

Translation control tunes *Drosophila* oogenesis

by Elliot T. Martin

A Thesis Submitted to
University at Albany, State University of New York
in Partial Fulfillment
of the Requirements for the Degree
Doctor of Philosophy

University at Albany, State University of New York
The Department of Biology

May 2022

Abstract

All dynamic biological processes require control over transcription, translation, or post-translation products. Stem cells in particular require dynamic control of gene expression. My work has focused on characterizing this control, primarily at the translation level, to better understand how stem cell differentiation occurs. Stem cells are cells with the unique ability to develop into more specialized cell types in a process called differentiation (Morrison & Spradling, 2008; Allan Spradling, Drummond-Barbosa, & Kai, 2001). Some stem cell, including those focused on in my work, also have the ability to “self-renew,” a process that allows one stem cell to copy itself giving rise to two stem cells (Cinalli, Rangan, & Lehmann, 2008; Allan Spradling, Drummond-Barbosa, & Kai, 2001). These processes must be carefully balanced as excess self-renewal will result in cells that do not give rise to differentiated cells necessary for further development or biological function (Cinalli, Rangan, & Lehmann, 2008). However, excess differentiation will result in the lack of an available pool of stem cells, preventing future differentiation and development (Cinalli, Rangan, & Lehmann, 2008). The decision of a stem cell to either self renew or differentiate is controlled by specific cellular pathways that can act at the level of transcription, translation, or post-translation (Blatt et al., 2020; Blatt, Martin, Breznak, & Rangan, 2020; Flora, Wong-Deyrup, et al., 2018b; Flora, McCarthy, Upadhyay, & Rangan, 2017; McCarthy et al., 2021; Sarkar et al.,

2021; Seydoux & Braun, 2006). To study the regulation of these pathways in-vivo I have used the female *Drosophila* germline as a model system. The female *Drosophila* germline is contained within two pairs of ovaries. Ovaries consist of two main types of tissue, soma and germline (Roth, 2001; Schüpbach, 1987; Xie & Spradling, 2000). Each ovary is made up of strands called ovarioles. Ovarioles represent an assembly line of successive development. At the anterior tip of each ovariole a structure called a germarium is present. At the anterior of the germarium two to three stem cells are housed in a somatic niche (Eliazer & Buszczak, 2011; Roth, 2001; Schupbach & Wieschaus, 1989; Xie & Spradling, 2000). These germline stem cells (GSCs) can self-renew, or differentiate giving rise to a daughter cell called a cystoblast (CB) (D. Chen & McKearin, 2003b; D. McKearin & Ohlstein, 1995; Xie & Spradling, 1998). The CB turns on a differentiation factor called bag of marbles (*bam*) (D. Chen & McKearin, 2003a; D. McKearin & Ohlstein, 1995). This CB then undergoes four incomplete cellular divisions, resulting in interconnected cysts consisting of two, four, eight, and finally sixteen cells (D. M. McKearin & Spradling, 1990; D. McKearin & Ohlstein, 1995). One of these cells is designated as the oocyte while the rest of the cells will become nurse cells (Bastock & St Johnston, 2008; J.-R. Huynh & St Johnston, 2004; J. Huynh & St Johnston, 2000; Navarro, Lehmann, & Morris, 2001; Navarro, Puthalakath, Adams, Strasser, & Lehmann, 2004; A. C. Spradling et al., 1997; Theurkauf, Alberts, Jan, & Jongens, 1993). The sixteen cell cyst is then encapsulated by somatic cells, forming egg chambers (Bastock & St Johnston, 2008; A. J. Forbes, Lin, Ingham, & Spradling, 1996; Xie & Spradling, 2000). Egg chambers successively grow in size in fourteen stages (A. Spradling, 1993). During this time the nurse cells produce mRNAs and proteins that are transported to the oocyte (Lilly & Duronio, 2005; Royzman & Orr-Weaver, 1998). The oocyte continues

to grow, while the nurse cells eventually die, dumping their contents into the oocyte (Guild, Connelly, Shaw, & Tilney, 1997; Jacob & Sirlin, 1959). Once the oocyte reaches the final, 14th stage it is known as an egg (A. Spradling, 1993). In concert with GSC differentiation, the differentiating progeny of GSCs also transition from a mitotic cell cycle to a meiotic cell cycle, in order to eventually undergo reductional cell division to form an egg [Kimble (2011); mckimMeioticRecombinationChromosome2002]. Several of the currently known factors that control this transition have been characterized as RNA binding proteins that likely facilitate the mitotic to meiotic transition by changing the translation landscape of the differentiating cysts [Tastan, Maines, Li, McKearin, & Buszczak (2010); Carreira-Rosario et al. (2016); Slaidina2014h; Blatt, Martin, Breznak, & Rangan (2020); Y. Li, Minor, Park, McKearin, & Maines (2009); Flora, Wong-Deyrup, et al. (2018b); Kim-Ha, Kerr, & Macdonald (1995)].

Each of the steps from GSC to egg require changes in cellular pathways. These changes can occur at the level of transcription, post-transcription, translation, or post-translation (Blatt, Martin, Breznak, & Rangan, 2020; Flora, McCarthy, Upadhyay, & Rangan, 2017). Decades of research has elucidated many of the changes that occur during oogenesis, however, many players in this process still remain mysterious. My work has helped to identify and characterize novel developmental mechanisms that are required for the successive developmental transitions that take place during oogenesis. I have leveraged RNAseq and polysome-seq to probe the global transcription and translation landscape over development and used the power of *Drosophila* genetics in concert with these sequencing techniques to identify and characterize misregulated pathways. To aid the research and hypothesis generation of other researchers in the field I have made a tool called Oo-site which democratizes access to our labs stage specific mRNAseq and polysome-seq data, as well as integrates publically available

single-cell seq data. This tool allows non-bioinformaticians to quickly and easily view expression data across *Drosophila* GSC differentiation and development. This work has revealed that *Ord*, a key meiotic gene is controlled post-transcriptionally, at the level of translation and suggests that other key genes involved in the transition of a GSC from a mitotic to a meiotic fate may be controlled though modulating their translation. A crucial participant in translation control is the ribosome which is the molecular machine that carries out translation (Brombin, Joly, & Jamen, 2015; Gabut, Bourdelais, & Durand, 2020; Genuth & Barna, 2018). Stem cells generally have high levels of ribosomes and ribosome biogenesis components, but relatively low levels of global translation (Gabut, Bourdelais, & Durand, 2020; Sanchez et al., 2016; Woolnough, Atwood, Liu, Zhao, & Giles, 2016; Zahradkal, Larson, & Sells, 1991; Q. Zhang, Shalaby, & Buszczak, 2014). When ribosome biogenesis is perturbed stem cells can differentiate inappropriately, at least sometimes in part because specific mRNAs become misregulated. This can result in tissue specific diseases called ribosomopathies. The tissue specific nature of these diseases has long been a question of study, but recently several examples have uncovered that in general these diseases arise from misregulation of stem cell differentiation. We have discovered a link between the efficient biogenesis of the translation apparatus, the ribosome, and the translation of the proteins constituent proteins of the ribosome. We found that three RNA helicases, Aramis, Athos, and Porthos, which were previously uncharacterized in *Drosophila* are all required for pre-rRNA processing and successful ribosome biogenesis. We found that proper ribosome biogenesis ensures that ribosomal proteins are translated at normal levels by preventing a translation inhibitor called Larp from binding its targets, which primarily consist of ribosomal proteins. We found that one of the mRNAs repressed by La-related protein (Larp) is Novel nucleolar protein (*Non1*),

which prevents cell cycle arrest in a p53 dependent manner. Therefore we discovered a novel connection between ribosome biogenesis and cell cycle. This resolves a longstanding question of why most genes involved in ribosome biogenesis all share the same phenotype when knocked down in *Drosophila* ovaries. Our work demonstrates that this likely occurs because when aspect of ribosome biogenesis is perturbed, translation of core ribosomal proteins are reduced to compensate for this loss in an attempt to balance ribosome biogenesis. This mechanism also results in a cell cycle arrest giving rise to a characteristic stem-like cyst where the GSC fails to divide from its progeny. More broadly, this connection has important implications in how stem cells regulate ribosome production which is known to play a crucial role in stem cell differentiation. Additionally, I have developed a tool called Oo-cyte to allow researchers to investigate changes in gene expression at the mRNA level and post-transcriptionally over the course of GSC differentiation. Using this tool I elucidated that crucial meiotic genes are in fact regulated post-transcriptionally. Overall, my work has emphasized the role the ribosome plays regulating stem cell differentiation. This regulation occurs both directly and indirectly. The ribosome regulation stem cell differentiation directly in that sufficient ribosome levels are required in order to overcome cell cycle blocks that ensure differentiation occurs properly. Indirectly, the ribosome carries out translation, which my work has demonstrated is a key point of regulation during stem cell differentiation. Moving forward, discovering the factors that enact translation regulation during differentiation is of critical importance to fully understanding stem cell differentiation and therefore differentiation related disease states.

Dedication

Dedicated to my wife and best friend Alli.

Acknowledgements

The work herein was only able to be completed thanks to the contribution of others. Foremost, my wife Allison Martin, without whom I would have given up countless times along the way to my PhD. She has been a sounding board, a life-coach, and my best friend for the years this work has taken. Secondly, my family including, Levi, who from childhood supported my curiosity and enabled me to pursue my interests and passions. Knowing that I have always had them to fall back on provided a cushion that has helped me from struggling in undergrad to the completion of my PhD. For direction, motivation, and guidance, I thank my mentors Dr. Prash Rangan and Dr. Gaby Fuchs. They agreed to mentor a disorganized student with less than stellar academics. Since that point they have helped me not only in developing a successful project, but also in maturing as an academic, a bench scientist, and generally, into adulthood. A thank you to my labmates who were always there to talk me through a failed experiment or get excited about an interesting result. To my collaborators, Elaine Nguyen, Roni Lahr, Dr. Andrea Berman, Dr. Shamsi Emtenani, and Dr. Daria Siekhaus, that contributed to this work I thank you for your expertise and beautiful results. Finally, to my committee members, Dr. Thomas Begley, Dr. Paolo Forni, and Dr. Joesph Wade for their guidance and advice throughout my graduate studies.

Attribution

1. Chapter 1: “Post-transcriptional gene regulation mediates critical cell fate transitions during *Drosophila* oogenesis” was published as Blatt P, Martin ET, Breznak SM, Rangan P. 2020. Post-transcriptional gene regulation regulates germline stem cell to oocyte transition during *Drosophila* oogenesis. Current Topics in Cell Biology 140: 3–34.
2. Except for minimal re-organization of the figures, the entire Chapter 2: “A translation control module coordinates germline stem cell differentiation with ribosome biogenesis during *Drosophila* oogenesis” was published as Martin, E.T., Blatt, P., Nguyen, E., Lahr, R., Selvam, S., Yoon, H.A.M., Pocchiari, T., Emtenani, S., Siekhaus, D., Berman, A.J., Fuchs, G., and Rangan, P. 2021. A translation control module coordinates germline stem cell differentiation with ribosome biogenesis during *Drosophila* oogenesis. bioRxiv.
3. Chapter 3: “Oo-site: A dashboard to visualize gene expression during *Drosophila* oogenesis reveals meiotic entry is regulated post-transcriptionally” was published as Martin, Elliot Todd, Kahini Sarkar, Alicia McCarthy, and Prashanth

Rangan. 2022. Oo-Site: A Dashboard to Visualize Gene Expression during Drosophila Oogenesis Reveals Meiotic Entry Is Regulated Post-Transcriptionally. bioRxiv.

These studies or articles are being included because they were part of the programmatic line of research that comprised the dissertation and that including them provides a coherent and appropriately sequenced investigation.

I was the primary researcher for the work reported in this dissertation.

Table of Contents

Abstract	ii
Dedication	vii
Acknowledgements	viii
Attribution	ix
Chapter 1: Post-transcriptional gene regulation instructs germline stem cell to oocyte transition during <i>Drosophila</i> oogenesis	1
1.1 Abstract	1
1.2 Introduction	2
1.3 Alternative splicing ensures accurate production of critical germline mRNAs to regulate sex determination and differentiation	6
1.4 RNA modifications direct splicing of sex determinants and translation of differentiation promoting genes in the germline	11
1.5 Production of ribosomes is finely tuned to facilitate differentiation	13
1.6 Hand off mechanisms facilitated by combinatorial RNA binding proteins dynamically shape the translational landscape during oogenesis	23
1.7 Summary	30
Chapter 2: A translation control module coordinates germline stem cell differentiation with ribosome biogenesis during <i>Drosophila</i> oogenesis	31
2.1 Summary:	31
2.2 Introduction	32
2.3 Results	37
2.3.1 Three conserved RNA helicases are required in the germline for GSC differentiation	37
2.3.2 Athos, Aramis, and Porthos are required for ribosome biogenesis	44
2.3.3 Aramis promotes cell cycle progression via p53 repression	50
2.3.4 Aramis-regulated targets contain a TOP motif in their 5'UTR	68
2.3.5 Larp binds TOP sequences in <i>Drosophila</i>	75
2.4 Discussion	81
2.4.1 Aramis, Athos, and Porthos are required for efficient ribosome biogenesis in <i>Drosophila</i>	82

2.4.2	Ribosome biogenesis defects leads to cell cycle defects mediated by p53	83
2.4.3	Ribosome biogenesis defects leads to repression of TOP-containing mRNA	86
2.4.4	Larp transduces growth status to ribosome biogenesis targets	87
2.4.5	Ribosome biogenesis in stem cell differentiation and ribosomopathies	89
2.5	Materials and Methods	94
Chapter 3:	Oo-site: A dashboard to visualize gene expression during <i>Drosophila</i> oogenesis reveals meiotic entry is regulated post-transcriptionally	117
3.1	Summary	117
3.2	Introduction	118
3.3	Results	121
3.4	Discussion	144
3.5	Acknowledgements	145
3.6	Materials and Methods	146
Chapter 4:	Conclusion	150
Appendix A:	The First Appendix	153
References		154

List of Tables

List of Figures

1.1	Schematic of <i>Drosophila</i> ovariole.	5
1.2	Schematic of the pathway that promotes alternative splicing of <i>sxl</i> .	11
1.3	Global translation rate, rRNA transcription rate, and mTorc1 activity during development.	22
1.4	Schematic of combinatorial and dynamic translation regulation in the <i>Drosophila</i> germarium.	29
2.1	RNA helicases Aramis, Athos and Porthos are required for GSC differentiation.	39
2.2	Aramis, Athos, and Porthos are required for proper cytokinesis and differentiation, related to Figure 2.1.	42
2.3	Athos, Aramis, and Porthos are required for efficient ribosome biogenesis.	46
2.4	Athos, Aramis, and Porthos are required for efficient ribosome biogenesis., related to Figure 2.3.	49
2.5	Athos, Aramis, and Porthos are required for cell cycle progression during early oogenesis.	53
2.6	Aramis is required for proper cell cycle progression, related to Figure 2.5.	57
2.7	Aramis is required for efficient translation of a subset of mRNAs.	60
2.8	The mRNA levels of Aramis polysome-seq targets are not significantly changing, related to Figure 2.7.	62
2.9	Non1 represses p53 expression to allow for GSC differentiation.	65
2.10	Non1 and p53 are inversely expressed, related to Figure 2.9.	67
2.11	Aramis regulated mRNAs contain a TOP motif.	71
2.12	TORC1 activity, Athos, and Porthos, regulate TOP expression in the germarium, related to Figure 2.11.	74
2.13	Larp binds to TOP mRNAs and binding is regulated by Aramis.	77
2.14	Larp binds specifically to TOP containing mRNAs and regulates cytokinesis, related to Figure 2.13.	80
3.1	Oo-site integrates and provides an interface for interacting with multi-omic data covering major stages of <i>Drosophila</i> GSC differentiation.	123
3.2	Sequencing strategy and clustered heatmaps of differential expression, related to Figure 3.1.	126

3.3	Oo-site allows for visualization of dynamically regulated genes.	128
3.4	Bulk RNA-seq recapitulates previously observed expression patterns of gene expression, related to Figure 3.3.	131
3.5	GO-terms enriched from differentially expressed genes between genetically enriched developmental milestones.	134
3.6	Ord expression is controlled post-transcriptionally.	137
3.7	Genes involved in meiotic cell cycle, including <i>ord</i> , may be controlled post-transcriptionally, related to Figure 3.6.	140
3.8	Genes involved in double-strand break repair may be controlled post-transcriptionally.	143

Chapter 1

Post-transcriptional gene regulation instructs germline stem cell to oocyte transition during *Drosophila* oogenesis

Patrick Blatt, Elliot T. Martin, Shane M. Breznak, Prashanth Rangan*

Department of Biological Sciences/RNA Institute, University at Albany SUNY, Albany,
NY University at Albany SUNY, 1400 Washington Avenue, Albany, 12222, USA *Corre-
spondence to: prangan@albany.edu

1.1 Abstract

During oogenesis, several developmental processes must be traversed to ensure effective completion of gametogenesis including, stem cell maintenance and asymmetric division, differentiation, mitosis and meiosis, and production of maternally contributed mRNAs, making the germ line a salient model for understanding how cell fate transitions are mediated. Due to silencing of the genome during meiotic divisions, there is little instructive transcription, barring a few examples, to mediate these critical transitions. In *Drosophila*, several layers of post-transcriptional regulation ensure that the mRNAs required for these processes are expressed in a timely manner and as needed during germline differentiation. These layers of

regulation include alternative splicing, RNA modification, ribosome production, and translational repression. Many of the molecules and pathways involved in these regulatory activities are conserved from *Drosophila* to humans making the *Drosophila* germline an elegant model for studying the role of post-transcriptional regulation during stem cell differentiation and meiosis.

Key words

Splicing, Translation Control, RNA Modifications, Ribosome Biogenesis,
Oogenesis, Drosophila, Germline Stem Cell, RNA regulation, Germline,
Differentiation, Gametogenesis, RNA Binding Proteins

1.2 Introduction

Gametogenesis gives rise to eggs or sperm in all sexually-reproducing organisms (Cinalli, Rangan, & Lehmann, 2008; Ellis & Kimble, 1994; Lesch & Page, 2012; Seydoux & Braun, 2006). Thus, understanding how gametogenesis is regulated is critical to comprehending this essential phenomenon that dictates fertility. Post-fertilization, the zygote gives rise to an entire organism, thus understanding how gametogenesis is regulated also has implications for the field of regeneration (Lasko, 2012; K.-A. Lee & Lee, 2014; Magnúsdóttir & Surani, 2014; Soldner & Jaenisch, 2018; Tadros & Lipshitz, 2009; Theunissen & Jaenisch, 2017).

Drosophila melanogaster has been one of the central organisms used to study heritability and gametogenesis for nearly a century due to its rapid generation time and genetic tractability (Mattox, Palmer, & Baker, 1990; Allan C. Spradling, 1993; A. C. Spradling et al., 1997;

Allan C. Spradling & Rubin, 1981; Allan Spradling, Fuller, Braun, & Yoshida, 2011; Xie & Li, 2007). These traits have facilitated the establishment of an extensive collection of informative and useful mutant and transgenic flies (Hales, Korey, Larracuente, & Roberts, 2015). In addition, many of the gametogenic regulatory factors described in the *Drosophila* germ line are conserved to mammals and also play critical roles in other tissues, such as neurons (Goldstrohm, Hall, & McKenney, 2018; H. Lin & Spradling, 1997; Reichardt et al., 2018; Vessey et al., 2010; Zamore, Bartel, Lehmann, & Williamson, 1999; K. Zhang & Smith, 2015). While both male and female *Drosophila* undergo meiosis to give rise to gametes, here we focus on the female germline as regulation of gametogenesis in males has been reviewed elsewhere (Barreau, Benson, Gudmannsdottir, Newton, & White-Cooper, 2008; Fuller, 1998; Allan Spradling, Fuller, Braun, & Yoshida, 2011; Yamashita & Fuller, 2005; G.-Q. Zhao & Garbers, 2002).

The spatiotemporal stages of *Drosophila* oogenesis are discrete and can be easily identified by their morphology and molecular markers (Gáspár & Ephrussi, 2017; D. Jia, Xu, Xie, Mio, & Deng, 2016; Allan Spradling, Fuller, Braun, & Yoshida, 2011). At the anterior end of the ovary, germline stem cells (GSCs) reside in a structure known as the germarium and initiate differentiation to give rise to gametes (Kai, Williams, & Spradling, 2005; Twombly et al., 1996; Xie & Li, 2007; Xie & Spradling, 1998, 2000). GSCs are maintained by signaling from the surrounding somatic niche. GSCs undergo asymmetric mitotic division, producing a stem cell daughter, or cystoblast (CB) which will begin the process of differentiation by expressing the essential differentiation factor *bag of marbles* (*bam*) (D. Chen & McKearin, 2003b; D. McKearin & Ohlstein, 1995). The differentiating CB then undergoes four incomplete mitotic divisions, giving rise to an interconnected 16-cell cyst (D. M. McKearin & Spradling, 1990;

D. McKearin & Ohlstein, 1995). In this cyst, one cell is designated to become the oocyte and the other 15 cells take on the role of nurse cells, which generate proteins and mRNAs that are provided to the developing oocyte (Navarro, Puthalakath, Adams, Strasser, & Lehmann, 2004; A. C. Spradling et al., 1997). The specified oocyte and its associated nurse cells are then encapsulated by somatic cells to form an egg chamber that buds off from the germarium (Figure 1B) (Gilboa & Lehmann, 2004; Margolis & Spradling, 1995). The nurse cells will enter into a unique state in which they undergo a modified version of the cell cycle without undergoing mitosis, creating polyploid nuclei capable of fulfilling the high transcriptional demand required to transcribe all of the mRNAs necessary for the egg (Lilly & Duronio, 2005; Royzman & Orr-Weaver, 1998). As this process ensues, the egg chambers and oocyte increase in size as the supply of mRNAs and proteins is created and deposited into the mature egg (Figure 1A) (Lasko, 2012; Richter & Lasko, 2011).

Oocyte development entails multiple processes that ensure effective completion of gametogenesis and fertility. Among these are stem cell maintenance and asymmetric division, differentiation, mitosis and meiosis, and production of the maternal mRNA contribution, thus the germ line is a salient model for understanding how cells navigate fate transitions (D. Chen & McKearin, 2003b; Fu et al., 2015; Harris, Pargett, Sutcliffe, Umulis, & Ashe, 2011; Lasko, 2012). During oogenesis, there is little instructive transcription, barring a few examples, to mediate these critical transitions (Cinalli, Rangan, & Lehmann, 2008; P. Rangan, DeGennaro, & Lehmann, 2008). Instead, the germline relies highly on post-transcriptional regulatory mechanisms to coordinate gametogenesis (Slaidina & Lehmann, 2014). These include: alternative splicing, RNA modifications to modulate splicing, protein-RNA interactions, small RNA biology, and organization of the translation machinery to

control the output of gene expression to mediate cell fate transitions. Here we focus on post-transcriptional processing of germline mRNAs and translational regulation both of which are required for successful oogenesis.

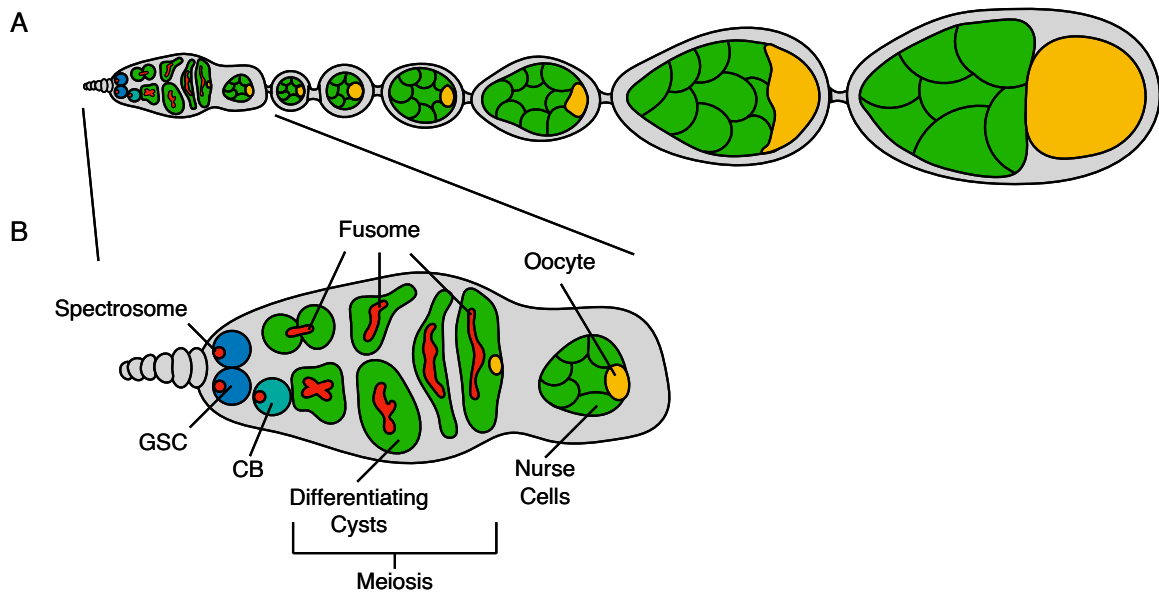


Figure 1.1: (A) **Schematic of *Drosophila* ovariole.** *Drosophila* females have two ovaries consisting of 16–20 ovarioles, which are assembly lines for producing mature eggs. The germarium, the structure that houses the germline stem cell (GSC), is present at anterior tip of the ovariole. The germline stem cell asymmetrically divides, giving rise to another GSC and a GSC daughter. The daughter cell then will undergo four incomplete rounds of mitosis, giving rise to a 16-cell cyst. Of the 16 cells one will be specified as the egg while the others serve as polyploid nurse cells that support oocyte and egg development. The surrounding somatic cells encapsulate the 16-cell cyst creating egg chambers. As development proceeds, the nurse cells provide mRNAs and proteins allowing the oocyte to grow in size and to eventually become a mature egg. (B) Inset of a germarium showing the developing germline, with the GSC located at the most anterior tip. Upon differentiation, the CB will undergo 4 incomplete mitotic divisions giving rise to a 16-cell cyst. Only one cell of the sixteen cells completes meiosis and is destined to become the oocyte.

1.3 Alternative splicing ensures accurate production of critical germline mRNAs to regulate sex determination and differentiation

Splicing decisions are crucial during the generation of mature mRNAs post-transcriptionally and significantly contribute to germline development. Splicing is mediated by a large ribonucleoprotein catalytic complex called the spliceosome, the core of which is made up of five small nuclear RNAs (snRNA), U1, U2, U4, U5 and U6, that work with spliceosomal proteins to form a small nuclear ribonucleoprotein complex (snRNP) (Madhani, Bordonne, & Guthrie, 1990; Wahl, Will, & Lührmann, 2009; Will & Lührmann, 2001, 2011). This complex removes introns from newly synthesized pre-mRNAs and links exonic sequences together (Wahl, Will, & Lührmann, 2009). Initially, U1 snRNP recognizes the donor site, which is located at the 5' end of the intron, and U2 snRNP binds the branch site located at the 3' end, leading to structural rearrangements of the complex and its associated substrate pre-mRNA (Matera & Wang, 2014). Catalytic actions of pre-mRNA splicing occur in two main steps. Cleavage at the 5' splice site forms a lariat-like structure such that a 2'-5' phosphodiester bond is created between the first nucleotide of the donor site and a conserved adenosine residue at the branch site (Rymond & Rosbash, 1985). Next, a second cleavage event occurs at the 3' splice site and is followed by ligation of flanking exons to complete splicing (Umen & Guthrie, 1995; Wahl, Will, & Lührmann, 2009).

Alternative splicing is a process by which a single locus can give rise to many unique mRNA isoforms and their resulting protein variants (Black, 2000). The selection of the

splice sites is exquisitely regulated to determine which exons will be included in the resulting alternatively spliced transcripts (Y. Wang et al., 2015). Alternative splicing is highly regulated and is critical to germline development (Hager & Cline, 1997; Kalsotra & Cooper, 2011). There are a myriad of RNA targets that must be differentially spliced, and a complex web of interacting proteins orchestrate production of their splice variants (Y. Lee & Rio, 2015). One of the first described instances of alternative splicing in *Drosophila* females is the splicing of the sex determination gene *sex-lethal* (*sxl*) (Bell, Maine, Schedl, & Cline, 1988). *sxl* is alternatively spliced to generate isoforms that control sex determination in somatic tissues (Chang, Dunham, Nuzhdin, & Arbeitman, 2011). In females, an autoregulatory loop forms between Sxl protein, U2AF splicing factor and U1 snRNP (Nagengast, Stitzinger, Tseng, Mount, & Salz, 2003). In *Drosophila*, the protein component of the U1 and U2 snRNPs are encoded by a gene called *sans fille* (*snf*) (Cline, Rudner, Barbash, Bell, & Vutien, 1999). Loss of *snf* results in a sterility phenotype in females that specifically affects germline *sxl* splicing and leads to a tumor comprised of undifferentiated cells (Johnson, Nagengast, & Salz, 2010; Nagengast, Stitzinger, Tseng, Mount, & Salz, 2003). When correctly spliced, the resulting Sxl protein recognizes its own pre-mRNAs by binding both upstream and downstream of Exon 3 (Penalva & Sánchez, 2003). In addition, Sxl protein interacts with the U2AF and U1 snRNP to block the recognition of splice sites at Exon 3 (Nagengast, Stitzinger, Tseng, Mount, & Salz, 2003). As a result, exon 3 is spliced out of the pre-mRNA in the final transcript that is capable of being translated into a fully functional protein (Penalva & Sánchez, 2003). In contrast, males include exon three in the final *sxl* transcript. Exon 3 contains a premature stop codon within the *sxl* transcript that results in a truncated protein that lacks the activity of the female-specific variant (Inoue, Hoshijima,

Sakamoto, & Shimura, 1990). Thus, *sxl* is differentially expressed in the male and the female gonad due to alternative splicing events.

In addition to control of *sxl* via alternative splicing, *sxl* expression is controlled at the level of transcription by several transcription factors, such as Ovo (Salles, Mével-Ninio, Vincent, & Payre, 2002). Ovo is a zinc finger DNA binding protein that is required in the germline for proper gametogenesis(Andrews et al., 2000). *ovo* is also alternatively spliced and each of its isoforms have different implications for *sxl* expression. Ovo-A and Ovo-B where the first splice variants of *ovo* shown to be expressed in the female germline during oogenesis (Salles, Mével-Ninio, Vincent, & Payre, 2002). In addition to differences due to alternative exon usage, Ovo-A, unlike Ovo-B, contains a 381 amino acid N-terminal extension which arises due to alternative transcription start sites (Andrews et al., 2000). Use of these promoters generates distinct Ova isoforms with unique temporal requirements during oocyte development; Ovo-B was found to be necessary and sufficient during early oogenesis and Ovo-A is critical in the later stages of egg development for a fully functional egg. The *ovo-B* gene has two characterized isoforms, Ovo+2B and Ovo-2B, which were discovered through a transposon insertion that disrupts exon splicing of *ovo-B*. This transposition event prevents inclusion of the exon 2b extension, producing a nonfunctional protein that accumulates during oogenesis. In the absence of retrotransposon insertion, the 178-amino acid extension encoded by exon 2b is included forming a fully functional Ovo protein, known as Ovo-+2B (Salles, Mével-Ninio, Vincent, & Payre, 2002). Interestingly, Ovo-B promotes transcription of *ovarian tumor* (*otu*), which enhances *sxl* expression (Figure 2) (J. Lu & Oliver, 2001). The mechanism by which Otu regulates *sxl* expression is unknown but various mutations in *otu* lead to a myriad of phenotypes such as loss of germ cell proliferation, and inability

to complete the differentiation process. The *otu* gene produces two cytoplasmic protein isoforms, a 104-kDA isoform (Otu-104) and a 98-kDA isoform (Otu-98) (Tirronen, Lahti, Heino, & Roos, 1995). Strikingly, only Otu-104 is capable of rescuing all the *otu* mutant phenotypes, indicating its requirement during oogenesis, while Otu-98 is dispensable during this process (Tirronen, Lahti, Heino, & Roos, 1995). Despite the lack of insight into how the *otu* splice forms regulate GSC development, its alternative splicing is critical for oogenesis (Sass, Comer, & Searles, 1995). Thus, a cascade of alternative splicing events regulate production of Sxl in the female germline to promote oogenesis (Figure 2).

Sxl expression in the female gonad regulates both sex determination as well as differentiation (Chau, Kulnane, & Salz, 2012). One critical task of Sxl is to represses Tudor domain containing protein 5-like (*tdrd5l*) (Primus, Pozmanter, Baxter, & Van Doren, 2019). Tdrd5l is present in the cytoplasm of the male germline, localizing to granules associated with RNA regulation, to promote male identity and differentiation. Sxl expression in the female gonad represses translation of Tdrd5l to promote female identity (Primus, Pozmanter, Baxter, & Van Doren, 2019). In addition, female Sxl has been found to regulate transcription of *PHD finger protein 7 (phf7)*, a key regulator of male identity (S. Y. Yang, Baxter, & Van Doren, 2012). Sxl was found to recruit SETDB1, a chromatin writer, to deposit trimethylated H3K9 (H3K9me3) repressing transcription of *phf7* (Smolko, Shapiro-Kulnane, & Salz, 2018). Thus, alternative splicing of *sxl* results in different sexes helps promote proper sex determination in the germline (Figure 2). Sxl also fulfills additional functions outside of sex determination. Sxl is required in the female germline for germline stem cell GSC differentiation. Loss of Sxl protein causes an accumulation of single cells and two cell cysts (Chau, Kulnane, & Salz, 2009). It is thought that Sxl binds *nanos (nos)* mRNA, an RNA binding protein that is

necessary for GSC self-renewal, using a canonical Sxl binding sequence in the 3' UTR (Chau, Kulnane, & Salz, 2012). Loss of Sxl leads to an accumulation of excess of Nanos protein, which is thought to limit? GSC differentiation (Boerner & Becker, 2016; Chau, Kulnane, & Salz, 2012; Y. Li et al., 2013). While regulation by Sxl is beginning to be deciphered, several aspects remain to be discovered. For example, Sxl, a splicing factor, is predominantly cytoplasmic in undifferentiated cells but becomes nuclear as differentiation proceeds (Chau, Kulnane, & Salz, 2009), yet, how it works as translational regulator while in the cytoplasm and how it is transported to the nucleus to function as splicing factor during differentiation are not known.

Polypyrimidine tract binding proteins (PTBs) promote splicing by binding polypyrimidine tracts that are ~10nt long and bring splice sites together by means of protein dimerization to promote alternative splicing (Polydorides, Okano, Yang, Stefani, & Darnell, 2000; Romanelli, Diani, & Lievens, 2013). A PTB, *half pint* (*hfp*), a homolog of human PUF60, is important for oogenesis (Maniatis & Tasic, 2002). Loss of *hfp* results in missplicing of the *otu* transcripts described above (Van Buskirk & Schüpbach, 2002). In addition, *hfp* also regulates alternative splicing of *eukaryotic initiation factor 4E* (*eIF4E*) during development through 3' splice site selection (Reyes & Izquierdo, 2008). Hfp is required to increase the relative abundance of the longer *eIF4E* transcript (Van Buskirk & Schüpbach, 2002). Lastly, *hfp* also regulates splicing of *gurken*, a critical regulator of dorsal-ventral patterning (Kalifa, Armenti, & Gavis, 2009). Thus, sex determination, differentiation and production of the determinants of embryonic patterning for the next generation are all regulated by mechanisms involving alternative splicing in the female germline.

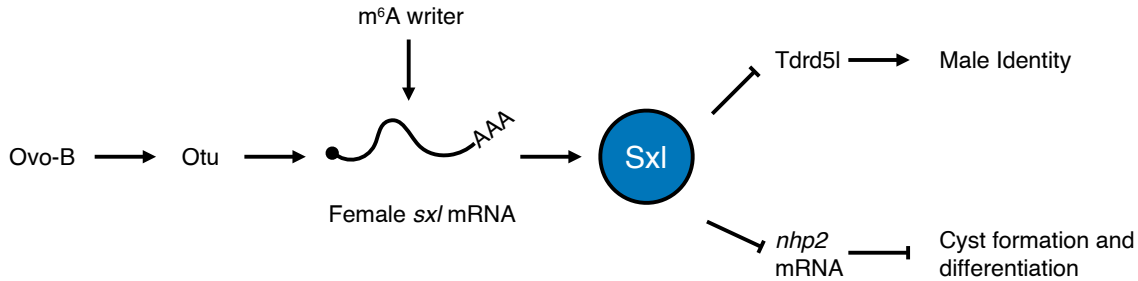


Figure 1.2: Schematic of the pathway that promotes alternative splicing of *sxl* to generate the female *sex determining* variant in the germline. Ovo-B promotes the transcription of *otu*, which enhances splicing of *sxl*. The female-specific splice form of *sxl* is further enhanced by RNA modification by the m6A writer. Formation of the female-specific form generates a functional Sxl protein. Sxl represses *Tdrd5l*, a protein that promotes male identify. Additionally, Sxl post-transcriptionally represses *nhp2* to promote cyst formation during differentiation.

1.4 RNA modifications direct splicing of sex determinants and translation of differentiation promoting genes in the germline

Post transcriptional RNA modifications are abundant and conserved in all branches of life (Yi & Pan, 2011). There have been over 100 described RNA modifications that can alter stability, function and splicing of RNAs (Licht & Jantsch, 2016; Roundtree, Evans, Pan, & He, 2017). A well-known example of an mRNA modification is the 5' methylguanosine cap that is added to all mRNAs to promote their stability and aid in translation initiation (Mitchell et al., 2010; Mukherjee et al., 2012). A variety of RNA modifications have been linked to developmental transitions, such as those affecting GSC fate (Batista et al., 2014; Roundtree, Evans, Pan, & He, 2017). Specifically during oogenesis, N6A-methyladenosine (m^6A) has been shown to be important for differentiation of germline stem cell daughter cells in females by ensuring

proper female-specific splicing of *sxl* (Haussmann et al., 2016). Additionally, the H/ACA box complex, an RNP complex responsible for depositing pseudouridine on rRNA, has been suggested to be regulated by Sxl during the germline stem cell to daughter cell transition and is required for proper cyst differentiation (T. Kiss, Fayet-Lebaron, & Jády, 2010; Morita, Ota, & Kobayashi, 2018).

m^6A is prevalent on mRNA and is mediated by a methyltransferase complex that deposits a methyl-group at the sixth nitrogen on adenosine (Y.-G. Y. Yang, Hsu, Chen, & Yang, 2018). In *Drosophila*, m^6A is placed by a m^6A writer complex consisting of Xio, Virilizer (Vir), Spenito (Nito), female lethal d (fl(2)d), Methyltransferase like 3 (Mettl3) and Methyltransferase like 14 (Mettl14) (Yan & Perrimon, 2015). Some described roles of m^6A involve modulating RNA-structure, facilitating mRNA degradation, promoting translation initiation and mediating alternative splicing (Roundtree, Evans, Pan, & He, 2017). Interestingly, the m^6A writer complex has been linked to *sxl* splicing during *Drosophila* oogenesis (Kan et al., 2017). miCLIP data revealed that m^6A must be placed at intergenic regions of the *sxl* mRNA in order to produce the female-specific isoform (Kan et al., 2017). Accordingly, loss of m^6A complex members such as *spenito* result in expression of the male specific isoform of *sxl*, and tumors of undifferentiated cells, similar to loss of *sxl* (Mattox, Palmer, & Baker, 1990); (Kan et al., 2017). This suggests that m^6A enables proper splicing of female-specific *sxl*, which allows for proper differentiation of germline stem cells into cystoblast daughter cells (Figure 2).

Pseudouridine is one of the most abundant RNA modifications (B. S. Zhao & He, 2015). Although most commonly found on tRNAs, pseudouridine is also found on mRNAs as well as rRNA (Penzo & Montanaro, 2018). Unlike the canonical nucleoside uridine which is attached

to the sugar via a nitrogen-carbon bond, pseudouridine is a uridine isomer attached through a carbon-carbon bond (Cohn, 1960). Pseudouridine can be placed by two different classes of enzymes; either by a sequence specific pseudouridine synthase or a small RNA guided complex called the box H/ACA ribonucleoprotein (De Zoysa & Yu, 2017). Depletion of the H/ACA box complex member Nucleolar Protein Family A Member 2 (NHP2) in the germline leads to an accumulation of 4- and 8- cell cysts that do not transition to the 16-cell cyst stage (Morita, Ota, & Kobayashi, 2018). Interestingly, the accumulation of single cells due to loss of *sxl* is partially rescued by loss of *NHP2* *indicating that this sxl phenotype is due to excess NHP2* (Morita, Ota, & Kobayashi, 2018). Consistent with this notion, Sxl interacts with *nhp2* mRNA suggesting that Sxl may impose a regulatory function, in this case likely repression of *nhp2* to allow initiation of the differentiation program (Figure 2) (Morita, Ota, & Kobayashi, 2018). Thus, although it is clear that RNA modifications help to ensure proper splicing of sex determination factors, but the pathway, mechanism, and direct targets remain unresolved.

1.5 Production of ribosomes is finely tuned to facilitate differentiation

While splicing mediates proper mRNA production, access of the mature mRNAs to ribosomes controls their translation. Once mRNAs are gated for translation, proper ribosome levels control protein production. The levels of ribosomes during early oogenesis are strictly regulated and shockingly dynamic. Ribosome biogenesis is the process of transcribing and

processing the ribosomal RNA (rRNA) components, as well as transcribing and translating the protein constituents of the ribosome (Granneman & Baserga, 2004; Nazar, 2004; Teng, Thomas, & Mercer, 2013; Yelick & Trainor, 2015). This process is exquisitely regulated as ribosome biogenesis is one of the most energy intensive tasks of maintaining cell homeostasis and is even more crucial in proliferative cells (Phipps, Charette, & Baserga, 2011). In addition to the high energy requirement of ribosome biogenesis, all of the components of the ribosome must be coordinated in their production. The process of ribosome biogenesis involves a series of coordinated steps of processing and assembly that involve dozens of non-coding RNAs and proteins and the molecular details of this process have been thoroughly covered in detail in several recent reviews (Granneman & Baserga, 2004; Yelick & Trainor, 2015; You, Park, & Kim, 2015). Briefly, ribosomal DNA (rDNA) is present in multicopy stretches within the genome; these areas of DNA are localized to a subnuclear organelle called the nucleolus (Karpen, Schaefer, & Laird, 1988; Ritossa & Spiegelman, 1965; Schwarzacher & Wachtler, 1993). rDNA is transcribed into rRNA in the nucleolus and processing steps begin cotranscriptionally (Koš & Tollervey, 2010) to remove internal and external spacers found in immature rRNA (Granneman & Baserga, 2004; Granneman, Petfalski, Tollervey, & Hurt, 2011; Schäfer, Strauß, Petfalski, Tollervey, & Hurt, 2003; Tafforeau et al., 2013). As these processing steps occur, the rRNA is covalently modified and ribosomal proteins begin to interact with the partially processed rRNA (Agalarov, Sridhar, Funke, Stout, & Williamson, 2000; Deshmukh, Tsay, Paulovich, & Woolford, 1993; Gumienny et al., 2017; Jady & Kiss, 2001; A. M. Kiss, Jady, Bertrand, & Kiss, 2004). When the rRNA is mostly mature it is exported from the nucleus to the cytoplasm where the small and large subunits of the ribosome fully mature and assemble (Lo et al., 2010; Schäfer, Strauß, Petfalski,

Tollervey, & Hurt, 2003; Sloan et al., 2017; Tschochner & Hurt, 2003; Zemp & Kutay, 2007).

Errors at any of these steps can result in ribosome biogenesis defects which in humans result in disease states known as ribosomopathies (Armistead & Triggs-Raine, 2014; Barlow et al., 2010; Brooks et al., 2014; Higa-Nakamine et al., 2012; Mills & Green, 2017; Sloan et al., 2017).

Curiously, despite the presence of ribosomes across cell types and sharing similar molecular origins, ribosomopathies manifest as tissue specific defects rather than pleiotropic phenotypes (Brooks et al., 2014; Higa-Nakamine et al., 2012; Mills & Green, 2017; Pereboom, van Weele, Bondt, & MacInnes, 2011; Yelick & Trainor, 2015). The reasons behind the unique, tissue-specific manifestations are still being investigated but in several cases it seems that stem cells may be particularly sensitive to perturbations in ribosome biogenesis (Brooks et al., 2014; Morgado-Palacin, Llanos, & Serrano, 2012; Pereboom, van Weele, Bondt, & MacInnes, 2011; Watanabe-Susaki et al., 2014). Indeed, a growing body of evidence is beginning to suggest that *Drosophila* GSCs not only have a specific requirement for ribosome biogenesis, but also that ribosome biogenesis, as well as global translation, vary greatly over the course of GSC differentiation and are uncoupled during early oogenesis (Sanchez et al., 2016; Q. Zhang, Shalaby, & Buszczak, 2014). These attributes make *Drosophila* oogenesis an excellent system to address how perturbations of ribosome levels affects stem cell differentiation.

In order to maintain stem cell fate, GSCs asymmetrically partition factors required for ribosome biogenesis by retaining more of this machinery than they pass on to daughter cells (Fichelson et al., 2009; Q. Zhang, Shalaby, & Buszczak, 2014). In particular, Underdeveloped (Udd), an rRNA transcription factor segregates asymmetrically to the GSC during mitosis

and seems to promote a high rate of rRNA synthesis within the GSC (Q. Zhang, Shalaby, & Buszczak, 2014). Furthermore, Wicked (Wcd), a U3 snoRNP complex member required for rRNA maturation, is also asymmetrically partitioned to GSCs and associates with the original spectrosome, an ER rich organelle found in GSCs and CBs (A. C. Spradling et al., 1997), of the dividing GSC. How GSCs carry out this specialized cellular division requires further investigation, however, asymmetric stem cell division is crucial for proper differentiation (D. Chen & McKearin, 2003a; D. Chen & McKearin, 2003b; H. Lin & Spradling, 1997). Consistent with this loss of *wcd* results in premature differentiation of GSCs (Fichelson et al., 2009). Nascent rRNA production, measured by BrUTP incorporation, and presumably ribosomes, are produced at high levels in GSCs but this production drops in CBs and in subsequent stages (Figure 3) (Q. Zhang, Shalaby, & Buszczak, 2014). Additionally, it has been observed that certain ribosome biogenesis components are expressed at high levels specifically in the germline (Kai, Williams, & Spradling, 2005). In particular, RNA exonuclease 5 (Rexo5) is an RNA exonuclease that facilitates ribosome biogenesis by trimming snoRNAs as well as rRNAs (Gerstberger et al., 2017). Depletion of *rexo5* in the germline results in an accumulation of egg chambers that bud off from the germarium, but do not grow in size, and causes defects in GSC proliferation (Gerstberger et al., 2017). These observations suggest that the machinery for ribosome biogenesis is not only critical for germline development but is also dynamically regulated.

Sanchez et al. demonstrated that the dynamic nature of rRNA transcription during germline development is not simply a consequence of the differentiation process. Instead, lowering ribosome biogenesis is required for timely differentiation, but severe loss of ribosome biogenesis causes formation of stem-cysts, a product of perturbed cytokinesis of GSC

daughters (Mathieu et al., 2013; Matias, Mathieu, & Huynh, 2015; Sanchez et al., 2016). Somewhat surprisingly, despite their increased retention of ribosome biogenesis components, GSCs exhibit a lower rate of translation compared to daughter cells and cyst stages (Figure 3). This finding invokes the hypothesis that despite the GSCs elevated capacity for ribosome biogenesis, GSCs do not intrinsically require higher ribosome levels for translation. Instead, the data is suggestive of the possibility that GSCs produce high levels of ribosomes in order to pass them on to and facilitate differentiation of their daughter cells. We thus hypothesize that a ribosome biogenesis checkpoint could couple ribosome production to cell cycle progression to ensure a sufficient ribosome concentration is passed from the GSC to the daughter CB. Conversely, increasing ribosome biogenesis via overexpression of TIF-IA, an RNA Pol I transcription initiation factor that is required for rRNA synthesis (Grewal, Evans, & Edgar, 2007), results in a failure of germ cells to differentiate, causing a marked overproliferation of undifferentiated GSC daughters (Q. Zhang, Shalaby, & Buszczak, 2014). This overproliferation may be caused by bypassing or rapid progression through the proposed ribosome biogenesis checkpoint such that the cell cycle is hastened in response to elevated ribosome biogenesis. The overproliferation of undifferentiated germ cells when ribosome levels are elevated is consistent with observations that high ribosome levels lead to rapidly growing cancers (Belin et al., 2009; Deisenroth & Zhang, 2010; Vlachos & Muir, 2010).

Although reducing ribosome biogenesis tends to result in the formation of a stem-cyst as previously described, some factors that play a role in ribosome biogenesis have a less severe phenotypes. For example, some mutants of the ribosomal protein S2 (*rps2*) gene have a repeating egg-chamber mid-oogenesis defect, wherein ovarian development halts at stage 5 and successive egg chambers do not grow in size and eventually die, resulting in

sterility (Cramton & Laski, 1994). This phenotype may be the consequence of incomplete loss of function as the allele that results in the repeating egg chamber phenotype reduces mRNA expression of *rps2*, incompletely, by 60-70%, while other allelic combinations result in embryonic lethality (Cramton & Laski, 1994). Incomplete loss of function alleles for another ribosomal protein, *ribosomal protein S3*, result in a similar repeating egg chamber phenotype [Sæbøe-Larssen1998]. These observations suggest that partial loss of ribosome biogenesis during oogenesis may be tolerated during differentiation but results in phenotypes at a later phase of egg production, consistent with the model that high levels of biogenesis in early stages supply the ribosomes for subsequent differentiation and development.

Not only do ribosome levels vary but a class of ribosomal protein paralogs are enriched specifically in early germ cells (Xue & Barna, 2012). Several variant ribosomal proteins such as *ribosomal proteins S5b* (*rps5b*), *s10a*, *s19b*, and *l22*-like are enriched in the germline and others are enriched during early oogenesis (Kai, Williams, & Spradling, 2005). The role of these ribosomal proteins has not been thoroughly explored, but their presence indicates either a role for specialized ribosomes early during germline development or as a way to further increase the availability of ribosomal proteins to facilitate the high level of ribosome production in GSCs. One of these ribosomal protein paralogs, RpS5b, has recently been characterized (Kong et al., 2019). *rps5b* is most highly expressed in ovaries in contrast to its paralog, *ribosomal protein S5a* (*rps5a*), which is expressed at high levels ubiquitously (Kong et al., 2019). Loss of *rps5a* in the germline does not cause a germline phenotype, however, loss of *rps5b* results in a mid-oogenesis defect that is further exacerbated when *rps5a* is depleted in a *rps5b* mutant background (Kong et al., 2019). This could suggest that RpS5a and RpS5b are functionally similar and that the RpS5b phenotype results from

lowering the overall amount of RpS5 available during oogenesis. However, RpS5b was also found to interact preferentially with mRNAs that encode proteins involved in mitochondrial electron transport, in contrast to RpS5a which binds mRNAs from a broad spectrum of gene categories (Kong et al., 2019). In accordance with the binding data, *rps5b* depleted ovaries expressed lower levels of proteins involved in oxidative phosphorylation and mitochondrial respiration (Kong et al., 2019). This evidence suggests that the expression of ribosomal protein paralogs may be a part of specialized ribosomes that translate specific groups of mRNAs; however, these ribosomal protein paralogs must be carefully analyzed to determine if they make up bonafide special ribosomes or instead have ribosome independent functions (Dinman, 2016).

What regulates ribosome biogenesis to allow for it to be dynamic during early *Drosophila* germline development? The best understood regulator of ribosome biogenesis is the Target of Rapamycin (TOR) pathway (Chymkowitch, Aanes, Robertson, Klungland, & Enserink, 2017; Magnuson, Ekim, & Fingar, 2012; Yuehua Wei & Zheng, 2009; Yerlikaya et al., 2016) TOR is a kinase that is part of two distinct subcomplexes, TOR complex 1 (TORC1) and TOR complex 2 (TORC2) (Wullschleger, Loewith, & Hall, 2006). These complexes have distinct biological roles. TORC2 has been shown to function as an important regulator of the cytoskeleton (Wullschleger, Loewith, & Hall, 2006). Whereas, TORC1 receives and integrates several different signals including nutritional and growth factors and its activity promotes pro-proliferative activities such as global translation, ribosomal protein translation, and cell cycle progression (E. Kim, Goraksha-Hicks, Li, Neufeld, & Guan, 2008; Magnuson, Ekim, & Fingar, 2012; Texada et al., 2019). TORC1 activity also helps to coordinate the transcription and translation of the components required for ribosome biogenesis (Grewal,

Evans, & Edgar, 2007; Magnuson, Ekim, & Fingar, 2012; D. E. Martin, Powers, & Hall, 2006). In *Drosophila*, TORC1 activity is high in GSCs through the 4-cell cyst, but TORC1 activity dips in 8 and 16 cell cysts and subsequently increases after the cyst stages (Youheng Wei, Bettledi, Kim, Ting, & Lilly, 2019). Interestingly, the landscape of TORC1 activity resembles the landscape of ribosome biogenesis, but not global translation (Figure 3) (Sanchez et al., 2016; Q. Zhang, Shalaby, & Buszczak, 2014). However, loss of TORC1 components does not phenocopy perturbation of ribosome biogenesis (Sanchez et al., 2016). This is possibly because TORC1 plays a broader role in early oogenesis given the myriad of regulatory functions TORC1 is known to play in other systems (E. Kim, Goraksha-Hicks, Li, Neufeld, & Guan, 2008; S. Li, Zhang, Takemori, Zhou, & Xiong, 2009; Moreno-Torres, Jaquenoud, & De Virgilio, 2015; Noda, 2017; Yuehua Wei & Zheng, 2009). A downstream effector of mTORC1, La related protein 1 (Larp1) is known to silence ribosomal protein translation in mammals through binding to terminal oligopyrimidine tracts in the 5'UTR of its targets (Bruno D. Fonseca et al., 2015; Hong et al., 2017; Roni M. Lahr et al., 2017; Tcherkezian et al., 2014); however, the same has yet to be demonstrated for the *Drosophila* ortholog, La related protein (Larp). Tantalizingly, Larp is required for male and female fertility in *Drosophila*, but details of Larp's precise role in the female and oogenesis are lacking (Blagden et al., 2009; Ichihara, Shimizu, Taguchi, Yamaguchi, & Inoue, 2007). In contrast, in males Larp is required for proper spindle pole formation as well as proper cytokinesis (Blagden et al., 2009). Given the regulatory role Larp plays in ribosome biogenesis in mammals and the data from *Drosophila* spermatogenesis, Larp could facilitate the dynamic nature of ribosome biogenesis during GSC differentiation and meiosis. However, further study is required to understand the role of Larp during GSC differentiation and oogenesis to determine its function.

in this context.

The process of differentiation requires major cellular reprogramming. Surprisingly, despite being required for cell viability ribosome biogenesis and global translation are two key programs that are modulated to shape GSC differentiation(Sanchez et al., 2016; Q. Zhang, Shalaby, & Buszczak, 2014). When ribosome production is improperly modulated during GSC differentiation it results in characteristic phenotypes, accumulation of single cells if biogenesis components are overexpressed and formation of a stem-like cyst if ribosome biogenesis components are knocked down in the germline (Sanchez et al., 2016; Q. Zhang, Shalaby, & Buszczak, 2014). Additionally, several ribosomal protein variants are highly enriched in ovaries and they may perform special functions, however, these variants are just beginning to be studied. Additionally, based on what we know of the mechanisms and networks that control ribosome biogenesis in *Drosophila* oocytes, the dynamic nature of ribosome biogenesis seems likely to be conserved; however, further investigation is required to determine and compare the basis of ribosome biogenesis control.

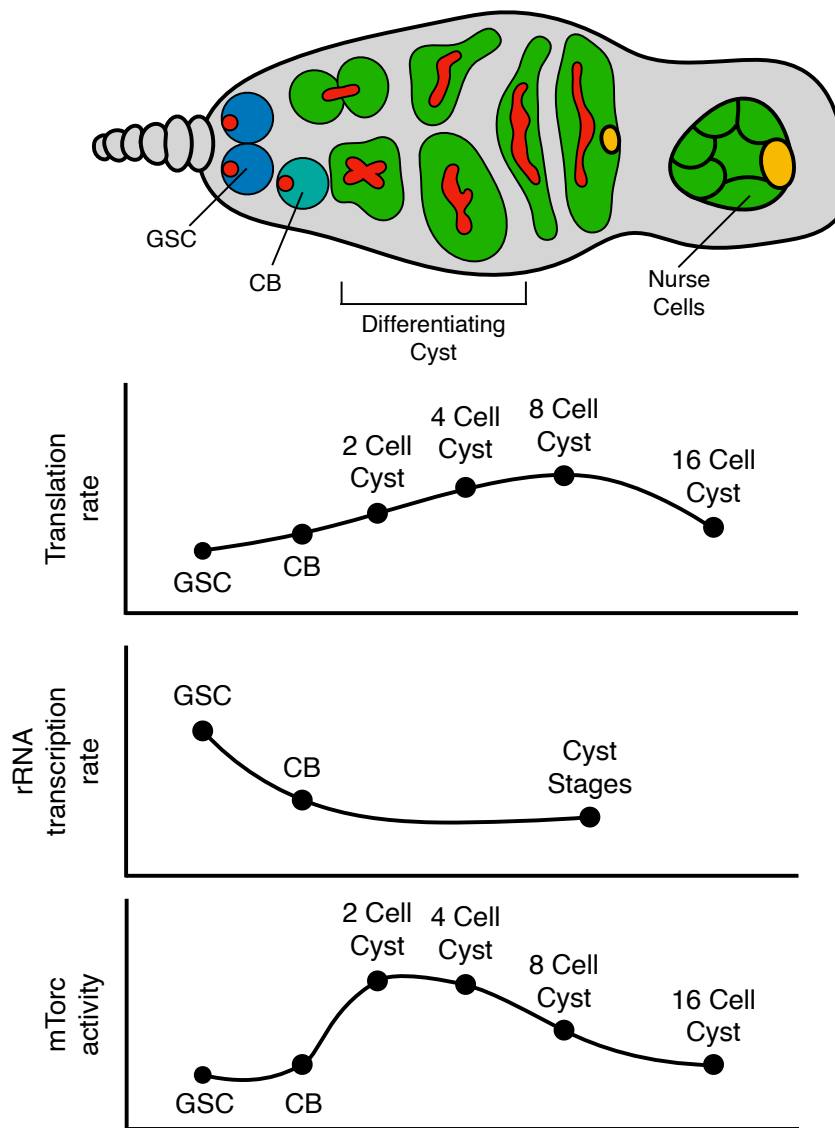


Figure 1.3: Global translation rate, rRNA transcription rate, and mTorc1 activity during development. Schematic representing the germarium and plots representing relative changes in global translation rate, rRNA transcription rate, and mTorc1 activity during development at the developmental stages indicated. As germline stem cell differentiation occurs rRNA production decreases, while global translation initially increases as differentiation occurs then falls off post differentiation. A global regulator of both translation and rRNA production, mTorc1 activity decreases during differentiation and increases post differentiation.

1.6 Hand off mechanisms facilitated by combinatorial RNA binding proteins dynamically shape the translational landscape during oogenesis

While some mRNAs are translated post-transcriptionally, other critical mRNAs are translationally regulated. For efficient translation of mRNAs, it is thought that the mRNAs must be circularized - bringing their 5' cap and 3' poly A tail in close proximity to each other (Fukao et al., 2009; Martineau et al., 2008; Preiss & Hentze, 1998). This interaction is mediated by cap binding proteins such as eukaryotic initiation factor 4E (eIF4E) and the poly-A binding protein (PABP)(Eichhorn et al., 2016; Kronja et al., 2014; Subtelny, Eichhorn, Chen, Sive, & Bartel, 2014; Tarun Jr, Wells, Deardorff, & Sachs, 1997). A longer poly-A tail and uninhibited access to the 5' cap for eIF4E is believed to promote efficient translation (Jalkanen, Coleman, & Wilusz, 2014). A major mode of translational regulation is that RNA binding proteins (RBPs) recognize cognate sequences in the 3' UTRs of their target mRNAs (Harvey et al., 2018). The binding of the RBP prevents circularization of the mRNA and inhibits efficient translation initiation, leading to reduced translation (Mazumder, Seshadri, Imataka, Sonenberg, & Fox, 2001). RBP binding to the 3' UTR can mediate translation inhibition by recruiting cofactors to inhibit circularization (Szostak & Gebauer, 2013). This inhibition of circularization can be achieved by RBP binding to the cap and competing with eIF4E, removal of the cap by the decapping machinery, or recruitment of factors such as the CCR4-Not complex to shorten poly-A tail length (Rissland, 2017). In some cases, RBPs can both block initiation as well as mediate shortening of the poly-A tail (Neve, Patel, Wang, Louey,

& Furger, 2017).

As mentioned in the germline several developmental processes such as stem cell maintenance, differentiation, mitosis and meiosis are coordinated and successful transition through these diverse programs relies on precise translational control (Figure 4) (Joshi, Riddle, Djabrayan, & Rothman, 2010; Slaidina & Lehmann, 2014). As factors that interfere with translation such as the decapping machinery and the poly-A tail shortening CCR4-Not complex are expressed continuously during oogenesis, and cannot support dynamic translational control on their own, a dynamic and diverse landscape of translational regulators has evolved to allow for fine-scale temporal control of mRNA translation (Eichhorn et al., 2016; Flora, Wong-Deyrup, et al., 2018b). To add an additional layer of complexity, the expression or abundance of several RBPs that regulate translational control oscillate as oogenesis progresses (Figure 4) (Flora, Wong-Deyrup, et al., 2018b; Prashanth Rangan et al., 2009; Richter & Lasko, 2011). As the levels of RBPs decrease, their bound mRNA targets are licensed for translation (Flora, Wong-Deyrup, et al., 2018b; Lasko, 2000; Linder & Lasko, 2006). There are three major themes that work to control mRNA translation: 1. RBPs collaborate in a combinatorial manner to regulate mRNAs, 2. Target mRNAs are handed off from one RBP complex to another as levels oscillate during oogenesis to consistently repress or promote target mRNA translation, and 3. Multiple feedback mechanisms operate to mediate each transition (Figure 4) (Flora, Wong-Deyrup, et al., 2018b). The feedback mechanism has been extensively reviewed elsewhere and is not the focus of this chapter (Flora, Wong-Deyrup, et al., 2018b; Slaidina & Lehmann, 2014). Here, we outline how RBPs both collaborate as well hand off mRNAs during the transition from GSC to mature oocyte.

GSCs rely on several factors to maintain self-renewal, two of the main factors are Pumilio

(Pum) and Nanos (Nos), which work in a combinatorial fashion to repress the translation of differentiation-promoting mRNAs (Figure 4) (A. Forbes & Lehmann, 1998; Gilboa & Lehmann, 2004; Joly, Chartier, Rojas-Rios, Busseau, & Simonelig, 2013; H. Lin & Spradling, 1997). Pum, a member of the conserved Pum- and Fem-3-binding factor (PUF) family of proteins, is present at high levels in the undifferentiated germline cells of the ovary, including GSCs, CBs, and early-differentiating cysts (A. Forbes & Lehmann, 1998; Kai, Williams, & Spradling, 2005). Independent of other factors, Pum can directly bind mRNA, but it requires the catalytic activity of other proteins to regulate translation of its targets in the *Drosophila* germline (Sonoda & Wharton, 1999; Tadauchi, Matsumoto, Herskowitz, & Irie, 2001). Pum is known to have dynamic interactions with two critical regulators, Nos in GSCs, and Brain tumor (Brat) in CBs (Figure 4) (Arvola, Weidmann, Tanaka Hall, & Goldstrohm, 2017; Goldstrohm, Hall, & McKenney, 2018; Harris, Pargett, Sutcliffe, Umulis, & Ashe, 2011; Reichardt et al., 2018; Sonoda & Wharton, 1999, 2001). Nos, a well conserved RNA binding protein, has the ability to bind mRNA, albeit at low affinity and requires the presence of Pum to recognize its targets (Arvola, Weidmann, Tanaka Hall, & Goldstrohm, 2017). Nanos directly interacts with Not1, a member of the CCR4-Not complex, recruiting it to target mRNAs, such as *meiotic P26* (*mei-p26*) and *brat*, to regulate their translation (Bhandari, Raisch, Weichenrieder, Jonas, & Izaurralde, 2014; Raisch et al., 2016; Temme, Simonelig, & Wahle, 2014). While in some systems Pum can directly recruit the CCR4-Not complex, activity of *nos* is required for this interaction in the *Drosophila* germline (Joly, Chartier, Rojas-Rios, Busseau, & Simonelig, 2013; Temme, Simonelig, & Wahle, 2014). Upon loss of Pum, Nanos or Twin, GSCs fail to maintain stem cell fate and differentiate into stem cell daughters, resulting in the inability to sustain oogenesis as outlined below.

An example of distinct, stage-specific translational control by Pum/Nos/CCR4-Not complex in the germline is the mechanism by which *polar granule component* (*pgc*), a germline-specific transcriptional repressor, is controlled (Figure 4) (Flora, Wong-Deyrup, et al., 2018b). *Pgc* interacts with the Positive Transcription Elongation Factor (P-TEFb) complex and inhibits the phosphorylation of the Serine-2 residue that is critical for transcriptional elongation, resulting in global transcriptional silencing (Hanyu-Nakamura, Sonobe-Nojima, Tanigawa, Lasko, & Nakamura, 2008). A single pulse of expression of *Pgc* protein in the CB allows for epigenetic and transcriptomic reprogramming during differentiation (Flora, Schowalter, et al., 2018). While *pgc* mRNA is expressed highly and ubiquitously throughout oogenesis, translation of *pgc* mRNA is tightly regulated to mitigate the effects of its potent transcriptional silencing activity. The *pgc* 3' UTR contains a conserved consensus sequence that is transiently and sequentially bound by multiple distinct, developmentally regulated RBPs (Flora, Wong-Deyrup, et al., 2018b). This 3' UTR sequence is required for post-transcriptional control of *pgc* as *Pgc* protein expression is restricted to the CB. In the GSCs, Pum and Nos bind the *pgc* 3' UTR and recruit Twin a component of the CCR4-Not complex to deadenylate *pgc* mRNA and inhibit its translation (Figure 4) (Flora, Wong-Deyrup, et al., 2018b). In addition to *pgc*, Pum/Nos and Twin also regulate Brain tumor (Brat) (Joly, Chartier, Rojas-Rios, Busseau, & Simonelig, 2013). Brat is a TRIM-NHL domain protein expressed in the germline that represses translation by engaging with d4EHP and competing with the cap-binding protein eIF4E to prevent translation initiation (Figure 4) (Arvola, Weidmann, Tanaka Hall, & Goldstrohm, 2017; Harris, Pargett, Sutcliffe, Umulis, & Ashe, 2011; Sonoda & Wharton, 2001). While *brat* mRNA is expressed in the GSC, it is specifically repressed by Nos and Pum . In addition to

these targets, several differentiation promoting mRNAs such as *meiP26* are also repressed (Joly, Chartier, Rojas-Rios, Busseau, & Simonelig, 2013). Thus, in the GSCs, a combination of Pum, Nos and CCR4-Not complex are required for repressing translation of several critical differentiation promoting mRNAs (Flora, Wong-Deyrup, et al., 2018b; Lasko, 2000, 2012; Slaidina & Lehmann, 2014).

Subsequent differentiation of the GSC daughters relies on several factors to repress expression of *nos* mRNA (Lasko, 2000, 2012). Differentiation is initiated upon Bam expression in the CB, where Bam and its binding partner benign gonial cell neoplasm (Bgcn) act through a sequence in the *nos* 3' UTR to inhibit translation (Figure 4) (Y. Li, Minor, Park, McKearin, & Maines, 2009; McCarthy, Deiulio, Martin, Upadhyay, & Rangan, 2018). This repression mechanism includes deadenylation activity by Twin, which works in conjunction with Bam and Bgcn (Fu et al., 2015). As Nos protein levels decrease in the CB, *pgc* and *brat* mRNAs are translated (Flora, Wong-Deyrup, et al., 2018b). The expressed Brat protein now partners with Pum to repress translation of GSC self-renewal genes (Figure 4) (Harris, Pargett, Sutcliffe, Umulis, & Ashe, 2011). In addition, expression of Mei-P26 increases initiating interactions with Bam, Bgcn and Sxl. Mei-P26 then promotes translational repression of GSC fate promoting genes such as *nos*, allowing for further differentiation by cooperating with Bam and Bgcn (Y. Li et al., 2013; Reichardt et al., 2018). As the CB differentiates into 2-, 4-, 8- and 16-cell cysts, levels of Nanos protein rebound. However, in spite of the presence of Nos, Pum partners with Brat to suppress *pgc* translation in the 4- to 16-cell cyst stages (Figure 4) (Flora, Wong-Deyrup, et al., 2018b). Thus, in CBs, absence of Nos allows for Pum to complex with a different subset of proteins as well as license expression of new translational regulators to promote differentiation.

After cyst differentiation, Pum protein levels decrease and expression of another translational repressor, Bruno (Bru), increases (Kim-Ha, Kerr, & Macdonald, 1995; Schupbach & Wieschaus, 1989, 1991; Webster, Liang, Berg, Lasko, & Macdonald, 1997). Downregulation of Pum expression is critical for the transition from GSC to an oocyte (Carreira-Rosario et al., 2016; A. Forbes & Lehmann, 1998). Rbfox1, an RBP whose cytoplasmic isoform regulates the translation of specific mRNAs in the germline is responsible for repressing Pum translation through binding of a consensus sequence in the *pum* 3' UTR (Figure 4) (Carreira-Rosario et al., 2016). Loss of Rbfox1 leads to an expansion of Pum protein expression and a disruption of differentiation (Carreira-Rosario et al., 2016). Repression of Pum levels by Rbfox1 allows for Bru expression (Carreira-Rosario et al., 2016). Surprisingly, Bru can bind to a sequence in the 3' UTR that is very similar to Pum binding sequence (Figure 4)(Reveal, Garcia, Ellington, & Macdonald, 2011). Bruno blocks translation initiation by interacting with Cup, a conserved eIF4E binding protein (G. Kim et al., 2015; Nakamura, Sato, & Hanyu-Nakamura, 2004). In fact, Bru binds the same sequence in the *pgc* 3' UTR as Nos/Pum to prevent *pgc* translation (Flora, Wong-Deyrup, et al., 2018b). This mode of translation repression is not restricted to *pgc*, rather a cohort of maternal mRNAs are co-regulated by Pum and Bru representing a hand-off mechanism for repression of maternal mRNAs (Flora, Wong-Deyrup, et al., 2018b).

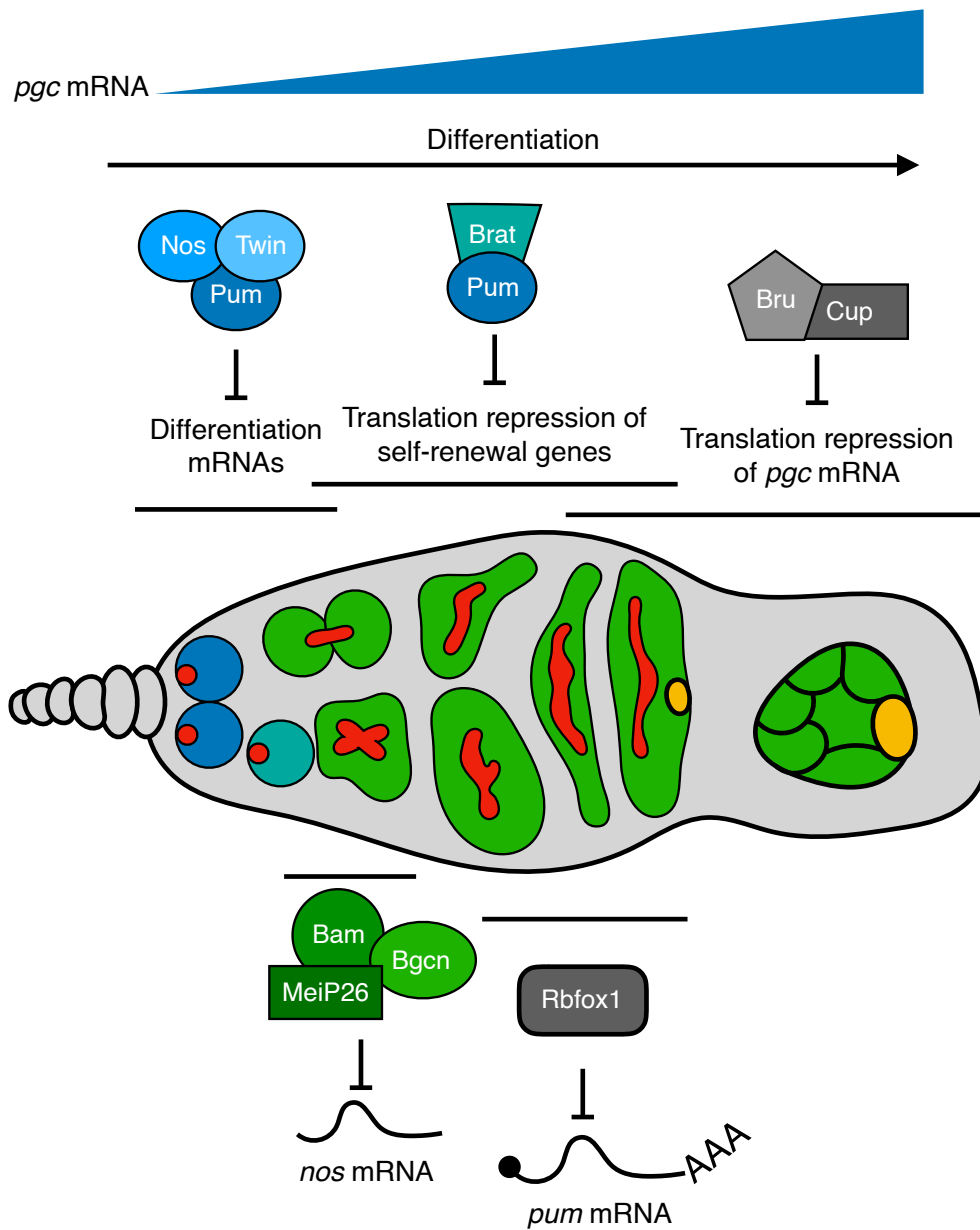


Figure 1.4: Schematic of combinatorial and dynamic translation regulation in the *Drosophila* germarium. In the GSCs Nos, Pum and Twin form a complex to inhibit the translation of differentiation mRNAs such as *pgc*, which increases throughout oogenesis. Expression of Bam in the CB initiates differentiation by interacting with its partner Bgcn and Mei-P26 to repress the translation of GSC-expressed mRNAs, specifically *nos*. As Nos protein levels decrease in the CB, Pum is available to partner with Brat to repress the translation of self-renewal genes and *pgc*. In cyst stages, Rbfox1 binds the *pum* 3' UTR to inhibit its translation. Throughout oogenesis Bru and Cup continuously block translation of *pgc*.

1.7 Summary

Decades of work using elegant genetics has revealed several paradigms in which splicing machinery, RNA modifying enzymes, ribosome levels, and translational regulation mediates the transition from GSC to oocyte fate. However, several critical details such as the direct targets and mechanisms still need to be deciphered. Together the advent of cost-effective sequencing technologies combined with the increasing ability to easily create mutants in previously uncharacterized genes will allow us to further elucidate the regulatory logic (underlying or of) this critical transition.

Chapter 2

A translation control module coordinates germline stem cell differentiation with ribosome biogenesis during *Drosophila* oogenesis

Elliot T. Martin^{1*}, Patrick Blatt^{1*}, Elaine Nguyen², Roni Lahr², Sangeetha Selvam¹, Hyun Ah M. Yoon^{1,3}, Tyler Pocchiari^{1,4}, Shamsi Emtenani⁵, Daria E. Siekhaus⁵, Andrea Berman², Gabriele Fuchs^{1†} and Prashanth Rangan^{1†}

¹Department of Biological Sciences/RNA Institute, University at Albany SUNY, Albany, NY 12202

²Department of Biological Sciences, University of Pittsburgh, Pittsburgh, PA 15260

³Albany Medical College, Albany, NY 12208

⁴SUNY Upstate Medical University, Syracuse, NY 13210-2375

⁵Institute of Science and Technology Austria, Klosterneuburg, Austria

*These authors contributed equally to this work

†Co-corresponding authors

Email: gfuchs@albany.edu, prangan@albany.edu

2.1 Summary:

Ribosomal defects perturb stem cell differentiation, causing ribosomopathies. How ribosome levels control stem cell differentiation is not fully known. Here we discovered that three RNA helicases govern ribosome biogenesis and *Drosophila* oogenesis. Loss of these helicases, which

we named Aramis, Athos and Porthos, aberrantly stabilized p53, arrested the cell cycle and stalled GSC differentiation. Aramis controls cell cycle progression by regulating translation of mRNAs containing a Terminal Oligo Pyrimidine (TOP) motif in their 5'-UTRs; we find TOP motifs confer sensitivity to ribosome levels mediated by La-related protein (Larp). One such TOP-containing mRNA codes for Novel Nucleolar protein 1 (Non1), a conserved p53 destabilizing protein. Upon a sufficient ribosome concentration, Non1 is expressed and promotes GSC cell cycle progression via p53 degradation. Thus, a previously unappreciated TOP-motif in *Drosophila* responds to reduced ribosome biogenesis to co-regulate the translation of ribosomal proteins and a p53 repressor, coupling ribosome biogenesis to GSC differentiation.

2.2 Introduction

All life depends on the ability of ribosomes to translate mRNAs into proteins. Despite this universal requirement, perturbations in ribosome biogenesis affects some cell types more than others. Stem cells, the unique cell type that underlies the generation and expansion of tissues, in particular have an increased ribosomal requirement (Gabut, Bourdelais, & Durand, 2020; Sanchez et al., 2016; Woolnough, Atwood, Liu, Zhao, & Giles, 2016; Zahradkal, Larson, & Sells, 1991; Q. Zhang, Shalaby, & Buszczak, 2014). Ribosome production and levels are dynamically regulated to maintain higher amounts in stem cells (Fichelson et al., 2009; Gabut, Bourdelais, & Durand, 2020; Sanchez et al., 2016; Woolnough, Atwood, Liu, Zhao, & Giles, 2016; Zahradkal, Larson, & Sells, 1991; Q. Zhang, Shalaby, & Buszczak, 2014). For example, ribosome biogenesis components are often differentially expressed, as observed

during the differentiation of embryonic stem cells, osteoblasts, and myotubes (Gabut, Bourdelais, & Durand, 2020; Watanabe-Susaki et al., 2014; Zahradkal, Larson, & Sells, 1991). In some cases, such as during *Drosophila* germline stem cell (GSC) division, ribosome biogenesis factors asymmetrically segregate during asymmetric cell division, such that a higher pool of ribosome biogenesis factors is maintained in the stem cell compared to the daughter cell (Blatt, Martin, Breznak, & Rangan, 2020; Fichelson et al., 2009; Q. Zhang, Shalaby, & Buszczak, 2014). Reduction of ribosome levels in several stem cell systems can cause differentiation defects (Corsini et al., 2018; Fortier, MacRae, Bilodeau, Sargeant, & Sauvageau, 2015; Khajuria et al., 2018; Q. Zhang, Shalaby, & Buszczak, 2014). In *Drosophila*, perturbations that reduce ribosome levels in the GSCs result in differentiation defects causing infertility (Sanchez et al., 2016). Similarly, humans with reduced ribosome levels are afflicted with clinically distinct diseases known as ribosomopathies, such as Diamond-Blackfan anemia, that often result from loss of proper differentiation of tissue-specific progenitor cells (Armistead & Triggs-Raine, 2014; Barlow et al., 2010; Brooks et al., 2014; Higa-Nakamine et al., 2012; Lipton, Kudisch, Gross, & Nathan, 1986; Mills & Green, 2017). However, the mechanisms by which ribosome biogenesis is coupled to proper stem cell differentiation remain incompletely understood.

Ribosome production requires the transcription of ribosomal RNAs (rRNAs) and of mRNAs encoding ribosomal proteins (Bousquet-Antonelli, Vanrobays, Gélugne, Caizeragues-Ferrer, & Henry, 2000; de la Cruz, Karbstein, & Woolford, 2015; Granneman, Bernstein, Bleichert, & Baserga, 2006; Granneman, Petfalski, Tollervey, & Hurt, 2011; Tafforeau et al., 2013; Venema, Cile Bousquet-Antonelli, Gelugne, Le Caizeragues-Ferrer, & Tollervey, 1997). Hundreds of factors including helicases and endonucleases, transiently associate with matur-

ing rRNAs to facilitate rRNA processing, modification, and folding (Granneman, Petfalski, Tollervey, & Hurt, 2011; Sloan et al., 2017; Tafforeau et al., 2013; Watkins & Bohnsack, 2012). Ribosomal proteins are imported into the nucleus, where they assemble with rRNAs to form precursors to the 40S and 60S ribosomal subunits, which are then exported to the cytoplasm (Baxter-Roshek, Petrov, & Dinman, 2007; Decatur & Fournier, 2002; Granneman, Bernstein, Bleichert, & Baserga, 2006; Granneman, Petfalski, Tollervey, & Hurt, 2011; Koš & Tollervey, 2010; Nerurkar et al., 2015; Tafforeau et al., 2013; Zemp & Kutay, 2007). Loss of RNA Polymerase I transcription factors, helicases, exonucleases, large or small subunit ribosomal proteins, or other processing factors all compromise ribosome biogenesis and trigger diverse stem cell-related phenotypes (Brooks et al., 2014; Calo et al., 2018; Sanchez et al., 2016; Yelick & Trainor, 2015; Q. Zhang, Shalaby, & Buszczak, 2014).

Nutrient availability influences the demand for *de novo* protein synthesis and thus ribosome biogenesis (Anthony, Anthony, Kimball, Vary, & Jefferson, 2000; Hong, Mannan, & Inoki, 2012; Mayer & Grummt, 2006; Shu, Swanda, & Qian, 2020). In mammals, mRNAs that encode the ribosomal proteins contain a Terminal Oligo Pyrimidine (TOP) motif within their 5' untranslated region (UTR), which regulates their translation in response to nutrient levels (Bruno D. Fonseca et al., 2015; Hong et al., 2017; Roni M. Lahr et al., 2017; Tcherkezian et al., 2014). Under growth-limiting conditions, La related protein 1 (Larp1) binds to the TOP sequences and to mRNA caps to inhibit translation of ribosomal proteins (Bruno D. Fonseca et al., 2015; J.-J. Jia et al., 2021; Roni M. Lahr et al., 2017; Philippe, Vasseur, Debart, & Thoreen, 2018). When growth conditions are suitable, Larp1 is phosphorylated by the nutrient/redox/energy sensor mammalian Target of rapamycin (mTOR) complex 1 (mTORC1), and does not efficiently bind the TOP sequence, thus allowing for

translation of ribosomal proteins (Bruno D. Fonseca et al., 2015; Bruno D. Fonseca et al., 2018; Hong et al., 2017; J.-J. Jia et al., 2021). In some instances, Larp1 binding can also stabilize TOP-containing mRNAs (Aoki et al., 2013; Berman et al., 2020; Gentilella et al., 2017; Ogami, Oishi, Nogimori, Sakamoto, & Hoshino, 2020), linking mRNA translation with mRNA stability to promote ribosome biogenesis (Aoki et al., 2013; Berman et al., 2020; Bruno D. Fonseca et al., 2015; Bruno D. Fonseca et al., 2018; Hong et al., 2017; Roni M. Lahr et al., 2017; Ogami, Oishi, Nogimori, Sakamoto, & Hoshino, 2020; Philippe, Vasseur, Debart, & Thoreen, 2018). Cellular nutrient levels are known to affect stem cell differentiation and oogenesis in *Drosophila* (Hsu, LaFever, & Drummond-Barbosa, 2008), however whether TOP motifs exist in *Drosophila* to coordinate ribosome protein synthesis is unclear. The *Drosophila* ortholog of Larp1, La related protein (Larp) is required for proper cytokinesis and meiosis in *Drosophila* testis as well as for female fertility, but its targets remain undetermined (Blagden et al., 2009; Ichihara, Shimizu, Taguchi, Yamaguchi, & Inoue, 2007).

Germline depletion of ribosome biogenesis factors manifests as a stereotypical GSC differentiation defect during *Drosophila* oogenesis (Sanchez et al., 2016). Female *Drosophila* maintain 2-3 GSCs in the germarium (**Figure 1A**) (Kai, Williams, & Spradling, 2005; Twombly et al., 1996; Xie & Li, 2007; Xie & Spradling, 1998, 2000). Asymmetric cell division of GSCs produces a self-renewing daughter GSC and a differentiating daughter, called the cystoblast (CB) (**Figure 1A**) (D. Chen & McKearin, 2003b; D. McKearin & Ohlstein, 1995). This asymmetric division is unusual: following mitosis, the abscission of the GSC and CB is not completed until the following G2 phase (**Figure 1A'**) (De Cuevas & Spradling, 1998; Hsu, LaFever, & Drummond-Barbosa, 2008). The GSC is marked by a round structure called the spectrosome, which elongates and eventually bridges the GSC

and CB, similar to the fusomes that connect differentiated cysts (**Figure 1A-A'**). During abscission the extended spectrosome structure is severed and a round spectrosome is established in the GSC and the CB (**Figure 1A'**) (De Cuevas & Spradling, 1998; Hsu, LaFever, & Drummond-Barbosa, 2008). Ribosome biogenesis defects result in failed GSC-CB abscission, causing cells to accumulate as interconnected cysts called “stem-cysts” that are marked by a fusome-like structure (**Figure 1A'**) (Mathieu et al., 2013; Sanchez et al., 2016). In contrast with differentiated cysts (D. M. McKearin & Spradling, 1990; D. McKearin & Ohlstein, 1995; Ohlstein & McKearin, 1997), these stem-cysts do not express the differentiation factor Bag of Marbles (Bam), do not differentiate, and typically die, resulting in sterility (**Figure 1A'**) (Sanchez et al., 2016). How proper ribosome biogenesis promotes GSC abscission and differentiation is not known.

By characterizing three RNA helicases and showing that they promote ribosome biogenesis, we identified a translational control module, which coordinates ribosome levels with GSC differentiation. When ribosome biogenesis is optimal, ribosomal proteins and a p53 repressor are both efficiently translated allowing for proper GSC cell cycle progression and its differentiation. However, when ribosome biogenesis is perturbed, we observe diminished translation of both ribosomal proteins and the p53 repressor. As a consequence, p53 is stabilized, cell cycle progression is blocked and GSC differentiation is stalled. Thus, our work reveals an elegant tuning mechanism that links ribosome biogenesis with a cell cycle progression checkpoint and thus stem cell differentiation. Given that ribosome biogenesis defects in humans result in ribosomopathies, which often result from stem cell differentiation defects, our data lay the foundation for understanding the etiology of developmental defects that arise due to ribosomopathies.

2.3 Results

2.3.1 Three conserved RNA helicases are required in the germline for GSC differentiation

We performed a screen to identify RNA helicases that are required for female fertility in *Drosophila*, and identified three predicted RNA helicases with previously uncharacterized functions, *CG5589*, *CG4901*, and *CG9253* (**Figure 2.1B-C**) (**Supplemental Table 2.1**) (Blatt et al., 2020). We named these candidate genes *aramis*, *athos*, and *porthos*, respectively, after Alexandre Dumas' three musketeers who fought in service of their queen. We evaluated the efficiency of RNAi in ovaries using qPCR and found that *aramis*, *athos*, and *porthos* was significantly downregulated (**Figure 2.2A**). We additionally drove RNAi of *aramis* and *athos* in the germline of flies expressing GFP::3XFLAG tagged versions of each gene respectively and performed immunostaining and found that the expression of Aramis and Athos was reduced specifically in the germline in contrast to the soma (**Figure 2.2B-E**). To further investigate how these helicases promote fertility, we depleted *aramis*, *athos*, and *porthos* in the germline using the germline-driver *nanos-GAL4* (*nosGAL4*) in combination with RNAi lines. We detected the germline and spectrosomes/fusomes in ovaries by immunostaining for Vasa and 1B1, respectively. In contrast to controls, *aramis*, *athos*, and *porthos* germline RNAi flies lacked spectrosome-containing cells, and instead displayed cells with fusome-like structures proximal to the self-renewal niche (**Figure 2.1D-H; Figure 2.2E-E''**). The cells in this cyst-like structure contained ring canals, a marker of cytoplasmic bridges, suggesting that they are indeed interconnected (**Figure 2.2F-F''**) (Q. Zhang, Shalaby, & Buszczak,

2014). In addition to forming cysts in an aberrant location, the *aramis*, *athos*, and *porthos* germline RNAi ovaries failed to form egg chambers (**Figure 2.2G-G'''**).

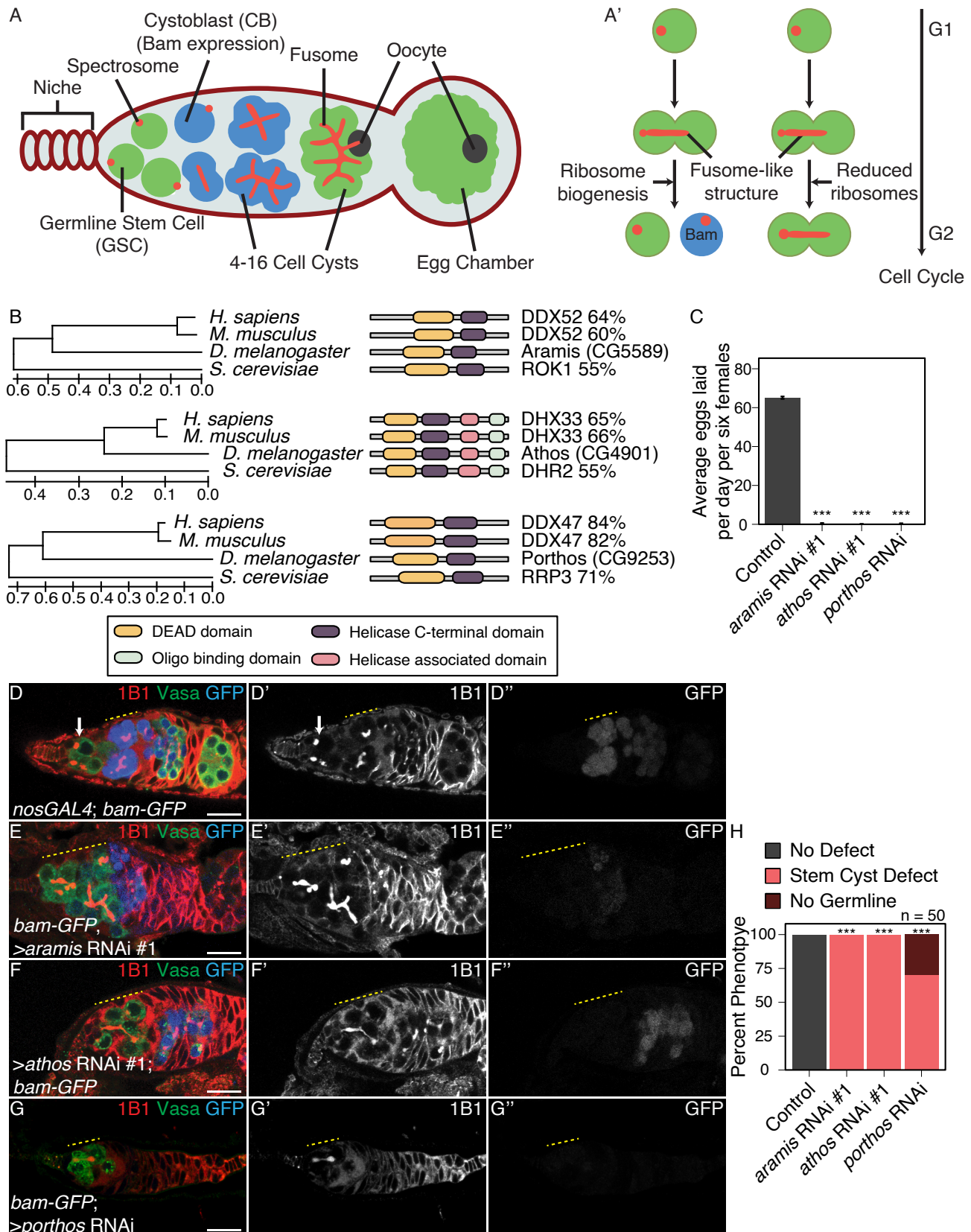


Figure 2.1: RNA helicases Aramis, Athos and Porthos are required for GSC differentiation.

(A) Schematic of *Drosophila* germarium. Germline stem cells are attached to the somatic niche (dark red). The stem cells divide and give rise to a stem cell and a cystoblast (CB) that expresses the differentiation factor Bag-of-marbles (Bam). GSCs and CBs are marked by spectrosomes. The CB undergoes four incomplete mitotic divisions giving rise to a 16-cell cyst (blue). Cysts are marked by branched spectrome structures known as fusomes (red). One cell of the 16-cell cyst is specified as the oocyte. The 16-cell cyst is encapsulated by the surrounding somatic cells giving rise to an egg chamber. **(A')** Ribosome biogenesis promotes GSC cytokinesis and differentiation. Disruption of ribosome biogenesis results in undifferentiated stem cyst accumulation. **(B)** Conservation of *aramis*, *athos*, and *porthos* between *H. sapiens*, *D. melanogaster*, and *S. cerevisiae* (left), trees are drawn to scale, with branch lengths measured in the number of substitutions per site. Representation of conserved protein domains for three RNA helicases in *Drosophila* compared to *H. sapiens* and *S. cerevisiae* orthologs (right). Percentage values represent similarity to *Drosophila* orthologs. **(C)** Egg laying assay after germline RNAi knockdown of *aramis*, *athos* or *porthos* indicating a loss of fertility compared to *nosGAL4*, driver control (n=3 trials). *** = p < 0.001, Tukey's post-hoc test after one-way ANOVA, p < 0.001. Error bars represent standard error (SE). **(D-G")** Confocal micrographs of ovaries from control, *UAS-Dcr2*; *nosGAL4*; *bam-GFP* (**D-D''**) and germline RNAi depletion targeting (**E-E''**) *aramis*, (**F-F''**) *athos* or (**G-G''**) *porthos* stained for 1B1 (red, left grayscale), Vasa (green), and Bam-GFP (blue, right grayscale). Depletion of these genes (**E-G''**) results in a characteristic phenotype in which early germ cells are connected marked by a 1B1 positive, fusome-like structure highlighted by a yellow dotted line in contrast to the single cells present in (**D-D''**) controls (white arrow) or differentiating cysts (yellow dashed line). Bam expression, if present, is followed by loss of the germline. **(H)** Phenotype quantification of ovaries depleted of *aramis*, *athos* or *porthos* compared to control ovaries (n=50 ovarioles, df=2, *** = p < 0.001, Fisher's exact tests with Holm-Bonferroni correction). Scale bars are 15 micron.

Aberrant cyst formation proximal to the niche could reflect stem cysts with GSCs that divide to give rise to CBs but fail to undergo cytokinesis or differentiated cysts that initiate differentiation but cannot progress further to form egg chambers. To discern between these possibilities, first we examined the expression of a marker of GSCs, phosphorylated Mothers against decapentaplegic (pMad). We observed pMad expression in the cells closest to the niche, but not elsewhere in the germline cysts of *aramis*, *athos*, and *porthos* germline RNAi flies (**Figure 2.2H-H'**) (Kai & Spradling, 2003). Additionally, none of the cells connected

to the GSCs in *aramis*, *athos*, and *porthos* germline RNAi flies expressed the differentiation reporter *bamGFP* (**Figure 2.1D-G”**) (D. McKearin & Ohlstein, 1995). Thus, loss of *aramis*, *athos*, or *porthos* in the germline results in the formation of stem cysts, however with variable severity. This variability could be due to a differential requirement for these genes or different RNAi efficiencies. Overall, we infer that Aramis, Athos, and Porthos are required for proper GSC cytokinesis to produce a stem cell and differentiating daughter.

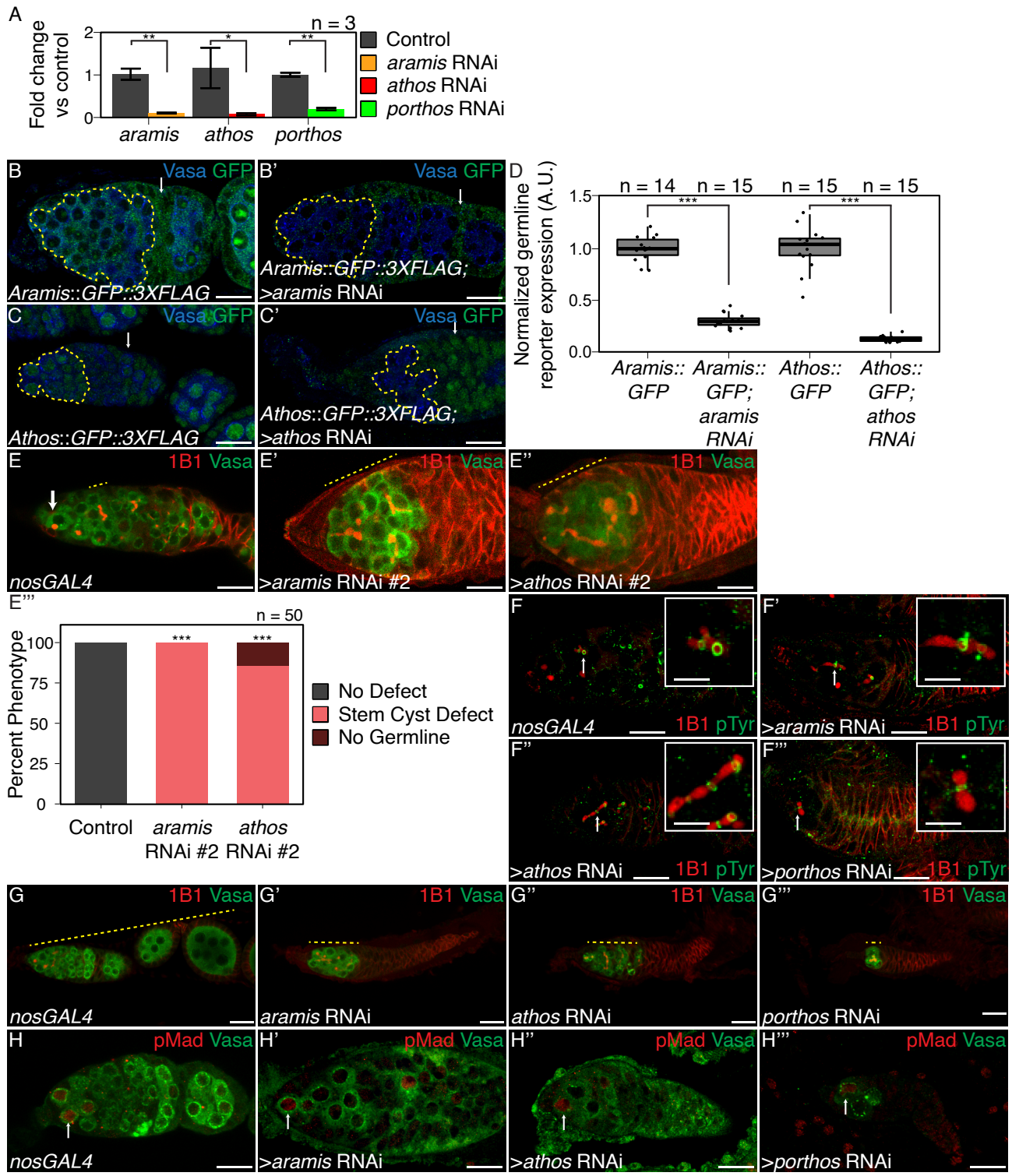


Figure 2.2: Aramis, Athos, and Porthos are required for proper cytokinesis and differentiation, related to Figure 2.1.

(A) qPCR targeting *aramis*, *athos*, *porthos* relative to α -*tub84B* to measure knockdown efficiency of *aramis*, *athos*, and *porthos* RNAi in the germline (n=3, Welch's t-test with Holm-Bonferroni correction, * = $p<0.05$, **= $p<0.01$). **(B-B')** Confocal images of **(B)** Aramis::GFP::3XFLAG and **(B')** Aramis::GFP::3XFLAG in conjunction with *aramis* germline knockdown stained for Vasa (blue), and GFP (green). **(C-C')** Confocal images of **(C)** Athos::GFP::3XFLAG and **(C')** Athos::GFP::3XFLAG in conjunction with *athos* germline knockdown stained for Vasa (blue), and GFP (green), early germline is outlined in yellow, representative somatic cell indicated by arrow. **(D)** Quantification of germline expression of GFP normalized to somatic GFP expression in Aramis::GFP::3XFLAG ovaries compared to Aramis::GFP::3XFLAG in conjunction with *aramis* germline knockdown and Athos::GFP::3XFLAG ovaries compared to Athos::GFP::3XFLAG in conjunction with *athos* germline knockdown showing that *aramis* RNAi and *athos* RNAi efficiently knockdown their targets in the germline. (n=14-15, Welch's t-test with Holm-Bonferroni correction, ***= $p<0.001$) **(E-E'')** Confocal images of **(E)** *nosGAL4*, driver control and germline RNAi knockdown using additional RNAi lines for **(E')** *aramis* and **(E'')** *athos* stained for 1B1 (red) and Vasa (green). **(E'')** Quantification of percentage of germaria with no defect (black), stem-cysts (salmon), or germline loss (dark red) in ovaries depleted of *athos*, *aramis*, or *porthos* compared to control ovaries recapitulates the phenotypes with independent RNAi lines (n=50, df=2, *** = $p<0.001$, Fisher's exact test with Holm-Bonferroni correction). **(F-F'')** Confocal images of germaria stained for 1B1 (red) and Phospho-tyrosine (green). Ring canals, marked by Phospho-tyrosine, connect differentiating cysts in **(F)** control *nosGAL4* ovaries and in between the interconnected cells of ovaries depleted of **(F')** *aramis*, **(F'')** *athos*, or **(F'')** *porthos* with 1B1 positive structures going through the ring canals. **(G-G'')** Confocal images of ovarioles stained for 1B1 (red) and Vasa (green). Control, *nosGAL* ovaries have egg chambers while ovaries depleted of **(G')** *aramis*, **(G'')** *athos*, or **(G'')** *porthos* lack egg chambers. **(H-H'')** Confocal images of germaria stained for pMad (red, grayscale) and Vasa (green). In **(H)** control ovaries nuclear pMad staining occurs in cells proximal to the niche marking GSCs. Nuclear pMad staining in ovaries depleted of **(H')** *aramis*, **(H'')** *athos*, and **(H'')** *porthos* demonstrates that the observed cysts are not composed of GSCs. Scale bar for main images is 15 micron, scale bar for insets is 3.75 micron.

2.3.2 Athos, Aramis, and Porthos are required for ribosome biogenesis

We found that Aramis, Athos, and Porthos are conserved from yeast to humans (**Figure 2.1B**). The closest orthologs of Aramis, Athos, and Porthos are Rok1, Dhr2, and Rrp3 in yeast and DExD-Box Helicase 52 (DDX52), DEAH-Box Helicase 33 (DHX33), and DEAD-Box Helicase 47 (DDX47) in humans, respectively (Hu et al., 2011). Both the yeast and human orthologs have been implicated in rRNA biogenesis (Bohnsack, Kos, & Tollervey, 2008; Khoshnevis et al., 2016; R. Martin et al., 2014; O 'day, Chavanikamannil, & Abelson, 1996; Sekiguchi, Hayano, Yanagida, Takahashi, & Nishimoto, 2006; Tafforeau et al., 2013; Venema, Cile Bousquet-Antonelli, Gelugne, Le Caizergues-Ferrer, & Tollervey, 1997; Venema & Tollervey, 1995; Vincent, Charette, & Baserga, 2017; Yandong Zhang, Forys, Miceli, Gwinn, & Weber, 2011). In addition, the GSC-cytokinesis defect that we observed in *aramis*, *athos*, and *porthos* RNAi flies is a hallmark of reduced ribosome biogenesis in the germline (Sanchez et al., 2016). Based on these observations, we hypothesized that Aramis, Athos, and Porthos could enhance ribosome biogenesis to promote proper GSC differentiation.

Many factors involved in rRNA biogenesis localize to the nucleolus and interact with rRNA (Arabi et al., 2005; Grandori et al., 2005; Henras et al., 2008; Karpen, Schaefer, & Laird, 1988). To detect the subcellular localization of Aramis and Athos, we used available lines that express Aramis::GFP::FLAG or Athos::GFP::FLAG fusion proteins under endogenous control. For Porthos, we expressed a Porthos::FLAG::HA fusion under the control of UAS t promoter in the germline using a previously described approach (DeLuca & Spradling, 2018). We found that in the germline, Aramis, Athos and Porthos colocalized with Fibrillarin, which

marks the nucleolus, the site of rRNA synthesis (**Figure 2.3A-C”**) (Ochs, Lischwe, Spohn, & Busch, 1985). Aramis was also in the cytoplasm of the germline and somatic cells of the gonad. To determine if Aramis, Athos, and Porthos directly interact with rRNA, we performed immunoprecipitation (IP) followed by RNA-seq. We found that rRNA immunopurified with Aramis, Athos, and Porthos (**Figure 2.3D-D”, Figure 2.4A-A”**). Thus, Aramis, Athos, and Porthos are present in the nucleolus and interact with rRNA, suggesting that they might regulate rRNA biogenesis.

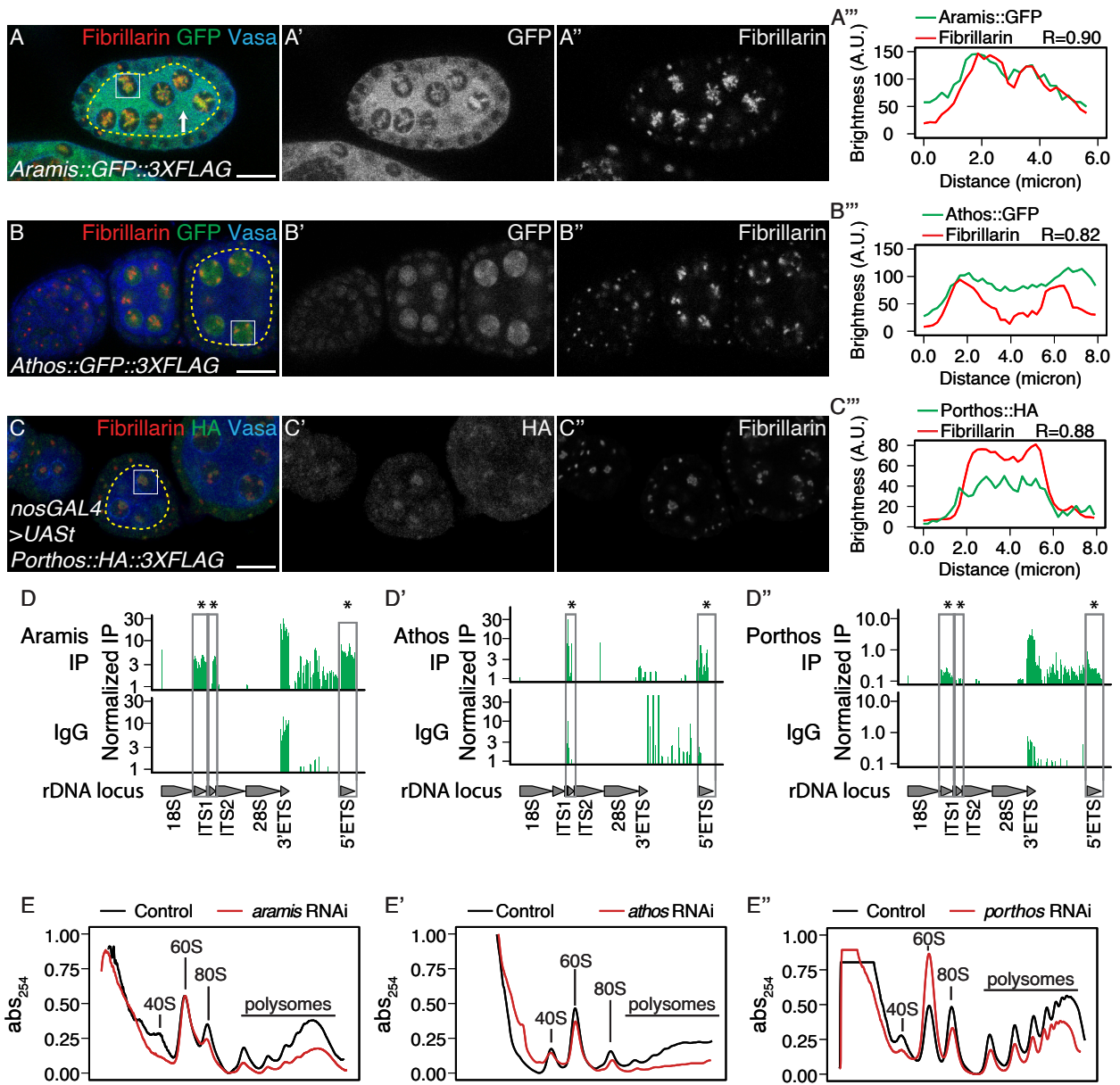


Figure 2.3: Athos, Aramis, and Porthos are required for efficient ribosome biogenesis.

(A-C'') Confocal images of ovariole immunostained for Fibrillarin (red, right grayscale), Vasa (blue), (A-A'') Aramis::GFP, (B-B'') Athos::GFP and (C-C'') Porthos::HA (green, left grayscale). (A''-C'') Fluorescence intensity plot generated from a box of averaged pixels centered around the punctate of Fibrillarin in the white box. The white box also indicates a nucleus, while the yellow dotted outline indicates the divide between soma and germline, with the germline on the interior of the outline and soma on the exterior. R values denote Spearman correlation coefficients between GFP and Fibrillarin from plot profiles generated using Fiji, taken from the nucleolus denoted by the white box. Aramis, Athos and Porthos are expressed throughout oogenesis and localize to the nucleolus. Aramis is

also present in the cytoplasm. (**D-D”**) RNA IP-seq of (**D**) Aramis, (**D’**) Athos, and (**D”**) Porthos aligned to rDNA locus displayed as genome browser tracks. Bar height represents log scaled rRNA reads mapping to rDNA normalized to input and spike-in. Grey boxes outline ETS (external spacers) and ITS (internal spacers) which are only present in pre-rRNA that are significantly enriched in the IP compared to the IgG control (bootstrapped paired t-tests, n=3, * = p-value < 0.05). (**E-E”**) Polysome traces from *Drosophila* S2 cells treated with dsRNA targeting *aramis*, (**E**) *athos*, (**E’**) *porthos* (red line) compared to a mock transfection control (black line). *aramis*, *athos* and *porthos* are required to maintain a proper 40S/60S ribosomal subunit ratio compared to control and have a smaller 40S/60S ratio. *athos* is required to maintain a proper 40S/60S ribosomal subunit ratio compared to control and has a larger 40S/60S ratio. Additionally, *aramis*, *athos*, and *porthos* are required to maintain polysome levels. All three helicases are required to maintain polysome levels. Scale bar for all images is 15 micron.

Nucleolar size, and in particular nucleolar hypotrophy, is associated with reduced ribosome biogenesis and nucleolar stress (Neumüller et al., 2008; Yandong Zhang, Forys, Miceli, Gwinn, & Weber, 2011). If Aramis, Athos, and Porthos promote ribosome biogenesis, then their loss would be expected to cause nucleolar stress and a reduction in mature ribosomes. Indeed, immunostaining for Fibrillarin revealed hypotrophy of the nucleolus in *aramis*, *athos*, and *porthos* germline RNAi flies compared to in control flies, consistent with nucleolar stress (**Figure 2.3B-C’**). Next, we used polysome profile analysis to evaluate the ribosomal subunit ratio and translation status of ribosomes in S2 cells depleted of *aramis*, *athos*, or *porthos* (Boamah, Kotova, Garabedian, Jarnik, & Tulin, 2012; Öunap, Käsper, Kurg, & Kurg, 2013). We found that upon the depletion of all three helicases, the heights of the polysome peaks were reduced (**Figure 2.3E-E”**). We found that depletion of *aramis* and *porthos* diminished the height of the 40S subunit peak compared to the 60S subunit peak, characteristic of defective 40S ribosomal subunit biogenesis (**Figure 2.3E, E”, Figure 2.4D**) (Cheng et al., 2019), whereas *athos* depletion diminished the height of the 60S subunit peak compared to

the 40S peaks, characteristic of a 60S ribosomal subunit biogenesis defect (**Figure 2.3E'**, **Figure 2.4D'**) (Cheng et al., 2019). Previous work indicates that the stem-cyst that arises from depletion of genes involved in ribosome biogenesis in the germline genetically interacts with Shrub (*shrb*) a member of the Escrt-III complex. To further determine if *aramis*, *athos*, and *porthos* regulates ribosome biogenesis, we performed trans-heterozygous crosses between *aramis*, *athos*, and *porthos* and *shrb*. We observed the presence of stem-cyst structures even heterozygotes mutants of *shrb*, consistent with previous observations (Matias, Mathieu, & Huynh, 2015; Sanchez et al., 2016), and in *aramis*, or *athos*, *porthos*. We found that in trans-heterozygous germaria of a *shrb* mutant our genes of interest result in a more frequent occurrence of stem-cysts than in their respective heterozygous background consistent with their role in ribosome biogenesis (**Figure S2.4E-L**). Taken together our findings indicate that these helicases promote ribosome biogenesis in *Drosophila*.

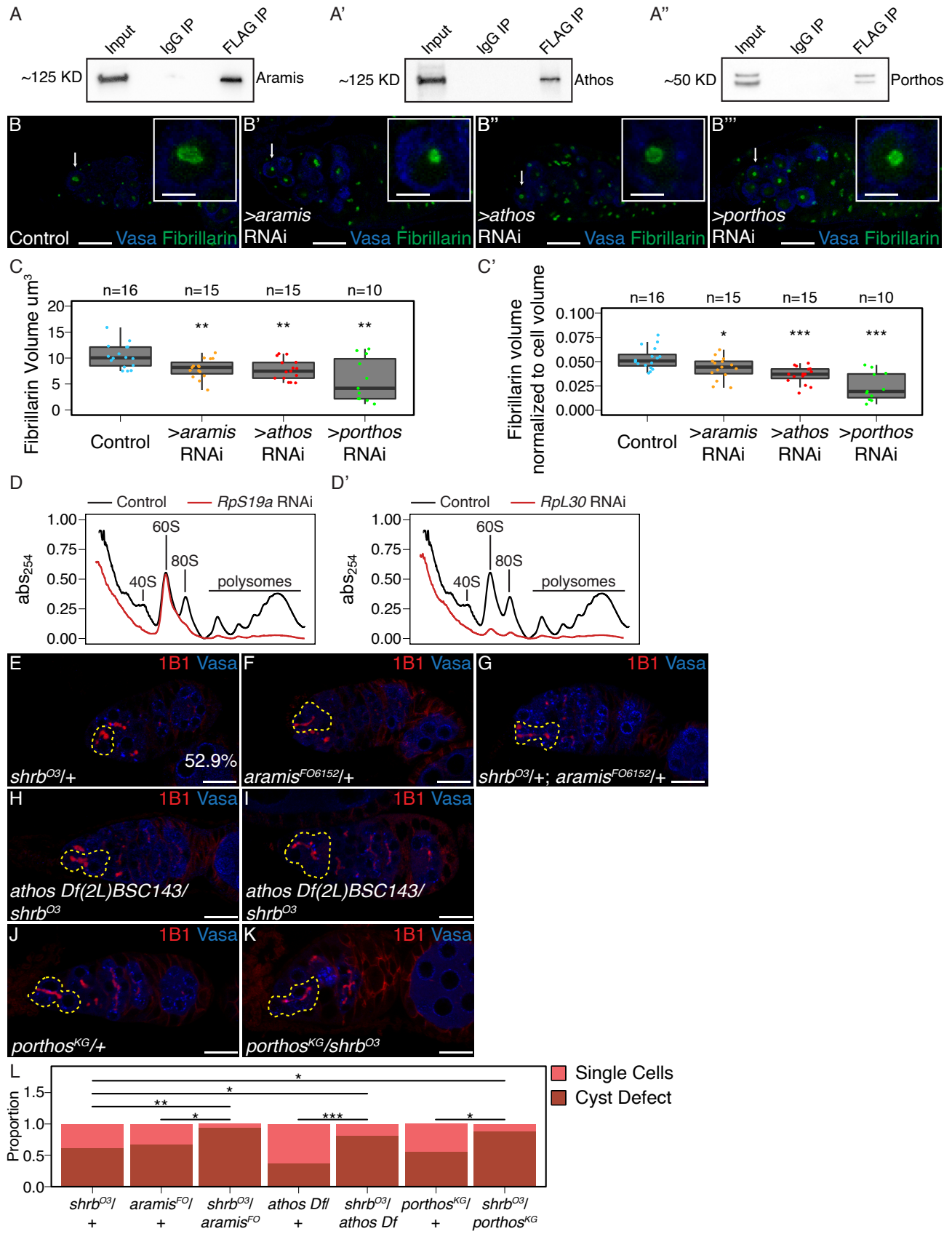


Figure 2.4: Athos, Aramis, and Porthos are required for efficient ribosome biogenesis., related to Figure 2.3.

(**A-A'**) Western blots of immunoprecipitations from ovaries for FLAG-tagged (**A**) Aramis, (**A'**) Athos, and (**A''**) Porthos. (**B-B''**) Confocal images of (**B**) *nosGAL4*, driver control, (**B'**) *aramis* (**B''**) *athos* and (**B'''**) *porthos* germline RNAi germaria stained for Fibrillarin (green), and Vasa (blue). (**C-C'**) Quantification of (**C**) raw nucleolar volume or (**C'**) normalized to cell volume nucleolar volume in GSCs of *aramis*, *athos*, and *porthos* RNAi, compared to control indicates loss of each helicase results in nucleolar stress. (n=12-16 GSCs per genotype, One-way ANOVA, p<0.001, with Welch's t-test, Holm-Bonferroni corrected, * = p<0.05, ** = p<0.01, *** = p<0.001). (**D-D'**) Polysome preparations from *Drosophila* S2 cells in cells treated with dsRNA targeting (**D**) *RpS19a* or (**D'**) *RpL30* (red line) compared to a mock transfection control (black line). (**E-K**) Confocal images of heterozygous (**E**) *shrb*^{O3}/+, (**F**) *aramis*^{f06152}/+ mutant ovaries, (**G**) *shrb*^{O3}/+; *aramis*^{f06152}/+ transheterozygous, (**H**) *athos* deficiency/+ mutant ovaries, (**I**) *athos* deficiency/*shrb*^{O3} transheterozygous, heterozygous (**J**) *porthos*^{KG05120}/+ mutant ovaries and (**K**) *porthos*^{KG05120}/*shrb*^{O3} transheterozygous ovaries stained for 1B1 (red) and Vasa (blue). (**L**) Quantification of proportion of germaria with presence of a stem-cyst or single cells from the indicated genotypes (pairwise one-sided Fisher's tests, Holm-Bonferroni corrected, * = p<0.05, ** = p<0.01, *** = p<0.001). Scale bar for main images is 15 micron, scale bar for insets is 3.75 micron.

2.3.3 Aramis promotes cell cycle progression via p53 repression

Our data so far indicate that Aramis, Athos and Porthos promote ribosome biogenesis, which is known to be required for GSC abscission (Sanchez et al., 2016). Yet the connections between ribosome biogenesis and GSC abscission are poorly understood. To explore the connection, we further examined the *aramis* germline RNAi line, as its defect was highly penetrant but maintained sufficient germline for analysis (**Figure 2.1E, H**). First, we compared the mRNA profiles of *aramis* germline RNAi ovaries to *bam* germline RNAi to determine if genes that are known to be involved in GSC abscission have altered expression. We used germline *bam* depletion as a control because it leads to the accumulation of CBs with no abscission defects (Flora, Schowalter, et al., 2018; Gilboa, Forbes, Tazuke, Fuller, & Lehmann,

2003; D. McKearin & Ohlstein, 1995; Ohlstein & McKearin, 1997), whereas loss of *aramis* resulted in accumulation of CBs that do not abscise from the GSCs.

We performed RNA-seq and found that 607 RNAs were downregulated and 673 RNAs were upregulated in *aramis* germline RNAi versus *bam* germline RNAi (cut-offs for differential gene expression were $\log_2(\text{foldchange}) > |1.5|$, FDR < 0.05) (**Figure 2.10A, Supplemental Table 2.2**). Gene Ontology (GO) analysis for biological processes on these genes encoding these differentially expressed mRNAs (Thomas et al., 2003) revealed that the genes that were downregulated upon *aramis* germline depletion were enriched for GO terms related to the cell cycle, whereas the upregulated genes were enriched for GO terms related to stress response (**Figure 2.5A, Figure 2.6B**). The downregulated genes included *Cyclin A*, which is required for cell cycle progression, *Cyclin B* (*CycB*) and *aurora B*, which are required for both cell cycle progression and cytokinesis; in contrast the housekeeping gene *Actin 5C* was unaffected (**Figure 2.5B-C, Figure 2.6C-C'**) (Mathieu et al., 2013; Matias, Mathieu, & Huynh, 2015). We confirmed that CycB was reduced in the ovaries of *aramis* germline RNAi flies compared to *bam* germline RNAi flies by immunofluorescence (**Figure 2.5D-F**). These changes to genes that promote cell cycle and cytokinesis were also seen *aramis; bam* double depletions as the Biological Process GO-terms we identified from targets downregulated in *aramis* RNAi were very similar to those we identified from in *bam* RNAi; *aramis* RNAi compared to their controls (**Figure 2.5A, Supplemental Table 2.3**). Similarly, all of the GO-terms we identified in from upregulated genes are also enriched GO terms from the double-knockdown upregulated targets (**Figure 2.6B, Supplemental Table 2.3**). Crucially, all the genes we refer to in the manuscript such as *CycB*, *AurB*, and *CycA* are also targets in *bam* RNAi; *aramis* RNAi. (**Figure 2.6B, Supplemental Table 2.3**). These

results suggest that *aramis* is required for the proper expression of key regulators of GSC abscission.

CycB is expressed during G2 phase after asymmetric cell division to promote GSC abscission (Flora, Schowalter, et al., 2018; Mathieu et al., 2013). To test if the loss of germline *aramis* leads to GSC abscission defects due to diminished expression of CycB, we attempted to express a functional CycB::GFP fusion protein in the germline under the control of a UAS/GAL4 system (**Figure 2.6F-G'**) (Mathieu et al., 2013). Unexpectedly, the CycB::GFP fusion protein was not expressed in the *aramis*-depleted germline, unlike the wild type (WT) germline (**Figure 2.6F-G**) (Glotzer, Murray, & Kirschner, 1991; Mathieu et al., 2013; Zielke et al., 2014). We considered the possibility that progression into G2 is blocked in the absence of *aramis*, precluding expression of CycB. To monitor the cell cycle, we used the Fluorescence Ubiquitin-based Cell Cycle Indicator (FUCCI) system. *Drosophila* FUCCI utilizes a GFP-tagged degron from E2f1 to mark G2, M, and G1 phases and an RFP-tagged degron from CycB to mark S, G2, and M phases (Zielke et al., 2014). We observed cells in different cell cycle stages in both WT and *bam*-depleted germaria, but the *aramis*-depleted germaria expressed neither GFP nor RFP (**Figure 2.6F-H''**). Double negative reporter expression is thought to indicate early S phase, when expression of E2f1 is low and CycB is not expressed (Hinnant, Alvarez, & Ables, 2017). The inability to express FPs is not due to a defect in translation as *aramis*-depleted germline can express GFP that is not tagged with the degron (**Figure 2.6K**). Taken together, we infer that loss of *aramis* blocks cell cycle progression around late G1 phase/early S phase and prevents progression to G2 phase, when GSCs abscise from CBs.

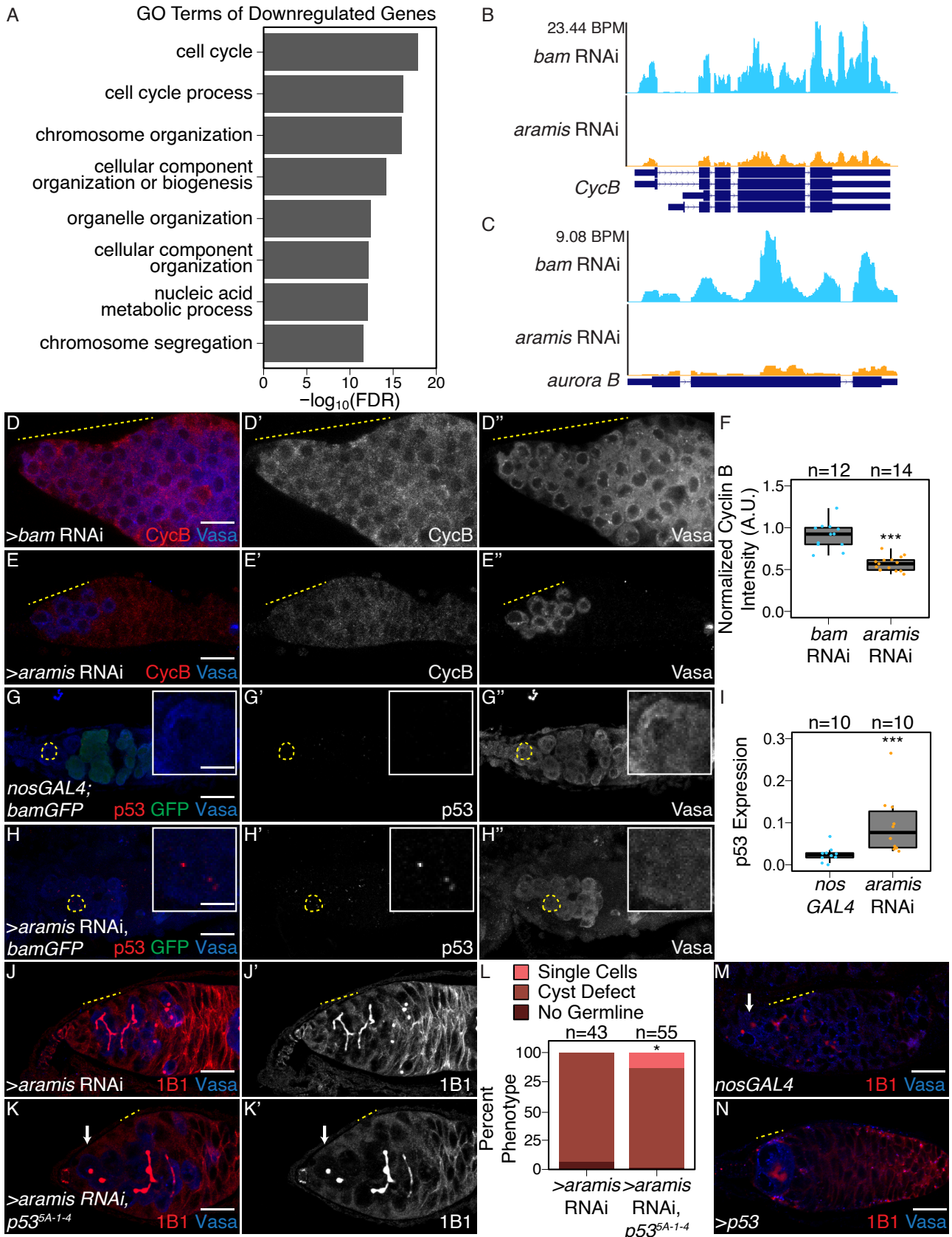


Figure 2.5: Athos, Aramis, and Porthos are required for cell cycle progression during early oogenesis.

(A) Bar plot representing the most significant Biological Process GO-terms of downregulated genes in ovaries depleted of *aramis* compared to *bam* RNAi control (FDR = False Discovery Rate from p-values using a Fisher's exact test). **(B-C)** Genome browser tracks representing the gene locus of **(B)** *CycB* and **(C)** *aurora B* in ovaries depleted of *aramis* compared to the developmental control, *bam* RNAi. Y-axis represents the number of reads mapping to the locus in bases per million (BPM). **(D-E")** Confocal images of germaria stained for CycB (red, left grayscale) and Vasa (blue, right grayscale) in **(D-D")** *bam* RNAi control ovaries and **(E-E")** *aramis* germline RNAi. **(F)** Boxplot of CycB intensity in the germline normalized to Cyc B intensity in the soma in *bam* RNAi and *aramis* RNAi (n=12-14 germaria per sample, *** = p < 0.001, Welch t-test). **(G-H")** Confocal images of germaria stained for p53 (red, left grayscale), GFP (green), and Vasa (blue, right grayscale) in **(G-G")** *nosGAL4*, driver control ovaries and **(H-H")** germline depletion of *aramis*. Cells highlighted by a dashed yellow circle represent cell shown in the inset. Driver control *nosGAL4* ovaries exhibit attenuated p53 expression in GSCs and CBs, but higher expression in cyst stages as previously reported, while p53 punctate are visible in the germline of *aramis* RNAi in the undifferentiated cells. **(I)** Box plot of percentage of pixel area exceeding the background threshold for p53 in GSCs and CBs in driver control *nosGAL4* ovaries and the germline of *aramis* RNAi indicates p53 expression is elevated in the germline over the GSCs/CBs of control ovaries. (n=10 germaria per sample, *** = p < 0.001, Welch's t-test). **(J-K")** Confocal images of germaria stained for 1B1 (red, left grayscale) and Vasa (blue, right grayscale) in **(J-J")** germline *aramis* RNAi in a wildtype background and **(K-K")** germline *aramis* RNAi with a mutant, null, *p53^{5-A-14}* background showing presence of spectrosomes upon loss of p53. **(L)** Quantification of stem-cyst phenotypes demonstrates a significant rescue upon of loss of *p53^{5-A-14}* in *aramis* germline depletion compared to the control (n=43-55 germaria per genotype, df=2, Fisher's exact test p < 0.05). **(M-N)** Confocal images of ovaries stained for 1B1 (red) and Vasa (blue) in *nosGAL4* ovaries **(M)** and ovaries overexpressing *p53* in the germline. Cysts are denoted by a dotted yellow line, single cells by a white arrow. **(N)**. We observed that 84% of germaria from *p53* overexpression ovaries had loss of germline while 12% of germaria contained a cyst, marked by an extended spectrosome structure connecting germline cells together, and an additional 4% of germaria contained an accumulation of single cells (n=55 germaria, Fisher's exact test, p < 0.001). Scale bar for main images is 15 micron, scale bar for insets is 3.75 micron

In mammals, cells defective for ribosome biogenesis stabilize p53, which is known to impede the G1 to S transition (Agarwal, Agarwal, Taylor, & Stark, 1995; Senturk & Manfredi, 2013). Therefore, we hypothesized that the reduced ribosome biogenesis in the *aramis*-depleted germline leads to p53 stabilization in undifferentiated cells, driving cell cycle arrest and

GSC abscission defects. To test this hypothesis, we detected p53 and Vasa in the germline by immunostaining. A hybrid dysgenic cross that expresses p53 in undifferentiated cells was utilized as a positive control, and *p53* null flies were used as negative controls (**Figure 2.6L-M**) (Moon et al., 2018). In WT, we observed p53 expression in the meiotic stages of germline but p53 expression in GSCs and CBs was attenuated as previously reported (**Figure 2.5G-G”**) (W.-J. Lu, Chapo, Roig, & Abrams, 2010). However, compared to WT GSCs/CBs, we observed p53 expression in the stem cysts of the *aramis*-depleted germline (**Figure 2.5G-I**). Similarly, we observed p53 expression in the stem cysts of *athos*- and *porthos*-depleted germlines (**Figure 2.6N-O**), further supporting that reduced ribosome biogenesis stabilizes p53. To determine if p53 stabilization is required for the cell cycle arrest in *aramis*, *athos*, and *porthos*-depleted germline cysts, we depleted *aramis*, *athos* and *porthos* in the germline of *p53* mutants using germline specific knockdown. We observed a partial but significant alleviation of the cyst phenotype, such that spectrosomes were restored (**Figure 2.5J-L**, **Figure 2.6P-T**). This finding indicates that p53 contributes to cytokinesis failure upon loss of *aramis*, but that additional factors are also involved.

To determine if p53 stabilization is required for the cell cycle arrest in *aramis*-, *athos*-, and *porthos*-depleted germline cysts, we depleted *aramis*, *athos* and *porthos* in the germline of *p53* mutants using germline specific knockdowns. We observed a partial but significant alleviation of the cyst phenotype, such that spectrosomes were restored (*Figure 2.5M-N*), This finding indicates that p53 contributes to cytokinesis failure upon loss of *aramis*, *athos* and *porthos* but that additional factors are also involved. To determine if aberrant expression of p53 is sufficient to cause the formation of stem-cysts, we overexpressed p53 in the germline under the control of a UAS/GAL4 system. While 84% of germaria had a complete loss of germline

as previously reported (Bakhrat, Pritchett, Peretz, McCall, & Abdu, 2010), excitingly in 12% of germaria the germline cells were connected by a fusome-like structure, phenocopying loss of *aramis*, *athos*, or *porthos* (**Figure 3M-N**), and in the rest, we observed several single germline cells, compared to the control (n=55, Fisher's exact test, p<0.001). Taken together, we find that *aramis-*, *athos-*, and *porthos-* depleted germ cells display reduced ribosome biogenesis, aberrant expression of p53 protein, and a block in cell cycle progression. Reducing p53 partially alleviates the cell cycle block and GSC cytokinesis defect, while inappropriate p53 expression results in loss of germline and cytokinesis defects in the GSCs., while inappropriate p53 expression results in loss of germline and cytokinesis defects.

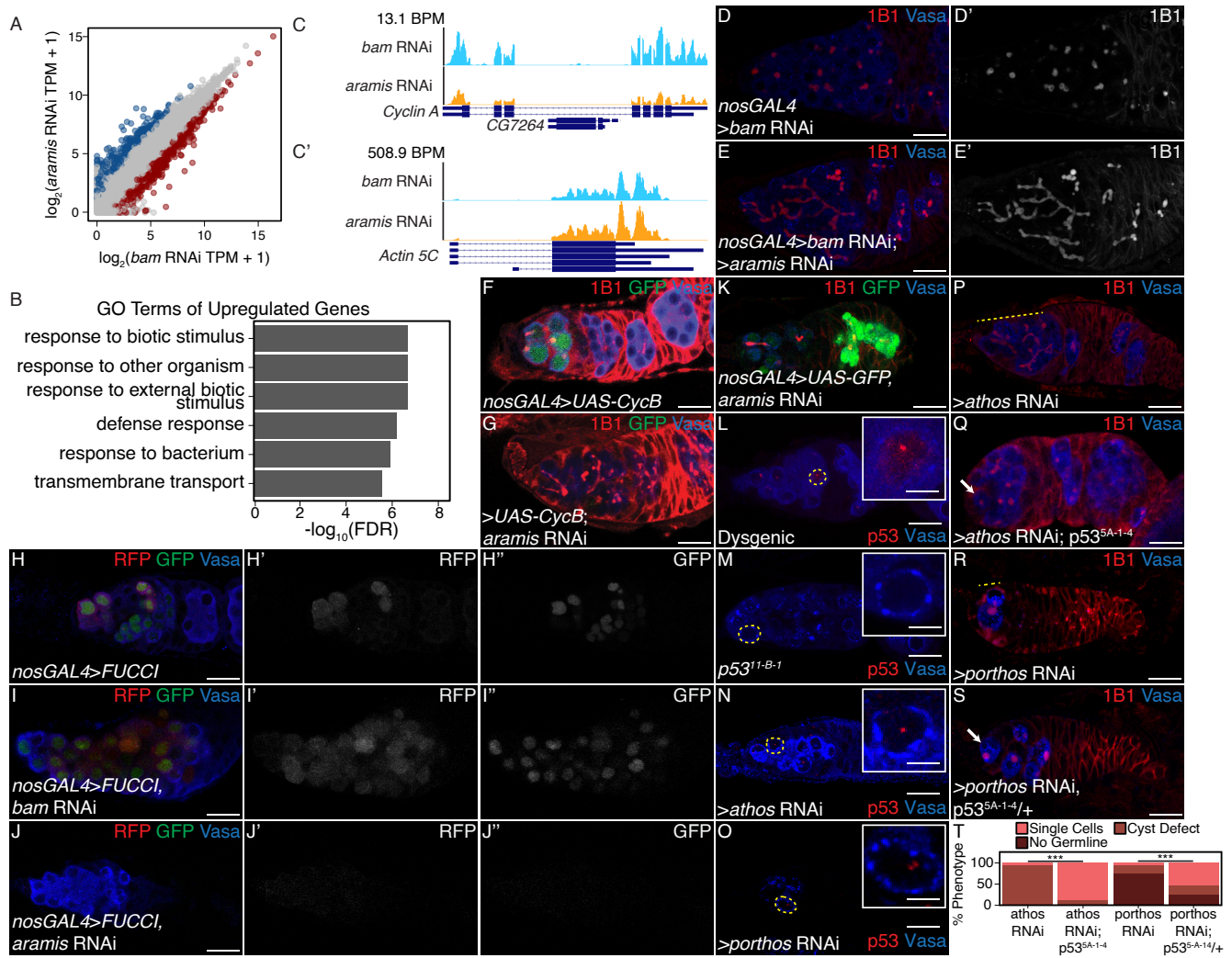


Figure 2.6: Aramis is required for proper cell cycle progression, related to Figure 2.5.

(A) Biplot of mRNA levels in *aramis* RNAi compared to *bam* RNAi. Blue points represent mRNAs significantly upregulated *aramis* RNAi compared to *bam* RNAi, red points represent mRNAs significantly downregulated *aramis* RNAi compared to *bam* RNAi. (B) Bar plot representing the most significant Biological Process GO-terms of upregulated genes in ovaries depleted of *aramis* compared to the developmental control, *bam* RNAi. (C-C') Genome browser tracks of mRNA levels at the (C) *Cyclin A* and (C') *Actin 5C* loci indicate that the RNaseq target gene *Cyclin A* expression is downregulated, while a non-target, *Actin 5C* is not downregulated. (D-E') Confocal images of germaria stained for 1B1 (red, greyscale) and Vasa (blue) (D-D') from ovaries with germline depletion of *bam* and (E-E') germline depletion of *bam* and *aramis* simultaneously demonstrates that simultaneous depletion of *bam* and *aramis* results in a stem-cyst similar to depletion of *aramis* alone. (F-G) Confocal images of germaria stained for 1B1 (red), Vasa (blue), and Cyclin B::GFP (green) in (F) control and (G) germline depletion of *aramis* demonstrates that functional Cyclin B::GFP cannot be efficiently expressed in germline depleted of *aramis*. (H-J") Confocal images of germaria stained for RFP, GFP, and Vasa. Panel T: Bar chart showing the percentage of phenotypes for different genotypes.

focal images of germaria that express Fly-FUCCI in the germline stained for Vasa (blue). GFP-E2f1^{degron} (green, right grayscale) and RFP-CycB^{degron} (red, left grayscale) in (**H-H”**) nosGAL4, driver control ovaries, (**I-I”**) bam RNAi as a developmental control, and (**J-J”**) ovaries with germline depletion of *aramis* demonstrates that the germline of *aramis* RNAi germline depleted ovaries are negative for both G1 and G2 cell cycle markers. (**K**) Confocal images of *aramis* germline RNAi expressing GFP in the germline, stained for 1B1 (red), Vasa (blue), and GFP (green) indicates productive translation of transgenes still occurs. (**L-M**) Confocal images of germaria stained for p53 (red) and Vasa (blue) in (**L**) hybrid dysgenic, Harwich, ovaries and (**M**) p53^{11-B-1} ovaries stained for p53 (red) and Vasa (blue) demonstrate the expected p53 staining patterns. (**N-O**) Confocal images of germaria stained for p53 (red) and Vasa (blue) in ovaries depleted of (**N**) *athos* or (**O**) *porthos* in the germline exhibit p53 punctate staining. Cells highlighted by a dashed yellow circle represent cells shown in the inset. (**P-Q**) Confocal images of germaria stained for 1B1 (red) and Vasa (blue) in (**P**) germline *athos* RNAi in a wildtype background and (**Q**) germline *athos* RNAi with a mutant, null, p53^{5-A-14} background showing presence of spectrosomes upon loss of p53. (**R-S**) Confocal images of germaria stained for 1B1 (red) and Vasa (blue) in (**R**) germline *porthos* RNAi in a wildtype background and (**S**) germline *porthos* RNAi with a mutant, heterozygous, p53^{5-A-14}/+ background showing presence of spectrosomes upon reduction of p53 (**T**) Phenotypic quantification of demonstrates a significant rescue upon of loss of p53^{5-A-14} in germline *athos* (n=63 *athos*, n=47 *athos* RNAi, p53^{5-A-14}, Fisher’s exact test p > 0.001) or *porthos*-depletion (n=34 *porthos* RNAi; n=41 *porthos* RNAi, p53^{5-A-14}/+, Fisher’s exact test p > 0.001) compared to the respective control.

Aramis promotes translation of Non1, a negative regulator of p53, linking ribosome biogenesis to the cell cycle

Although p53 protein levels were elevated upon loss of *aramis* in the germline, p53 mRNA levels were not significantly altered (log₂ fold change: -0.49; FDR: 0.49). Given that ribosome biogenesis is affected, we considered that translation of p53 or one of its regulators was altered in *aramis*-depleted germlines. To test this hypothesis, we performed polysome-seq of gonads enriched for GSCs or CBs as developmental controls, as well as gonads depleted for *aramis* in the germline (Flora, Wong-Deyrup, et al., 2018b). We plotted the ratios of polysome-associated RNAs to total RNAs (**Figure 2.7A-A”, Supplemental Table 2.4**)

and identified 87 mRNAs with a reduced ratio upon depletion of *aramis*, suggesting that they were translated less efficiently compared to developmental controls. Loss of *aramis* reduced the levels of these 87 downregulated transcripts in polysomes, without significantly affecting their total mRNA levels (**Figure 2.7B**, **Figure 2.8A-A'**). These 87 transcripts encode proteins mostly associated with translation including ribosomal proteins (**Figure 2.7C**). To validate that Aramis regulates translation of these target mRNAs, we utilized a reporter line for the Aramis-regulated transcript encoding Ribosomal protein S2 (RpS2) that is expressed in the context of the endogenous promoter and regulatory sequences (Buszczak et al., 2007; Q. Zhang, Shalaby, & Buszczak, 2014). We observed reduced levels of RpS2::GFP in germlines depleted of *aramis* but not in those depleted of *bam* (**Figure 2.7D-F**). RpS2::GFP expression is also reduced in *bam* RNAi, *aramis* RNAi double germline knockdown compared to *bam* RNAi (**Figure 2.8B-D**). To ensure that reduced RpS2::GFP levels did not reflect a global decrease in translation, we visualized nascent translation using O-propargyl-puromycin (OPP). OPP is incorporated into nascent polypeptides and can be detected using click-chemistry (Sanchez et al., 2016). We observed that global translation in the germlines of ovaries depleted of *aramis* was not reduced compared to single cells of control ovaries or *bam* (**Figure 2.7G-J**). Notably, the regulation of these genes do not appear to be directly mediated by Aramis as none of the target genes are enriched from Aramis::GFP::3XFLAG RNA IP-seq (**Supplemental Table 2.5**). Thus, loss of *aramis* results in reduced translation of a subset of transcripts compared to the rest of the transcriptome.

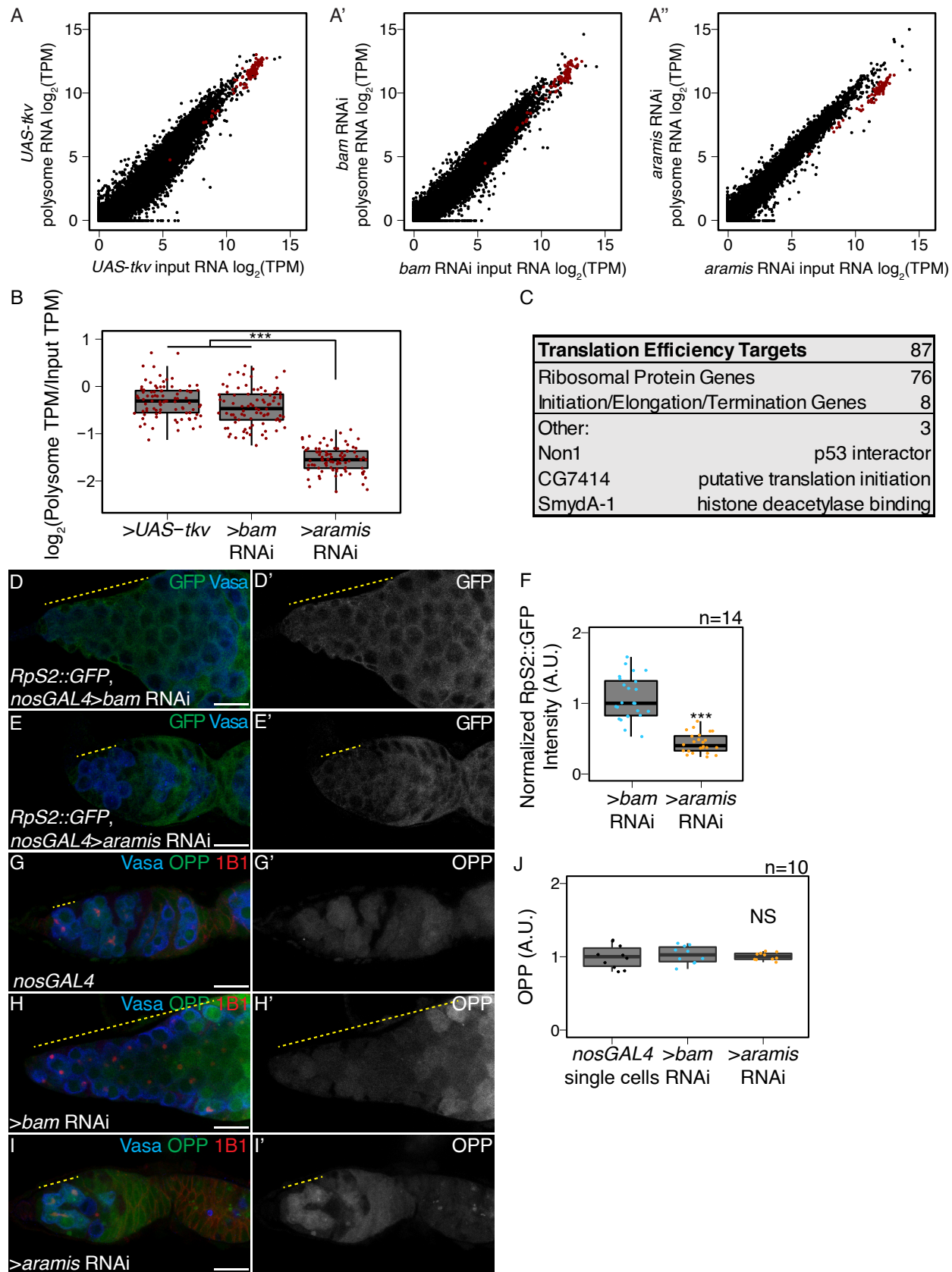


Figure 2.7: Aramis is required for efficient translation of a subset of mRNAs.

(A-A') Biplots of poly(A)+ mRNA Input versus polysome associated mRNA from **(A)** ovaries genetically enriched for GSCs (*UAS-tkv*), **(A')** Undifferentiated GSC daughter cells (*bam* RNAi) or **(A'')** germline *aramis* RNAi ovaries. **(B)** Boxplot of translation efficiency of target genes in *UAS-tkv*, *bam* RNAi, and *aramis* RNAi samples (ANOVA p<0.001, post-hoc Welch's t-test, n=87, *** = p < 0.001). **(C)** Summary of downregulated target genes identified from polysome-seq. **(D-E')** Confocal images of germaria stained for 1B1 (red), RpS2::GFP (green, grayscale), and Vasa (blue) in **(D-D')** *bam* RNAi control and **(E-E')** *aramis* RNAi (yellow dashed line marks approximate region of germline used for quantification). **(F)** A.U. quantification of germline RpS2::GFP expression normalized to RpS2::GFP expression in the surrounding soma in undifferentiated daughter cells of *bam* RNAi compared to *aramis* RNAi. RpS2::GFP expression is significantly lower in *aramis* RNAi compared to control (n=14 germaria per sample, Welch's t-test, *** = p < 0.001). **(G-I')** Confocal images of germaria stained for 1B1 (red), OPP (green, grayscale), and Vasa (blue) in **(G-G')** *nosGAL4*, **(H-H')** *bam* RNAi, and **(I-I')** *aramis* RNAi (yellow dashed line marks approximate region of germline used for quantification). **(J)** A.U. quantification of OPP intensity in single cells of *nosGAL4* control germeria and undifferentiated daughter cells in *bam* RNAi as controls and *aramis* RNAi (n = 10 germaria per genotype, Welch's t-test, NS = p > 0.05). OPP intensity is not significantly downregulated in *aramis* RNAi compared to either control. Scale bar for all images is 15 micron.

Previous work has indicated that excess ribosomal protein expression may be deleterious to cellular functions and induce cell stress. We hypothesized that the decrease in translation we observe may be the result of a regulatory mechanism to mitigate such affects. To test if overexpression of ribosomal proteins is deleterious to germline development, we overexpressed several ribosomal proteins in the germline. We found no obvious phenotype as a result of overexpression of single ribosomal proteins (**Figure 2.8E-G'**). We reason that individual overexpression may not be as detrimental as the excess expression of nearly all ribosomal proteins that we observed in our experiments, which is not technically possible to recapitulate through exogenous expression lines.

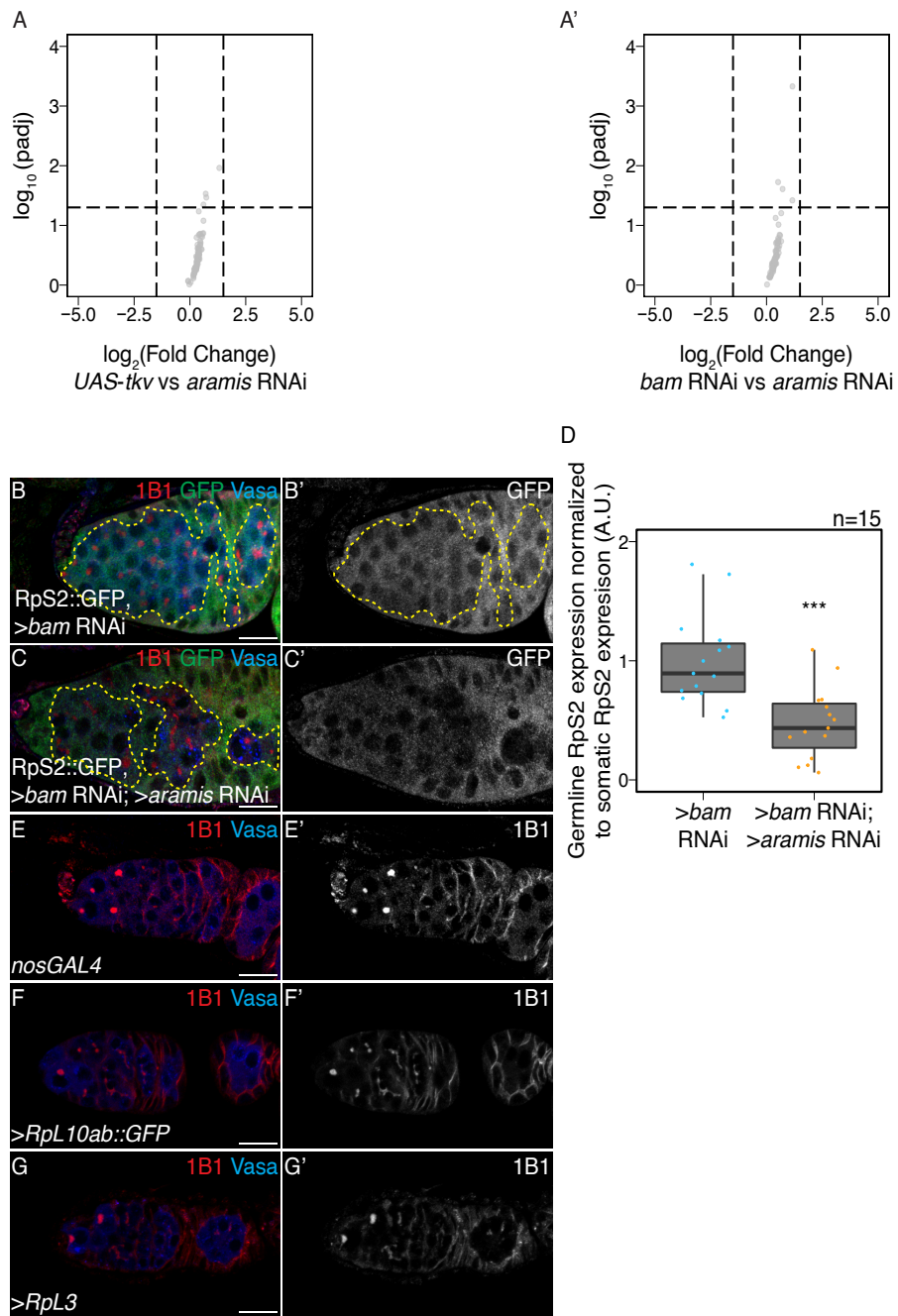


Figure 2.8: The mRNA levels of Aramis polysome-seq targets are not significantly changing, related to Figure 2.7.

(A-A') Volcano plot of mRNA levels from poly(A)+ mRNA input libraries in germline *aramis* RNAi compared to (A) germline driven *UAS-tkv* and (A') *bam* RNAi of targets identified from polysome-seq. No target genes identified from polysome-seq meet the differential expression cutoff for mRNA in *UAS-tkv* compared to *aramis* RNAi or *bam* RNAi compared to *aramis* RNAi input libraries. (B-C') Confocal images of germaria stained for

1B1 (red) RpS2::GFP (green, greyscale) and Vasa (blue) in (**B-B'**) germline *bam* RNAi as a control and (**C-C'**) germline *bam* RNAi; *aramis* RNAi. Yellow dotted outline denotes the germline on the interior of the outline with the soma on the exterior of the outline. (**D**) Quantification of RpS2::GFP expression in the germline normalized to the soma in germline *bam* RNAi compared to *bam* RNAi; *aramis* RNAi demonstrates a significant decrease in RpS2::GFP expression when *aramis* is knocked down in a germline *bam* RNAi background (Welch's t-test, *** = p<0.001, n=15).

None of these 87 translational targets have been implicated in directly controlling abscission (Mathieu et al., 2013; Matias, Mathieu, & Huynh, 2015). However, we noticed that the mRNA encoding Novel Nucleolar protein 1 (Non1/CG8801) was reduced in polysomes upon loss of *aramis* in the germline (**Figure 2.7C**). The human ortholog of Non1 is GTP Binding Protein 4 (GTPBP4), and these proteins are known to physically interact with p53 in both *Drosophila* and human cells and have been implicated in repressing p53 (mentioned as CG8801 in Lunardi et al.) (L. Li et al., 2018; Lunardi et al., 2010). To determine if the protein level of Non1 is reduced upon depletion of *aramis*, we monitored the abundance of Non1::GFP, a transgene that is under endogenous control (Sarov et al., 2016), and found that Non1::GFP was expressed in the undifferentiated GSCs and CBs (**Figure 2.9A-A''**). Non1::GFP levels were reduced in the *aramis*, *athos* or *porthos*-depleted stem cysts compared to the CBs that accumulated upon *bam*-depletion (**Figure 2.9B-D**, **Figure 2.10C-F**), suggesting that efficient ribosome biogenesis promotes efficient translation of Non1. During normal oogenesis, p53 protein is expressed in cyst stages in response to recombination-induced double strand breaks (W.-J. Lu, Chapo, Roig, & Abrams, 2010). We found that Non1 was highly expressed at undifferentiated stages and in two- and four-cell cysts when p53 protein levels were low, whereas its expression was attenuated

at eight- and 16-cell cyst stages when p53 protein levels were high (**Figure 2.9A-A'**, **Figure 2.10A-B'**). Non1 was highly expressed in egg chambers, which express low levels of p53 protein suggesting that Non1 could regulate p53 protein levels. To determine if Non1 regulates GSC differentiation and p53, we depleted *Non1* in the germline. We found that germline-depletion of *Non1* results in stem cyst formation and loss of later stages, as well as increased p53 expression, phenocopying germline-depletion of *aramis*, *athos*, and *porthos* (**Figure 2.9E-F, H, Figure 2.10G-I**). In addition, we found that loss of *p53* from *Non1*-depleted germaria partially suppressed the phenotype (**Figure 5F-H**). Thus, *Non1* is regulated by *aramis* and is required for p53 suppression, cell cycle progression, and GSC abscission.

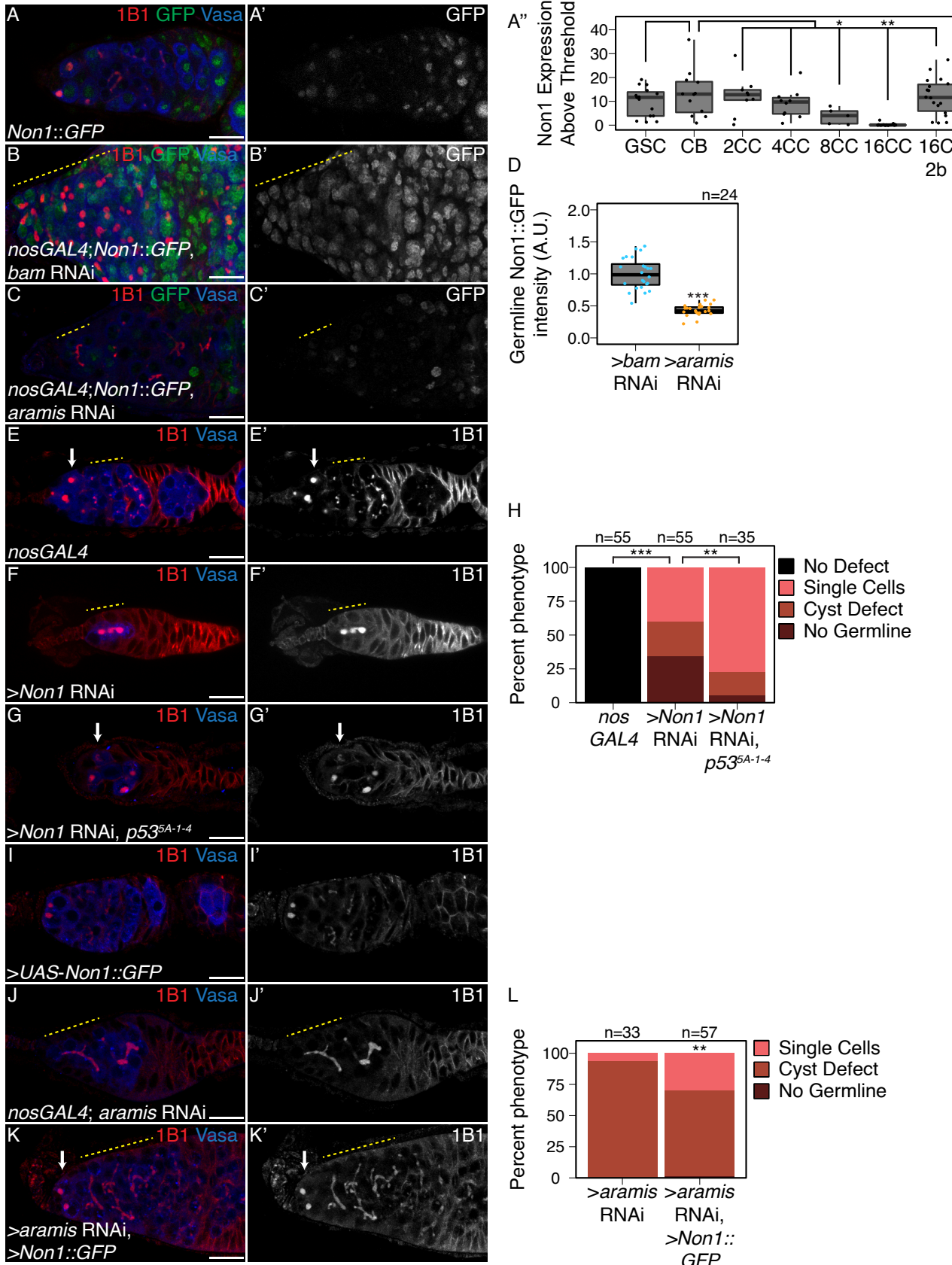


Figure 2.9: Non1 represses p53 expression to allow for GSC differentiation.

(A-A') Confocal images of Non1::GFP germaria stained for 1B1 (red), GFP (green, grayscale), and Vasa (blue). **(A'')** Boxplot of Non1::GFP expression over germline development in GSCs, CBs and Cyst (CC) stages (n=5-25 cysts of each type, * = p < 0.05, ** = p < 0.01, ANOVA with Welch's post-hoc tests). **(B-C')** Confocal images of **(B-B')** *bam* RNAi and **(C-C')** *aramis* RNAi germaria both carrying *Non1::GFP* transgene stained for 1B1 (red), Vasa (blue), and Non1::GFP (green, grayscale). Yellow dashed line marks region of germline used for quantification. **(D)** Boxplot of Non1::GFP expression in the germline normalized to somatic Non1::GFP expression in *bam* RNAi and *aramis* RNAi (n=24 germaria per genotype, Welch's t-test, *** = p < 0.001). Non1 expression is significantly lower in the germline of *aramis* RNAi compared to *bam* RNAi control. **(E-G')** Confocal images of germaria stained for 1B1 (red, grayscale) and Vasa (blue) in **(E-E')** *nosGAL4*, driver control ovaries, **(F-F')** germline *Non1* RNAi, and **(G-G')** germline *Non1* RNAi in a *p53^{5-A-14}* background. Arrow marks the presence of a single cell (**E, G**), yellow dashed line marks a stem-cyst emanating from the niche (**F-F'**) or the presence of proper cysts (**E-E'**). **(H)** Quantification of percentage of germaria with no defect (black), presence of single cell (salmon), presence of a stem-cyst emanating from the niche (brown-red), or germline loss (dark red) demonstrates a significant rescue of stem-cyst formation upon of loss of *Non1* in *p53^{5-A-14}* compared to the *p53* wildtype control (n=35-55 germaria per genotype, df=3, Fisher's exact test with Holm-Bonferroni correction ** = p < 0.01, *** = p < 0.001). **(I-K')** Confocal images of germaria stained for 1B1 (red, grayscale) and Vasa (blue) in ovaries with **(I-I')** germline *Non1* overexpression, **(J-J')** *aramis* germline RNAi exhibiting stem-cyst phenotype (yellow dashed line) and **(K-K')** *aramis* germline RNAi with *Non1* overexpression exhibiting single cells (arrow). **(L)** Phenotypic quantification of *aramis* RNAi with *Non1* overexpression demonstrates a significant alleviation of the stem-cyst phenotype (n=33-57 germaria per genotype, df=2, Fisher's exact test, ** = p < 0.01). Scale bar for all images is 15 micron.

To determine if Aramis, Athos, and Porthos promotes GSC differentiation via translation of Non1, we restored *Non1* expression in germ cells depleted of *aramis*, *athos*, or *porthos*. Briefly, we cloned *Non1* with heterologous UTR elements under the control of the UAS/GAL4 system (see Methods) (Rørth, 1998). We found that restoring *Non1* expression in the *aramis*, *athos*, or *porthos* -depleted germline significantly attenuated the stem cysts and increased the number of cells with spectrosomes, however overexpression of Non1 alone did not cause any noticeable defect (**Figure 2.9I-K**, **Figure 2.10J-N**). Taken together, we

conclude that Non1 can partially suppress the cytokinesis defect caused by germline *aramis* depletion.

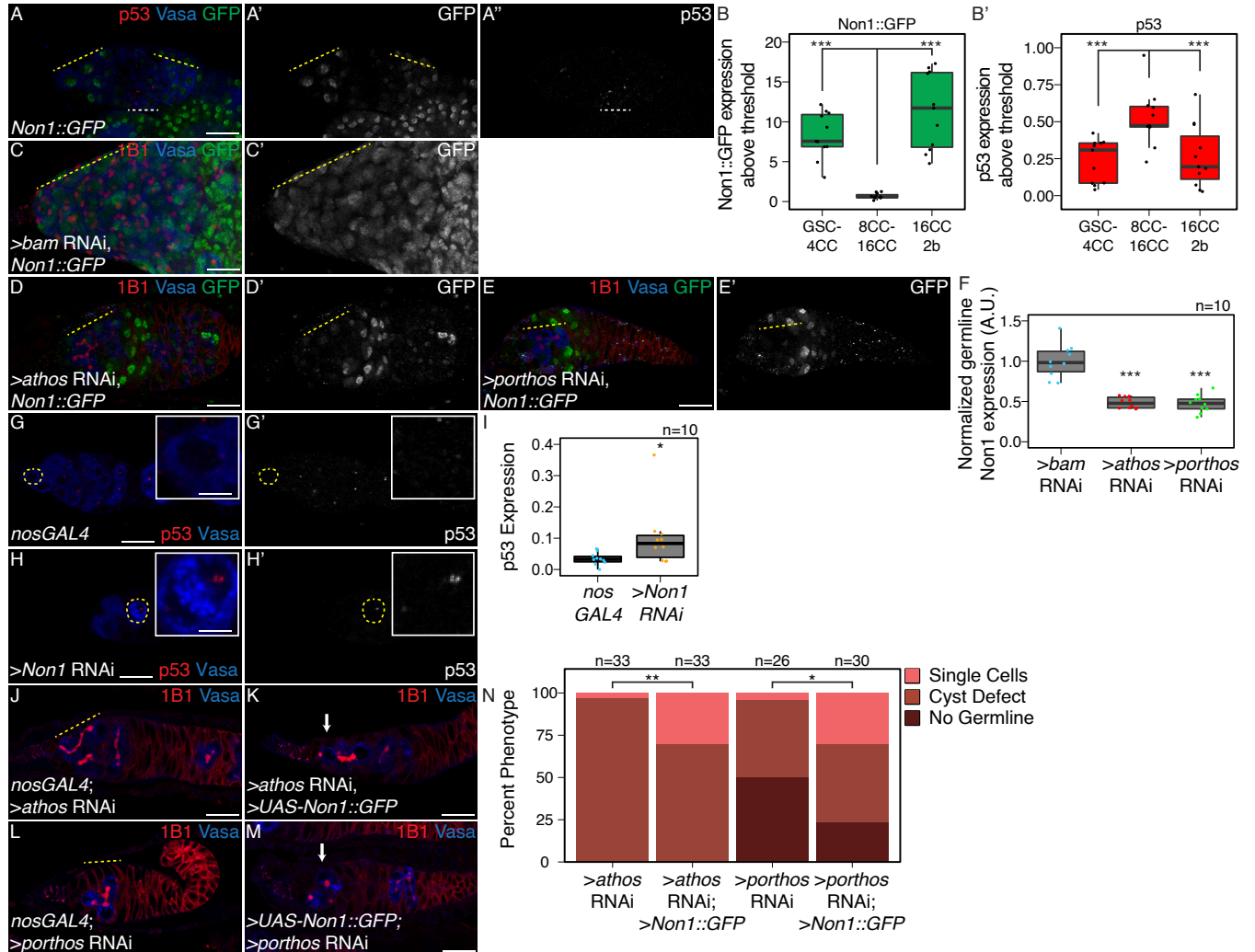


Figure 2.10: Non1 and p53 are inversely expressed, related to Figure 2.9.

(A-A'') Confocal images of ovarioles expressing Non1::GFP stained for p53 (red, right grayscale), Vasa (blue), and Non1::GFP (green, left grayscale). **(B-B')** Quantifications of staining, (B) peak Non1 expression in control ovaries occurs in GSC-4 cell cyst stages and 16-cell cyst-region 2b stages where (B') p53 expression is low. **(C-E')** Confocal images of germline (**C-C'**) *bam* RNAi, (**D-D'**) germline *athos* RNAi, or (**E-E'**) germline *porthos* RNAi germaria stained for 1B1 (red), Non1::GFP (green, greyscale), and Vasa (blue). **(F)** Quantification of Non1:GFP expression in germline *athos*, or *porthos* RNAi compared to germline *bam* RNAi as a developmental control demonstrates there is significantly lower Non1::GFP expression in *athos*, or *porthos* RNAi compared to *bam* RNAi (n=10 germaria per genotype, Welch's t-test, *** = p<0.001) **(G-H')** Confocal images of (**G-G'**) *nosGAL4*, driver control and germline (**H-H'**) *Non1* RNAi germaria stained for p53 (red, grayscale)

and Vasa (blue). (**I**) Quantification of p53 punctate area above cutoff are markedly brighter in the germline of *Non1* RNAi depleted ovaries compared to the control (n=10 germaria per genotype, Welch's t-test, * = p<0.05). Cells highlighted by a dashed yellow circle represent cells shown in the inset. (**J-M**) Confocal images of germaria stained for 1B1 (red, grayscale), and Vasa (blue) in (**J**) *athos* germline RNAi exhibiting stem-cyst phenotype (yellow dashed line) and (**K**) *athos* germline RNAi with *Non1* overexpression exhibiting single cells (arrow), (**L**) *porthos* germline RNAi exhibiting stem-cyst phenotype (yellow dashed line) and (**M**) *porthos* germline RNAi with *Non1* overexpression exhibiting single cells (arrow). (**N**) Phenotypic quantification of germline *athos* RNAi or *porthos* RNAi with *Non1* overexpression demonstrates a significant alleviation of the stem-cyst phenotype compared to germline *athos* or *porthos* RNAi alone (n=26-33 germaria per genotype, df=2, Fisher's exact test, * = p<0.05, ** = p< 0.01). Scale bar for main images is 15 micron, scale bar for insets is 3.75 micron.

2.3.4 Aramis-regulated targets contain a TOP motif in their 5'UTR

We next asked how *aramis* and efficient ribosome biogenesis promote the translation of a subset of mRNAs, including *Non1*, to regulate GSC differentiation. We hypothesized that the 87 mRNA targets share a property that make them sensitive to rRNA and ribosome levels. To identify shared characteristics, we performed *de novo* motif discovery of target genes compared to non-target genes (Bailey, Williams, Misleh, & Li, 2006) and identified a polypyrimidine motif in the 5'UTRs of most target genes (UCUUU; E-value: 6.6e⁻⁰⁹⁴). This motif resembles the previously described TOP motif at the 5' end of mammalian transcripts (Philippe, Vasseur, Debart, & Thoreen, 2018; Thoreen et al., 2012). Although the existence of TOP-containing mRNAs in *Drosophila* has been speculated, to our knowledge their presence has not been explicitly demonstrated (T. Chen & Steensel, 2017; Qin, Ahn, Speed, &

Rubin, 2007). This observation motivated us to precisely determine the 5' end of transcripts, so we analyzed previously published Cap Analysis of Gene Expression sequencing (CAGE-seq) data that had determined transcription start sites (TSS) in total mRNA from the ovary (**Figure 6A**) (Boley, Wan, Bickel, & Celniker, 2014; Z.-X. Chen et al., 2014; dos Santos et al., 2015). Of the 87 target genes, 76 had sufficient expression in the CAGE-seq dataset to define their TSS. We performed motif discovery using the CAGE-seq data and found that 72 of 76 Aramis-regulated mRNAs have a polypyrimidine motif that starts within the first 50 nt of their TSS (**Figure 2.11B-C**). In mammals, it was previously thought that the canonical TOP motif begins with an invariant 'C' (Meyuhas, 2000; Philippe, van den Elzen, Watson, & Thoreen, 2020). However, systematic characterization of the sequence required in order for an mRNA to be regulated as a TOP containing mRNA revealed that TOP mRNAs can start with either a 'C' or a 'U' (Philippe, van den Elzen, Watson, & Thoreen, 2020). Thus, mRNAs whose efficient translation is dependent on *aramis* share a terminal polypyrimidine-rich motif in their 5'UTR that resembles a TOP motif.

In vertebrates, most canonical TOP-regulated mRNAs encode ribosomal proteins and translation initiation factors that are coordinately upregulated in response to growth cues mediated by the Target of Rapamycin (TOR) pathway and the TOR complex 1 (mTORC1) (Hornstein, Tang, & Meyuhas, 2001; Iadevaia, Liu, & Proud, 2014; E. Kim, Goraksha-Hicks, Li, Neufeld, & Guan, 2008; Meyuhas & Kahan, 2015; Pallares-Cartes, Cakan-Akdogan, & Teleman, 2012) Indeed, 76 of the 87 Aramis targets were ribosomal proteins, and 9 were known or putative translation factors, consistent with TOP-containing RNAs in vertebrates (**Figure 2.7C, Supplemental Table 2.6**). To determine if the putative TOP motifs that we identified are sensitive to TORC1 activity, we designed "TOP reporter" constructs.

Specifically, the germline-specific *nanos* promoter was employed to drive expression of an mRNA with 1) the 5'UTR of the *aramis* target *RpL30*, which contains a putative TOP motif, 2) the coding sequence for a GFP-HA fusion protein and 3) a 3'UTR (K10) that is not translationally repressed (Flora, Wong-Deyrup, et al., 2018b; Serano, Cheung, Frank, & Cohen, 1994), referred to as the WT-TOP reporter (**Figure 2.11D**). As a control, we created a construct in which the polypyrimidine sequence was mutated to a polypurine sequence referred to as the Mut-TOP reporter (**Figure 2.11D**).

In *Drosophila*, TORC1 activity increases during meiotic cyst stages (Youheng Wei et al., 2014; Youheng Wei, Bettledi, Kim, Ting, & Lilly, 2019). We found that the WT-TOP reporter displayed peak expression in 8-cell cysts, whereas the Mutant-TOP reporter did not (**Figure 2.11E-F**”), suggesting that the WT-TOP reporter is sensitive to TORC1 activity. Moreover, depletion of *Nitrogen permease regulator-like 3* (*Nprl3*), an inhibitor of TORC1 (Youheng Wei et al., 2014), led to a significant increase in expression of the WT-TOP reporter but not the Mutant-TOP reporter (**Figure 2.12A-E**). Additionally, to attenuate TORC1 activity, we depleted *raptor*, one of the subunits of the TORC1 complex (Hong, Mannan, & Inoki, 2012; Loewith & Hall, 2011). Here we found that the WT-TOP reporter had a significant decrease in reporter expression while the Mutant-TOP reporter did not show a decrease in expression (**Figure 2.12F-J**). Taken together, our data suggest that Aramis-target transcripts contain TOP motifs that are sensitive to TORC1 activity. However, we note that our TOP reporter did not recapitulate the pattern of Non1::GFP expression, suggesting that Non1 may have additional regulators that modulate its protein levels in the cyst stages.

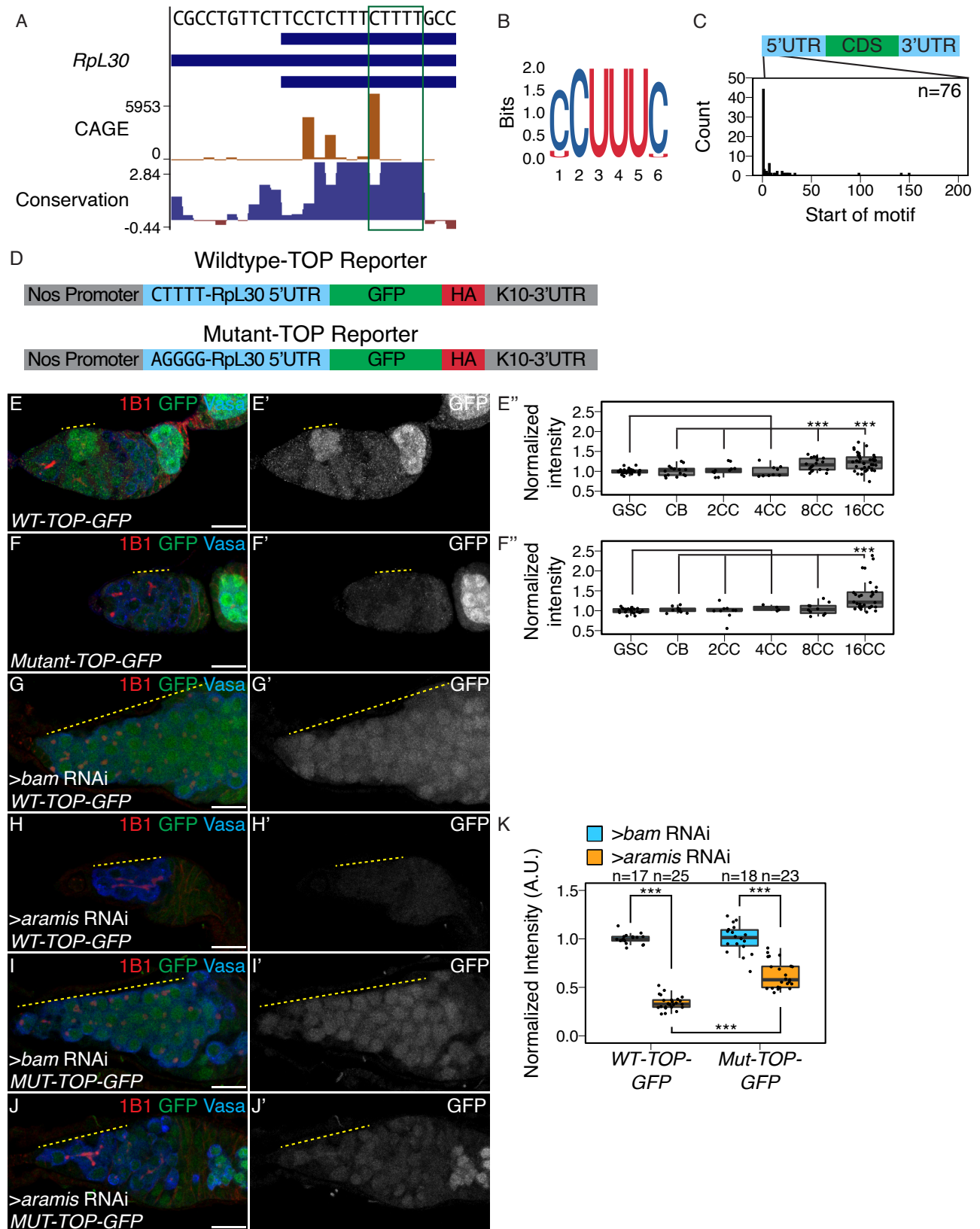


Figure 2.11: Aramis regulated mRNAs contain a TOP motif.

(A) Genome browser tract of *RpL30* locus in ovary CAGE-seq data showing the proportion of transcripts that are produced from a given TSS (orange). Predominant TSSs are shown in orange and putative TOP motif indicated with a green box. The bottom blue and red graph represents sequence conservation of the locus across *Diptera*. The dominant TSS initiates with a canonical TOP motif. **(B)** Sequence logo generated from *de novo* motif discovery on the first 200 bases downstream of CAGE derived TSSs of *aramis* translation target genes resembles a canonical TOP motif. **(C)** Histogram representing the location of the first 5-mer polypyrimidine sequence from each CAGE based TSS of *aramis* translation target genes demonstrates that the TOP motifs occur proximal to the TSS (n=76 targets). **(D)** Diagram of the *WT* and *Mut-TOP-GFP* reporter constructs indicating the TOP sequence that is mutated by transversion in the Mutant reporter (blue). **(E-F”)** Confocal images and quantifications of **(E-E’)** *WT-TOP-GFP* and **(F-F’)** *Mut-TOP-GFP* reporter expression stained for 1B1 (red), GFP (green, grayscale), and Vasa (blue). Yellow dotted-line marks increased reporter expression in 8-cell cysts of *WT-TOP-GFP* but not in *Mut-TOP-GFP*. Reporter expression was quantified over germline development for **(E”)** *WT-TOP-GFP* and **(F”)** *Mut-TOP-GFP* reporter expression and normalized to expression in the GSC reveals dynamic expression based on the presence of a TOP motif. **(G-H’)** Confocal images of *WT-TOP-GFP* reporter ovarioles showing 1B1 (red), GFP (green, grayscale), and Vasa (blue) in **(G-G’)** *bam* germline depletion as a developmental control and **(H-H’)** *aramis* germline depleted ovaries. Yellow dotted lines indicate germline. **(I-J’)** Confocal images of *Mut-TOP-GFP* reporter expression showing 1B1 (red), GFP (green, grayscale), and Vasa (blue) in **(I-I’)** *bam* RNAi and **(J-J’)** *aramis* germline RNAi. Yellow dotted lines indicate germline. **(K)** A.U. quantification of WT and Mutant TOP reporter expression in undifferentiated daughter cells in *bam* RNAi compared *aramis* RNAi demonstrates that the *WT-TOP-GFP* reporter shows significantly lower expression in *aramis* RNAi than the *Mut-TOP-GFP* relative to the expression of the respective reporters in *bam* RNAi indicating that the presence of a TOP motif sensitizes transcripts to regulation (n=17-25 germaria per genotype, with Welch's t-test *** = p<0.001). Scale bar for all images is 15 micron.

TOP mRNAs show increased translation in response to TOR signaling, leading to increased ribosome biogenesis (Jefferies et al., 1997; J.-J. Jia et al., 2021; Powers & Walter, 1999; Thoreen et al., 2012). However, to our knowledge, whether reduced ribosome biogenesis can coordinately diminish the translation of TOP mRNAs to balance and lower ribosome protein production and thus balance the levels of the distinct components needed for full ribosome assembly is not known. To address this question, we crossed the transgenic flies carrying

the WT-TOP reporter and Mutant-TOP reporter into *bam* and *aramis*, *athos*, and *porthos* germline RNAi backgrounds. We found that the expression from the WT-TOP reporter was reduced by 2.9-fold in the germline of *aramis* RNAi ovaries compared to *bam* RNAi ovaries (**Figure 2.11F-G, J**). In contrast, the Mutant-TOP reporter was only reduced by 1.6-fold in the germline of *aramis* RNAi ovaries compared to *bam* RNAi ovaries (**Figure 2.11H-J**). We observed the same trend for *athos* and *porthos* (**Figure 2.12K-Q**). This suggests that the TOP motif-containing mRNAs are sensitive to ribosome biogenesis.

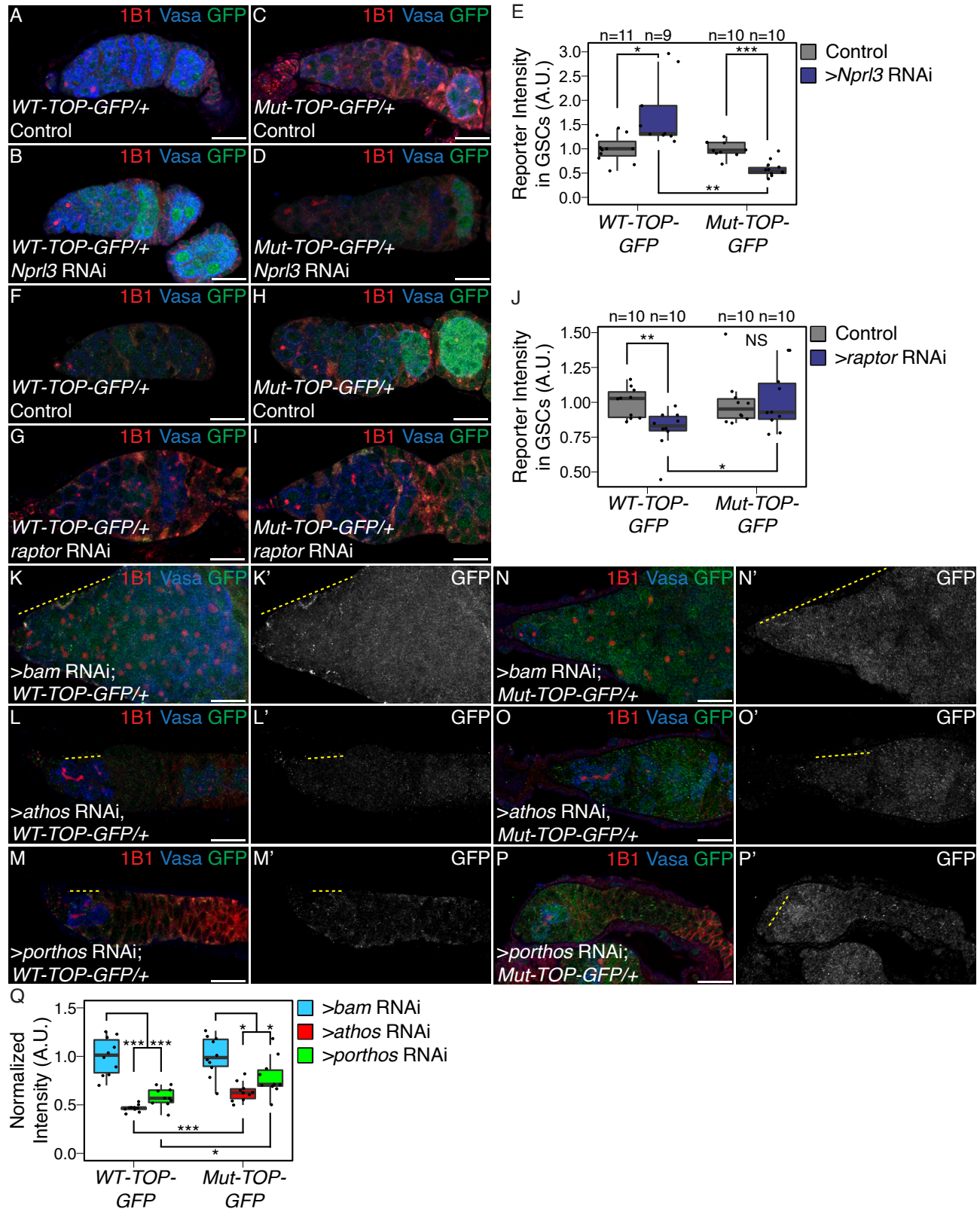


Figure 2.12: TORC1 activity, Athos, and Porthos, regulate TOP expression in the germarium, related to Figure 2.11.

(A-B) Confocal images of *WT-TOP* reporter expression stained for 1B1 (red), GFP (green), and Vasa (blue) in **(A)** *nosGAL4*, driver control ovaries and **(B)** ovaries depleted of *Nprl3* in the germline. **(C-D)** Confocal images of *Mut-TOP-GFP* reporter expression stained for 1B1 (red), GFP (green, grayscale), and Vasa (blue) in **(C)** *nosGAL4*, driver control ovaries and **(D)** ovaries depleted of *Nprl3* in the germline. **(E)** A.U. quantification of WT and Mutant TOP reporter expression in GSCs of *nosGAL4*, driver control ovaries and GSCs of *Nprl3* germline depleted ovaries normalized to Vasa expression indicate that the relative expression of the *WT-TOP-GFP* reporter is higher than the *Mut-TOP-GFP* reporter (n=9-11 germania per genotype, Welch's t-test, * = p<0.05, ** = p<0.01, *** = p<0.001). **(F-G)** Confocal images of *WT-TOP* reporter expression stained for 1B1 (red), GFP (green), and Vasa (blue) in **(F)** *nosGAL4*, driver control ovaries and **(G)** ovaries depleted of *raptor* in the germline. **(H-I)** Confocal images of *Mut-TOP-GFP* reporter expression stained for 1B1 (red), GFP (green), and Vasa (blue) in **(H)** *nosGAL4*, driver control ovaries and **(I)** ovaries depleted of *raptor* in the germline. **(J)** A.U. quantification of WT and Mutant TOP reporter expression in GSCs of *nosGAL4*, driver control ovaries and GSCs of *raptor* germline depleted ovaries normalized to Vasa expression indicate that the relative expression of the *WT-TOP-GFP* reporter is lower than the *Mut-TOP-GFP* reporter (n=10 germania per genotype, Welch's t-test, * = p<0.05, ** = p<0.01). **(K-M')** Confocal images of *WT-TOP-GFP* reporter ovarioles showing 1B1 (red), GFP (green, grayscale), and Vasa (blue) in **(K-K')** *bam* germline depletion as a developmental control, **(L-L')** *athos* germline depleted ovaries, and **(M-M')** *porthos* germline depleted ovaries. Yellow dotted lines indicate germline. **(N-P')** Confocal images of *Mut-TOP-GFP* reporter expression showing 1B1 (red), GFP (green, grayscale), and Vasa (blue) in **(N-N')** *bam* RNAi, **(O-O')** *athos* germline RNAi, and **(P-P')** *porthos* germline depleted ovaries. Yellow dotted lines indicate germline. **(Q)** A.U. quantification of WT and Mutant TOP reporter expression in undifferentiated daughter cells in *bam* RNAi compared *athos* or *porthos* RNAi demonstrates that the *WT-TOP-GFP* reporter shows significantly lower expression in *athos* and *porthos* RNAi than the *Mut-TOP-GFP* relative to the expression of the respective reporters in *bam* RNAi indicating that the presence of a TOP motif sensitizes transcripts to regulation (n=17-25 germania per genotype, with Welch's t-test with , ** = p<0.01, *** = p<0.001). Scale bar for images is 15 micron.

2.3.5 Larp binds TOP sequences in *Drosophila*

Next, we sought to determine how TOP-containing mRNAs are regulated downstream of Aramis. In mammalian cells, Larp1 is a critical negative regulator of TOP-containing RNAs during nutrient deprivation (Berman et al., 2020; Bruno D. Fonseca et al., 2015; Hong et

al., 2017; Philippe, van den Elzen, Watson, & Thoreen, 2020; Tcherkezian et al., 2014).

Therefore, we hypothesized that *Drosophila* Larp reduces the translation of TOP-containing mRNAs when rRNA biogenesis is reduced upon loss of *aramis*. First, using an available gene-trap line in which endogenous Larp is tagged with GFP and 3XFLAG, we confirmed that Larp was robustly expressed throughout all stages of oogenesis including in GSCs (**Figure 2.14A-A'**).

Next, we performed electrophoretic mobility shift assays (EMSA) to examine protein-RNA interactions with purified *Drosophila* Larp-DM15, the conserved domain that binds to TOP sequences in vertebrates (Roni M. Lahr et al., 2017). As probes, we utilized capped 42-nt RNAs corresponding to the 5'UTRs of *RpL30* and *Non1*, including their respective TOP sequences. We observed a gel shift with these RNA oligos in the presence of increasing concentrations of Larp-DM15 (**Figure 2.13A-A'**, **Figure 2.14B**), and this shift was abrogated when the TOP sequences were mutated to purines (**Figure 2.14C-C'**). To determine if Larp interacts with TOP-containing mRNAs *in vivo*, we immunopurified Larp::GFP::3XFLAG from the ovaries of the gene-trap line and performed RNA-seq (**Figure 2.14D**). We uncovered 156 mRNAs that were bound to Larp, and 84 of these were among the 87 *aramis* translationally regulated targets, including *Non1*, *RpL30*, and *RpS2* (**Figure 2.13B-C**, **Supplemental Table 2.7**). Thus, *Drosophila* Larp binds to TOP sequences *in vitro* and TOP-containing mRNAs *in vivo*.

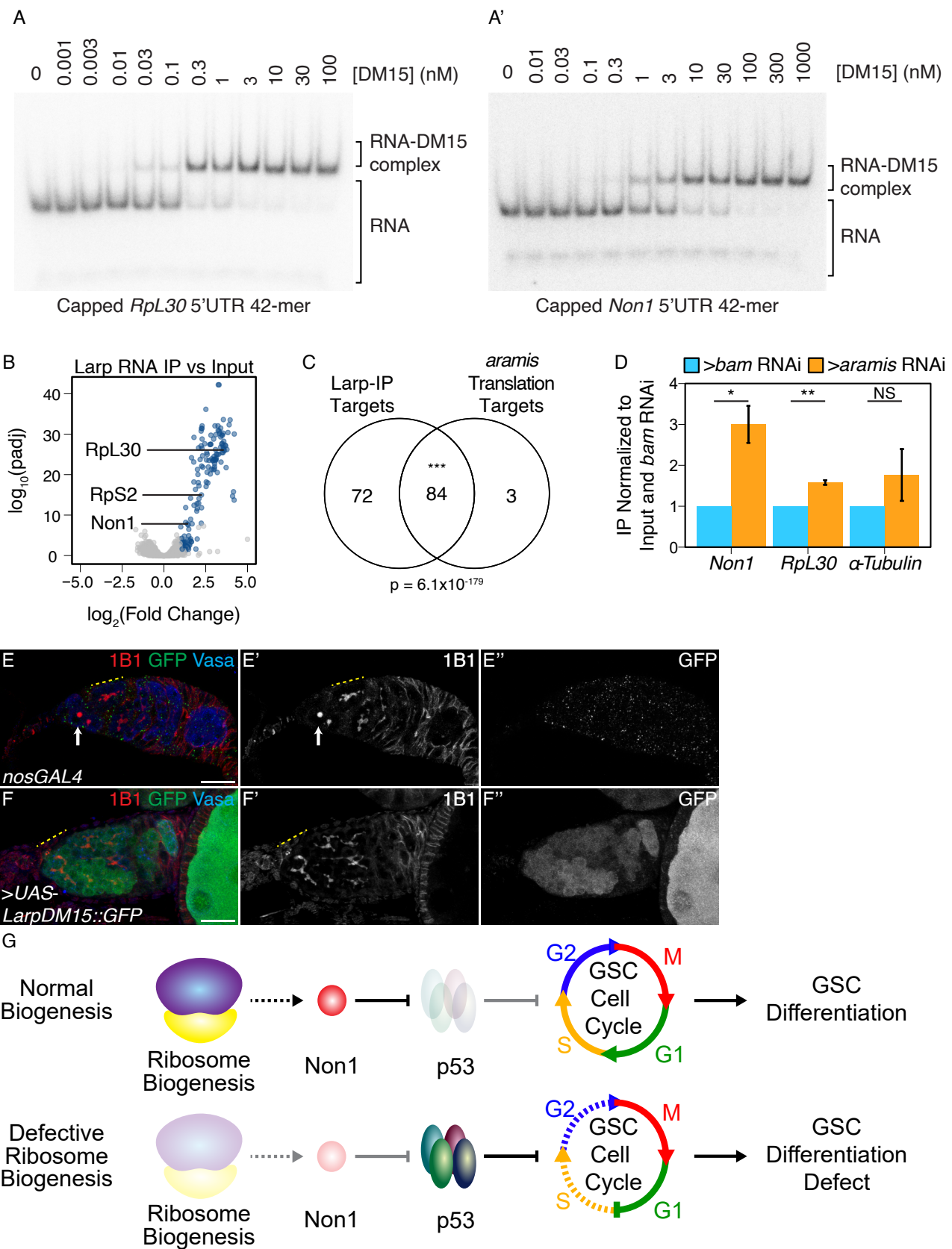


Figure 2.13: Larp binds to TOP mRNAs and binding is regulated by Aramis.

(A-A') EMSA of Larp-DM15 and the leading 42 nucleotides of **(A)** *RpL30* and **(A')** *Non1* with increasing concentrations of Larp-DM15 from left to right indicates that both RNAs bind to Larp-DM15. **(B)** Volcano plot of mRNAs in Larp::GFP::3XFLAG IP compared to input. Blue points represent mRNAs significantly enriched in Larp::GFP::3XFLAG compared to input, but not enriched in an IgG control compared to input. **(C)** Venn diagram of overlapping Larp IP targets and *aramis* RNAi polysome seq targets indicates that Larp physically associates with mRNAs that are translationally downregulated in germline *aramis* RNAi ($p < 0.001$, Hypergeometric Test). **(D)** Bar plot representing the fold enrichment of mRNAs from Larp RNA IP in germline *aramis* RNAi relative to matched *bam* RNAi ovaries as a developmental control measured with qPCR ($n=3$, * = $p < 0.5$, ** = $p < 0.01$, NS = non-significant, One-sample t-test, $\mu=1$) indicates that more of two *aramis* translation targets *Non1* and *RpL30* are bound by Larp in *aramis* RNAi. **(E-F")** Confocal images of **(E-E")** *nosGAL4*, driver control and **(F-F")** ovaries overexpressing the DM15 region of Larp in the germline ovaries stained for 1B1 (red, left grayscale), Vasa (blue), and Larp-DM15::GFP (green, right grayscale). Overexpression of Larp results in an accumulation of extended 1B1 structures (highlighted with a dotted yellow line), marking interconnected cells when Larp-DM15 is overexpressed compared to *nosGAL4*, driver control ovaries. **(G)** In conditions with normal ribosome biogenesis *Non1* is efficiently translated, downregulating p53 levels allowing for progression through the cell cycle. When ribosome biogenesis is perturbed *Non1* is not translated to sufficient levels, resulting in the accumulation of p53 and cell cycle arrest. Dotted lines indicate indirect affects. Scale bar for all images is 15 micron.

To test our hypothesis that *Drosophila* Larp inhibits the translation of TOP-containing mRNAs upon loss of *aramis*, we immunopurified Larp::GFP::3XFLAG from germline *bam* RNAi ovaries and germline *aramis* RNAi ovaries. Larp protein is not expressed at higher levels in *aramis* RNAi compared to developmental control *bam* RNAi (**Figure 2.14E-G**). Larp protein is also not expressed at higher levels in *bam* RNAi; *aramis* RNAi germline knockdown compared to *bam* RNAi as a control (**Figure 2.14H-I**). We found that Larp binding to *aramis* target mRNAs *Non1* and *RpL30* was increased in *aramis* RNAi ovaries compared to *bam* RNAi ovaries (**Figure 2.13D**, **Figure 2.14J**). In contrast, a non-target mRNA that does not contain a TOP motif, *alpha-tubulin* mRNA, did not have a significant increase in binding to Larp in *aramis* RNAi ovaries compared to *bam* RNAi ovaries. Overall,

these data suggest that reduced rRNA biogenesis upon loss of *aramis* increases Larp binding to the TOP-containing mRNAs *Non1* and *RpL30*.

If loss of *aramis* inhibits the translation of TOP-containing mRNAs due to increased binding of Larp to its targets, then overexpression of Larp would be expected to phenocopy germline depletion of *aramis*. Unphosphorylated Larp binds to TOP motifs more efficiently, but the precise phosphorylation sites of *Drosophila* Larp, to our knowledge, are currently unknown (Hong et al., 2017). To circumvent this issue, we overexpressed the DM15 domain of Larp which we showed binds the *RpL30* and *Non1* TOP motifs *in vitro* (**Figure 2.13A-A'**), and, based on homology to mammalian Larp1, lacks majority of the putative phosphorylation sites (J.-J. Jia et al., 2021; Roni M. Lahr et al., 2017; Philippe, Vasseur, Debart, & Thoreen, 2018). We found that overexpression of a Larp-DM15::GFP fusion in the germline resulted in fusome-like structures extending from the niche (**Figure 2.13E-F'**). Additionally, ovaries overexpressing Larp-DM15 had 32-cell egg chambers, which were not observed in control ovaries (**Figure 2.14K-K'**). The presence of 32-cell egg chambers is emblematic of cytokinesis defects that occur during early oogenesis (Mathieu et al., 2013; Matias, Mathieu, & Huynh, 2015; Sanchez et al., 2016). Our findings indicate that these cells are delayed in cytokinesis and that over expression of Larp partially phenocopies depletion of *aramis*.

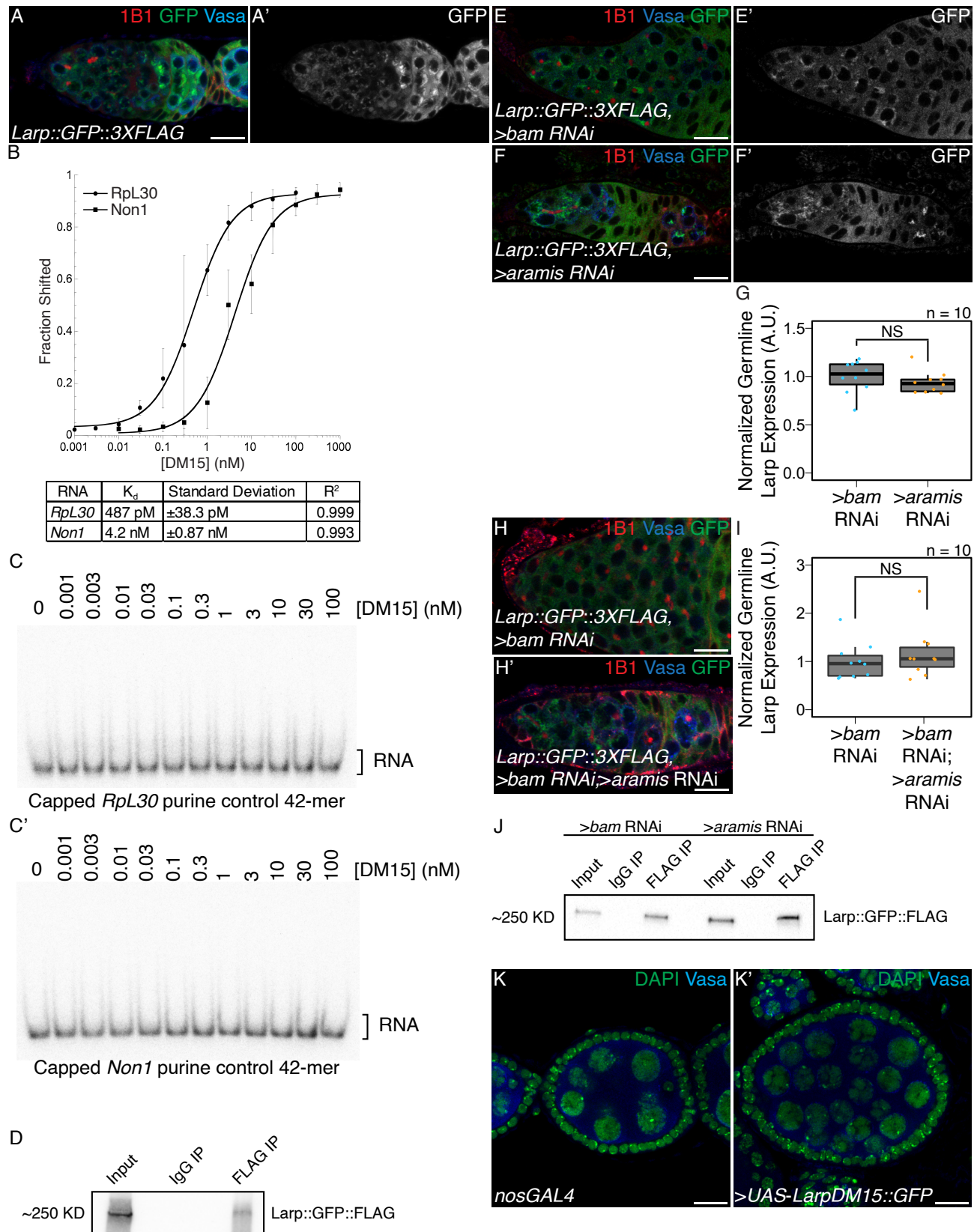


Figure 2.14: Larp binds specifically to TOP containing mRNAs and regulates cytokinesis, related to Figure 2.13.

(A-A') Confocal images of germaria stained for 1B1 (red), Vasa (blue), and *Larp GFP-3XFLAG* (green, grayscale) indicates Larp is expressed throughout early oogenesis. **(B)** Quantification of EMSAs and summary of K_d of the protein-RNA interactions. **(C-C')** EMSA of Larp-DM15 and the leading 42 nucleotides of **(B)** *RpL30* and **(B')** *Non1* with their TOP sequence mutated to purines as a negative control with increasing concentrations of Larp-DM15 from left to right indicates that Larp-DM15 requires a leading TOP sequence for its binding. **(D)** Western of representative IP of Larp::GFP::3XFLAG from ovary tissue used for RNA IP-seq. **(E-F')** Confocal images of Larp::GFP::3XFLAG reporter expression stained for 1B1 (red), GFP (green, grayscale), and Vasa (blue) in **(E-E')** *bam* and **(F-F')** *aramis*-depleted germaria. **(G)** A.U. quantification of Larp::GFP::3XFLAG reporter expression in the germline of *bam* RNAi and *aramis* RNAi normalized to germline Vasa intensity demonstrates that the germline expression of Larp is not elevated in *aramis* germline RNAi compared to *bam* germline RNAi as a developmental control ($n=10$, NS = $p>0.05$, Welch's t-test). **(H-H')** Confocal images of Larp::GFP::3XFLAG reporter expression stained for 1B1 (red), GFP (green), and Vasa (blue) in **(H)** *bam* and **(H')** *bam*; *aramis*-depleted germaria. **(I)** A.U. quantification of Larp::GFP::3XFLAG reporter expression in the germline of *bam* RNAi and *bam* RNAi ; *aramis* RNAi demonstrates that the germline expression of Larp normalized to somatic Larp expression is not elevated in *bam*; *aramis* germline RNAi compared to *bam* germline RNAi as a developmental control ($n=10$, NS = $p>0.05$, Welch's t-test). **(J)** Western of representative IP of Larp::GFP::3XFLAG from ovary tissue used for RNA IP qPCR. **(K-K')** Confocal images of **(K)** *nosGAL4*, driver control and **(K')** ovaries overexpressing the DM15 region of Larp in the germline ovaries stained for DAPI (green) and Vasa (blue). Overexpression of Larp-DM15 results in the production of 32-cell egg chambers which indicates it causes a cytokinesis defect. Scale bar for all images is 15 micron.

2.4 Discussion

During *Drosophila* oogenesis, efficient ribosome biogenesis is required in the germline for proper GSC cytokinesis and differentiation. The outstanding questions that needed to be addressed were: 1) Why does disrupted ribosome biogenesis impair GSC abscission and differentiation? And 2) How does the GSC monitor and couple ribosome abundance to differentiation? Our results suggest that a germline ribosome biogenesis defect stalls the

cell cycle, resulting a loss of differentiation and the formation of stem-cysts. We discovered that proper ribosome biogenesis is monitored through a translation control module that allows for co-regulation of ribosomal proteins and a p53 repressor. Loss of *aramis*, *athos* and *porthos* reduces ribosome biogenesis and inhibits translation of a p53 repressor, leading to p53 stabilization, cell cycle arrest and loss of stem cell differentiation (**Figure 2.13G**).

2.4.1 Aramis, Athos, and Porthos are required for efficient ribosome biogenesis in *Drosophila*

We provide evidence that Aramis, Athos and Porthos play a role in ribosome biogenesis in *Drosophila*, similar to their orthologs in yeast (Bohnsack, Kos, & Tollervey, 2008; Granneman, Bernstein, Bleichert, & Baserga, 2006; Khoshnevis et al., 2016; O 'day, Chavanikamanil, & Abelson, 1996) and mammals (Sekiguchi, Hayano, Yanagida, Takahashi, & Nishimoto, 2006; Tafforeau et al., 2013; Yandong Zhang, Forys, Miceli, Gwinn, & Weber, 2011). Their role in ribosome biogenesis is likely a direct function of these helicases as they physically interact with precursor rRNA. In yeast, Rok1, the ortholog of Aramis, binds to several sites on pre-rRNA, predominantly in the 18S region (Bohnsack, Kos, & Tollervey, 2008; Khoshnevis et al., 2016; R. Martin et al., 2014). This is consistent with the small subunit ribosome biogenesis defect we observe upon loss of *aramis* in *Drosophila*. Rrp3, the yeast ortholog of Porthos, promotes proper cleavage of pre-rRNA and is required for proper 18S rRNA production (Granneman, Bernstein, Bleichert, & Baserga, 2006; O 'day, Chavanikamanil, & Abelson, 1996). DDX47, the mammalian ortholog of Porthos, binds to early rRNA precursors as well as proteins involved in ribosome biogenesis (Sekiguchi, Hayano, Yanagida,

Takahashi, & Nishimoto, 2006). Consistent with these findings, we find that Aramis and Porthos promote 40S ribosome biogenesis. DHX33, the mammalian ortholog of Athos, has been implicated in facilitating rRNA synthesis (Yandong Zhang, Forys, Miceli, Gwinn, & Weber, 2011). In contrast, we find that Athos promotes 60S ribosome biogenesis by directly interacting with rRNA. However, we cannot exclude the possibility that Athos also affects transcription of rRNA in *Drosophila* as it does in mammals (Yandong Zhang, Forys, Miceli, Gwinn, & Weber, 2011). Overall, we find that each mammalian ortholog of Aramis, Athos, and Porthos has consistent ribosome subunit defects, suggesting that the function of these helicases is conserved from flies to mammals. Intriguingly, DDX52 (Aramis) is one of the 15 genes deleted in 17q12 syndrome (Hendrix, Clemens, Canavan, Surti, & Rajkovic, 2012). 17q12 syndrome results in delayed development, intellectual disability, and, more rarely, underdevelopment of organs such as the uterus (Bernardini et al., 2009; Hendrix, Clemens, Canavan, Surti, & Rajkovic, 2012). Our finding that Aramis disrupts stem cell differentiation could explain some of the poorly understood defects in 17q12 syndrome.

2.4.2 Ribosome biogenesis defects leads to cell cycle defects mediated by p53

Here we report that three RNA helicases, *aramis*, *athos*, and *porthos*, that promote proper ribosome biogenesis in *Drosophila* are required in the germline for fertility. Loss of *aramis*, *athos*, and *porthos* causes formation of a “stem-cyst” and loss of later stage oocytes. Stem-cysts are a characteristic manifestation of ribosome biogenesis deficiency wherein GSCs are unable to complete cytokinesis and fail to express the differentiation factor Bam, which in

GSC daughters is initiated at G2 of the cell cycle (Sanchez et al., 2016; Q. Zhang, Shalaby, & Buszczak, 2014). Our RNA seq and cell cycle analysis indicates that depletion of *aramis* blocks the cell cycle at G1, and that failure to progress to G2 prevents abscission and expression of Bam. Thus, our results suggest that ribosome biogenesis defects in the germline stall the cell cycle, resulting in formation of stem-cysts and sterility.

In most tissues in *Drosophila*, p53 primarily activates apoptosis, however, in the germline p53 is activated during meiosis and does not cause cell death (Fan et al., 2010; W.-J. Lu, Chapo, Roig, & Abrams, 2010). Furthermore, p53 activation in the germline is required for germline repopulation and GSC survival after genetic insult, implicating p53 as a potential cell cycle regulator (Ma et al., 2016; Tasnim & Kelleher, 2018). Our observation that reduction of *p53* partially rescues a stem-cyst defect caused by ribosome deficiency due to germline depletion of *aramis* indicates that the G1 block in GSCs is, in part, mediated by p53 activation. Thus, in *Drosophila* GSCs, p53 blocks the GSC cell cycle and is sensitive to ribosome biogenesis. Furthermore, while overexpression of p53 causes germline death, it is also sufficient to induce the formation of stem-like cysts demonstrating p53 plays a key regulatory role in GSC cell cycle. The developmental upregulation of p53 during GSC differentiation concomitant with lower ribosome levels parallels observations in disease states, such as ribosomopathies (Calo et al., 2018; Deisenroth & Zhang, 2010; Pereboom, van Weele, Bondt, & MacInnes, 2011; Yelick & Trainor, 2015).

We find that p53 levels in GSCs are regulated by the conserved p53 regulator Non1. In mammalian cells, increased free RpS7 protein due to nucleolar stress binds and sequesters a repressor of p53, MDM2, freeing p53, resulting in G1 cell cycle arrest (Deisenroth & Zhang, 2010; Yanping Zhang & Lu, 2009). *Drosophila* have no identified homolog to MDM2. It is

not fully known how ribosome levels are monitored in *Drosophila* in the absence of MDM2 and how this contributes to cell cycle progression. In *Drosophila*, Non1 levels are high in the GSCs and p53 is low, and reciprocally Non1 levels are low during meiosis, but p53 is expressed. Our finding that loss of Aramis leads to diminished Non1 and elevated p53, and that either loss of p53 or elevated Non1 suppress differentiation defects caused by loss of Aramis, suggests that, in the female germline, Non1 may fulfill the function of Mdm2 by promoting p53 degradation during *Drosophila* oogenesis. While Non1 has been shown to directly interact with p53, how it regulates p53 levels in both humans and *Drosophila* is not known (L. Li et al., 2018; Lunardi et al., 2010). Overall, our data place Non1 downstream of ribosome biogenesis and upstream of p53 in controlling cell cycle progression and GSC differentiation. However, our data do not rule out that Non1 may also act upstream of or in parallel to Aramis.

The vertebrate ortholog of Non1, GTPBP4, also controls p53 levels and is upregulated in some cancers (L. Li et al., 2018; Lunardi et al., 2010; Yu, Jin, Zhang, & Xu, 2016). This suggests that there may be parallel pathways for monitoring ribosome levels via p53 in different tissue types. Unlike *Drosophila* Non1, its ortholog, GTPBP4 has not been identified as a TOP mRNA, so if it similarly acts as a mediator between ribosome biogenesis and the cell cycle it is likely activated in a somewhat different manner (Philippe, van den Elzen, Watson, & Thoreen, 2020). However, mammalian Larp1 is required for proper cell cycle progression and cytokinesis (Burrows et al., 2010; Tcherkezian et al., 2014). Excitingly several differentiation and cell cycle regulation genes in mammals are TOP mRNAs regulated by Larp1, including Tumor Protein, Translationally-Controlled 1 (TPT1) and Nucleosome Assembly Protein 1 Like 1 (NAP1L1) (Philippe, van den Elzen, Watson, & Thoreen, 2020).

TPT1 is a cancer associated factor that has been implicated in activating pluripotency (Koziol, Garrett, & Gurdon, 2007). Similarly, NAP1L1, a nucleosome assembly protein, is required to maintain proper cell cycle control as loss of NAP1L1 results in cell cycle exit and premature differentiation (Qiao et al., 2018). Overall, although the specific targets of Larp1 in mammals may differ from those in *Drosophila*, the mechanism by which Larp modulates cell cycle and differentiation may be conserved.

2.4.3 Ribosome biogenesis defects leads to repression of TOP-containing mRNA

TOP-containing mRNAs are known to be coregulated to coordinate ribosome production in response to nutrition or other environmental cues (Kimball, 2002; Meyuhas & Kahan, 2015; H. Tang et al., 2001). Surprisingly, our observation that loss of *aramis* reduces translation, albeit indirectly via regulation of ribosome biogenesis, of a cohort of TOP-containing mRNAs, including Non1, suggests that the TOP motif also sensitizes their translation to lowered levels of ribosome biogenesis. This notion is supported by TOP reporter assays demonstrating that reduced translation upon loss of *aramis* requires the TOP motif. We hypothesize that limiting TOP mRNA translation lowers ribosomal protein production to maintain a balance with reduced rRNA production. This feedback mechanism would prevent the production of excess ribosomal proteins that cannot be integrated into ribosomes and the ensuing harmful aggregates (Tye et al., 2019). Additionally, it would coordinate rRNA production and ribosomal protein translation during normal germline development, where it is known that the level of ribosome biogenesis and of global translation are dynamic (Blatt,

Martin, Breznak, & Rangan, 2020; Fichelson et al., 2009; Sanchez et al., 2016; Q. Zhang, Shalaby, & Buszczak, 2014).

2.4.4 Larp transduces growth status to ribosome biogenesis targets

Recent work has shown that the translation and stability of TOP-containing mRNAs are mediated by Larp1 and its phosphorylation (Berman et al., 2020; Hong et al., 2017; J.-J. Jia et al., 2021). We found that perturbing rRNA production and thus ribosome biogenesis, without directly targeting ribosomal proteins, similarly results in dysregulation of TOP mRNAs. Our data show that *Drosophila* Larp binds the *RpL30* and *Non1* 5'UTR in a TOP-dependent manner *in vitro* and to 97% of the translation targets we identified *in vivo*. Together these data suggest that rRNA production regulates TOP mRNAs via Larp. Furthermore, the cytokinesis defect caused by overexpression of Larp-DM15 in the germline suggests that Larp regulation could maintain the homeostasis of ribosome biogenesis more broadly by balancing the expression of ribosomal protein production with the rate of other aspects of ribosome biogenesis, such as rRNA processing, during development.

Previous studies indicate that unphosphorylated Larp1 binds to and represses its targets more efficiently than phosphorylated Larp1 (Bruno D. Fonseca et al., 2018; Hong et al., 2017; J.-J. Jia et al., 2021). In mammalian systems Larp1 has been shown to be phosphorylated by the TORC1 complex, AKT, and CDK1 (Berman et al., 2020; Hong et al., 2017; J.-J. Jia et al., 2021). In *Drosophila*, it has been shown that Pink1 can phosphorylates Larp, and the Pink1 dependent phosphorylation sites have been identified in *Drosophila* Larp (Yi

Zhang et al., 2019). However, to our knowledge, Larp phosphorylation sites have not been systematically catalogued, nor has it been studied if TORC1, AKT, or CDK1 phosphorylate Larp in *Drosophila*. We have demonstrated that expression of our TOP-reporter is dependent on Raptor and TOP-reporter expression is repressed by Nprl3 (**Figure 2.12A-J**). These results suggest a model where TORC1 either directly or indirectly monitors ribosome biogenesis status by regulating the activity of Larp. Thus, although we do not know the identity of the kinase that phosphorylates Larp in *Drosophila* definitively, we hypothesize that Larp is not phosphorylated upon loss of *aramis*, *athos* and *porthos*, when ribosome biogenesis is perturbed. We propose that until ribosome biogenesis homeostasis is reached, this kinase will remain inactive, continuously increasing the pool of dephosphorylated Larp. In this scenario, as dephosphorylated Larp accumulates, it begins to bind its targets. Initially, it will bind its highest affinity targets, presumably encoding ribosomal proteins and repress their translation to rebalance ribosomal protein production with rRNA production. Consistent with this model, the TOP motif in *RpL30* is bound by Larp even more tightly with a nearly 9-fold higher affinity compared to the *Non1* TOP site (**Figure 2.14B**). We propose that such differences in affinity may allow Larp to repress ribosomal protein translation to facilitate cellular homeostasis without immediately causing cell cycle arrest. However, if homeostasis cannot be achieved and sufficient dephosphorylated Larp accumulates, Larp will also bind and repress the translation of lower affinity targets. Repression of *Non1* in this manner would result in cell cycle arrest and block differentiation as occurs upon *aramis* depletion.

2.4.5 Ribosome biogenesis in stem cell differentiation and ribosomopathies

Ribosomopathies arise from defects in ribosomal components or ribosome biogenesis and include a number of diseases such as Diamond-Blackfan anemia, Treacher Collins syndrome, Shwachman-Diamond syndrome, and 5q-myelodysplastic syndrome (Armistead & Triggs-Raine, 2014; Drapchinskaia et al., 1999; McGowan et al., 2011; Valdez, Henning, So, Dixon, & Dixon, 2004; Warren, 2018). Despite the ubiquitous requirement for ribosomes and translation, ribosomopathies cause tissue-specific disease (Armistead & Triggs-Raine, 2014). The underlying mechanisms of tissue specificity remain unresolved.

In this study we demonstrate that loss of helicases involved in rRNA processing lead to perturbed ribosome biogenesis and, ultimately, cell cycle arrest. Given that *Drosophila* germ cells undergo an atypical cell cycle program as a normal part of their development it may be that this underlying cellular program in the germline leads to the tissue-specific symptom of aberrant stem-cyst formation (D. M. McKearin & Spradling, 1990). This model implies that other tissues would likewise exhibit unique tissue-specific manifestations of ribosomopathies due to their underlying cell state and underscores the need to further explore tissue-specific differentiation programs and development to shed light not only on ribosomopathies but also on other tissue-specific diseases associated with ubiquitous processes. Although it is also possible that phenotypic differences arise from a common molecular cause, our data suggests two sources of potential tissue specificity: 1) tissues express different cohorts of mRNAs, such as *Non1*, that are sensitive to ribosome levels. For example, we find that in *Drosophila* macrophages, RNAs that regulate the metabolic state of macrophages and influence their

migration require increased levels of ribosomes for their translation (Emtenani et al., 2021). 2) p53 activation, as has been previously described, is differentially tolerated in different developing tissues (Bowen & Attardi, 2019; Calo et al., 2018; Jones et al., 2008). Together, both mechanisms could begin to explain the tissue-specific nature of ribosomopathies and their link to differentiation.

Acknowledgements

We are grateful to all members of the Rangan and Fuchs labs for their discussion and comments on the manuscript. We also thank Dr. Sammons, Dr. Marlow and Life Science Editors for their thoughts and comments on the manuscript. Additionally, we thank the Bloomington Stock Center, the Vienna *Drosophila* Resource Center, the BDGP Gene Disruption Project, and Flybase for fly stocks, reagents, and other resources. P.R. is funded by the NIH/NIGMS (R01GM111779-06 and R01GM135628-01), G.F. is funded by NSF MCB-2047629 and NIH RO3 AI144839, D.E.S. was funded by Marie Curie CIG 334077/IRTIM and the Austrian Science Fund (FWF) grant ASI_FWF01_P29638S, and A.B is funded by NIH R01GM116889 and American Cancer Society RSG-17-197-01-RMC.

Author Contributions

Conceptualization, E.T.M., P.B., G.F., and P.R.; Methodology, E.T.M., P.B., G.F., and P.R.; Investigation, E.T.M., P.B., E.N., R.L., S.S., H.Y., T.P., and S.E.; Writing – Original Draft, E.T.M., D.E.S., and P.R.; Writing – Review & Editing, E.T.M., P.B., D.E.S., A.B., G.F., and P.R.; Funding Acquisition, G.F. and P.R.; Visualization, E.T.M., E.N.; Supervision, G.F. and P.R.

Supplemental Tables can be found along with the original publication here: XXX

Supplemental Table 2.1. Results of germline helicase RNAi screen on ovariole morphology. Results of screen of RNA helicases depleted from the germline. Reported is the majority phenotype from n=50 ovarioles.

Supplemental Table 2.2. Differential expression analysis from RNaseq of ovaries depleted of *aramis* in the germline compared to a developmental control. DEseq2 output from RNaseq of ovaries depleted of *aramis* in the germline compared to ovaries depleted of *bam* in the germline as a developmental control. Sheet 1 (Downregulated Genes) contains genes and corresponding Deseq2 output meeting the cutoffs to be considered downregulated in *aramis* RNAi compared to *bam* RNAi. Sheet 2 (Upregulated Genes) contains genes and corresponding Deseq2 output meeting the cutoffs to be considered upregulated in *aramis* RNAi compared to *bam* RNAi. Sheet 3 (All Genes) contains Deseq2 output for all genes in the dm6 assembly.

Supplemental Table 2.3. Differential expression analysis from RNaseq of ovaries depleted of *bam* and *aramis* in the germline compared to ovaries depleted of *bam* in the germline. DEseq2 output from RNaseq of ovaries depleted of *bam* and *aramis* in the germline compared to ovaries depleted of *bam* in the germline as a control. Sheet 1 (Downregulated Genes) contains genes and corresponding DEseq2 output meeting

the cutoffs to be considered downregulated in *bam*; *aramis* RNAi compared to *bam* RNAi. Sheet 2 (Upregulated Genes) contains genes and corresponding DEseq2 output meeting the cutoffs to be considered upregulated in *bam*; *aramis* RNAi compared to *bam* RNAi. Sheet 3 (All Genes) contains DEseq2 output for all genes in the dm6 assembly. Sheet 4(BP GO terms - downregulated) contains the output of a Biological Process PANTHER Overrepresentation Test of significantly enriched GO terms performed on genes identified as downregulated targets from Sheet 1. Sheet 5 (BP GO terms - upregulated) contains the output of a Biological Process PANTHER Overrepresentation Test of significantly enriched GO terms performed on genes identified as upregulated targets from Sheet 2.

Supplemental Table 2.4. Analysis of polysome-seq of ovaries depleted of *aramis* in the germline compared to developmental controls. Results of polysome-seq from ovaries depleted of *aramis* in the germline, ovaries depleted of *bam*, and ovaries overexpressing tkv in the germline as developmental controls. Sheet 1 (Downregulated Genes) contains genes and corresponding polysome/input ratio values and values representing the difference in the polysome/input ratios between *aramis* RNAi and the developmental controls meeting the cutoffs to be considered downregulated in *aramis* RNAi. Sheet 2 (Upregulated Genes) contains genes and corresponding polysome/input ratio values and values representing the difference in the polysome/input ratios between *aramis* RNAi and the developmental controls meeting the cutoffs to be considered upregulated in *aramis* RNAi. Sheet 3 (All Genes) contains DEseq2 output for all genes in the dm6 assembly.

Supplemental Table 2.5. Enrichment analysis of Aramis RNA IPmRNA-seq.

Results of Aramis::GFP::FLAG IP/IgG/Input mRNASeq. Each sheet contains the output of results from DEseq2. Sheet 1 (aramis polysome IP Enrichment) contains the enrichment value of all *aramis* polysome targets from Aramis IP. Sheet 2 (aramis polysome IgG Enrichment) contains the enrichment value of all *aramis* polysome targets from Aramis IgG control. Sheet 3 (Aramis IP Targets) contains Aramis IP targets as defined in methods. Sheet 4 (IP vs In Enriched) contains genes significantly enriched in the Aramis IP samples compared to the input samples. Sheet 5 (IgG vs In Enriched) contains genes significantly enriched (see methods) in the IgG samples compared to the input samples. Sheet 6 (IPvsIn All Genes) contains the DEseq2 output of all genes in the Aramis IP samples compared to the input samples. Sheet 7 (IgG vs In All Genes) contains the DEseq2 output of all genes in the IgG samples compared to the input samples.

Supplemental Table 2.6. Aramis translation targets contain TOP sequences.

Sheet 1 (aramisRNAi target CAGE 5'UTRs) contains the CAGE corrected 5'UTRs of *aramis* RNAi polysome downregulated targets with leading TOP sequences and start codons annotated. Sheet 2 (TOP location) contains a list of *aramis* RNAi polysome downregulated targets and the position and sequence of the first instance of a 5-mer pyrimidine sequence downstream of the CAGE-defined TSS of each gene.

Supplemental Table 2.7. Enrichment analysis of Larp RNA IP mRNA-seq. Results of Larp::GFP::3XFLAG IP/IgG/Input mRNASeq. Each sheet contains the output of DEseq2. Sheet 1 (Larp Targets) contains Larp IP targets as defined in methods. Sheet 2 (IP vs In Enriched) contains genes significantly enriched in the Larp IP samples compared to the input samples. Sheet 3 (IgG vs In Enriched) contains genes significantly enriched (see methods) in the IgG samples compared to the input samples. Sheet 4 (IPvsIn All Genes) contains the DEseq2 output of all genes in the Larp IP samples compared to the input samples. Sheet 5 (IgG vs In All Genes) contains the DEseq2 output of all genes in the IgG samples compared to the input samples.

2.5 Materials and Methods

Resource Availability

Lead Contact:

Further information and requests for resources and reagents should be directed to and will be fulfilled by the lead contact, Prashanth Rangan (prangan@albany.edu).

Materials availability:

Materials generated during this study are available upon request.

Data and Code availability:

Sequencing data generated during this study are available on GEO under the accession GSE171350. Other data generated during this study are available from the lead contact.

Fly lines

The following Bloomington Stock Center lines were used in this study: #25751 *UAS-Dcr2;nosGAL4*, #4442 *nosGAL4;MKRS/TM6*, #32334 Aramis RNAi#1 CG5589^{HMS00325}, #56977 Athos RNAi#1 CG4901^{HMC04417}, #36589 Porthos RNAi#1 CG9253^{GL00549}, #36537 UAS-tkv.CA, #33631 bam RNAi^{HMS00029}, #6815 p53^{5A-1-4}, #4264 Harwich, #6816 p53^{11-1B-1}, #55101 FUCCI: UASp-GFP.E2f1.1-230, UASp-mRFP1.CycB.1-266/TM6B, #5431 UAS-EGFP, #18942 aramis^{f06152} Pbac{WH}CG5589f06152/TM6B, Tb1, #9503 athos Df Df(2L)BSC143/CyO, #13988 porthos^{KG} P{SUPor-P}CG9253^{KG05120}, #58178 bam RNAi P{TriP.HMJ22155}, #78777 Non1 RNAi P{TriP.HMS05872}, #61790 Larp::GFP::3XFLAG Mi{PT-GFSTF.1}larp^{MI06928-GFSTF.1}, #8841 w1118; Df(3R)Hsp70A, Df(3R)Hsp70B, #55384 Nprl3 RNAi P{TriP.HMC04072}attP40, #34814 raptor RNAi P{TriP.HMS00124}attP2

The following Vienna Stock Center lines were used in this study: Aramis RNAi#2 CG5589^{v44322}, Athos RNAi#2 CG4901^{v34905}, Aramis::GFP Pbac{fTRG01033.sfGFP-TVPTBF}VK00002, Athos::GFP Pbac{fTRG01233.sfGFP-TVPTBF}VK00033, Non1::GFP Pbac{fTRG00617.sfGFP-TVPTBF}VK00033

The following additional fly lines were used in the study: UASp-CycB::GFP (Mathieu et al., 2013), *UAS-Dcr2;nosGAL4;bamGFP*, *If/CyO;nosGAL4* (Lehmann Lab), w1118 (Lehmann lab), *tjGAL4/CyO* (Tanentzapf, Devenport, Godt, & Brown, 2007), UASp-p53 (Bakhrat, Pritchett, Peretz, McCall, & Abdu, 2010), RpS2::GFP^{CB02294} (Buszczak et al., 2007; Q. Zhang, Shalaby, & Buszczak, 2014), UASt-porthos::3XFLAG::3XHA (Emtenani et al., 2021), UASp-Non1 (this study), UASp-Larp-DM15 (this study), WT-TOP-Reporter (this study),

Mutant-TOP-Reporter (this study).

Antibodies IF

The following antibodies were used for immunofluorescence: mouse anti-1B1 1:20 (DSHB 1B1), rabbit anti-Vasa 1:833-1:4000 (Rangan Lab), chicken anti-Vasa 1:833-1:4000 (Rangan Lab) (Upadhyay et al., 2016), rabbit anti-pTyr 1:500 (Sigma T1235), rabbit anti-pMad 1:200 (Abcam ab52903), rabbit anti-GFP 1:2000 (abcam, ab6556), mouse anti-p53 1:200 (DSHB 25F4), Rabbit anti-CycB 1:200 (Santa Cruz Biotechnology, 25764), Rabbit anti-Fibrillarin 1:200 (Abcam ab5821), Mouse anti-Fibrillarin 1:50 (Fuchs Lab) (McCarthy, Deiulio, Martin, Upadhyay, & Rangan, 2018). Alexa 488 (Molecular Probes), Cy3 and Cy5 (Jackson Labs) were used at a dilution of 1:500.

Antibodies Western/IP

Mouse anti-FLAG-HRP 1:5000 (Sigma Aldrich, A8592)

Mouse anti-FLAG (Sigma Aldrich, F1804)

Anti-GAPDH-HRP 1:10,000 (Cell Signaling, 14C10)

Rabbit anti-DDX52 1:5000 (Bethyl, A303-053A)

Rabbit anti-DHX33 1:5000 (Bethyl, A300-800A)

Rabbit anti-DDX47 1:1000 (Bethyl, A302-977A)

Protein Domain Analysis

Protein domain figures were adapted from: The Pfam protein families database in 2019: S. El-Gebali et al. Nucleic Acids Research (2019). Protein Similarity values were obtained from

the DRSC/TRiP Functional Genomics Resources.

Protein Conservation Analysis

Evolutionary trees were generated using MEGA. The evolutionary history was inferred by using the Maximum Likelihood method and JTT matrix-based model. The tree with the highest log likelihood is shown. Initial tree(s) for the heuristic search were obtained automatically by applying Neighbor-Join and BioNJ algorithms to a matrix of pairwise distances estimated using a JTT model, and then selecting the topology with superior log likelihood value. Trees are drawn to scale, with branch lengths measured in the number of substitutions per site.

TOP Reporter Cloning

gBlocks (see primer list for details) were cloned into pCasper2 containing a Nos promoter, HA-tag, GFP-tag, and K10 3'UTR. PCR was used in order to amplify the gBlock and to remove the 5'-end of the RpL30 5'UTR in order to generate the 5'-UTR discovered via CAGE-seq. In order to clone the Nos promoter followed by the RpL30 5'UTR without an intervening restriction site, the portion of the plasmid 5' of the 5'UTR consisting of a portion of the plasmid backbone, a NotI restriction site, and the Nos Promoter was amplified from the pCasper plasmid using PCR. HiFi cloning was performed on the amplified fragments. The backbone was cut with NotI and SpeI and HiFi cloning was performed according to the manufacturers' instructions except the HiFi incubation was performed for 1 hour to increase cloning efficiency. Colonies were picked and cultured and plasmids were purified using standard techniques. Sequencing was performed by Eton Bioscience Inc. to confirm

the correct sequence was present in the final plasmids. Midi-prep scale plasmid was prepared using standard methods and plasmids were sent to BestGene Inc. for microinjection.

Gateway Cloning

Gateway cloning was performed as described according to the manufacturer's manual. Briefly, primers containing the appropriate Gateway *attB* sequence on the 5'-ends and gene specific sequences on the 3'-ends (see primer list for sequences) were used to PCR amplify each gene of interest. PCR fragments were BP cloned into pENTR221 as detailed in the ThermoFisher Gateway Cloning Manual and used to transform Invitrogen One Shot OmniMAX 2 T1 Phage-Resistant Cells. Resulting clones were picked and used to perform LR cloning into either pPGW or pPWG as appropriate. Cloning was carried out according to the ThermoFisher Gateway Cloning Manual except the LR incubation was carried out up to 16 hours. Colonies were picked and cultured and plasmids were purified using standard techniques. Sequencing was performed by Eton Bioscience Inc. to confirm the correct sequence was present in the final plasmids. Midi-prep scale plasmid was prepared using standard methods and plasmids were sent to BestGene Inc. for microinjection.

Egg Laying Test

Newly eclosed flies were collected and fattened overnight on yeast. Six female flies were crossed to 4 male controls and kept in cages at 25°C. Flies were allowed to lay for three days, and plates were changed and counted daily. Total number of eggs laid over the three day laying periods were determined and averaged between three replicate crosses for control and experimental crosses.

Immunostaining

Ovaries were dissected and teased apart with mounting needles in cold PBS and kept on ice for subsequent dissections. All incubations were performed with nutation. Ovaries were fixed for 10-15 min in 5% methanol-free formaldehyde in PBS. Ovaries were washed with PBT (1x PBS, 0.5% Triton X-100, 0.3% BSA) once quickly, twice for 5 min, and finally for 15 min. Ovaries were incubated overnight, up to 72 hours in PBT with the appropriate primary antibodies. Ovaries were again washed with PBT once quickly, twice for 5 min, and finally for 15 min. Ovaries were then incubated with the appropriate secondary antibodies in PBT overnight up to 72 hours at 4°C. Ovaries were washed once quickly, twice for 5 min, and finally for 15 min in PBST (1x PBS, 0.2% Tween 20 Ovaries). Ovaries were mounted with Vectashield with 4',6-diamidino-2-phenylindole (DAPI) (Vector Laboratories) and imaged on a Zeiss 710. All gain, laser power, and other relevant settings were kept constant for any immunostainings being compared. Image processing was performed in Fiji, gain was adjusted, and images were cropped in Photoshop CC 2018.

Fluorescent Imaging

Tissues were visualized and imaged were acquired using a Zeiss LSM-710 confocal microscope under the 20x— and 40x— oil objectives.

Measurement of global protein synthesis

OPP (Thermo Fisher, C10456) treatment was performed as in McCarthy (McCarthy et al., 2019). Briefly, ovaries were dissected in Schneider's media (Thermo Fisher, 21720024) and incubated in 50 µM of OPP reagent for 30 minutes. Tissue was washed in 1x PBS and fixed

for 10 minutes in 1x PBS plus 5% methanol-free formaldehyde. Tissue was permeabilized with 1% Triton X-100 in 1x PBST (1x PBS, 0.2% Tween 20) for 30 minutes. Samples were washed with 1x PBS and incubated with Click-iT reaction cocktail, washed with Click-iT reaction rinse buffer according to manufacturer's instructions. Samples were then immunostained according to previously described procedures.

Image Quantifications

All quantifications were performed on images using the same confocal settings. A.U. quantifications were performed in Fiji on images taken with identical settings using the "Measure" function. Intensities were normalized as indicated in the figure legends, boxplots of A.U. measurements were plotted using R and statistics were calculated using R.

Quantification of nucleolar size was measured in Fiji by measuring the diameter of the nucleolus using the measure tool in Fiji. Volumes were calculated using the formula for a sphere.

Quantification of p53 area of expression was performed from control, *nosGAL4* and *nosGAL4>aramis* RNAi germaria. A manual threshold was set based off of qualitative assessment of a "punctate." For control ovaries, cells proximal to the niche consisting of GSCs/CBs were outlined and for *aramis* RNAi the entire germline proximal to the niche was outlined and a Fiji script was used to determine the number of pixels above the threshold and the total number of pixels. Data from each slice for each replicate was summed prior to plotting and statistical analysis.

Colocalization analysis of helicases with Fibrillarin was performed in Fiji using the Plot Profile tool. A selection box was drawn over a Fibrillarin punctate of interest (indicated

with a box in the images) and Plot Profiles was acquired for each channel of interest. Data was plotted and Spearman correlations calculated using R.

Quantification of Non1-GFP expression and p53 expression over development was calculated in Fiji using the Auto Threshold tool with the Yen method (Sezgin & Sankur, 2004) to threshold expression. Quantifications were performed on 3 merged slices and egg chambers were cropped out of quantified images prior to thresholding to prevent areas outside of the germarium from influencing the thresholding algorithm. Areas of germline with “high” and “low” expression of Non1-GFP were outlined manually and a custom Fiji script was used in order to quantify the proportion of pixels in the selected marked as positive for expression for either Non1-GFP or p53, staging was inferred from the results of the Non1-GFP quantification performed using 1B1 to determine the stages of peak Non1 expression. Percent area was plotted with ggplot2 as boxplots in a custom R script.

RNA Extraction from Ovaries

RNA extraction was performed using standard methods. Ovaries were dissected into PBS and transferred to microcentrifuge tubes. PBS was removed and 100ul of Trizol was added and ovaries were flash frozen and stored at -80°C. Ovaries were lysed in the microcentrifuge tube using a plastic disposable pestle. Trizol was added to 1 mL total volume and sample was vigorously shaken and incubated for 5 min at RT. The samples were centrifuged for x min at >13,000 g at 4°C and the supernatant was transferred to a fresh microcentrifuge tube. 500 ul of chloroform was added and the samples were vigorously shaken and incubated for 5 minutes at RT. Samples were spun at max speed for 10 minutes at 4°C. The supernatant was transferred to a fresh microcentrifuge tube and ethanol precipitated. Sodium acetate

was added equaling 10% of the volume transferred and 2-2.5 volumes of 100% ethanol were added. The samples were shaken thoroughly and left to precipitate at -20°C overnight. The samples were centrifuged at max speed at 4°C for 15 min to pellet the RNA. The supernatant was discarded and 500 ul of 75% ethanol was added to wash the pellet. The samples were vortexed to dislodge the pellet to ensure thorough washing. The samples were spun at 4°C for 5 min and the supernatant was discarded. The pellets were left for 10-20 min until dry. The pellets were resuspended in 20-50ul of RNase free water and the absorbance at 260 was measured on a nanodrop to measure the concentration of each sample.

S2 Cell RNAi

DRSC-S2 cells (Stock #181, DGRC) were cultured according to standard methods in M3+BPYE media supplemented with 10% heat-inactivated FBS. dsRNA for RNAi was prepared as described by the SnapDragon manual. Briefly, template was prepared from S2 cell cDNA using the appropriate primers (see primer list) designed using SnapDragon (<https://www.flyrnai.org/snapdragon>). Template was either used directly for *in-vitro* transcription or TA-cloned into the pCR2.1-TOPO vector (K450002) followed by transformation into TOP-10 cells (K450002), plasmid purified, and digested with *Eco*R I prior to *in-vitro* transcription. For *in-vitro* transcription the T7 Megascript kit (AM1334) was used following manufacturer's instructions and in-vitro transcriptions were incubated overnight at 37°C. The RNA was treated with DNase according to the T7 Megascript manual and the RNA was purified using acid-phenol chloroform extraction and ethanol precipitated. The resulting RNA was annealed by heating at 65°C for 5 minutes and slow cooling to 37°C for an hour. S2 cell RNAi was performed essentially as previously described using

Effectine (Zhou, Mohr, Hannon, & Perrimon, 2013). 1.0×10^6 cells were seeded 30 minutes prior to transfection and allowed to attach. After 30 minutes, just prior to transfection, the media was changed for 500 μ l of fresh media. 500 μ l of transfection complexes using 1 μ g of dsRNA was prepared per well of a 6-well plate and pipetted dropwise onto seeded cells. After 24 hours an additional 1 mL of media was added to each well. After an additional 24 hours cells were passaged to 10 cm dishes. After an additional 3 days cells were harvested for further analysis.

Polysome-profiling

Polysome-profiling in S2 cells was performed as in Fuchs et al. (Fuchs, Diges, Kohlstaedt, Wehner, & Sarnow, 2011) with minor modifications. S2 cells were resuspended by pipetting, pelleted by centrifugation at 800g for one minute, and washed in cold PBS. Cells were again pelleted and resuspended in 400 μ l of lysis buffer (300 mM NaCl, 15 mM Tris-HCl, pH 7.5, 15 mM EDTA, 100 g/mL cycloheximide, 1% Triton X-100). Cells were then allowed to continue to lyse for 15 min on ice. Lysate was cleared by centrifugation at 8500g for 5 min at 4°C. Cleared lysate was loaded onto 10%-50% sucrose gradients (300 mM NaCl, 15 mM Tris-HCl, pH 7.5, 15 mM MgCl₂, 100 g/mL cycloheximide) and centrifuged in an SW41 rotor at 35,000 RPM, for 3 hours. Gradients were fractionated on a Density Gradient Fractionation System (Brandel, #621140007) at 0.75 mL/min. Data generated from gradients were plotted using R.

Western Blot

HeLa cells were harvested for Western by in RIPA buffer by scraping. Western blotting were performed according to standard methods, briefly, each sample was loaded onto a 4-20% commercial, precast gels and run at 100V for 60-90m depending on the size of the protein of interest. Gels were transferred to nitrocellulose membranes at 100V for 1hr at 4°C. Blot was blocked in 1% milk in PBS and washed 3 times with PBS-T for 5 minutes. Primary antibodies were diluted in PBS-T+5% BSA and incubated overnight. Blot was washed once quickly, once for 5m, and once for 10m in PBS-T. Blot was subsequently imaged with ECL for conjugated primaries. For unconjugated primaries, the appropriate secondary was diluted 1:10,000 in 5% milk and incubated for 2-4 hours at RT. Blot was washed once quickly, once for 5m, and once for 10m in PBS-T and imaged. Images were quantified using Fiji.

mRNaseq Library Preparation and Analysis

Libraries were prepared with the Biooscientific kit (Bioo Scientific Corp., NOVA-5138-08) according to manufacturer's instructions with minor modifications. Briefly, RNA was prepared with Turbo DNase according to manufacturer's instructions (TURBO DNA-free Kit, Life Technologies, AM1907), and incubated at 37°C for 30 min. DNase was inactivated using the included DNase Inactivation reagent and buffer according to manufactures instructions. The RNA was centrifuged at 1000 g for 1.5 min and 19 µl of supernatant was transferred into a new 1.5 mL tube. This tube was again centrifuged at 1000 g for 1.5 min and 18 µl of supernatant was transferred to a new tube to minimize any Inactivation reagent carry-over. RNA concentration was measured on a nanodrop. Poly-A selection was performed

on a normalized quantity of RNA dependent on the lowest amount of RNA in a sample, but within the manufacturer's specifications for starting material. Poly-A selection was performed according to manufacturer's instructions (Bioo Scientific Corp., 710 NOVA-512991). Following Poly-A selection mRNA libraries were generated according to manufactures instructions (Bioo Scientific Corp., NOVA-5138-08) except RNA was incubated for 13 min at 95°C to generate optimal fragment sizes. Library quantity was assessed via Qubit according to manufacturer's instructions and library quality was assessed with a Bioanalyzer or Fragment Analyzer according to manufacturer's instructions to assess the library size distribution. Sequencing was performed on biological duplicates from each genotype on an Illumina NextSeq500 by the Center for Functional Genomics (CFG) to generate single end 75 base pair reads. Reads were aligned to the dm6.01 assembly of the Drosophila genome using HISAT v2.1.0. Reads were counted using featureCounts v1.4.6.p5. UCSC genome browser tracks were generated using the bam coverage module of deeptools v3.1.2.0.0. Differential expression analysis was performed using DEseq2 (v1.24.0) and data was plotted using R. Differentially expressed genes were those with $\log_2(\text{foldchange}) > |1.5|$ and FDR < 0.05 in the *aramis* RNAi versus *bam* RNAi experiment and foldchange $> |1.5|$ and FDR < 0.05 in the *bam* RNAi; *aramis* RNAi versus *bam* RNAi experiment. GO-term analysis of GO biological processes was performed on differentially expressed genes using PANTHER via <http://geneontology.org/>. Fisher's exact test was used to calculate significance and FDR was used to correct for multiple testing. GO-term analysis results were plotted using R.

Polysome-seq

Polysome-seq was performed as in Flora et al. (Flora, Wong-Deyrup, et al., 2018b) with minor modifications. Ovaries were dissected in PBS and transferred to a microcentrifuge tube in liquid nitrogen. Ovaries were lysed in 300 μ l of lysis buffer (300 mM NaCl, 15 mM Tris-HCl, pH 7.5, 15 mM EDTA, 100 μ g/mL cycloheximide, 1% Triton X-100) and allowed to lyse for 15 min on ice. Lysate was cleared by centrifugation at 8500g for 5 min at 4°C. 20% of the lysate was reserved as input, 1 mL of Trizol (Invitrogen, 15596026) was added and RNA was stored at -80°C. Cleared lysate was loaded onto 10%-50% sucrose gradients (300 mM NaCl, 15 mM Tris-HCl, pH 7.5, 15 mM MgCl₂, 100 g/mL cycloheximide) and centrifuged in an SW41 rotor at 35,000 RPM, for 3 hours. Gradients were fractionated on a Density Gradient Fractionation System (Brandel, #621140007) at 0.75 mL/min, 20 μ l of 20% SDS, 8 μ l of 0.5 M pH 8 EDTA, and 16 μ l of proteinase K (NEB, P8107S) was added to each polysome fraction. Fractions were incubated for 30m at 37°C. Standard acid phenol chloroform purification followed by ethanol precipitation was performed on each fraction. The RNA from polysome fractions was pooled and RNAseq libraries were prepared.

Polysome-seq Data Analysis

Reads were checked for quality using FastQC. Reads were mapped to the *Drosophila* genome (dm6.01) using Hisat version 2.1.0. Mapped reads were assigned to features using feature-Count version v1.6.4. Translation efficiency was calculated as in (Flora et al., 2018; Kronja et al., 2014) using an R script. Briefly, TPMs (transcripts per million) values were calculated. Any gene having zero reads in any library was discarded from further analysis. The

\log_2 ratio of CPMs between the polysome fraction and total mRNA was calculated and averaged between replicates. This ratio represents the TE. TE of each replicate was averaged. Targets were defined as transcripts falling greater or less than two standard deviations from the median TE in aramis RNAi for upregulated and downregulated genes respectively, but not in either of the two developmental controls (Nos-GAL4 UAS-*tkv* or Nos-GAL4 UAS-*bam* RNAi). Additionally, genes were only considered targets if their mean TE value in Nos-GAL4 UAS-*aramis* RNAi was higher (for upregulated targets) or lower (for downregulated targets) than their mean TE values in both of the two developmental controls. Finally, only targets meeting a conservative expression cutoff of $\log_2(\text{TPM})$ expression greater than five were considered to exclude more lowly expressed genes as they are highly influenced by noise in polysome-seq in both controls.

CAGE-seq Tracks

CAGE-seq tracks were visualized using the UCSC Genome Browser after adding the publicly available track hub 'EPD Viewer Hub'.

CAGE-seq Data Reanalysis

Publicly available genome browser tracks were obtained of CAGE-seq data (generated by Chen et al. (2014) and viewed through the UCSC Genome Browser. The original CAGE-seq data from ovaries was obtained from SRA under the accession number SRR488282. Reads were aligned to the dm6.01 assembly of the *Drosophila* genome using HISAT v2.1.0. cageFightR was used to determine the dominant TSS for every gene with sufficient expression in from the aligned dataset according to its documentation with default parameters excepting

the following: For getCTSS, a mappingQualityThreshold of 10 was used. For normalizeTagCount the method used was “simpleTPM.” For clusterCTSS the following parameters were used; threshold = 1, thresholdIsTPM = TRUE, nrPassThreshold = 1, method = “paraclu,” maxDist = 20, removeSingletons = TRUE, keepSingletonsAbove = 5. R was used to obtain genome sequence information downstream of the TSS of each gene identified.

To generate a table of *aramis* polysome-seq target 5’UTRs adjusted using CAGE-seq data, bigwig files of CAGE-seq from ovaries were obtained from EPD Viewer Hub. The most highly expressed TSS within a CAGE cluster (obtained as described in this section) was used to determine the new 5’-end coordinate associated with each *aramis* polysome-seq target gene at the transcript level. These coordinates were used to obtain the corrected 5’UTR using R and transcripts with identical sequences were discarded.

Motif Enrichment Analysis

Motif enrichment analysis was performed using Homer (Heinz et al., 2010) using the find-motifs.pl module, supplying Homer with the first 200 nucleotides downstream of the TSS as determined by CAGE-seq for polysome-seq targets and non-targets as a background control with the following parameters “-rna -nogo -p 6 -len 6.” Only motifs not marked as potential false positives were considered. The position of the putative TOP motifs was determined using a custom R script by searching for the first instance of any five pyrimidines in a row within the first 200 nucleotides of the TSS using the Biostrings package (Pagès, Aboyoun, Gentleman, & DebRoy, 2019). Results were plotted as a histogram in R.

RNA Immunoprecipitation (RNA IP)

All RIPs were performed with biological triplicates. 50-60 ovary pairs were dissected for each sample in RNase free PBS and dissected ovaries were kept on ice during subsequent dissections. After dissection, ovaries were washed with 500 μ l of PBS to remove any debris. This PBS was removed, and ovaries were lysed in 100 μ l of RIPA buffer (10 mM Tris-Cl Buffer (pH 8.0), 1 mM EDTA, 1% Triton X-100, 0.1% Sodium deoxycholate, 0.1% SDS, 140 mM NaCl, 1 mM PMSF, 1 cOmplete, EDTA-free Protease Inhibitor/10mL buffer (Roche, 11873580001), RNase free H₂O) supplemented with 8 μ l of RNase Out. Following lysis an additional 180 μ l of RIPA was added to each sample. Lysate was cleared with centrifugation at 14,000g for 20m at 4°C. Cleared lysate was transferred to a new 1.5 mL tube. 10% of this lysate was reserved for RNA input and 5% was reserved as a protein input. To the RNA input 100 μ l of Trizol was added and the input was stored at -80°C. To the protein input SDS loading buffer was added to a 1X working concentration and the sample was heated at 95°C for 5m and stored at -20°C. The remaining lysate was equally divided into two new 1.5 mL tubes. To one tube 3 μ g of mouse anti-FLAG antibody was added and to the other tube 3 μ g of mouse IgG was added. These samples were incubated for 3 hours with nutation at 4°C. NP40 buffer was diluted to a 1X working concentration from a 10X stock (10x NP40 Buffer: 50 mM Tris-Cl Buffer (pH 8.0), 150 mM NaCl, 10% NP-40, 1 cOmplete, EDTA-free Protease Inhibitor Cocktail Pill/10mL buffer, RNase free H₂O). 30 μ l of Protein-G beads per RIP were pelleted on a magnetic stand and supernatant was discarded. 500 μ l of 1X NP40 buffer was used to resuspend Protein-G beads by nutation. Once beads were resuspended, they were again pelleted on the magnetic stand. This washing process was repeated a total

of 5 times. Washed Protein-G beads were added to each lysate and incubated overnight. The next day fresh 1X NP40 buffer was prepared. Lysates were pelleted on a magnetic stand at 4°C and supernatant was discarded. 300 μ l of 1X NP40 buffer was added to each sample and samples were resuspended by nutation at 4°C. Once samples were thoroughly resuspended, they were pelleted on a magnetic stand. These washing steps were repeated 6 times. Following the final washing steps, beads were resuspended in 25 ul of 1X NP40 Buffer. 5 μ l of beads were set aside for Western and the remaining beads were stored at -80°C in 100 μ l of Trizol. SDS loading buffer was added was added to a 1X working concentration and the sample was heated at 95°C for 5m and stored at -20°C or used for Western (refer to Western Blot section).

Helicase RNA IPseq

RNA was purified as previously described. RNA yield was quantified using Qubit or nanodrop according to manufactures instructions. RNA was run on a Fragment Analyzer according to manufactures instructions to assess quality. Inputs were diluted 1:50 to bring them into a similar range as the IgG and IP samples. To each sample 0.5 ng of Promega Luciferase Control RNA was added as a spike-in. Libraries were prepared as previously described except Poly(A) selection steps were skipped and library preparation was started with between 1-100 ng of total RNA. Reads were mapped to the M21017.1 NCBI *Drosophila* rRNA sequence record and the sequence of Luciferase obtained from Promega. All further analysis was performed using custom R scripts. Reads were assigned to features using featureCounts based off of a custom GTF file assembled based off of the Flybase record of rRNA sequences. Reads mapping to rRNA were normalized to reads mapping to the Lu-

ciferase spike-in control. Reads were further normalized to the reads from the corresponding input library to account for differences in input rRNA concentration between replicates and replicates were subsequently averaged. Tracks were visualized using the R package 'ggplot2', with additional formatting performed using 'scales' and 'egg'. The rRNA GTF was read into R using 'rtracklayer' and visualized using 'gggenes'. Average reads mapping to rRNA from IgG control and IP was plotted and a one-sided bootstrapped paired t-test for was performed on regions on rRNA that appeared to be enriched in the IP samples compared to the IgG control as it is a non-parametric test suitable for use with low n using R with 100,000 iterations.

Larp Gel Shifts

Cloning, Protein expression and purification The Larp-DM15 protein expression construct (amino acids 1330-1481 corresponding to isoform D) was cloned into a modified pET28a vector by PCR using cDNA corresponding to accession ID NP_733244.5. The resulting fusion protein has an N-fHis₁₀-maltose binding protein (MBP)-tobacco etch virus (TEV) protease recognition site tag. Protein expression and purification were performed as described previously (Roni M. Lahr et al., 2015). Briefly, plasmid was transformed into BL21(DE3) *E. coli* cells and plated onto kanamycin-supplemented agar plates. A confluent plate was used to inoculate 500 mL of autoinduction media (Studier, 2005). Cells were grown for three hours at 37°C and induced overnight at 18°C. Cells were harvested, flash frozen, and stored at -80°C.

Cells were resuspended in lysis buffer (50 mM Tris, pH 8, 400 mM NaCl, 10 mM imidazole, 10% glycerol) supplemented with aprotinin (Gold Bio), leupeptin (RPI Research), and PMSF

(Sigma) protease inhibitors. Cells were lysed via homogenization. Lysate was clarified by centrifugation and incubated with Ni-NTA resin (ThermoScientific) for batch purification. Resin was washed with lysis buffer supplemented with 35 mM imidazole to remove non-specific interactions. His₁₀-MBP-DM15 was eluted with 250 mM imidazole. The tag was removed via proteolysis using TEV protease and simultaneously dialyzed overnight (3 mg TEV to 40 mL protein elution). Larp-DM15 was further purified by tandem anion (GE HiTrap Q) and cation exchange (GE HiTrap SP) chromatography using an AKTA Pure (GE) to remove nucleic acid and protein contaminants. The columns were washed with in buffer containing 50 mM Tris, pH 7, 175 mM NaCl, 0.5 mM EDTA, and 10% glycerol and eluted with a gradient of the same buffer containing higher salt (1 M NaCl). Fractions containing Larp-DM15 were pooled, and 3 M ammonium sulfate was added to a final concentration of 1 M. A butyl column (GE HiTrap Butyl HP) was run to remove TEV contamination. The wash buffer contained 50 mM Tris, pH 7, 1 M ammonium sulfate, and 5% glycerol, and the elution buffer contained 50 mM Tris pH 7 and 2 mM DTT. Fractions containing Larp-DM15 were buffer exchanged into storage buffer (50 mM Tris pH, 7.5, 250 mM NaCl, 2 mM DTT, 25% glycerol), flash frozen in liquid nitrogen, and stored at -80°C. The purification scheme and buffer conditions were the same as with *HsDM15* (Roni M. Lahr et al., 2015), except cation and anion exchange buffers were at pH 7, as noted above.

RNA preparation 5'-triphosphorylated *RpL30* and *Non1* 42-mers were synthesized (ChemGenes). Purine-substituted controls were synthesized by *in vitro* transcription using homemade P266L T7 RNAP polymerase (Guillerez, Lopez, Proux, Launay, & Dreyfus, 2005). The transcription reaction containing 40 mM Tris, pH 8, 10 mM DTT, 5 mM

spermidine, 2 mM NTPs, and 10-15 mM MgCl₂ was incubated at 37°C for 4 hours. Transcripts were subsequently purified from an 8% polyacrylamide/6M urea/1XTBE denaturing gel, eluted passively using 10 mM sodium cacodylate, pH 6.5, and concentrated using spin concentrators (Millipore Amicon). All oligos were radioactively capped using Vaccinia virus capping system (NEB) and α^{32} -GTP (Perkin-Elmer). Labelled oligos were purified using a 10% polyacrylamide/6M urea/1XTBE denaturing gel, eluted with 10 mM sodium cacodylate, pH 6.5, and concentrated by ethanol precipitation.

The RNA sequences used were:

RpL30:

CUUUUGCCAUUGUCAGCCACGAAGUGCUUAACCAAACUA

Non1:

CUUUUUGGAAUACGAAGCUGACACCGCGUGGUUUUGCUU

*Purine-substituted RPL30 control:

GAAAAGCCAUUGUCAGCCACGAAGUGCUUAACCAAACUA

*Purine-substituted Non1 control:

GAAAAAGGAAUACGAAGCUGACACCGCGUGGUUUUGCUU

Oligos used for run-off transcription

DNA oligo	Sequence (5' to 3')
**RpL30 control gene block (with 3' HDV)	GCGCGCGAATTCTAATACGACTCACTATA <u>GAAAAGCCATTGTCAGCCGACGAAGTG</u> <u>CTTTAACCCAAACTAGGGTGGCATGG</u> CATCTCACCTCCTCGCGGTCCGACCTG GGCTACTTCGGTAGGCTAAGGGAGAAG CTTGGCACTGGCCGTCGTTTGGCACTG GCCGTCGTTT

DNA oligo	Sequence (5' to 3')
Non1 control	GCGCGCGAATTCTAATACGACTCACTATA
Forward	<u>GGAAAAAGGAATACGAAG</u>
	<u>CTGACA</u>
Non1 control	<u>AAGCAAAAACACCACCGCGGTGTCAGCTT</u>
Reverse	<u>CGTATTCCCTTTCTATAGTGAG</u>
5' GEN amp	GCGCGCGAATTCTAATACGACTCA
RpL30 amp Reverse	TAGTTGGGTTAAAGCACTTCGTCGGC
Non1 amp Reverse	AAGCAAAAACACCACCGCGGTGTCAGCTA

* These RNAs were synthesized using run-off transcription.

Electrophoretic mobility shift assays (EMSA)** Each binding reaction contained 125 total radioactive counts with final reaction conditions of: 20 mM Tris-HCl, pH 8, 150 mM NaCl, 10% glycerol, 1 mM DTT, 0.5 µg tRNA (Ambion), 1 µg BSA (Invitrogen), and <90 pM RNA. To anneal RNA, oligos were snap-cooled by heating at 95°C for 1 min and cooled on ice for 1 hour. For capped RpL30 shifts and capped purine-substituted controls, final concentrations of 0, 0.001, 0.003, 0.01, 0.03, 0.1, 0.3, 1, 3, 10, 30, and 100 nM Larp-DM15 were titrated. For capped Non1 shifts, final concentrations of 0, 0.01, 0.03, 0.1, 0.3, 1, 3, 10, 30, 100, 300, and 1000 nM Larp-DM15 were titrated. Native 7% polyacrylamide 0.5X TBE gels were pre-run on ice at 120 V for 30 min. Binding reactions were run at 120 V on ice for 45-52 min. Gels were dried for 30 min and allowed to expose overnight using a phosphor screen (GE). Screens were imaged using GE Amersham Typhoon. Bands were quantified using ImageQuant TL (GE). Background subtraction was first done using the rolling ball method and then subtracting the signal from the zero-protein lane from each of the shifted bands. Fraction shifted was determined by dividing the background-corrected intensity of

the shifted band by total intensity of bands in each lane. Three independent experiments were done for each oligo, with the average plotted and standard deviation shown.

mRNA IPseq

IPs of Larp and Aramis were performed as described in the RNA IP-seq section above in triplicate. mRNA libraries were prepared as described in mRNASeq Library Preparation and Data Processing using a constant volume of RNA from each sample with input samples having been diluted 1:50. Data was processed as described as in the mRNASeq Library Preparation and Data Processing section. Targets are defined as genes with >2 fold enrichment and an adjusted p-value <0.05 in the Larp-IP libraries compared to input libraries, but not meeting those criteria in the IgG libraries compared to input.

Larp RNA IP qPCR

Larp RNA IP was performed as described in the Larp RNA IPseq section with the following modifications. As the ovaries used were small, they were flash frozen in order to accumulate 40-50 ovaries for each biological replicate. Additionally, 5% input was taken for both RNA and protein samples. Once RNA was purified all of the RNA was treated with Turbo DNase as in the **mRNASeq Library Preparation and Analysis** section. Reverse transcription (RT) was performed using Superscript II according to the manufacturer's protocol with equivalent volumes of RNA for each sample. cDNA was diluted 1:8 before performing qPCR using Syber Green. Each reaction consisted of 5ul Syber Green master mix, 0.4 ul water, 0.3 ul of each primer, and 4 ul of diluted cDNA. For each sample 3 biological and 3 technical replicates were performed. Oulier values of technical replicates were removed using

a Dixon test with a cutoff of $p < 0.05$. Remaining technical replicates were averaged, and the IP Input Ct value, the \log_2 of the Input dilution (20) was also subtracted to account for the Input being 5% of the total sample as follows:

$$\Delta Ct[\text{normalized IP}] = (\text{Average } Ct[\text{IP}]/(\text{Average } Ct[\text{Input}] - \log 2(\text{Input Dilution Factor}))$$

Next, RNA recovery was normalized using the spike-in control for each sample as follows:

$$\Delta\Delta Ct = \Delta Ct[\text{normalized IP}] - \Delta Ct[\text{Luciferase}]$$

Next, Each sample was normalized to it's matched *bam* RNAi control as follows:

$$\text{bam RNAi normalizedCt} = \Delta\Delta Ct[\text{aramis RNAi IP}] - \Delta\Delta Ct[\text{bam RNAi IP}]$$

Finally, fold increase of IP from *aramis* RNAi over *bam* RNAi was calculated as follows:

$$\text{FoldEnrichment} = 2^{-\text{bam RNAi normalized Ct}}$$

Fold enrichment was plotted and One-sample t-test performed on *aramis* RNAi samples in R using a mu of 1.

Chapter 3

Oo-site: A dashboard to visualize gene expression during *Drosophila* oogenesis reveals meiotic entry is regulated post-transcriptionally

Elliot T. Martin^{1*}, Kahini Sarkar^{1, 4}, Alicia McCarthy¹, and Prashanth Rangan^{1,4*}

¹Department of Biological Sciences/RNA Institute, University at Albany SUNY, Albany, NY 12202

⁴Black Family Stem Cell Institute, Department of Cell, Developmental, and Regenerative Biology, Icahn School of Medicine at Mount Sinai, 1 Gustave L. Levy Place, New York, NY 10029, USA

*Co-corresponding authors

Email: etmartin@albany.edu and prashanth.rangan@mssm.edu

3.1 Summary

Determining how stem cell differentiation is controlled has important implications for understanding the etiology of degenerative disease and designing regenerative therapies. *In vivo* analyses of stem cell model systems have revealed regulatory paradigms for stem cell self-renewal and differentiation. The germarium of the female *Drosophila* gonad, which houses both germline and somatic stem cells, is one such model system. Bulk mRNA sequencing (RNA-seq), single-cell (sc) RNA-seq, and bulk translation efficiency of mRNAs

are available for stem cells and their differentiating progeny within the *Drosophila* germarium. However, visualizing those data is hampered by the lack of a tool to spatially map gene expression and translational data in the germarium. Here, we have developed Oosite (<https://www.ranganlab.com/Oo-site>), a tool for visualizing bulk RNA-seq, scRNA-seq, and translational efficiency data during different stages of germline differentiation, that makes these data accessible to non-bioinformaticians. Using this tool, we recapitulated previously reported expression patterns of developmentally regulated genes and discovered that meiotic genes, such as those that regulate the synaptonemal complex, are regulated at the level of translation.

3.2 Introduction

The *Drosophila* ovary provides a powerful system to study stem cell differentiation *in vivo* (Bastock & St Johnston, 2008; Eliazer & Buszczak, 2011; Lehmann, 2012; Allan Spradling, Fuller, Braun, & Yoshida, 2011). The *Drosophila* ovary consists of two main cell lineages, the germline, which ultimately gives rise to eggs, and the soma, which surrounds the germline and plays a supportive role in egg development (Eliazer & Buszczak, 2011; Roth, 2001; Schüpbach, 1987; Xie & Spradling, 2000). Each stage of *Drosophila* female germline stem cell (GSC) differentiation is observable and identifiable, allowing GSC development to be easily studied (Bastock & St Johnston, 2008; Lehmann, 2012; Xie & Spradling, 1998). Specifically, female *Drosophila* GSCs undergo an asymmetric division, giving rise to another GSC and a cystoblast (CB) (**Figure 3.1A**) (D. Chen & McKearin, 2003b; D. McKearin & Ohlstein, 1995; Xie & Spradling, 1998). The GSC and CB are marked by a round structure called the

spectrosome (**Figure 3.1A**) (De Cuevas & Spradling, 1998; Zaccai & Lipshitz, 1996). The CB then undergoes four incomplete divisions resulting in 2-, 4-, 8-, and finally 16-cell cysts (CC), which are marked by an extended structure called the fusome (**Figure 3.1A**) (D. Chen & McKearin, 2003a; D. Chen & McKearin, 2003b; De Cuevas & Spradling, 1998). In the 16-CC, one of the cyst cells is specified as the oocyte, while the other 15 cells become nurse cells, which provide proteins and mRNAs to support the development of the oocyte (**Figure 3.1A**) (Bastock & St Johnston, 2008; Carpenter, 1975; J.-R. Huynh & St Johnston, 2004; J. Huynh & St Johnston, 2000; Navarro, Lehmann, & Morris, 2001; Theurkauf, Alberts, Jan, & Jongens, 1993). The 16-CC is encapsulated by somatic cells and buds off from the germarium, forming an egg chamber (**Figure 3.1A**) (Bastock & St Johnston, 2008; A. J. Forbes, Lin, Ingham, & Spradling, 1996; Xie & Spradling, 2000). In each chamber, the oocyte grows as the nurse cells synthesize and then deposit mRNAs and proteins into the oocyte, which eventually gives rise to a mature egg (Bastock & St Johnston, 2008; J. Huynh & St Johnston, 2000).

Expression of differentiation factors, including those that regulate translation, results in progressive differentiation of GSCs to an oocyte (Blatt, Martin, Breznak, & Rangan, 2020; Slaidina & Lehmann, 2014). In the CB, Bag-of-marbles (Bam) expression promotes differentiation and the transition from CB to 8-CC stage (D. Chen & McKearin, 2003a; D. McKearin & Ohlstein, 1995; Ohlstein & McKearin, 1997). In the 8-CC, RNA-binding Fox protein 1 (Rbfox1) promotes exit from the mitotic cell cycle into meiosis (Carreira-Rosario et al., 2016). Both the differentiation factors Bam and Rbfox1 affect the translation of mRNAs to promote differentiation (Carreira-Rosario et al., 2016; Y. Li, Minor, Park, McKearin, & Maines, 2009; Tastan, Maines, Li, McKearin, & Buszczak, 2010). In addition, in

8-CCs, recombination is initiated across many cyst cells and then eventually is restricted to the specified oocyte (Hinnant, Merkle, & Ables, 2020; J. Huynh & St Johnston, 2000). Neither the mRNAs that are translationally regulated during this progressive differentiation nor how recombination is temporally regulated is fully understood (Cahoon & Hawley, 2016; Carreira-Rosario et al., 2016; Flora, Wong-Deyrup, et al., 2018a; Rubin, Macaisne, & Huynh, 2020; Slaidina & Lehmann, 2014; Tanneti, Landy, Joyce, & McKim, 2011; Youheng Wei et al., 2014).

Within the germarium, the germline is surrounded by and relies on distinct populations of somatic cells for signaling, structure, and organization (Roth, 2001; Schüpbach, 1987; Xie & Spradling, 1998, 2000). For example, the terminal filament, cap, and anterior-escort cells act as a somatic niche for the GSCs (Decotto & Spradling, 2005; Haifan Lin & Spradling, 1993; X. Wang & Page-McCaw, 2018; Xie & Spradling, 2000). Once GSCs divide to give rise to CBs, posterior escort cells guide CB differentiation by encapsulating the CB and the early-cyst stages (Kirilly, Wang, & Xie, 2011; Shi et al., 2021; Upadhyay et al., 2016). Follicle stem cells (FSCs), which are present towards the posterior of the germarium, divide and differentiate to give rise to follicle cells, (FCs) which surround the late-stage cysts that give rise to egg chambers (Margolis & Spradling, 1995; Nystul & Spradling, 2010; Rust et al., 2020). FSCs also give rise to stalk cells and polar cells which connect the individual egg chambers that comprise the ovariole (Margolis & Spradling, 1995; Nystul & Spradling, 2010; Rust et al., 2020; Sahai-Hernandez, Castanieto, & Nystul, 2012).

While there is a wealth of bulk RNA-seq, single-cell mRNA-seq (scRNA-seq), and translational efficiency data from polysome-seq experiments for the cells in the germarium, there are several hurdles for easy utilization of this data:

1. scRNA-seq has exquisite temporal resolution but it can miss some lowly expressed transcripts which are better captured by bulk RNA-seq (Lähnemann et al., 2020). However, there is no easy way to compare these two data sets.
2. While scRNA-seq provides mRNA levels, it does not indicate if these mRNAs are translated, especially in the germline where translation control plays an important role (Blatt, Martin, Breznak, & Rangan, 2020; Slaidina & Lehmann, 2014).
3. Lastly, there is a barrier to the visualization of the data for those who are not experienced in bioinformatics.

Here, we have developed a tool that we call Oo-site which integrates bulk RNA-seq, scRNA-seq, and polysome-seq data to spatially visualize gene expression and translational efficiency in the germarium.

3.3 Results

To make bulk RNA-, scRNA-, and polysome-, seq data accessible to the community, we have collated and reprocessed previously published sequencing datasets of ovaries enriched for GSCs, CBs, cysts, and egg chambers (**Figure 3.1B**). Notably, each genetically enriched sample had matched bulk RNA-seq and polysome-seq libraries prepared, allowing for simultaneous read-out of mRNA level and translation status (**Figure 3.2A**). One limitation is that the enriched cyst stages do not resolve each distinct stage of cyst development, instead, these samples represent a mixture of cyst stages. Therefore to supplement the enrichment data, we have integrated scRNA-seq data from Slaidina *et al.* which provides a more discrete

temporal resolution of the cyst stages (Slaidina, Gupta, Banisch, & Lehmann, 2021). We present these data as a tool called Oo-site (<https://www.ranganlab.com/Oo-site>), a collection of interactive visualizations that allows researchers to easily input a gene or collection of genes of interest to determine their expression pattern(s).

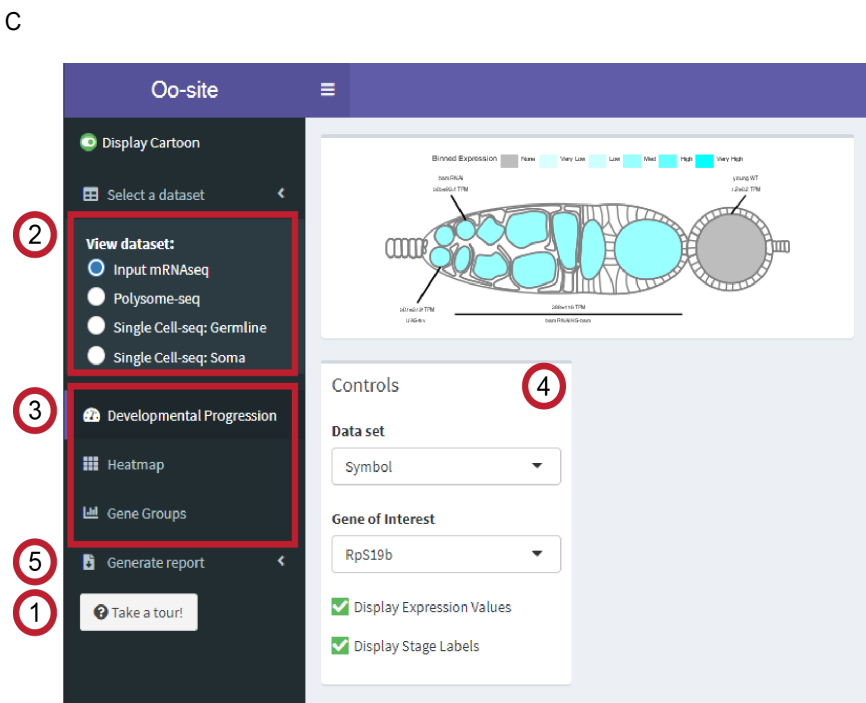
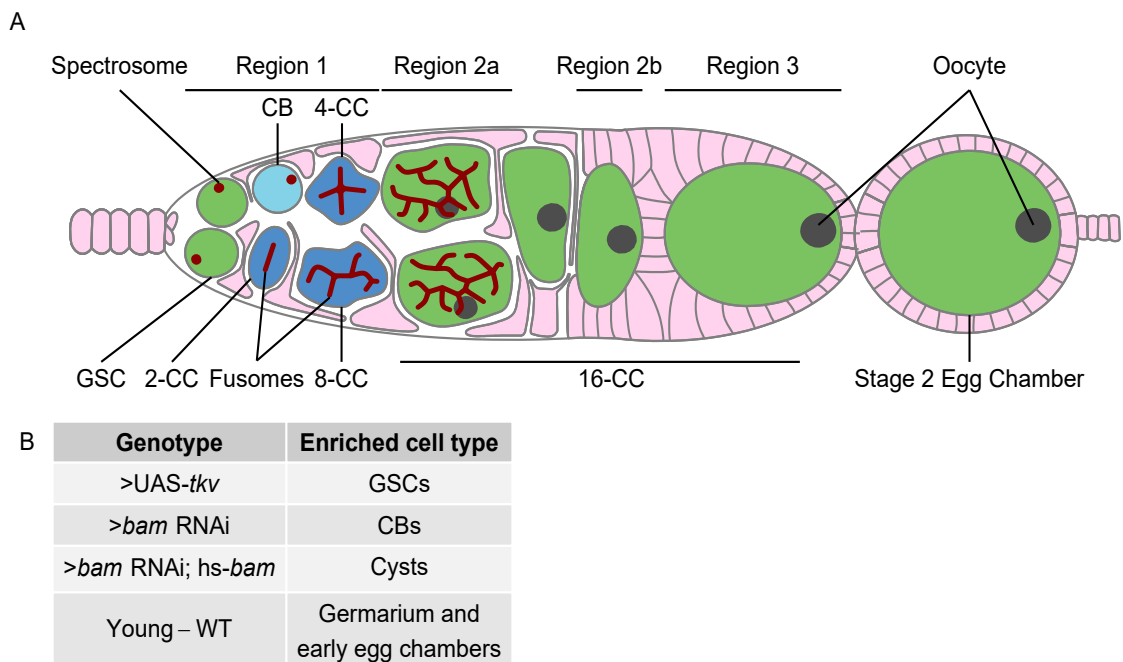


Figure 3.1: Oo-site integrates and provides an interface for interacting with multi-omic data covering major stages of *Drosophila* GSC differentiation.

(A) Schematic illustrating developmental stages of germline development. **(B)** Summary of the samples used for bulk RNA-seq and polysome-seq and the cell types these samples are enriched for. **(C)** Screenshot of Oo-site dashboard, indicating: (1) “Take a Tour!” function, which guides the user through the functionality and operation of Oo-site. (2) The available seq datasets which the user can view, including RNA-seq of ovaries genetically enriched for developmental stages (bulk RNA-seq), polysome-seq of ovaries genetically enriched for developmental stages (Polysome-seq), single-cell seq of germline stages (Single-Cell seq: Germline), and single-cell seq of somatic stages in the germarium (Single-Cell seq: Soma). (3) the available visualizations which the user can use, including viewing the expression of genes over development at the level of a single gene (Developmental Progression), viewing all significantly changing genes as heatmaps (Heatmap), and viewing groups of genes either derived from GO-term categories or supplied by the user (Gene Groups). (4) The control panel, which the user can use to control the current visualization, and (5) the Generate Report Function, which can be used to download a PDF report of either the current visualization or all active visualizations.

Oo-site consists of three modules: ovary-map, ovary-heatmap, and ovary-violin (**Figure 3.1C**). Each module allows users to visualize expression from matched mRNA-seq and polysome-seq data of genetically enriched stages of early GSC differentiation as well as previously published scRNA-seq data (Slaidina, Gupta, Banisch, & Lehmann, 2021). Additionally, we have integrated scRNA-seq expression data for genes that cluster in somatic cell populations that reside in the germarium (Slaidina, Gupta, Banisch, & Lehmann, 2021), however, here we focus on the germline (Slaidina, Gupta, Banisch, & Lehmann, 2021). Ovary-map allows users to visualize the expression of a single gene over the course of differentiation in the framework of a germarium schematic, which contextualizes staging for those less familiar with *Drosophila* oogenesis. Ovary-heatmap consists of a clustered, interactive heatmap of genes determined to be differentially expressed that allows users to explore expression trends over-development (**Figure 3.1B**, **Figure 3.2B-C'**). Finally, ovary-violin allows users to visualize the expression of multiple genes over the course of differentiation (**Figure 3.1C**). These groups of genes can be selected either by a GO-term of interest or a custom list of genes supplied by the user. The user can download a spreadsheet of gene ex-

pressions corresponding to the subset of selected or input genes. Finally, Oo-site incorporates a reporting tool that generates a downloadable report of the visualization(s) in a standardized format to facilitate their use for publication (**Figure 3.1C**). Researchers can use these datasets to enhance hypothesis generation or to confirm expression patterns observed from other methods.

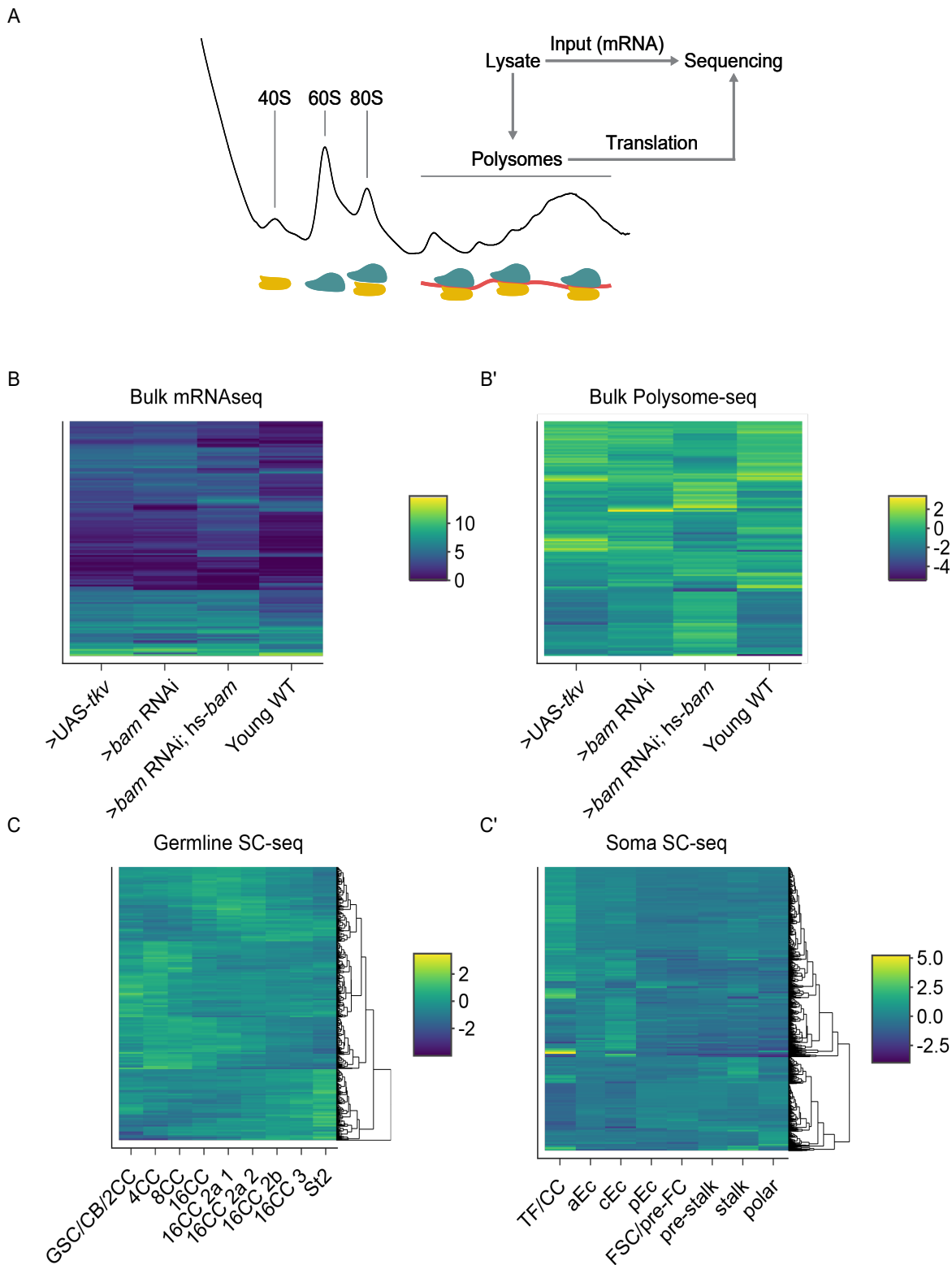


Figure 3.2: Sequencing strategy and clustered heatmaps of differential expression, related to Figure 3.1.

(A) Schematic of strategy used to obtain input mRNA samples and matched polysome-seq libraries of ovaries genetically enriched for developmental milestones. **(B-B')** Clustered heatmaps of (B) bulk RNA-seq and (B') $\log_2(\text{TE})$ from bulk polysome-seq of the developmental milestones indicated on the X-axis. Each row in the heatmap indicates a gene that is differentially expressed in at least one of the milestones compared to all others in a pairwise fashion. Color scale denotes average relative expression. **(C)** scRNA-seq of early germline cells and **(C')** scRNA-seq of somatic cells in the germarium. X-axis denotes cell-type and each row in the heatmap indicates a gene that is differentially expressed in at least one of the cell-types compared to all others in a pairwise fashion.

Using Oo-site, we first determined if the bulk RNA-seq data that was acquired by enriching for specific stages of germline development is representative of the gene expression patterns from purified cell types. We compared bulk RNA-seq data obtained by enriching for GSC and CB cell types without purification from somatic cells (**Figure 3.1C**) to the GSC and CB data from Wilcockson *et al.* where they included a fluorescent-assisted cell sorting (FACS) step to eliminate somatic cells so that a pure population of these germline cells was sequenced (Wilcockson & Ashe, 2019). We analyzed the expression of genes that Wilcockson *et al.* identified as 2-fold or more down- or upregulated with a p-value < 0.01. We found that in the enriched bulk RNA-seq data these genes followed similar trends as identified by Wilcockson *et al.*, indicating that despite the lack of FACS purification, enrichment of cell types reproduces meaningful mRNA expression changes over these stages (**Figure 3.4A-A'**).

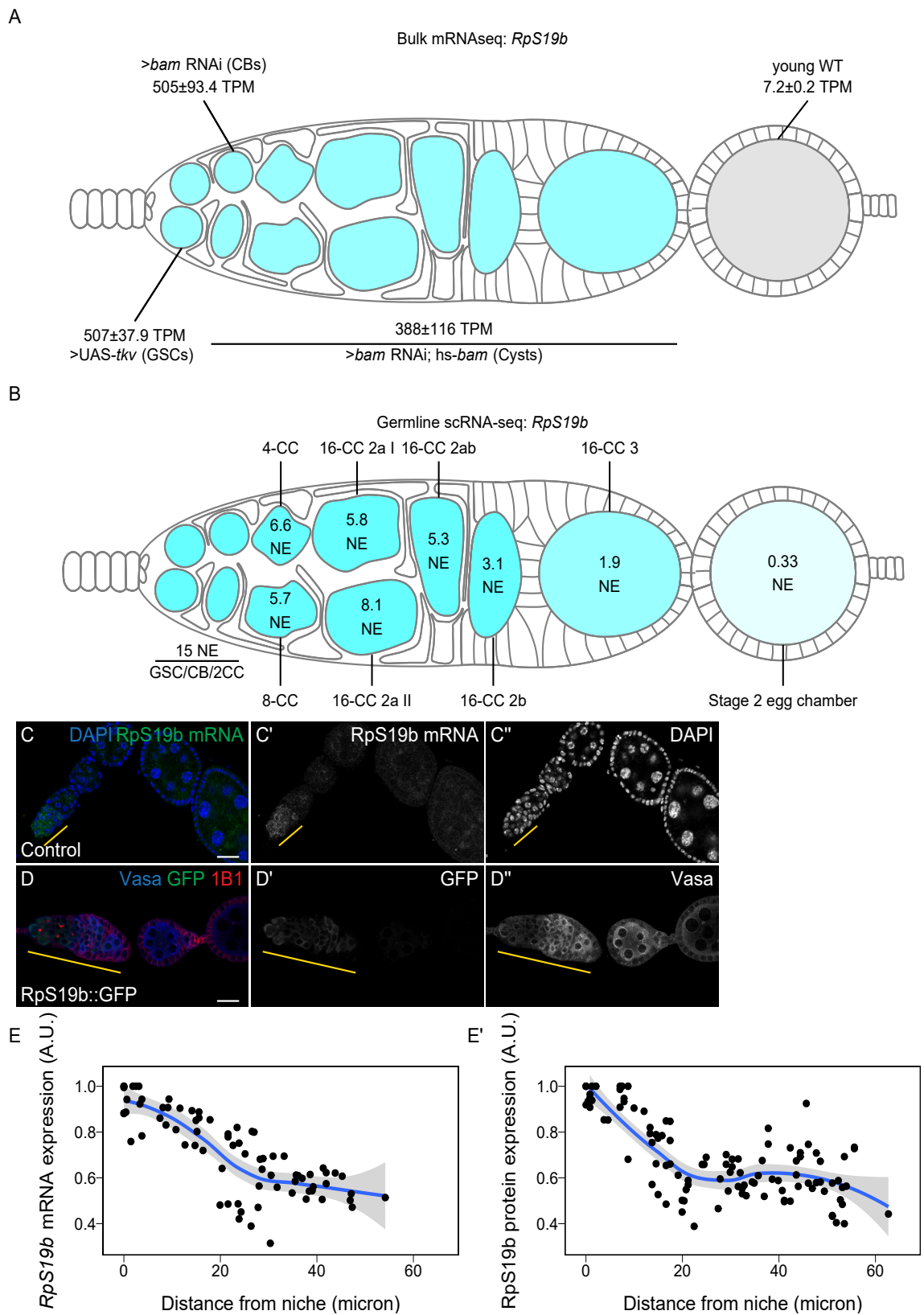


Figure 3.3: Oo-site allows for visualization of dynamically regulated genes.

(A-B) Visualization of expression of *RpS19b* over germline development from (A) developmentally enriched stages and (B) single-cell seq data indicate that the mRNA level of *RpS19b* decreases starting in the cysts and is dramatically decreased in early egg chambers. Color indicates relative expression and values indicate the (A) mean TPM \pm standard error or (B) the normalized expression of *RpS19b* in each given stage. **(C-C')** Confocal images of ovaries with *in situ* hybridization of *RpS19b* (green, middle greyscale) and stained for DAPI (blue, right greyscale) demonstrate that the mRNA level of *RpS19b* decreases starting in the cyst stages and are dramatically lower in early egg chambers consistent with the seq data. **(D-D')** Confocal images of ovaries expressing RpS19b::GFP, visualizing (D') GFP (green, middle greyscale), (D'') Vasa staining (blue, right greyscale), and 1B1 (red) demonstrate that the protein expression of RpS19b::GFP is consistent with its mRNA levels. **(E-E')** Quantifications of normalized mean intensity of staining, X-axis represents the distance in microns from the niche, Y-axis represents mean intensity normalized to the maximum mean intensity per germarium of (E) *RpS19b* mRNA or (E') RpS19b::GFP. The line represents fit using a loess regression, shaded area represents the standard error of the fit. (n=5 germaria).

To determine if the bulk RNA-seq data recapitulates genuine changes in gene expression, we compared the expression of *ribosomal small subunit protein 19b* (*RpS19b*) in bulk RNA-seq to scRNA-seq data. Our bulk RNA-seq data, as well as the available scRNA-seq data indicated that *RpS19b* was highly expressed in GSCs, decreased during differentiation in the cyst stages and was greatly decreased in expression in early egg chambers, consistent with previous reports (**Figure 3.3A-B**) (McCarthy et al., 2021; Sarkar et al., 2021). To further validate this expression pattern, we probed the expression of *RpS19b* *in vivo* using *in situ* hybridization as well as an RpS19b::GFP line that is under endogenous control elements (McCarthy et al., 2021). We found that *RpS19b* was present in the GSCs and diminishes in the cyst stages both at the mRNA and protein level (**Figure 3.3C-E'**). Additionally, RpS19b::GFP expression resembled its mRNA expression indicating that its dynamic expression is achieved primarily through modulating the mRNA level of *RpS19b*, consistent with its moderate to high translational efficiency in early stages (**Figure 3.3C-D**, **Figure 3.4B**). Thus, enriching for specific germline stages captures changes to gene expression in the germline. However, we note that care should be taken in interpreting bulk RNA-seq

results as the data may be influenced by the somatic cells present in the samples. However, simultaneous comparison with scRNA-seq can alleviate this problem.

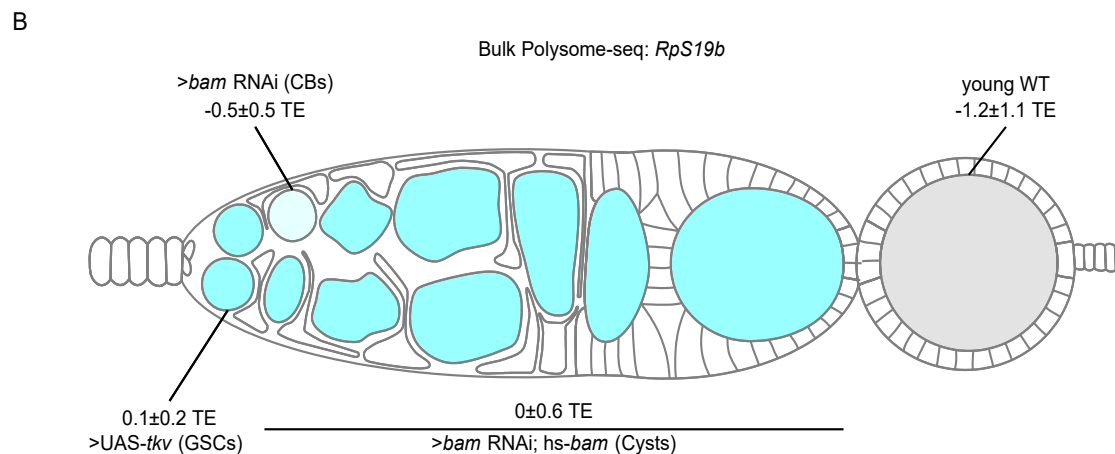
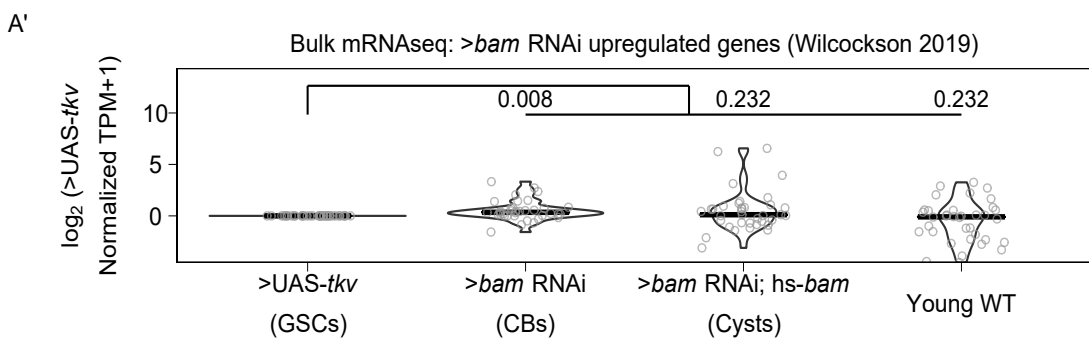
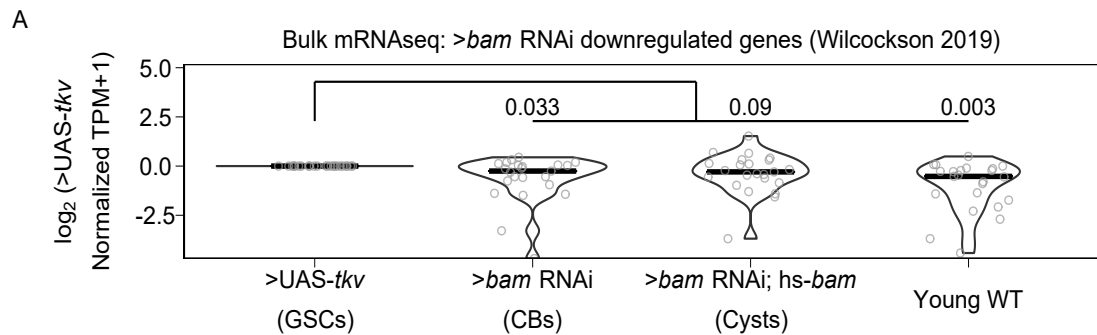


Figure 3.4: Bulk RNA-seq recapitulates previously observed expression patterns of gene expression, related to Figure 3.3.

(A-A') Violin plots of expression from bulk RNA-seq of genes 2-fold or more (A) down or (A') upregulated in bam RNAi germline cells compared to UAS-TKV overexpressing germline cell with a p-value < 0.01 over germline development from Wilcockson *et al.* demonstrate that bulk RNA-seq identifies similar trends in gene expression compared to the FACS based method employed by Wilcockson *et al.* Values above plots represent Holm-Bonferroni adjusted p-values from a Welch's t-test between the indicated genotypes. **(B)** Visualization of expression of *RpS19b* over germline development from polysome-seq data. Color indicates TE and values indicate the log₂ mean TE±standard error. *RpS19b* TE is relatively consistent during early oogenesis and decreases in the egg chambers.

To determine the groups of genes that change as the GSCs differentiate into an egg, we used gene ontology (GO)-term analysis to probe for pathways that change at the level of RNA using bulk RNA-seq data. We did not identify any significant GO-terms in genes that are differentially expressed between GSCs and CBs. We found that genes with lower expression in GSCs compared to differentiating cysts are enriched in the GO-term polytene chromosome puffing which is consistent with GO-terms identified in Wilcockson *et al.* for genes that are expressed at lower levels in GSCs than in differentiating cysts than GSCs (**Figure 3.5A**). We also identified the polytene chromosome puffing GO-term in genes downregulated in CBs compared to cysts. Additionally, we observed that several GO-terms involving peptidase activity were enriched in genes upregulated in GSCs and CBs compared to cysts (**Figure 3.5B**). This is consistent with findings suggesting that peptidases can be actively regulated during differentiation and can influence stem cell fate (Han, Wang, Bachovchin, Zukowska, & Osborn, 2015; Perišić Nanut, Pečar Fonović, Jakoš, & Kos, 2021; Tiaden *et al.*, 2012). We found that two GO-terms related to glutathione transferase activity were enriched in genes downregulated in GSCs and CBs compared to ovaries from young-wildtype (young-WT) flies and in CBs compared to differentiating cysts, suggesting that metabolic processes may be altered during GSC differentiation. Additionally, comparison of CBs and differentiating cysts to young-WT, which contain early egg chambers, indicated that downregulated genes

were enriched in GO-terms involving vitelline and eggshell coat proteins (**Figure 3.5A**).

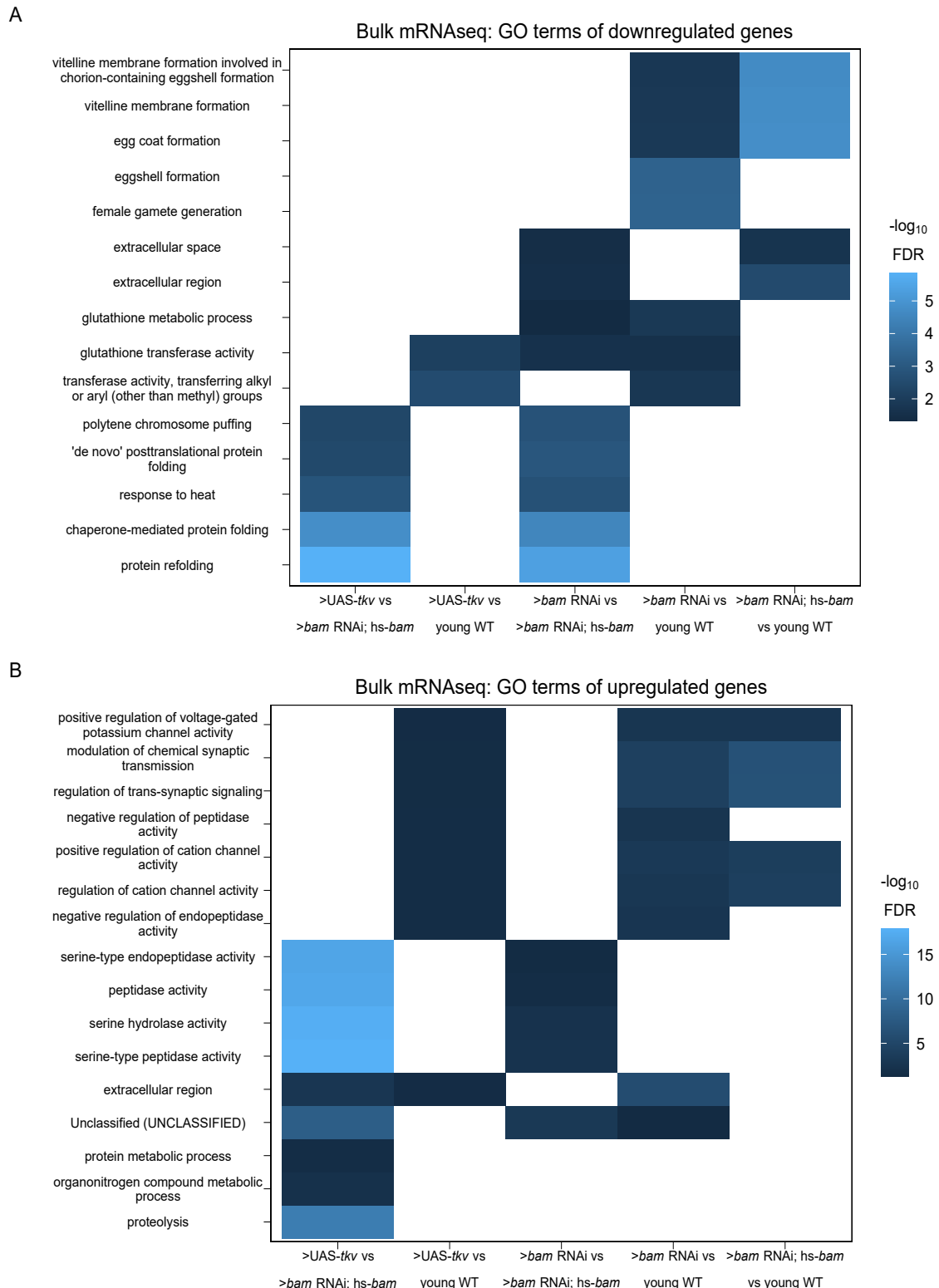


Figure 3.5: GO-terms enriched from differentially expressed genes between genetically enriched developmental milestones.

(A-B) Heatmaps of top five significant GO-terms by fold enrichment resulting from each pairwise comparison of significantly (A) downregulated or (B) upregulated genes in the first genotype listed relative to the second genotype listed in the x-axis from bulk RNA-seq of each developmentally enriched stage. Comparisons that did not generate any significant GO-terms are omitted.

Next, to determine if our data could resolve large-scale expression changes that occur during oogenesis we examined the expression of genes in the GO-term meiotic cell cycle. Meiosis is initiated during the cyst stages of differentiation and therefore we would expect genes in the category, in general, to increase in expression in the *>bam* RNAi; hs-*bam* samples (Carpenter, 1979; Tanneti, Landy, Joyce, & McKim, 2011). We were surprised to find no significant change in the mean mRNA expression of genes in this GO-term in any of our enriched stages compared to enriched GSCs, though this does not preclude gene expression changes for individual genes (**Figure 3.7A**). However, this is consistent with the observation that several factors that promote meiosis I are transcribed in the GSCs and the cells that follow (McCarthy et al., 2021). This suggests that, in general, a transition from a mitotic state to a meiotic state is not driven by large changes in mRNA levels of meiotic genes.

As we did not see overall changes to mRNA levels of genes in the GO-term meiotic cell cycle, we next examined the polysome-seq data of those genes to determine if changes in expression might occur at the level of translation. Polysome-seq uses polysome profiling to separate mRNAs that are associated with polysomes which form by mRNAs engagement with multiple ribosomes. To quantify the degree to which an mRNA is associated with polysome fractions, we compared the relative abundance of mRNAs from the polysome fractions to their relative expression using corresponding input lysates to calculate a metric referred to as translational efficiency (TE). Indeed, genes in the meiotic cell cycle GO-term had a significant increase in translation efficiency in CBs and a more dramatic increase in cysts despite no significant

changes to the overall mRNA level of these genes (**Figure 3.7A-B**). Based on scRNA-seq data, the expression of meiotic cell cycle genes increased slightly but significantly in the 4-CC cluster with a median increase in expression of 1.25 fold (**Figure 3.7C**). This suggests that some genes in the meiotic cell cycle GO-term may be regulated at the mRNA level, but as a group this regulation is modest. This is likely because genes in this GO-term are robustly expressed even in GSCs as the median mRNA level of meiotic cell cycle genes in enriched GSCs is 36.1 TPM, which exceeds the 70th expression percentile among all genes in enriched GSCs.

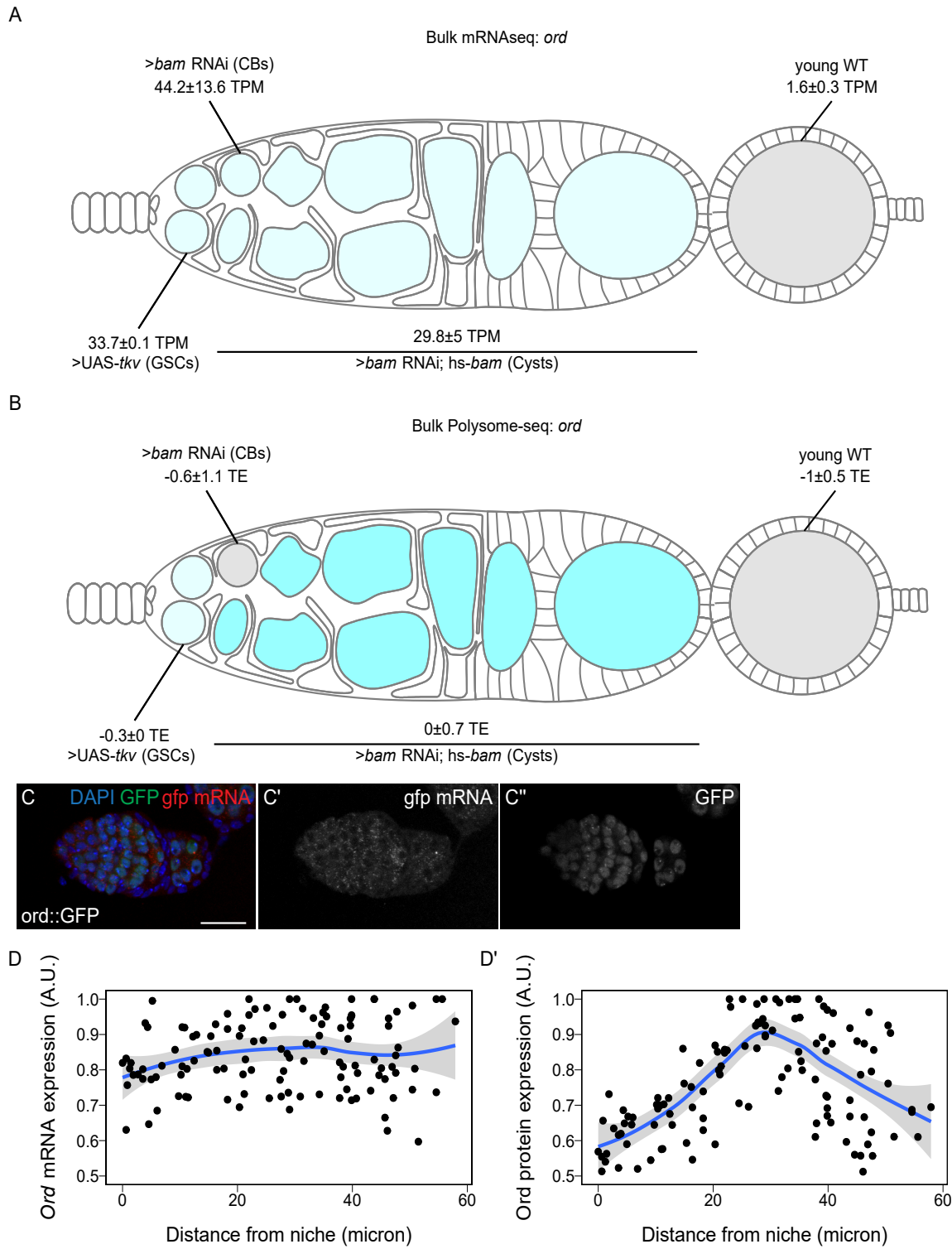


Figure 3.6: Ord expression is controlled post-transcriptionally.

(A-B) Visualization of expression of *ord* over germline development from (A) bulk RNA-seq of developmentally enriched stages and (B) polysome-seq of developmentally enriched stages indicates that the mRNA level of *ord* is consistent from GSCs to cysts, until decreasing in early egg chambers, but the translation efficiency of *ord* increases during the cyst stages compared to other stages. Color indicates (A) relative expression or (B) TE and values indicate the (A) mean TPM±standard error or (B) the log₂ mean TE±standard error **(C-C')** Confocal images of ovaries expressing Ord::GFP with *in situ* hybridization of *gfp* mRNA (red, middle greyscale) and stained for GFP protein (green, right greyscale) and DAPI (blue) demonstrate that the mRNA level of Ord::GFP is consistent throughout the germarium. **(D-D')** Quantification of normalized mean intensity of stainings (C-C'). X-axis represents the distance in microns from the niche, Y-axis represents mean intensity normalized to the maximum mean intensity per germarium of *ord* mRNA (D) or Ord protein (D'). The line represents fit using a loess regression, shaded area represents the standard error of the fit. (n=8 germaria).

To validate this finding, we examined *orientation disrupter* (*ord*) because it is a well-characterized gene, is required for sister chromatid cohesion, and has previously been reported to peak in expression as meiosis begins in *Drosophila* (S. E. Bickel, Wyman, Miyazaki, Moore, & Orr-Weaver, 1996; Sharon E. Bickel, Wyman, & Orr-Weaver, 1997; Khetani & Bickel, 2007). Our Oo-site results suggested that *ord* mRNA was expressed before meiosis, both from bulk RNA-seq (**Figure 3.6A**) and scRNA-seq (**Figure 3.7D**) consistent with reports that chromosome pairing initiates before meiotic entry (Christophorou, Rubin, & Huynh, 2013; Joyce, Apostolopoulos, Beliveau, & Wu, 2013). However, polysome-seq data were consistent with the observation that Ord protein expression increases during the cyst stages due to translation (**Figure 3.6B**). This led us to predict that *ord* mRNA would be expressed before meiosis, and that Ord protein expression would increase during the cyst stages as previously observed, implying a change in the translation status of *ord* mRNA. To test this, we performed fluorescent *in situ* hybridization against GFP in a fly expressing Ord-GFP under the control of the *ord* promoter and 5'UTR. We visualized both the GFP protein and the mRNA and observed increased expression of Ord::GFP protein but consistent

ord::GFP mRNA expression, indicating that Ord is controlled post-transcriptionally, likely at the level of translation based on our polysome-seq data (**Figure 3.6C-D'**). This finding also underscores the utility of Oo-site in exploring post-transcriptional gene expression changes.

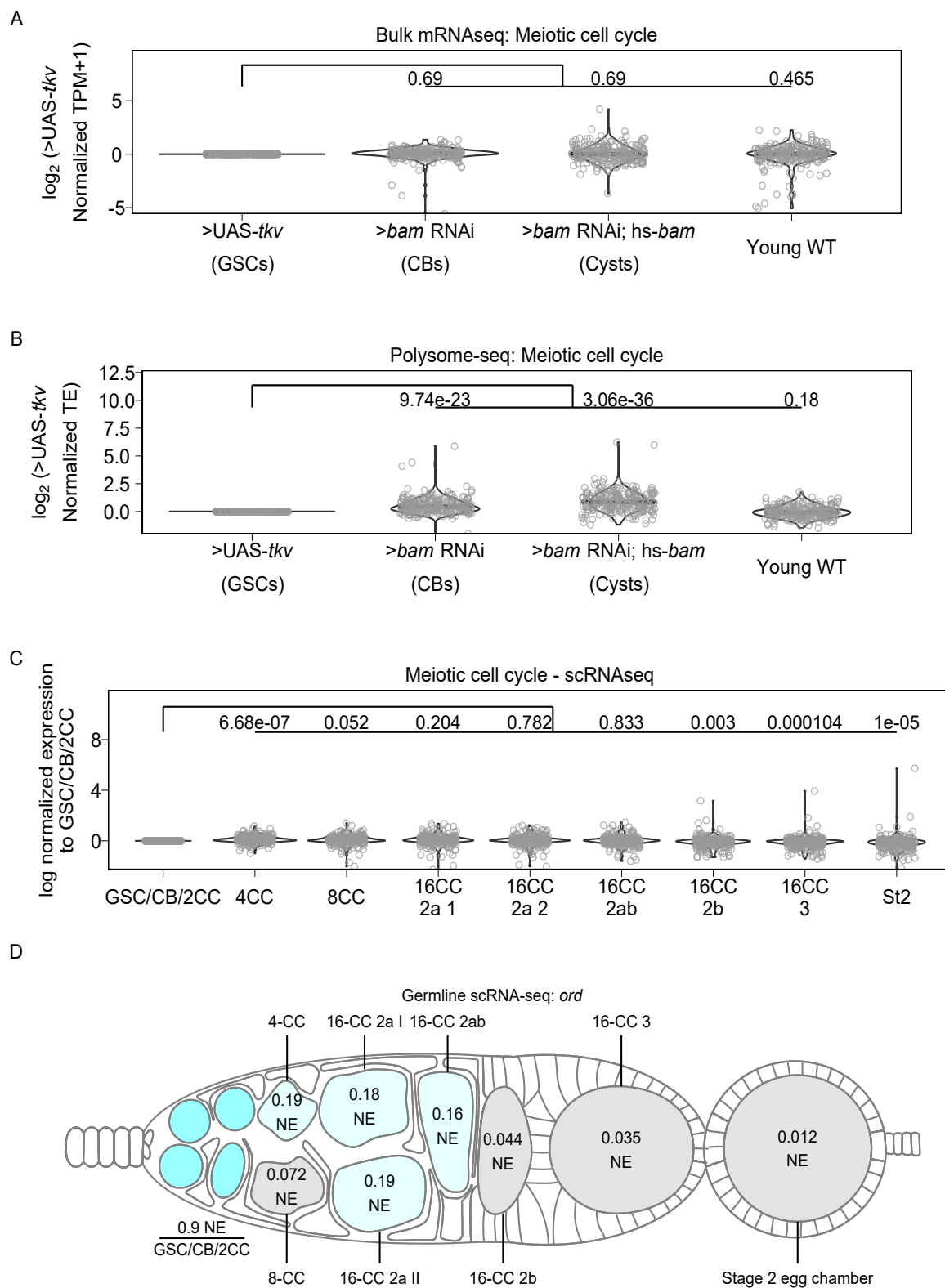


Figure 3.7: Genes involved in meiotic cell cycle, including *ord*, may be controlled post-transcriptionally, related to Figure 3.6.

(A) Violin plots of gene expression from RNA-seq of genes in the GO-term category meiotic cell cycle. No significant overall change occurs to expression of these genes at any of the developmental milestones compared to GSCs. Values above plots represent Holm-Bonferroni adjusted p-values from a Welch's t-test between the indicated genotypes. **(B)** Violin plots of TE from polysome-seq of genes in the GO-term category meiotic cell cycle. Overall TE increases in CBs and cysts significantly compared to GSCs indicating that meiotic entry may be partially controlled post-transcriptionally. Values above plots represent Holm-Bonferroni adjusted p-values from a Welch's t-test between the indicated genotypes. **(C)** Violin plot of expression of genes in the GO category "meiotic cell cycle" from scRNA-seq. Overall expression of these genes increases in CBs, cysts, and young-WT ovaries compared to the GSC/CB/2CC cluster. Values above plots represent Holm-Bonferroni adjusted p-values from a Welch's t-test between the indicated genotypes. **(D)** scRNA-seq data indicate that the mRNA level of *ord* is highest in the GSC/CB/2CC cluster, but remains relatively consistent in its expression starting in the 4-CC through 16-CC 2ab clusters and is dramatically decreased in early egg chambers. Color and values indicate the normalized expression of *ord* in each given stage.

To further determine if meiosis is regulated post-transcriptionally, we examined the expression of genes in the GO-term "Double-strand break repair," which is known to occur during meiosis 1 (Hughes, Miller, Miller, & Hawley, 2018; Page & Hawley, 2003). Double-stranded breaks are resolved before egg chamber formation (Hughes, Miller, Miller, & Hawley, 2018; Mehrotra & McKim, 2006; Page & Hawley, 2003). At the level of input mRNA, we found no significant changes in the expression of genes in this category compared to enriched GSCs (**Figure 3.8A**). From scRNA-seq data, the median expression of double-strand break repair genes significantly increases, but the median increase was only 1.05 fold in 4-CCs and 1.06 in 8-CCs compared to the GSC/CB/2CC group (**Figure 3.8B**). This suggests that double-strand break repair gene transcription begins in GSC stages and increases modestly during the cyst stages.

In contrast, we found a significant increase in the median translational efficiency of double-strand break repair genes, with a 1.20 fold increase in the median translational efficiency in enriched CBs and a 1.56 fold increase in enriched cysts compared to enriched GSCs (**Figure**

5C). In young-WT the median fold change in translational efficiency decreased slightly but significantly compared to enriched GSCs at 0.95 fold. This is consistent with the observed progression of double-stranded break repair that occurs *in vivo*. This demonstrates that Oosite can be used to derive insights into biological processes that may be changing during early oogenesis (Mehrotra & McKim, 2006; Page & Hawley, 2003). That key processes related to meiosis and differentiation are controlled post-transcriptionally is consistent with the importance of proteins that regulate translation such as Bam and Rbfox1 in differentiation and meiotic commitment during *Drosophila* oogenesis (Blatt, Martin, Breznak, & Rangan, 2020; Carreira-Rosario et al., 2016; Flora, Wong-Deyrup, et al., 2018a; Kim-Ha, Kerr, & Macdonald, 1995; Y. Li, Minor, Park, McKearin, & Maines, 2009; Slaidina & Lehmann, 2014; Tastan, Maines, Li, Mckearin, & Buszczak, 2010).

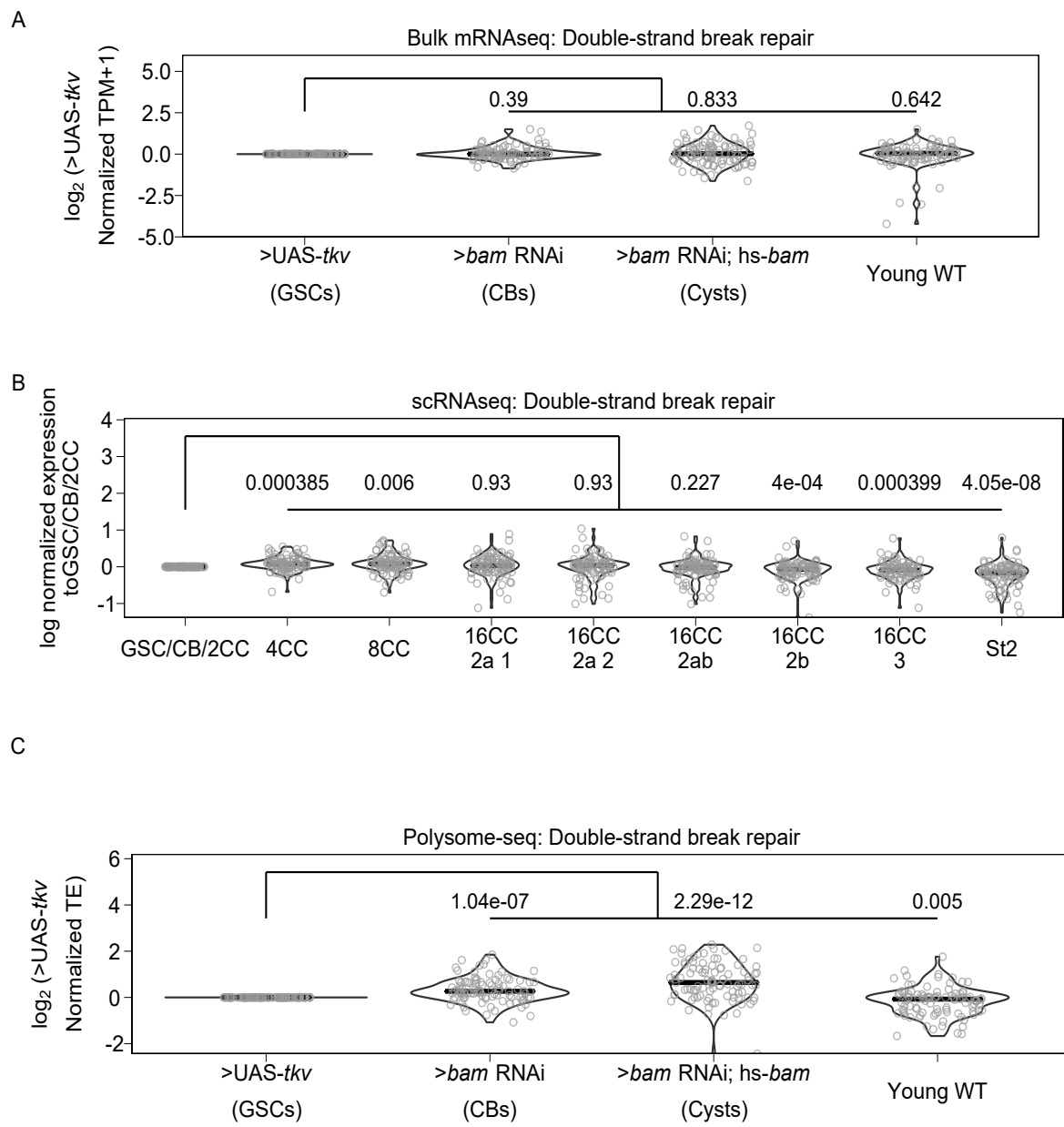


Figure 3.8: Genes involved in double-strand break repair may be controlled post-transcriptionally.

(A) Violin plot of expression of genes in the GO category “Double-strand break repair” from bulk RNA-seq. No significant overall change in expression of these genes occurs comparing each genetically enriched developmental stage to GSCs. **(B)** Violin plot of expression of genes in the GO category “Double-strand break repair” from scRNA-seq. Overall expression of these genes increases in CBs, cysts, and young-WT ovaries compared to the GSC/CB/2CC cluster. Values above plots represent Holm-Bonferroni adjusted p-values from a Welch’s t-test between the indicated genotypes **(C)** Violin plot of expression of genes in the GO category “Double-strand break repair” from polysome-seq. Overall expression of these genes increases in CBs, cysts, and young-WT ovaries compared to GSCs. Values above plots represent Holm-Bonferroni adjusted p-values from a Welch’s t-test between the indicated genotypes.

3.4 Discussion

We have developed an application that facilitates analysis of bulk RNA-seq, sc RNA-seq, and polysome-seq data of early *Drosophila* oogenesis that is accessible to non-bioinformaticians.

We have demonstrated its utility in representing expression at the mRNA and translation level. Additionally, we have demonstrated that it can be used to visualize the expression of groups of genes over development to facilitate hypothesis development. As with all sequencing data, care should be taken to validate findings from Oo-site as sequencing can be influenced by a myriad of factors.

We have used Oo-site to discover that key meiosis regulators such as proteins of the synaptonemal complex and proteins of the double-strand break machinery are regulated at the level of translation. This adds to our understanding of the mechanisms regulating the mitotic to meiotic transition. In future work, identifying the factors mediating the widespread post-transcriptional regulation of crucial meiotic genes and mechanistically how it drives the mitotic to meiotic transition is of high importance.

High-throughput sequencing has enabled researchers to generate more data than ever before

However, the development of analysis tools that are usable without bioinformatics training that enable users to make sense of these data to generate hypotheses and novel discoveries has lagged (Shachak, Shuval, & Fine, 2007). Oo-site allows for hypothesis generation and discovery using the powerful model system of *Drosophila* oogenesis. We believe Oo-site might also have utility as a teaching and demonstration tool to introduce students to the power of genomics in developmental biology. The open-source nature of this software facilitates future tool development, which will be crucial as more researchers delve into more data-intensive scRNA-seq, where visualization tools are limited and produce plots that may be difficult to interpret for those not versed in bioinformatics. Oo-site can be supplemented in the future to include additional data such as Cut and Run for various chromatin marks, nascent mRNA transcription using transient transcriptome sequencing or similar techniques, or protein levels from mass-spectroscopy to further extend its utility in hypothesis development.

3.5 Acknowledgements

We thank the Drs. Ruth Lehmann and Maija Sladina for sharing scRNA-seq data with us before publication of the manuscript. We are grateful to all members of the Rangan laboratory for discussion and comments on the manuscript. We thank Noor Kotb for naming the dashboard Oo-site. We also thank Dr. Florence L. Marlow for critically reading and editing the manuscript. P.R. is funded by the National Institutes of Health NIGMS (RO1GM11177 and RO1GM135628).

3.6 Materials and Methods

The following RNAi stocks were used in this study; *ord-GFP* (Bickel Lab), *Rps19b::GFP* (McCarthy et al., 2021), *UAS-Dcr2;nosGAL4* (Bloomington stock #25751), *bam* RNAi (Bloomington #58178), *hs-bam/TM3* (Bloomington #24637),

Sequencing data

Polysome-seq data were obtained from previous studies conducted by the Rangan lab. Data are available via the following GEO accession numbers:

>UAS-*tkv* GSE171349

>*bam* RNAi GSE171349, GSE166275

>*bam* RNAi; *hs-bam* GSE143728, GSE195893

Young-WT GSE119458

Single-cell sequencing data were obtained from Slaidina *et al.*, GEO accession: GSE162192

Code Availability

All code used in the preparation of this manuscript is available on GitHub at <https://github.com/elliotmartin92/Developmental-Landscape/tree/master/Paper>

The codebase underlying Oo-site is available on GitHub at <https://github.com/elliotmartin92/Developmental-Landscape/tree/master/ShinyExpresionMap>

Antibodies

Mouse anti-1B1 1:20 (DSHB 1B1), rabbit anti-GFP 1:2000 (abcam, ab6556), rabbit anti-Vasa 1:4000 (Upadhyay et al., 2016), chicken anti-Vasa 1:4000 (Upadhyay et al., 2016)

Polysome-seq

Flies ready for heat shock were placed at 37°C for 2 hours, moved to room temperature for

4 hours, and placed back into 37°C for 2 additional hours. Flies were then left overnight at room temperature and the same heat shocking procedure was repeated for a total of 2 days. Flies were then dissected in 1x PBS. Polysome-seq was performed as previously described (McCarthy et al., 2021).

Polysome-seq data processing

Reads were mapped to the *Drosophila* genome (dm6.01) using STAR version 2.6.1c. Mapped reads were assigned to features also using STAR. Translation efficiency was calculated as in (Flora et al., 2018) using an R script which is available in the Oo-site Github repo. Briefly, TPMs (transcripts per million) values were calculated. The log₂ ratio of TPMs between the polysome fraction and total mRNA was calculated as such to prevent zero counts from overly influencing the data and to prevent divide by zero errors: $\frac{\text{Polysome}_{\text{TPM}}+1}{\text{Input}_{\text{TPM}}+1}$. This ratio represents TE, TE of each replicate was averaged and standard error about the calculated average for each gene was calculated.

Differential Expression

Differential expression analysis between all bulk RNA-seq samples in a pairwise manner was performed using DEseq2 (Love, Huber, & Anders, 2014). Differential expression was considered as Foldchange > |4| fold, FDR < 0.05.

Differential expression analysis between all polysome-seq samples in a pairwise manner was performed using DEseq2 (Love, Huber, & Anders, 2014) using the model ~ type + genotype + genotype:type with LRT (reduced = ~ type + genotype) to test for changes in polysome counts controlling for input counts. Differential expression was considered as (Foldchange > |2| fold, pvalue < 0.05)

Differentially expressed genes between all germline clusters from scRNA-seq was determined

using the FindAllMarkers function from Seurat (Hao et al., 2021). Cutoff was logfc.threshold = 0.75.

Differentially expressed genes between all germarium soma clusters from scRNA-seq was determined using the FindAllMarkers function from Seurat (Hao et al., 2021). Cutoff was logfc.threshold = 0.75.

GO term heatmaps

GO-term enrichment analysis was performed using Panther (release 20210224) using the default settings for an Overrepresentation Test of genes differentially expressed between Input samples. Top 5 GO-terms based on fold enrichment of each category were plotted using ggplot2 (Wickham, 2016).

Fluorescent *in situ* hybridization

A modified *in situ* hybridization procedure for Drosophila ovaries was followed from Sarkar *et al.* (Sarkar et al., 2021). Probes were designed and generated by LGC Biosearch Technologies using Stellaris® RNA FISH Probe Designer, with specificity to target base pairs of target mRNAs. Ovaries (3 pairs per sample) were dissected in RNase free 1X PBS and fixed in 1 mL of 5% formaldehyde for 10 minutes. The samples were then permeabilized in 1mL of Permeabilization Solution (PBST+1% Triton X-100) rotating in RT for 1 hour. Samples were then washed in wash buffer for 5 minutes (10% deionized formamide and 10% 20x SSC in RNase-free water). Ovaries were covered and incubated overnight with 1ul of the probe in hybridization solution (10% dextran sulfate, 1 mg/ml yeast tRNA, 2 mM RNaseOUT, 0.02 mg/ml BSA, 5x SSC, 10% deionized formamide, and RNase-free water) and primary antibody at 30°C. Samples were then washed 2 times in 1 mL wash buffer with 1ul of corresponding secondary antibody for 30 minutes each and mounted in Vectashield

(VectaLabs).

Quantification of Stainings

Stainings were quantified using the Fiji Measure tool. Images were aligned and cropped to place the stem cell niche at $x=0$. Individual cells were outlined within the germarium and Measure was used to calculate the Mean intensity of staining within the cell as well as the X coordinate of the centroid of the cell. Values were normalized to 1 by dividing Mean Intensity values by the maximum of the Mean Intensity per germarium. Data were plotted using ggplot2 and a fit line was added using ggplot2 geom_smooth with a “loess” function with default settings. The shaded area around the line represents standard error.

Chapter 4

Conclusion

My work has shined a spotlight on the role of post-transcriptional control in GSC differentiation. Specifically, the ribosome is a nexus for gene expression regulation in three ways. The ribosome is the subject of post-transcriptional gene regulation in order to balance the production of ribosomal proteins with the production of ribosomal RNA, ribosomal proteins are regulated post-transcriptionally. This role oddly ouroboric because the mechanism behind this regulation works by inhibiting translation initiation by the ribosome onto ribosomal mRNAs. Second, the ribosome plays its “traditional” role as a factory to translate genetic instructions into protein products. Although the role of the ribosome in this aspect is “passive” mRNAs must make their way from the nucleus to the ribosome and are subject to degradation, sequestration, and interaction with hundreds or thousands of potential regulators on their journey. Finally, less explored by my work, is the role of post-translational modifications on ribosomal proteins and mRNAs and the role that these modifications play in gene regulation. My work has specifically has highlighted the importance of the first two facets in controlling GSC differentiation and future work should seek to understand the role

of post-translational modifications is GSC differentiation and stem cell differentiation more broadly.

This work has developed tools to study and described the crucial role of post-transcriptional gene regulation in GSC differentiation and entry into meiosis in *Drosophila*. Work in other systems has underscored the importance of translation control in stem cell differentiation in general (Gabut, Bourdelais, & Durand, 2020; Sanchez et al., 2016; Woolnough, Atwood, Liu, Zhao, & Giles, 2016; Zahradkal, Larson, & Sells, 1991; Q. Zhang, Shalaby, & Buszczak, 2014). Historically, study of post-transcriptional control has lagged behind that of control at the level of transcription. This is in part due to the lack of equity in tools and techniques between the two areas of study. One salient example is the lag in single-cell sequencing of mRNA which was first published in 2009 compared to the first published example of single-cell Ribo-seq, the first example of which was published in 2021, a 12 year lag (F. Tang et al., 2009; VanInsberghe, van den Berg, Andersson-Rolf, Clevers, & van Oudenaarden, 2021). This exemplifies that those interested in understanding translation control must continue to develop tools and use those tools to better understand developmental systems, regeneration, and disease states. Without equity in understanding between the domains of transcription control and translation control, gaps in our knowledge will prevent our understanding of fundamental biological questions. However, as our toolkits grow we must also remember that every year we generate more data than the previous, but only a subset of the scientific community has the skills necessary to process that data. Therefore, we must attempt to democratize access to the high-throughput data we generate to empower the research of others.

Future work should aim to understand the pathways that underlie stem cell differentiation

and meiotic entry, in particular the interplay and feedback between the Torc1 pathway and the synthesis of ribosomes. Our work has demonstrated that a feedback loop exists between Larp activity and ribosome biogenesis, but future work in other systems should determine if this loop is conserved and if Torc1 acts upstream of Larp as has been shown in other systems. More importantly, how the balance of the Larp-ribosome axis informs differentiation and what levers upstream of Larp might play a role in the initiation of differentiation are of great interest to better understand differentiation, regeneration, and developmental diseases. Emerging techniques such as single-cell Ribo-seq will no doubt allow for these questions to be studied in complex tissues including developmental systems and disease states.

Additionally, future work should examine whether the Larp-ribosome axis is tissue specific. So far we have demonstrated its importance in GSCs, but it remains an open question whether this mechanism acts in other stem cell populations or perhaps in unipotent cells. With our collaborators, we have found certain translational changes related to mitochondrial function that result when perturbing ribosome biogenesis in S2 cells. As Larp has been previously implicated in playing a role in mitochondrial translation in spermatogenesis, this may speak to a tissue specific mode of regulation, however, additional work is required to solidify the linkage between ribosome biogenesis, Larp, and Larp's targets outside of GSCs. These questions are of great interest as understanding whether Larp may have tissue specific targeting or activity could help explain the tissue specific nature of ribosomeopathies, which has been intensely studied for decades.

Appendix A

The First Appendix

References

- Agalarov, S. C., Sridhar, G., Funke, P. M., Stout, C. D., & Williamson, J. R. (2000). Structure of the S15, S6, S18-rRNA complex: Assembly of the 30S ribosome central domain. *Science*, 288(5463), 107–112.
- Agarwal, M. L., Agarwal, A., Taylor, W. R., & Stark, G. R. (1995). P53 controls both the G2/M and the G1 cell cycle checkpoints and mediates reversible growth arrest in human fibroblasts. *Proceedings of the National Academy of Sciences*, 92(18), 8493–8497.
- Andrews, J., Garcia-Estefania, D., Delon, I., Lu, J., Mével-Ninio, M., Spierer, A., ... Oliver, B. (2000). OVO transcription factors function antagonistically in the Drosophila female germline. *Development (Cambridge, England)*, 127(4), 881–892.
- Anthony, J. C., Anthony, T. G., Kimball, S. R., Vary, T. C., & Jefferson, L. S. (2000). Orally Administered Leucine Stimulates Protein Synthesis in Skeletal Muscle of Postabsorptive Rats in Association with Increased eIF4F Formation. *The Journal of Nutrition*, 130(2), 139–145. <http://doi.org/10.1093/jn/130.2.139>

- Aoki, K., Adachi, S., Homoto, M., Kusano, H., Koike, K., & Natsume, T. (2013). LARP1 specifically recognizes the 3' terminus of poly(A) mRNA. *FEBS Letters*, 587(14), 2173–2178. <http://doi.org/10.1016/j.febslet.2013.05.035>
- Arabi, A., Wu, S., Ridderstråle, K., Bierhoff, H., Shiue, C., Fatyol, K., ... Wright, A. P. H. (2005). C-Myc associates with ribosomal DNA and activates RNA polymerase I transcription. *Nature Cell Biology*, 7(3), 303–310. <http://doi.org/10.1038/ncb1225>
- Armistead, J., & Triggs-Raine, B. (2014). Diverse diseases from a ubiquitous process: The ribosomopathy paradox. *FEBS Letters*, 588(9), 1491–1500. <http://doi.org/10.1016/j.febslet.2014.03.024>
- Arvola, R. M., Weidmann, C. A., Tanaka Hall, T. M., & Goldstrohm, A. C. (2017). Combinatorial control of messenger RNAs by Pumilio, Nanos and Brain Tumor Proteins. *RNA Biology*, 14(11), 1445–1456. <http://doi.org/10.1080/15476286.2017.1306168>
- Bailey, T. L., Williams, N., Misleh, C., & Li, W. W. (2006). MEME: Discovering and analyzing DNA and protein sequence motifs. *Nucleic Acids Research*, 34(suppl_2), W369–W373.
- Bakhrat, A., Pritchett, T., Peretz, G., McCall, K., & Abdu, U. (2010). Drosophila Chk2 and P53 proteins induce stage-specific cell death independently during oogenesis. *Apoptosis*, 15(12), 1425–1434. <http://doi.org/10.1007/s10495-010-0539-z>
- Barlow, J. L., Drynan, L. F., Trim, N. L., Erber, W. N., Warren, A. J., & Mckenzie, A. N. J. (2010). Cell Cycle New insights into 5q-syndrome as a ribosomopathy. *Cell Cycle*, 9, 4286–4293. <http://doi.org/10.4161/cc.9.21.13742>

- Barreau, C., Benson, E., Gudmannsdottir, E., Newton, F., & White-Cooper, H. (2008). Post-meiotic transcription in Drosophila testes. *Development*, 135(11), 1897–1902.
- Bastock, R., & St Johnston, D. (2008). Drosophila oogenesis. *Current Biology*, 18(23), R1082–R1087.
- Batista, P. J., Molinie, B., Wang, J., Qu, K., Zhang, J., Li, L., ... Daneshvar, K. (2014). m6A RNA modification controls cell fate transition in mammalian embryonic stem cells. *Cell Stem Cell*, 15(6), 707–719.
- Baxter-Roshek, J. L., Petrov, A. N., & Dinman, J. D. (2007). Optimization of ribosome structure and function by rRNA base modification. *PLoS ONE*, 2(1), e174. <http://doi.org/10.1371/journal.pone.0000174>
- Belin, S., Beghin, A., Solano-González, E., Bezin, L., Brunet-Manquat, S., Textoris, J., ... Diaz, J.-J. (2009). Dysregulation of ribosome biogenesis and translational capacity is associated with tumor progression of human breast cancer cells. *PloS One*, 4(9), e7147.
- Bell, L. R., Maine, E. M., Schedl, P., & Cline, T. W. (1988). Sex-lethal, a Drosophila sex determination switch gene, exhibits sex-specific RNA splicing and sequence similarity to RNA binding proteins. *Cell*, 55(6), 1037–1046.
- Berman, A. J., Thoreen, C. C., Dedeic, Z., Chettle, J., Roux, P. P., & Blagden, S. P. (2020). Controversies around the function of LARP1. *RNA Biology*, 1–11. <http://doi.org/10.1080/15476286.2020.1733787>

- Bernardini, L., Gimelli, S., Gervasini, C., Carella, M., Baban, A., Frontino, G., ... Dallapiccola, B. (2009). Recurrent microdeletion at 17q12 as a cause of Mayer-Rokitansky-Kuster-Hauser (MRKH) syndrome: Two case reports. *Orphanet Journal of Rare Diseases*, 4(1), 25. <http://doi.org/10.1186/1750-1172-4-25>
- Bhandari, D., Raisch, T., Weichenrieder, O., Jonas, S., & Izaurrealde, E. (2014). Structural basis for the Nanos-mediated recruitment of the CCR4-NOT complex and translational repression. *Genes & Development*, 28(8), 888–901. <http://doi.org/10.1101/gad.237289.113>
- Bickel, S. E., Wyman, D. W., Miyazaki, W. Y., Moore, D. P., & Orr-Weaver, T. L. (1996). Identification of ORD, a Drosophila protein essential for sister chromatid cohesion. *The EMBO Journal*, 15(6), 1451.
- Bickel, Sharon E., Wyman, D. W., & Orr-Weaver, T. L. (1997). Mutational Analysis of the Drosophila Sister-Chromatid Cohesion Protein ORD and Its Role in the Maintenance of Centromeric Cohesion. *Genetics*, 146(4), 1319–1331. <http://doi.org/10.1093/genetics/146.4.1319>
- Black, D. L. (2000). Protein diversity from alternative splicing: A challenge for bioinformatics and post-genome biology. *Cell*, 103(3), 367–370.
- Blagden, S. P., Gatt, M. K., Archambault, V., Lada, K., Ichihara, K., Lilley, K. S., ... Glover, D. M. (2009). Drosophila Larp associates with poly (A)-binding protein and is required for male fertility and syncytial embryo development. *Developmental Biology*, 334(1), 186–197. <http://doi.org/10.1016/J.YDBIO.2009.07.016>

Blatt, P., Martin, E. T., Breznak, S. M., & Rangan, P. (2020). Post-transcriptional gene regulation regulates germline stem cell to oocyte transition during Drosophila oogenesis. In *Current Topics in Developmental Biology* (Vol. 140, pp. 3–34). Elsevier.
<http://doi.org/10.1016/bs.ctdb.2019.10.003>

Blatt, P., Wong-Deyrup, S. W., McCarthy, A., Breznak, S., Hurton, M. D., Upadhyay, M., ... Rangan, P. (2020). RNA degradation sculpts the maternal transcriptome during Drosophila oogenesis. *bioRxiv*, 2020.06.30.179986.
<http://doi.org/10.1101/2020.06.30.179986>

Boamah, E. K., Kotova, E., Garabedian, M., Jarnik, M., & Tulin, A. V. (2012). Poly(ADP-Ribose) Polymerase 1 (PARP-1) Regulates Ribosomal Biogenesis in Drosophila Nucleoli. *PLoS Genetics*, 8(1). <http://doi.org/10.1371/journal.pgen.1002442>

Boerner, K., & Becker, P. B. (2016). Splice variants of the SWR1-type nucleosome remodeling factor Domino have distinct functions during Drosophila melanogaster oogenesis. *Development*, 143(17), 3154–3167.

Bohnsack, M. T., Kos, M., & Tollervey, D. (2008). Quantitative analysis of snoRNA association with pre-ribosomes and release of snR30 by Rok1 helicase. *EMBO Reports*, 9(12), 1230–1236. <http://doi.org/10.1038/embor.2008.184>

Boley, N., Wan, K. H., Bickel, P. J., & Celniker, S. E. (2014). Navigating and Mining modENCODE Data. *Methods (San Diego, Calif.)*, 68(1), 38–47.
<http://doi.org/10.1016/j.ymeth.2014.03.007>

- Bousquet-Antonelli, C. C., Vanrobays, E., Gélugne, J.-P., Caizergues-Ferrer, M., & Henry, Y. (2000). Rrp8p is a yeast nucleolar protein functionally linked to Gar1p and involved in pre-rRNA cleavage at site A2. *Rna*, 6(6), 826–843.
- Bowen, M. E., & Attardi, L. D. (2019). The role of P53 in developmental syndromes. *Journal of Molecular Cell Biology*, 11(3), 200–211. <http://doi.org/10.1093/jmcb/mjy087>
- Brombin, A., Joly, J.-S., & Jamen, F. (2015). New tricks for an old dog: Ribosome biogenesis contributes to stem cell homeostasis. *Current Opinion in Genetics & Development*, 34, 61–70. <http://doi.org/10.1016/j.gde.2015.07.006>
- Brooks, S. S., Wall, A. L., Golzio, C., Reid, D. W., Kondyles, A., Willer, J. R., ... Davis, E. E. (2014). A novel ribosomopathy caused by dysfunction of RPL10 disrupts neurodevelopment and causes X-linked microcephaly in humans. *Genetics*, 198(2), 723–33. <http://doi.org/10.1534/genetics.114.168211>
- Burrows, C., Abd Latip, N., Lam, S.-J., Carpenter, L., Sawicka, K., Tzolovsky, G., ... Blagden, S. P. (2010). The RNA binding protein Larp1 regulates cell division, apoptosis and cell migration. *Nucleic Acids Research*, 38(16), 5542–5553. <http://doi.org/10.1093/nar/gkq294>
- Buszczak, M., Paterno, S., Lighthouse, D., Bachman, J., Planck, J., Owen, S., ... Spradling, A. C. (2007). The Carnegie Protein Trap Library: A Versatile Tool for Drosophila Developmental Studies. *Genetics*, 175(3), 1505–1531. <http://doi.org/10.1534/genetics.106.065961>

Cahoon, C. K., & Hawley, R. S. (2016). Regulating the construction and demolition of the synaptonemal complex. *Nature Structural & Molecular Biology*, 23(5), 369–377.
<http://doi.org/10.1038/nsmb.3208>

Calo, E., Gu, B., Bowen, M. E., Aryan, F., Zalc, A., Liang, J., ... Attardi, L. D. (2018). Tissue-selective effects of nucleolar stress and rDNA damage in developmental disorders. *Nature*, 554(7690), 112.

Carpenter, A. T. C. (1975). Electron microscopy of meiosis in *Drosophila melanogaster* females. *Chromosoma*, 51(2), 157–182. <http://doi.org/10.1007/BF00319833>

Carpenter, A. T. C. (1979). Synaptonemal Complex and Recombination Nodules in Wild-Type *Drosophila melanogaster* Females. *Genetics*, 92(2), 511.

Carreira-Rosario, A., Bhargava, V., Hillebrand, J., Kollipara, R. K. K., Ramaswami, M., & Buszczak, M. (2016). Repression of Pumilio Protein Expression by Rb-fox1 Promotes Germ Cell Differentiation. *Developmental Cell*, 36(5), 562–571.
<http://doi.org/10.1016/j.devcel.2016.02.010>

Chang, P. L., Dunham, J. P., Nuzhdin, S. V., & Arbeitman, M. N. (2011). Somatic sex-specific transcriptome differences in *Drosophila* revealed by whole transcriptome sequencing. *BMC Genomics*, 12(1), 364.

Chau, J., Kulnane, L. S., & Salz, H. K. (2009). Sex-lethal facilitates the transition from germline stem cell to committed daughter cell in the *Drosophila* ovary. *Genetics*, 182(1), 121–132.

Chau, J., Kulnane, L. S., & Salz, H. K. (2012). Sex-lethal enables germline stem cell differentiation by down-regulating Nanos protein levels during *Drosophila* oogenesis. *Proceedings of the National Academy of Sciences*, 109(24), 9465–9470.

Chen, D., & McKearin, D. (2003a). Dpp Signaling Silences bam Transcription Directly to Establish Asymmetric Divisions of Germline Stem Cells. *Current Biology*, 13(20), 1786–1791. <http://doi.org/10.1016/J.CUB.2003.09.033>

Chen, D., & McKearin, D. M. (2003b). A discrete transcriptional silencer in the bam gene determines asymmetric division of the *Drosophila* germline stem cell. *Development*, 130(6), 1159–1170. <http://doi.org/10.1242/dev.00325>

Chen, T., & Steensel, B. van. (2017). Comprehensive analysis of nucleocytoplasmic dynamics of mRNA in *Drosophila* cells. *PLOS Genetics*, 13(8), e1006929. <http://doi.org/10.1371/journal.pgen.1006929>

Chen, Z.-X., Sturgill, D., Qu, J., Jiang, H., Park, S., Boley, N., . . . Richards, S. (2014). Comparative validation of the *D. Melanogaster* modENCODE transcriptome annotation. *Genome Research*, 24(7), 1209–1223. <http://doi.org/10.1101/gr.159384.113>

Cheng, Z., Mugler, C. F., Keskin, A., Hodapp, S., Chan, L. Y.-L., Weis, K., . . . Brar, G. A. (2019). Small and Large Ribosomal Subunit Deficiencies Lead to Distinct Gene Expression Signatures that Reflect Cellular Growth Rate. *Molecular Cell*, 73(1), 36–47.e10. <http://doi.org/10.1016/j.molcel.2018.10.032>

Christophorou, N., Rubin, T., & Huynh, J.-R. (2013). Synaptonemal Complex Components Promote Centromere Pairing in Pre-meiotic Germ Cells. *PLOS Genetics*, 9(12),

e1004012. <http://doi.org/10.1371/journal.pgen.1004012>

Chymkowitch, P., Aanes, H., Robertson, J., Klungland, A., & Enserink, J. M. (2017).

TORC1-dependent sumoylation of Rpc82 promotes RNA polymerase III assembly and activity. *Proceedings of the National Academy of Sciences*, 114(5), 1039–1044.

Cinalli, R. M., Rangan, P., & Lehmann, R. (2008). Germ Cells Are Forever. *Cell*, 132(4),

559–562. <http://doi.org/10.1016/j.cell.2008.02.003>

Cline, T. W., Rudner, D. Z., Barbash, D. A., Bell, M., & Vutien, R. (1999). Functioning

of the Drosophila integral U1/U2 protein Snf independent of U1 and U2 small nuclear ribonucleoprotein particles is revealed by snf+ gene dose effects. *Proceedings of the National Academy of Sciences*, 96(25), 14451–14458.

Cohn, W. E. (1960). Pseudouridine, a carbon-carbon linked ribonucleoside in ribonucleic acids: Isolation, structure, and chemical characteristics. *Journal of Biological Chemistry*, 235(5), 1488–1498.

Corsini, N. S., Peer, A. M., Moeseneder, P., Roiuk, M., Burkard, T. R., Theussl, H.-C., ...

Knoblich, J. A. (2018). Coordinated Control of mRNA and rRNA Processing Controls Embryonic Stem Cell Pluripotency and Differentiation. *Cell Stem Cell*, 22(4), 543–558.e12. <http://doi.org/10.1016/j.stem.2018.03.002>

Cramton, S. E., & Laski, F. A. (1994). String of pearls encodes Drosophila ribosomal protein S2, has Minute-like characteristics, and is required during oogenesis. *Genetics*, 137(4), 1039–1048.

De Cuevas, M., & Spradling, A. C. (1998). Morphogenesis of the *Drosophila* fusome and its implications for oocyte specification. *Development*, 125(15), 2781 LP–2789.

de la Cruz, J., Karbstein, K., & Woolford, J. L. (2015). Functions of ribosomal proteins in assembly of eukaryotic ribosomes in vivo. *Annual Review of Biochemistry*, 84, 93–129.
<http://doi.org/10.1146/annurev-biochem-060614-033917>

De Zoysa, M. D., & Yu, Y.-T. (2017). Posttranscriptional RNA pseudouridylation. In *The Enzymes* (Vol. 41, pp. 151–167). Elsevier.

Decatur, W. A., & Fournier, M. J. (2002). rRNA modifications and ribosome function. *Trends in Biochemical Sciences*, 27(7), 344–351. [http://doi.org/10.1016/S0968-0004\(02\)02109-6](http://doi.org/10.1016/S0968-0004(02)02109-6)

Decotto, E., & Spradling, A. C. (2005). The *Drosophila* ovarian and testis stem cell niches: Similar somatic stem cells and signals. *Developmental Cell*, 9(4), 501–510.
<http://doi.org/10.1016/j.devcel.2005.08.012>

Deisenroth, C., & Zhang, Y. (2010). Ribosome biogenesis surveillance: Probing the ribosomal protein-Mdm2-p53 pathway. *Oncogene*, 29(30), 4253–4260.
<http://doi.org/10.1038/onc.2010.189>

DeLuca, S. Z., & Spradling, A. C. (2018). Efficient Expression of Genes in the *Drosophila* Germline Using a UAS Promoter Free of Interference by Hsp70 piRNAs. *Genetics*, 209(2), 381–387. <http://doi.org/10.1534/genetics.118.300874>

Deshmukh, M., Tsay, Y. F., Paulovich, A. G., & Woolford, J. L. (1993). Yeast ribosomal protein L1 is required for the stability of newly synthesized 5S rRNA and the assembly

of 60S ribosomal subunits. *Molecular and Cellular Biology*, 13(5), 2835–2845.

Dinman, J. D. (2016). Pathways to specialized ribosomes: The Brussels lecture. *Journal of Molecular Biology*, 428(10), 2186–2194.

dos Santos, G., Schroeder, A. J., Goodman, J. L., Strelets, V. B., Crosby, M. A., Thurmond, J., ... Gelbart, W. M. (2015). FlyBase: Introduction of the *Drosophila melanogaster* Release 6 reference genome assembly and large-scale migration of genome annotations. *Nucleic Acids Research*, 43(Database issue), D690–D697.
<http://doi.org/10.1093/nar/gku1099>

Draptchinskaia, N., Gustavsson, P., Andersson, B., Pettersson, M., Willig, T.-N., Dianzani, I., ... Dahl, N. (1999). The gene encoding ribosomal protein S19 is mutated in Diamond-Blackfan anaemia. *Nature Genetics*, 21(2), 169–175.
<http://doi.org/10.1038/5951>

Eichhorn, S. W., Subtelny, A. O., Kronja, I., Kwasnieski, J. C., Orr-Weaver, T. L., & Bartel, D. P. (2016). mRNA poly(A)-tail changes specified by deadenylation broadly reshape translation in *Drosophila* oocytes and early embryos. *eLife*, 5, e16955.
<http://doi.org/10.7554/eLife.16955>

Eliazer, S., & Buszczak, M. (2011). Finding a niche: Studies from the *Drosophila* ovary. *Stem Cell Research & Therapy*, 2(6), 45. <http://doi.org/10.1186/scrt86>

Ellis, R. E., & Kimble, J. (1994). Control of germ cell differentiation in *Caenorhabditis elegans*. *Ciba Foundation Symposium*, 182, 179–192.

Emtenani, S., Martin, E. T., Gyoergy, A., Bicher, J., Genger, J.-W., Hurd, T. R., ... Siekhaus, D. E. (2021). A genetic program boosts mitochondrial function to power macrophage tissue invasion. *bioRxiv*, 2021.02.18.431643.

<http://doi.org/10.1101/2021.02.18.431643>

Fan, Y., Lee, T. V., Xu, D., Chen, Z., Lamblin, A.-F., Steller, H., & Bergmann, A. (2010). Dual roles of Drosophila P53 in cell death and cell differentiation. *Cell Death & Differentiation*, 17(6), 912–921. <http://doi.org/10.1038/cdd.2009.182>

Fichelson, P., Moch, C., Ivanovitch, K., Martin, C., Sidor, C. M., Lepesant, J.-A., ... Huynh, J.-R. (2009). Live-imaging of single stem cells within their niche reveals that a U3snoRNP component segregates asymmetrically and is required for self-renewal in Drosophila. *Nature Cell Biology*, 11(6), 685.

Flora, P., McCarthy, A., Upadhyay, M., & Rangan, P. (2017). Role of Chromatin Modifications in Drosophila Germline Stem Cell Differentiation. In S. Arur (Ed.), *Signaling-Mediated Control of Cell Division : From Oogenesis to Oocyte-to-Embryo Development* (pp. 1–30). Cham: Springer International Publishing. http://doi.org/10.1007/978-3-319-44820-6_1

Flora, P., Schowalter, S., Wong-Deyrup, S., DeGennaro, M., Nasrallah, M. A., & Rangan, P. (2018). Transient transcriptional silencing alters the cell cycle to promote germline stem cell differentiation in Drosophila. *Developmental Biology*, 434(1), 84–95. <http://doi.org/10.1016/j.ydbio.2017.11.014>

Flora, P., Wong-Deyrup, S. W., Martin, E. T., Palumbo, R. J., Nasrallah, M., Oligney, A., ... Rangan, P. (2018a). Sequential regulation of maternal mRNAs through a conserved cis-acting element in their 3' UTRs. *Cell Reports*, 25(13), 3828–3843.

Flora, P., Wong-Deyrup, S. W., Martin, E. T., Palumbo, R. J., Nasrallah, M., Oligney, A., ... Rangan, P. (2018b). Sequential Regulation of Maternal mRNAs through a Conserved cis-Acting Element in Their 3' UTRs. *Cell Reports*, 25(13), 3828–3843.e9.
<http://doi.org/10.1016/j.celrep.2018.12.007>

Fonseca, Bruno D., Jia, J.-J., Hollensen, A. K., Pointet, R., Hoang, H.-D., Niklaus, M. R., ... Alain, T. (2018). *LARP1 is a major phosphorylation substrate of mTORC1* (Preprint). Biochemistry.

Fonseca, Bruno D., Zakaria, C., Jia, J.-J., Graber, T. E., Svitkin, Y., Tahmasebi, S., ... Diao, I. T. (2015). La-related protein 1 (LARP1) represses terminal oligopyrimidine (TOP) mRNA translation downstream of mTOR complex 1 (mTORC1). *Journal of Biological Chemistry*, 290(26), 15996–16020.

Forbes, A. J., Lin, H., Ingham, P. W., & Spradling, A. C. (1996). Hedgehog is required for the proliferation and specification of ovarian somatic cells prior to egg chamber formation in Drosophila. *Development (Cambridge, England)*, 122(4), 1125–1135.

Forbes, A., & Lehmann, R. (1998). Nanos and Pumilio have critical roles in the development and function of Drosophila germline stem cells. *Development*, 125(4), 679 LP–690.

Fortier, S., MacRae, T., Bilodeau, M., Sargeant, T., & Sauvageau, G. (2015). Haploinsufficiency screen highlights two distinct groups of ribosomal protein genes essential for embryonic stem cell fate. *Proceedings of the National Academy of Sciences*, 112(7), 2127–2132. <http://doi.org/10.1073/pnas.1418845112>

Fu, Z., Geng, C., Wang, H., Yang, Z., Weng, C., Li, H., ... Xie, T. (2015). Twin Promotes the Maintenance and Differentiation of Germline Stem Cell Lineage through Modulation of Multiple Pathways. *Cell Reports*, 13(7), 1366–1379. <http://doi.org/10.1016/j.celrep.2015.10.017>

Fuchs, G., Diges, C., Kohlstaedt, L. A., Wehner, K. A., & Sarnow, P. (2011). Proteomic Analysis of Ribosomes: Translational Control of mRNA populations by Glycogen Synthase GYS1. *Journal of Molecular Biology*, 410(1), 118–130. <http://doi.org/10.1016/j.jmb.2011.04.064>

Fukao, A., Sasano, Y., Imataka, H., Inoue, K., Sakamoto, H., Sonenberg, N., ... Fujiwara, T. (2009). The ELAV Protein HuD Stimulates Cap-Dependent Translation in a Poly(A)- and eIF4A-Dependent Manner. *Molecular Cell*, 36(6), 1007–1017. <http://doi.org/10.1016/j.molcel.2009.11.013>

Fuller, M. T. (1998). Genetic control of cell proliferation and differentiation in Drosophilaspermatogenesis. In *Seminars in cell & developmental biology* (Vol. 9, pp. 433–444). Elsevier.

Gabut, M., Bourdelais, F., & Durand, S. (2020). Ribosome and Translational Control in Stem Cells. *Cells*, 9(2), 497. <http://doi.org/10.3390/cells9020497>

Gáspár, I., & Ephrussi, A. (2017). RNA localization feeds translation. *Science*, 357(6357), 1235 LP–1236. <http://doi.org/10.1126/science.aao5796>

Gentilella, A., Morón-Duran, F. D., Fuentes, P., Zweig-Rocha, G., Riaño-Canalias, F., Pelletier, J., . . . Thomas, G. (2017). Autogenous Control of 5'TOP mRNA Stability by 40S Ribosomes. *Molecular Cell*, 67(1), 55–70.e4. <http://doi.org/10.1016/j.molcel.2017.06.005>

Genuth, N. R., & Barna, M. (2018). The discovery of ribosome heterogeneity and its implications for gene regulation and organismal life. *Molecular Cell*, 71(3), 364. <http://doi.org/10.1016/j.molcel.2018.07.018>

Gerstberger, S., Meyer, C., Benjamin-Hong, S., Rodriguez, J., Briskin, D., Bognanni, C., . . . Tuschl, T. (2017). The conserved RNA exonuclease Rexo5 is required for 3' end maturation of 28S rRNA, 5S rRNA, and snoRNAs. *Cell Reports*, 21(3), 758–772.

Gilboa, L., Forbes, A., Tazuke, S. I., Fuller, M. T., & Lehmann, R. (2003). Germ line stem cell differentiation in Drosophila requires gap junctions and proceeds via an intermediate state. *Development*, 130(26), 6625–6634. <http://doi.org/10.1242/dev.00853>

Gilboa, L., & Lehmann, R. (2004). Repression of Primordial Germ Cell Differentiation Parallels Germ Line Stem Cell Maintenance. *Current Biology*, 14(11), 981–986. <http://doi.org/10.1016/j.cub.2004.05.049>

Glotzer, M., Murray, A. W., & Kirschner, M. W. (1991). Cyclin is degraded by the ubiquitin pathway. *Nature*, 349(6305), 132–138. <http://doi.org/10.1038/349132a0>

Goldstrohm, A. C., Hall, T. M. T., & McKenney, K. M. (2018). Post-transcriptional Regulatory Functions of Mammalian Pumilio Proteins. *Trends in Genetics*, 34(12),

972–990. <http://doi.org/10.1016/j.tig.2018.09.006>

Grandori, C., Gomez-Roman, N., Felton-Edkins, Z. A., Ngouenet, C., Galloway, D. A., Eisenman, R. N., & White, R. J. (2005). C-Myc binds to human ribosomal DNA and stimulates transcription of rRNA genes by RNA polymerase I. *Nature Cell Biology*, 7(3), 311–318. <http://doi.org/10.1038/ncb1224>

Granneman, S., & Baserga, S. J. (2004). Ribosome biogenesis: Of knobs and RNA processing. *Experimental Cell Research*, 296(1), 43–50.

Granneman, S., Bernstein, K. A., Bleichert, F., & Baserga, S. J. (2006). Comprehensive Mutational Analysis of Yeast DEXD/H Box RNA Helicases Required for Small Ribosomal Subunit Synthesis Downloaded from. *MOLECULAR AND CELLULAR BIOLOGY*, 26(4), 1183–1194. <http://doi.org/10.1128/MCB.26.4.1183-1194.2006>

Granneman, S., Petfalski, E., Tollervey, D., & Hurt, E. C. (2011). A cluster of ribosome synthesis factors regulate pre-rRNA folding and 5.8S rRNA maturation by the Rat1 exonuclease. *The EMBO Journal*, 30(19), 4006–19. <http://doi.org/10.1038/emboj.2011.256>

Grewal, S. S., Evans, J. R., & Edgar, B. A. (2007). Drosophila TIF-IA is required for ribosome synthesis and cell growth and is regulated by the TOR pathway. *Journal of Cell Biology*, 179(6), 1105–1113. <http://doi.org/10.1083/jcb.200709044>

Guild, G. M., Connelly, P. S., Shaw, M. K., & Tilney, L. G. (1997). Actin Filament Cables in Drosophila Nurse Cells Are Composed of Modules That Slide Passively Past One Another during Dumping. *Journal of Cell Biology*, 138(4), 783–797.

<http://doi.org/10.1083/jcb.138.4.783>

Guillerez, J., Lopez, P. J., Proux, F., Launay, H., & Dreyfus, M. (2005). A mutation in T7 RNA polymerase that facilitates promoter clearance. *Proceedings of the National Academy of Sciences*, 102(17), 5958–5963. <http://doi.org/10.1073/pnas.0407141102>

Gumienny, R., Jedlinski, D. J., Schmidt, A., Gypas, F., Martin, G., Vina-Vilaseca, A., & Zavolan, M. (2017). High-throughput identification of C/D box snoRNA targets with CLIP and RiboMeth-seq. *Nucleic Acids Research*, 45(5), 2341–2353. <http://doi.org/10.1093/nar/gkw1321>

Hager, J. H., & Cline, T. W. (1997). Induction of female Sex-lethal RNA splicing in male germ cells: Implications for Drosophila germline sex determination. *Development*, 124(24), 5033–5048.

Hales, K. G., Korey, C. A., Larracuente, A. M., & Roberts, D. M. (2015). Genetics on the Fly: A Primer on the Drosophila Model System. *Genetics*, 201(3), 815–842. <http://doi.org/10.1534/genetics.115.183392>

Han, R., Wang, X., Bachovchin, W., Zukowska, Z., & Osborn, J. W. (2015). Inhibition of dipeptidyl peptidase 8/9 impairs preadipocyte differentiation. *Scientific Reports*, 5(1), 12348. <http://doi.org/10.1038/srep12348>

Hanyu-Nakamura, K., Sonobe-Nojima, H., Tanigawa, A., Lasko, P., & Nakamura, A. (2008). Drosophila Pgc protein inhibits P-TEFb recruitment to chromatin in primordial germ cells. *Nature*, 451(7179), 730–733. <http://doi.org/10.1038/nature06498>

Hao, Y., Hao, S., Andersen-Nissen, E., Mauck, W. M., Zheng, S., Butler, A., ... Satija, R. (2021). Integrated analysis of multimodal single-cell data. *Cell*, 184(13), 3573–3587.e29. <http://doi.org/10.1016/j.cell.2021.04.048>

Harris, R. E., Pargett, M., Sutcliffe, C., Umulis, D., & Ashe, H. L. (2011). Brat promotes stem cell differentiation via control of a bistable switch that restricts BMP signaling. *Developmental Cell*, 20(1), 72–83. <http://doi.org/10.1016/j.devcel.2010.11.019>

Harvey, R. F., Smith, T. S., Mulroney, T., Queiroz, R. M. L., Pizzinga, M., Dezi, V., ... Willis, A. E. (2018). Trans-acting translational regulatory RNA binding proteins. *Wiley Interdisciplinary Reviews. RNA*, 9(3), e1465–e1465. <http://doi.org/10.1002/wrna.1465>

Haussmann, I. U., Bodík, Z., Sanchez-Moran, E., Mongan, N. P., Archer, N., Fray, R. G., & Soller, M. (2016). M 6 A potentiates Sxl alternative pre-mRNA splicing for robust Drosophila sex determination. *Nature*, 540(7632), 301.

Heinz, S., Benner, C., Spann, N., Bertolino, E., Lin, Y. C., Laslo, P., ... Glass, C. K. (2010). Simple combinations of lineage-determining transcription factors prime cis-regulatory elements required for macrophage and B cell identities. *Molecular Cell*, 38(4), 576–589. <http://doi.org/10.1016/j.molcel.2010.05.004>

Hendrix, N. W., Clemens, M., Canavan, T. P., Surti, U., & Rajkovic, A. (2012). Prenatally Diagnosed 17q12 Microdeletion Syndrome with a Novel Association with Congenital Diaphragmatic Hernia. *Fetal Diagnosis and Therapy*, 31(2), 129–133. <http://doi.org/10.1159/000332968>

Hernas, A. K., Soudet, J., Gérus, M., Lebaron, S., Caizergues-Ferrer, M., Mougin, A., & Henry, Y. (2008). The post-transcriptional steps of eukaryotic ribosome biogenesis. *Cellular and Molecular Life Sciences*, 65(15), 2334–2359. <http://doi.org/10.1007/s00018-008-8027-0>

Higa-Nakamine, S., Suzuki, T. T., Uechi, T., Chakraborty, A., Nakajima, Y., Nakamura, M., ... Kenmochi, N. (2012). Loss of ribosomal RNA modification causes developmental defects in zebrafish. *Nucleic Acids Research*, 40(1), 391–398. <http://doi.org/10.1093/nar/gkr700>

Hinnant, T. D., Alvarez, A. A., & Ables, E. T. (2017). Temporal remodeling of the cell cycle accompanies differentiation in the Drosophila germline. *Developmental Biology*, 429(1), 118–131. <http://doi.org/10.1016/j.ydbio.2017.07.001>

Hinnant, T. D., Merkle, J. A., & Ables, E. T. (2020). Coordinating Proliferation, Polarity, and Cell Fate in the Drosophila Female Germline. *Frontiers in Cell and Developmental Biology*, 0. <http://doi.org/10.3389/fcell.2020.00019>

Hong, S., Freeberg, M. A., Han, T., Kamath, A., Yao, Y., Fukuda, T., ... Inoki, K. (2017). LARP1 functions as a molecular switch for mTORC1-mediated translation of an essential class of mRNAs. *Elife*, 6, e25237.

Hong, S., Mannan, A. M., & Inoki, K. (2012). Evaluation of the Nutrient-Sensing mTOR Pathway. In T. Weichhart (Ed.), *mTOR: Methods and Protocols* (pp. 29–44). Totowa, NJ: Humana Press. http://doi.org/10.1007/978-1-61779-430-8_3

Hornstein, E., Tang, H., & Meyuhas, O. (2001). Mitogenic and nutritional signals are transduced into translational efficiency of TOP mRNAs. In *Cold Spring Harbor symposia on quantitative biology* (Vol. 66, pp. 477–484). Cold Spring Harbor Laboratory Press.

Hsu, H.-J., LaFever, L., & Drummond-Barbosa, D. (2008). Diet controls normal and tumorous germline stem cells via insulin-dependent and -independent mechanisms in *Drosophila*. *Developmental Biology*, 313(2), 700–712. <http://doi.org/10.1016/j.ydbio.2007.11.006>

Hu, Y., Flockhart, I., Vinayagam, A., Bergwitz, C., Berger, B., Perrimon, N., & Mohr, S. E. (2011). An integrative approach to ortholog prediction for disease-focused and other functional studies. *BMC Bioinformatics*, 12(1), 357. <http://doi.org/10.1186/1471-2105-12-357>

Hughes, S. E., Miller, D. E., Miller, A. L., & Hawley, R. S. (2018). Female Meiosis: Synapsis, Recombination, and Segregation in *Drosophila melanogaster*. *Genetics*, 208(3), 875–908. <http://doi.org/10.1534/genetics.117.300081>

Huynh, J.-R., & St Johnston, D. (2004). The Origin of Asymmetry: Early Polarisation of the *Drosophila* Germline Cyst and Oocyte. *Current Biology*, 14(11), R438–R449. <http://doi.org/10.1016/j.cub.2004.05.040>

Huynh, J., & St Johnston, D. (2000). The role of BicD, egl, orb and the microtubules in the restriction of meiosis to the *Drosophila* oocyte. *Development*, 127(13), 2785–2794. <http://doi.org/10.1242/dev.127.13.2785>

Iadevaia, V., Liu, R., & Proud, C. G. (2014). mTORC1 signaling controls multiple steps in ribosome biogenesis. *Seminars in Cell & Developmental Biology*, 36, 113–120.
<http://doi.org/10.1016/j.semcd.2014.08.004>

Ichihara, K., Shimizu, H., Taguchi, O., Yamaguchi, M., & Inoue, Y. H. (2007). A Drosophila orthologue of larp protein family is required for multiple processes in male meiosis. *Cell Structure and Function*, 710190003.

Inoue, K., Hoshijima, K., Sakamoto, H., & Shimura, Y. (1990). Binding of the Drosophila sex-lethal gene product to the alternative splice site of transformer primary transcript. *Nature*, 344(6265), 461.

Jacob, J., & Sirlin, J. L. (1959). Cell function in the ovary of drosophila. *Chromosoma*, 10(1), 210–228. <http://doi.org/10.1007/BF00396572>

Jalkanen, A. L., Coleman, S. J., & Wilusz, J. (2014). Determinants and implications of mRNA poly(A) tail size—does this protein make my tail look big? *Seminars in Cell & Developmental Biology*, 34, 24–32. <http://doi.org/10.1016/j.semcd.2014.05.018>

Jády, B. E., & Kiss, T. (2001). A small nucleolar guide RNA functions both in 2'-O-ribose methylation and pseudouridylation of the U5 spliceosomal RNA. *EMBO Journal*, 20(3), 541–551. <http://doi.org/10.1093/emboj/20.3.541>

Jefferies, H. B. J., Fumagalli, S., Dennis, P. B., Reinhard, C., Pearson, R. B., & Thomas, G. (1997). Rapamycin suppresses 5'TOP mRNA translation through inhibition of P70s6k. *The EMBO Journal*, 16(12), 3693–3704.
<http://doi.org/10.1093/emboj/16.12.3693>

Jia, D., Xu, Q., Xie, Q., Mio, W., & Deng, W.-M. (2016). Automatic stage identification of Drosophila egg chamber based on DAPI images. *Scientific Reports*, 6, 18850.
<http://doi.org/10.1038/srep18850>

Jia, J.-J., Lahr, R. M., Solgaard, M. T., Moraes, B. J., Pointet, R., Yang, A.-D., ... Fonseca, B. D. (2021). mTORC1 promotes TOP mRNA translation through site-specific phosphorylation of LARP1. *Nucleic Acids Research*.
<http://doi.org/10.1093/nar/gkaa1239>

Johnson, M. L., Nagengast, A. A., & Salz, H. K. (2010). PPS, a large multidomain protein, functions with sex-lethal to regulate alternative splicing in Drosophila. *PLoS Genetics*, 6(3), e1000872.

Joly, W., Chartier, A., Rojas-Rios, P., Busseau, I., & Simonelig, M. (2013). The CCR4 deadenylase acts with Nanos and Pumilio in the fine-tuning of Mei-P26 expression to promote germline stem cell self-renewal. *Stem Cell Reports*, 1(5), 411–424.
<http://doi.org/10.1016/j.stemcr.2013.09.007>

Jones, N. C., Lynn, M. L., Gaudenz, K., Sakai, D., Aoto, K., Rey, J.-P., ... Trainor, P. A. (2008). Prevention of the neurocristopathy Treacher Collins syndrome through inhibition of P53 function. *Nature Medicine*, 14(2), 125–133.
<http://doi.org/10.1038/nm1725>

Joshi, P. M., Riddle, M. R., Djabrayan, N. J. V., & Rothman, J. H. (2010). *Caenorhabditis elegans* as a model for stem cell biology. *Developmental Dynamics : An Official Publication of the American Association of Anatomists*, 239(5), 1539–1554.

<http://doi.org/10.1002/dvdy.22296>

- Joyce, E. F., Apostolopoulos, N., Beliveau, B. J., & Wu, C. (2013). Germline Progenitors Escape the Widespread Phenomenon of Homolog Pairing during Drosophila Development. *PLOS Genetics*, 9(12), e1004013. <http://doi.org/10.1371/journal.pgen.1004013>
- Kai, T., & Spradling, A. (2003). An empty Drosophila stem cell niche reactivates the proliferation of ectopic cells.
- Kai, T., Williams, D., & Spradling, A. C. (2005). The expression profile of purified Drosophila germline stem cells. *Developmental Biology*, 283(2), 486–502.
- Kalifa, Y., Armenti, S. T., & Gavis, E. R. (2009). Glorund interactions in the regulation of gurken and oskar mRNAs. *Developmental Biology*, 326(1), 68–74.
- Kalsotra, A., & Cooper, T. A. (2011). Functional consequences of developmentally regulated alternative splicing. *Nature Reviews Genetics*, 12(10), 715.
- Kan, L., Grozhik, A. V., Vedanayagam, J., Patil, D. P., Pang, N., Lim, K.-S., ... Despic, V. (2017). The m 6 A pathway facilitates sex determination in Drosophila. *Nature Communications*, 8, 15737.
- Karpen, G. H., Schaefer, J. E., & Laird, C. D. (1988). A Drosophila rRNA gene located in euchromatin is active in transcription and nucleolus formation. *Genes & Development*, 2(12b), 1745–1763.
- Khajuria, R. K., Munschauer, M., Ulirsch, J. C., Fiorini, C., Ludwig, L. S., McFarland, S. K., ... Sankaran, V. G. (2018). Ribosome levels selectively regulate

translation and lineage commitment in human hematopoiesis. *Cell*, 173(1), 90–103.

<http://doi.org/10.1016/J.CELL.2018.02.036>

Khetani, R. S., & Bickel, S. E. (2007). Regulation of meiotic cohesion and chromosome core morphogenesis during pachytene in *Drosophila* oocytes. *Journal of Cell Science*, 120(Pt 17), 3123–3137. <http://doi.org/10.1242/jcs.009977>

Khoshnevis, S., Askenasy, I., Johnson, M. C., Dattolo, M. D., Young-Erdos, C. L., Stroupe, M. E., & Karbstein, K. (2016). The DEAD-box Protein Rok1 Orchestrates 40S and 60S Ribosome Assembly by Promoting the Release of Rrp5 from Pre-40S Ribosomes to Allow for 60S Maturation. *PLOS Biology*, 14(6), e1002480. <http://doi.org/10.1371/journal.pbio.1002480>

Kim, E., Goraksha-Hicks, P., Li, L., Neufeld, T. P., & Guan, K.-L. (2008). Regulation of TORC1 by Rag GTPases in nutrient response. *Nature Cell Biology*, 10(8), 935.

Kim, G., Pai, C.-I., Sato, K., Person, M. D., Nakamura, A., & Macdonald, P. M. (2015). Region-Specific Activation of oskar mRNA Translation by Inhibition of Bruno-Mediated Repression. *PLOS Genetics*, 11(2), e1004992.

Kimball, S. R. (2002). Regulation of Global and Specific mRNA Translation by Amino Acids. *The Journal of Nutrition*, 132(5), 883–886. <http://doi.org/10.1093/jn/132.5.883>

Kimble, J. (2011). Molecular Regulation of the Mitosis/Meiosis Decision in Multicellular Organisms. *Cold Spring Harbor Perspectives in Biology*, 3(8), a002683. <http://doi.org/10.1101/cshperspect.a002683>

Kim-Ha, J., Kerr, K., & Macdonald, P. M. (1995). Translational regulation of oskar mRNA by Bruno, an ovarian RNA-binding protein, is essential. *Cell*, 81(3), 403–412.
[http://doi.org/10.1016/0092-8674\(95\)90393-3](http://doi.org/10.1016/0092-8674(95)90393-3)

Kirilly, D., Wang, S., & Xie, T. (2011). Self-maintained escort cells form a germline stem cell differentiation niche. *Development*, 138(23), 5087–5097.
<http://doi.org/10.1242/dev.067850>

Kiss, A. M., Jady, B. E., Bertrand, E., & Kiss, T. (2004). Human Box H/ACA Pseudouridylation Guide RNA Machinery. *Molecular and Cellular Biology*, 24(13), 5797–5807. <http://doi.org/10.1128/MCB.24.13.5797-5807.2004>

Kiss, T., Fayet-Lebaron, E., & Jády, B. E. (2010). Box H/ACA small ribonucleoproteins. *Molecular Cell*, 37(5), 597–606.

Kong, J., Han, H., Bergalet, J., Bouvrette, L. P. B., Hernández, G., Moon, N.-S., ... Lasko, P. (2019). Drosophila ribosomal protein S5b is essential for oogenesis and interacts with distinct RNAs. *bioRxiv*, 600502.

Koš, M., & Tollervey, D. (2010). Yeast pre-rRNA processing and modification occur cotranscriptionally. *Molecular Cell*, 37(6), 809–820.

Koziol, M. J., Garrett, N., & Gurdon, J. B. (2007). Tpt1 Activates Transcription of Oct4 and nanog in Transplanted Somatic Nuclei. *Current Biology*, 17(9), 801–807.
<http://doi.org/10.1016/j.cub.2007.03.062>

Kronja, I., Yuan, B., Eichhorn, S. W. W., Dzeyk, K., Krijgsveld, J., Bartel, D. P. P., & Orr-Weaver, T. L. L. (2014). Widespread Changes in the Posttranscriptional Land-

scape at the Drosophila Oocyte-to-Embryo Transition. *Cell Reports*, 7(5), 1495–1508.

<http://doi.org/10.1016/j.celrep.2014.05.002>

Lahr, Roni M., Fonseca, B. D., Ciotti, G. E., Al-Ashtal, H. A., Jia, J.-J., Niklaus, M. R., ... Berman, A. J. (2017). La-related protein 1 (LARP1) binds the mRNA cap, blocking eIF4F assembly on TOP mRNAs. *Elife*, 6, e24146.

Lahr, Roni M., Mack, S. M., Héroux, A., Blagden, S. P., Bousquet-Antonelli, C., Deragon, J.-M., & Berman, A. J. (2015). The La-related protein 1-specific domain repurposes HEAT-like repeats to directly bind a 5'TOP sequence. *Nucleic Acids Research*, 43(16), 8077–8088. <http://doi.org/10.1093/nar/gkv748>

Lasko, P. (2000). The *Drosophila melanogaster* genome: Translation factors and RNA binding proteins. *Journal of Cell Biology*, 150(2), 51–56. <http://doi.org/10.1083/jcb.150.2.F51>

Lasko, P. (2012). mRNA localization and translational control in *Drosophila* oogenesis. *Cold Spring Harbor Perspectives in Biology*, 4(10), a012294. <http://doi.org/10.1101/cshperspect.a012294>

Lähnemann, D., Köster, J., Szczurek, E., McCarthy, D. J., Hicks, S. C., Robinson, M. D., ... Schönhuth, A. (2020). Eleven grand challenges in single-cell data science. *Genome Biology*, 21(1), 31. <http://doi.org/10.1186/s13059-020-1926-6>

Lee, K.-A., & Lee, W.-J. (2014). *Drosophila* as a model for intestinal dysbiosis and chronic inflammatory diseases. *Developmental & Comparative Immunology*, 42(1), 102–110. <http://doi.org/10.1016/j.dci.2013.05.005>

Lee, Y., & Rio, D. C. (2015). Mechanisms and regulation of alternative pre-mRNA splicing. *Annual Review of Biochemistry*, 84, 291–323.

- Lehmann, R. (2012). Germline Stem Cells: Origin and Destiny. *Cell Stem Cell*, 10(6), 729–739. <http://doi.org/10.1016/j.stem.2012.05.016>
- Lesch, B. J., & Page, D. C. (2012). Genetics of germ cell development. *Nature Reviews Genetics*, 13, 781.
- Li, L., Pang, X., Zhu, Z., Lu, L., Yang, J., Cao, J., & Fei, S. (2018). GTPBP4 Promotes Gastric Cancer Progression via Regulating P53 Activity. *Cellular Physiology and Biochemistry*, 45(2), 667–676.
- Li, S., Zhang, C., Takemori, H., Zhou, Y., & Xiong, Z.-Q. (2009). TORC1 regulates activity-dependent CREB-target gene transcription and dendritic growth of developing cortical neurons. *Journal of Neuroscience*, 29(8), 2334–2343.
- Li, Y., Minor, N. T., Park, J. K., McKearin, D. M., & Maines, J. Z. (2009). Bam and Bgcn antagonize Nanos-dependent germ-line stem cell maintenance. *Proceedings of the National Academy of Sciences*, 106(23), 9304 LP–9309. <http://doi.org/10.1073/pnas.0901452106>
- Li, Y., Zhang, Q., Carreira-Rosario, A., Maines, J. Z., McKearin, D. M., & Buszczak, M. (2013). Mei-P26 Cooperates with Bam, Bgcn and Sxl to Promote Early Germline Development in the Drosophila Ovary. *PLOS ONE*, 8(3), e58301.
- Licht, K., & Jantsch, M. F. (2016). Rapid and dynamic transcriptome regulation by RNA editing and RNA modifications. *J Cell Biol*, 213(1), 15–22.
- Lilly, M. A., & Duronio, R. J. (2005). New insights into cell cycle control from the Drosophila endocycle. *Oncogene*, 24(17), 2765–2775. <http://doi.org/10.1038/sj.onc.1208610>

- Lin, Haifan, & Spradling, A. C. (1993). Germline Stem Cell Division and Egg Chamber Development in Transplanted Drosophila Germaria. *Developmental Biology*, 159(1), 140–152. <http://doi.org/10.1006/dbio.1993.1228>
- Lin, H., & Spradling, A. C. (1997). A novel group of pumilio mutations affects the asymmetric division of germline stem cells in the Drosophila ovary. *Development (Cambridge, England)*, 124(12), 2463–2476.
- Linder, P., & Lasko, P. (2006). Bent out of Shape: RNA Unwinding by the DEAD-Box Helicase Vasa. *Cell*, 125(2), 219–221. <http://doi.org/10.1016/j.cell.2006.03.030>
- Lipton, J. M., Kudisch, M., Gross, R., & Nathan, D. G. (1986). Defective Erythroid Progenitor Differentiation System in Congenital Hypoplastic (Diamond-Blackfan) Anemia. *Blood*, 67(4), 962–968. <http://doi.org/10.1182/blood.V67.4.962.962>
- Lo, K.-Y., Li, Z., Bussiere, C., Bresson, S., Marcotte, E. M., & Johnson, A. W. (2010). Defining the pathway of cytoplasmic maturation of the 60S ribosomal subunit. *Molecular Cell*, 39(2), 196–208.
- Loewith, R., & Hall, M. N. (2011). Target of Rapamycin (TOR) in Nutrient Signaling and Growth Control. *Genetics*, 189(4), 1177–1201. <http://doi.org/10.1534/genetics.111.133363>
- Love, M. I., Huber, W., & Anders, S. (2014). Moderated estimation of fold change and dispersion for RNA-seq data with DESeq2. *Genome Biology*, 15(12), 550. <http://doi.org/10.1186/s13059-014-0550-8>
- Lu, J., & Oliver, B. (2001). Drosophila OVO regulates ovarian tumor transcription by binding unusually near the transcription start site. *Development*, 128(9), 1671–1686.

Lu, W.-J., Chapo, J., Roig, I., & Abrams, J. M. (2010). Meiotic Recombination Provokes Functional Activation of the P53 Regulatory Network. *Science*, 328(5983), 1278–1281.
<http://doi.org/10.1126/science.1185640>

Lunardi, A., Di Minin, G., Provero, P., Dal Ferro, M., Carotti, M., Del Sal, G., & Collavin, L. (2010). A genome-scale protein interaction profile of Drosophila P53 uncovers additional nodes of the human P53 network. *Proceedings of the National Academy of Sciences*, 107(14), 6322–6327.

Ma, X., Han, Y., Song, X., Do, T., Yang, Z., Ni, J., & Xie, T. (2016). DNA damage-induced Lok/CHK2 activation compromises germline stem cell self-renewal and lineage differentiation. *Development*, 143(23), 4312–4323. <http://doi.org/10.1242/dev.141069>

Madhani, H. D., Bordonne, R., & Guthrie, C. (1990). Multiple roles for U6 snRNA in the splicing pathway. *Genes & Development*, 4(12b), 2264–2277.

Magnusson, B., Ekim, B., & Fingar, D. C. (2012). Regulation and function of ribosomal protein S6 kinase (S6K) within mTOR signalling networks. *Biochem. J*, 441, 1–21.
<http://doi.org/10.1042/BJ20110892>

Magnúsdóttir, E., & Surani, M. A. (2014). How to make a primordial germ cell. *Development*, 141(2), 245 LP–252. <http://doi.org/10.1242/dev.098269>

Maniatis, T., & Tasic, B. (2002). Alternative pre-mRNA splicing and proteome expansion in metazoans. *Nature*, 418(6894), 236.

Margolis, J., & Spradling, A. (1995). Identification and behavior of epithelial stem cells in the Drosophila ovary. *Development*, 121(11), 3797 LP–3807.

Martin, D. E., Powers, T., & Hall, M. N. (2006). Regulation of ribosome biogenesis: Where is TOR? *Cell Metabolism*, 4(4), 259–260.

Martin, R., Hackert, P., Ruprecht, M., Simm, S., Brüning, L., Mirus, O., ... Bohnsack, M. T. (2014). A pre-ribosomal RNA interaction network involving snoRNAs and the Rok1 helicase. *RNA*, 20(8), 1173–1182. <http://doi.org/10.1261/rna.044669.114>

Martineau, Y., Derry, M. C., Wang, X., Yanagiya, A., Berlanga, J. J., Shyu, A.-B., ... Sonenberg, N. (2008). Poly(A)-binding protein-interacting protein 1 binds to eukaryotic translation initiation factor 3 to stimulate translation. *Molecular and Cellular Biology*, 28(21), 6658–6667. <http://doi.org/10.1128/MCB.00738-08>

Matera, A. G., & Wang, Z. (2014). A day in the life of the spliceosome. *Nature Reviews Molecular Cell Biology*, 15(2), 108.

Mathieu, J., Cauvin, C., Moch, C., Radford, S. J. J., Sampaio, P., Perdigoto, C. N., ... Huynh, J.-R. (2013). Aurora B and cyclin B have opposite effects on the timing of cytokinesis abscission in Drosophila germ cells and in vertebrate somatic cells. *Developmental Cell*, 26(3), 250–265. <http://doi.org/10.1016/J.DEVCEL.2013.07.005>

Matias, N. R., Mathieu, J., & Huynh, J.-R. (2015). Abscission is regulated by the ESCRT-III protein shrub in Drosophila germline stem cells. *PLoS Genetics*, 11(2), e1004653. <http://doi.org/10.1371/journal.pgen.1004653>

Mattox, W., Palmer, M. J., & Baker, B. S. (1990). Alternative splicing of the sex determination gene transformer-2 is sex-specific in the germ line but not in the soma. *Genes & Development*, 4(5), 789–805.

Mayer, C., & Grummt, I. (2006). Ribosome biogenesis and cell growth: mTOR coordinates transcription by all three classes of nuclear RNA polymerases. *Oncogene*, 25(48), 6384–6391. <http://doi.org/10.1038/sj.onc.1209883>

Mazumder, B., Seshadri, V., Imataka, H., Sonenberg, N., & Fox, P. L. (2001). Translational silencing of ceruloplasmin requires the essential elements of mRNA circularization: Poly(A) tail, poly(A)-binding protein, and eukaryotic translation initiation factor 4G. *Molecular and Cellular Biology*, 21(19), 6440–6449. <http://doi.org/10.1128/mcb.21.19.6440-6449.2001>

McCarthy, A., Deiulio, A., Martin, E. T., Upadhyay, M., & Rangan, P. (2018). Tip60 complex promotes expression of a differentiation factor to regulate germline differentiation in female Drosophila. *Molecular Biology of the Cell*, 29(24), 2933–2945. <http://doi.org/10.1091/mbc.E18-06-0385>

McCarthy, A., Sarkar, K., Martin, E. T., Upadhyay, M., James, J. R., Lin, J. M., ... Rangan, P. (2019). MSL3 coordinates a transcriptional and translational meiotic program in female Drosophila. *bioRxiv*, 2019.12.18.879874. <http://doi.org/10.1101/2019.12.18.879874>

McCarthy, A., Sarkar, K., Martin, E. T., Upadhyay, M., Jang, S., Williams, N. D., ... Rangan, P. (2021). MSL3 promotes germline stem cell differentiation in female Drosophila. *Development*, dev.199625. <http://doi.org/10.1242/dev.199625>

McGowan, K. A., Pang, W. W., Bhardwaj, R., Perez, M. G., Pluvinage, J. V., Glader, B. E., ... Barsh, G. S. (2011). Reduced ribosomal protein gene dosage and

P53 activation in low-risk myelodysplastic syndrome. *Blood*, 118(13), 3622–3633.

<http://doi.org/10.1182/blood-2010-11-318584>

McKearin, D. M., & Spradling, A. C. (1990). Bag-of-marbles: A *Drosophila* gene required to initiate both male and female gametogenesis. *Genes & Development*, 4(12b), 2242–2251. <http://doi.org/10.1101/gad.4.12b.2242>

McKearin, D., & Ohlstein, B. (1995). A role for the *Drosophila* bag-of-marbles protein in the differentiation of cystoblasts from germline stem cells. *Development*, 121(9), 2937 LP–2947.

Mehrotra, S., & McKim, K. S. (2006). Temporal Analysis of Meiotic DNA Double-Strand Break Formation and Repair in *Drosophila* Females. *PLOS Genetics*, 2(11), e200. <http://doi.org/10.1371/journal.pgen.0020200>

Meyuhas, O. (2000). Synthesis of the translational apparatus is regulated at the translational level. *European Journal of Biochemistry*, 267(21), 6321–6330. <http://doi.org/10.1046/j.1432-1327.2000.01719.x>

Meyuhas, O., & Kahan, T. (2015). The race to decipher the top secrets of TOP mRNAs. *Biochimica Et Biophysica Acta (BBA) - Gene Regulatory Mechanisms*, 1849(7), 801–811. <http://doi.org/10.1016/j.bbagr.2014.08.015>

Mills, E. W., & Green, R. (2017). Ribosomopathies: There's strength in numbers. *Science*, 358(6363), eaan2755. <http://doi.org/10.1126/SCIENCE.AAN2755>

Mitchell, S. F., Walker, S. E., Algire, M. A., Park, E.-H., Hinnebusch, A. G., & Lorsch, J. R. (2010). The 5'-7-methylguanosine cap on eukaryotic mRNAs serves both to stim-

ulate canonical translation initiation and to block an alternative pathway. *Molecular Cell*, 39(6), 950–962.

Moon, S., Cassani, M., Lin, Y. A., Wang, L., Dou, K., & Zhang, Z. Z. Z. (2018). A Robust Transposon-Endogenizing Response from Germline Stem Cells. *Developmental Cell*, 47(5), 660–671.

Moreno-Torres, M., Jaquenoud, M., & De Virgilio, C. (2015). TORC1 controls G 1S cell cycle transition in yeast via Mpkl and the greatwall kinase pathway. *Nature Communications*, 6, 8256.

Morgado-Palacin, L., Llanos, S., & Serrano, M. (2012). Ribosomal stress induces L11-and P53-dependent apoptosis in mouse pluripotent stem cells. *Cell Cycle*, 11(3), 503–510.

Morita, S., Ota, R., & Kobayashi, S. (2018). Downregulation of NHP 2 promotes proper cyst formation in Drosophila ovary. *Development, Growth & Differentiation*, 60(5), 248–259.

Morrison, S. J., & Spradling, A. C. (2008). Stem Cells and Niches: Mechanisms That Promote Stem Cell Maintenance throughout Life. *Cell*, 132(4), 598–611.
<http://doi.org/10.1016/j.cell.2008.01.038>

Mukherjee, C., Patil, D. P., Kennedy, B. A., Bakthavachalu, B., Bundschuh, R., & Schoenberg, D. R. (2012). Identification of cytoplasmic capping targets reveals a role for cap homeostasis in translation and mRNA stability. *Cell Reports*, 2(3), 674–684.

Nagengast, A. A., Stitzinger, S. M., Tseng, C.-H., Mount, S. M., & Salz, H. K. (2003). Sex-lethal splicing autoregulation in vivo: Interactions between SEX-LETHAL, the

U1 snRNP and U2AF underlie male exon skipping. *Development*, 130(3), 463–471.

Nakamura, A., Sato, K., & Hanyu-Nakamura, K. (2004). Drosophila Cup Is an eIF4E Binding Protein that Associates with Bruno and Regulates oskar mRNA Translation in Oogenesis. *Developmental Cell*, 6(1), 69–78. [http://doi.org/10.1016/S1534-5807\(03\)00400-3](http://doi.org/10.1016/S1534-5807(03)00400-3)

Navarro, C., Lehmann, R., & Morris, J. (2001). Oogenesis: Setting one sister above the rest. *Current Biology*, 11(5), R162–R165. [http://doi.org/10.1016/S0960-9822\(01\)00083-5](http://doi.org/10.1016/S0960-9822(01)00083-5)

Navarro, C., Puthalakath, H., Adams, J. M., Strasser, A., & Lehmann, R. (2004). Egali-tarian binds dynein light chain to establish oocyte polarity and maintain oocyte fate. *Nature Cell Biology*, 6(5), 427–435. <http://doi.org/10.1038/ncb1122>

Nazar, R. (2004). Ribosomal RNA Processing and Ribosome Biogenesis in Eukaryotes. *IUBMB Life (International Union of Biochemistry and Molecular Biology: Life)*, 56(8), 457–465. <http://doi.org/10.1080/15216540400010867>

Nerurkar, P., Altvater, M., Gerhardy, S., Schütz, S., Fischer, U., Weirich, C., & Panse, V. G. (2015). Eukaryotic ribosome assembly and nuclear export. *International Review of Cell and Molecular Biology*, 319, 107–40. <http://doi.org/10.1016/bsircmb.2015.07.002>

Neumüller, R. A., Betschinger, J., Fischer, A., Bushati, N., Poernbacher, I., Mechtler, K., ... Knoblich, J. A. (2008). Mei-P26 regulates microRNAs and cell growth in the Drosophila ovarian stem cell lineage. *Nature*, 454(7201), 241–5. <http://doi.org/10.1038/nature07014>

Neve, J., Patel, R., Wang, Z., Louey, A., & Furger, A. M. (2017). Cleavage and polyadenylation: Ending the message expands gene regulation. *RNA Biology*, 14(7), 865–890.
<http://doi.org/10.1080/15476286.2017.1306171>

Noda, T. (2017). Regulation of autophagy through TORC1 and mTORC1. *Biomolecules*, 7(3), 52.

Nystul, T., & Spradling, A. (2010). Regulation of Epithelial Stem Cell Replacement and Follicle Formation in the Drosophila Ovary. *Genetics*, 184(2), 503–515.
<http://doi.org/10.1534/genetics.109.109538>

O ’day, C. L., Chavanikamannil, F., & Abelson, J. (1996). 8S rRNA processing requires the RNA helicase-like protein Rrp3. *Nucleic Acids Research*, 24(16).

Ochs, R. L., Lischwe, M. A., Spohn, W. H., & Busch, H. (1985). Fibrillarin: A new protein of the nucleolus identified by autoimmune sera. *Biology of the Cell*, 54(2), 123–133. <http://doi.org/10.1111/j.1768-322X.1985.tb00387.x>

Ogami, K., Oishi, Y., Nogimori, T., Sakamoto, K., & Hoshino, S. (2020). LARP1 facilitates translational recovery after amino acid refeeding by preserving long poly(A)-tailed TOP mRNAs. *bioRxiv*, 716217. <http://doi.org/10.1101/716217>

Ohlstein, B., & McKearin, D. (1997). Ectopic expression of the Drosophila Bam protein eliminates oogenic germline stem cells. *Development*, 124(18), 3651–3662.

Öunap, K., Käspér, L., Kurg, A., & Kurg, R. (2013). The Human WBSCR22 Protein Is Involved in the Biogenesis of the 40S Ribosomal Subunits in Mammalian Cells. *PLoS ONE*, 8(9). <http://doi.org/10.1371/journal.pone.0075686>

Page, S. L., & Hawley, R. S. (2003). Chromosome Choreography: The Meiotic Ballet. *Science*. <http://doi.org/10.1126/science.1086605>

Pagès, H., Aboyoun, P., Gentleman, R., & DebRoy, S. (2019). Biostrings: Efficient manipulation of biological strings.

Pallares-Cartes, C., Cakan-Akdogan, G., & Teleman, A. A. (2012). Tissue-specific coupling between insulin/IGF and TORC1 signaling via PRAS40 in Drosophila. *Developmental Cell*, 22(1), 172–182.

Penalva, L. O. F., & Sánchez, L. (2003). RNA binding protein sex-lethal (Sxl) and control of Drosophila sex determination and dosage compensation. *Microbiol. Mol. Biol. Rev.*, 67(3), 343–359.

Penzo, M., & Montanaro, L. (2018). Turning uridines around: Role of rRNA pseudouridylation in ribosome biogenesis and ribosomal function. *Biomolecules*, 8(2), 38.

Pereboom, T. C., van Weele, L. J., Bondt, A., & MacInnes, A. W. (2011). A zebrafish model of dyskeratosis congenita reveals hematopoietic stem cell formation failure resulting from ribosomal protein-mediated P53 stabilization. *Blood*, 118(20), 5458–5465.

Perišić Nanut, M., Pečar Fonović, U., Jakoš, T., & Kos, J. (2021). The Role of Cysteine Peptidases in Hematopoietic Stem Cell Differentiation and Modulation of Immune System Function. *Frontiers in Immunology*, 12.

Philippe, L., van den Elzen, A. M. G., Watson, M. J., & Thoreen, C. C. (2020). Global analysis of LARP1 translation targets reveals tunable and dynamic features of 5' TOP motifs. *Proceedings of the National Academy of Sciences*, 117(10), 5319–5328.

<http://doi.org/10.1073/pnas.1912864117>

Philippe, L., Vasseur, J.-J., Debart, F., & Thoreen, C. C. (2018). La-related protein 1 (LARP1) repression of TOP mRNA translation is mediated through its cap-binding domain and controlled by an adjacent regulatory region. *Nucleic Acids Research*, 46(3), 1457–1469. <http://doi.org/10.1093/nar/gkx1237>

Phipps, K. R., Charette, J. M., & Baserga, S. J. (2011). The small subunit processome in ribosome biogenesisprogress and prospects. *Wiley Interdisciplinary Reviews: RNA*, 2(1), 1–21.

Polydorides, A. D., Okano, H. J., Yang, Y. Y. L., Stefani, G., & Darnell, R. B. (2000). A brain-enriched polypyrimidine tract-binding protein antagonizes the ability of Nova to regulate neuron-specific alternative splicing. *Proceedings of the National Academy of Sciences*, 97(12), 6350–6355.

Powers, T., & Walter, P. (1999). Regulation of ribosome biogenesis by the rapamycin-sensitive TOR-signaling pathway in *Saccharomyces cerevisiae*. *Molecular Biology of the Cell*, 10(4), 987–1000.

Preiss, T., & Hentze, M. W. (1998). Dual function of the messenger RNA cap structure in poly(A)-tail-promoted translation in yeast. *Nature*, 392(6675), 516–520. <http://doi.org/10.1038/33192>

Primus, S., Pozmanter, C., Baxter, K., & Van Doren, M. (2019). Tudor-domain containing protein 5-like promotes male sexual identity in the *Drosophila* germline and is repressed in females by Sex lethal. *PLoS Genetics*, 15(7), e1007617.

Qiao, H., Li, Y., Feng, C., Duo, S., Ji, F., & Jiao, J. (2018). Nap1l1 Controls Embryonic Neural Progenitor Cell Proliferation and Differentiation in the Developing Brain. *Cell Reports*, 22(9), 2279–2293. <http://doi.org/10.1016/j.celrep.2018.02.019>

Qin, X., Ahn, S., Speed, T. P., & Rubin, G. M. (2007). Global analyses of mRNA translational control during early Drosophila embryogenesis. *Genome Biology*, 8(4), R63. <http://doi.org/10.1186/gb-2007-8-4-r63>

Raisch, T., Bhandari, D., Sabath, K., Helms, S., Valkov, E., Weichenrieder, O., & Izaurralde, E. (2016). Distinct modes of recruitment of the CCR4-NOT complex by Drosophila and vertebrate Nanos. *The EMBO Journal*, 35(9), 974–990. <http://doi.org/10.15252/embj.201593634>

Rangan, Prashanth, DeGennaro, M., Jaime-Bustamante, K., Coux, R.-X. X., Martinho, R. G., & Lehmann, R. (2009). Temporal and Spatial Control of Germ-Plasm RNAs. *Current Biology*, 19(1), 72–77. <http://doi.org/10.1016/j.cub.2008.11.066>

Rangan, P., DeGennaro, M., & Lehmann, R. (2008). Regulating Gene Expression in the Drosophila Germ Line. *Cold Spring Harbor Symposia on Quantitative Biology*, 73, 1–8. <http://doi.org/10.1101/sqb.2008.73.057>

Reichardt, I., Bonnay, F., Steinmann, V., Loedige, I., Burkard, T. R., Meister, G., & Knoblich, J. A. (2018). The tumor suppressor Brat controls neuronal stem cell lineages by inhibiting Deadpan and Zelda. *EMBO Reports*, 19(1), 102–117. <http://doi.org/10.15252/embr.201744188>

Reveal, B., Garcia, C., Ellington, A., & Macdonald, P. M. (2011). Multiple RNA binding domains of Bruno confer recognition of diverse binding sites for translational repression. *RNA Biology*, 8(6), 1047–1060. <http://doi.org/10.4161/rna.8.6.17542>

Reyes, R., & Izquierdo, J. M. (2008). Half pint couples transcription and splicing of eIF4E-1, 2 gene during fly development. *Biochemical and Biophysical Research Communications*, 374(4), 758–762.

Richter, J. D., & Lasko, P. (2011). Translational control in oocyte development. *Cold Spring Harbor Perspectives in Biology*, 3(9), a002758–a002758. <http://doi.org/10.1101/cshperspect.a002758>

Rissland, O. S. (2017). The organization and regulation of mRNA/protein complexes. *Wiley Interdisciplinary Reviews: RNA*, 8(1), e1369. <http://doi.org/10.1002/wrna.1369>

Ritossa, F. M., & Spiegelman, S. (1965). Localization of DNA complementary to ribosomal RNA in the nucleolus organizer region of *Drosophila melanogaster*. *Proceedings of the National Academy of Sciences of the United States of America*, 53(4), 737.

Romanelli, M., Diani, E., & Lievens, P. (2013). New insights into functional roles of the polypyrimidine tract-binding protein. *International Journal of Molecular Sciences*, 14(11), 22906–22932.

Roth, S. (2001). Drosophila oogenesis: Coordinating germ line and soma. *Current Biology*, 11(19), R779–R781. [http://doi.org/10.1016/S0960-9822\(01\)00469-9](http://doi.org/10.1016/S0960-9822(01)00469-9)

Roundtree, I. A., Evans, M. E., Pan, T., & He, C. (2017). Dynamic RNA modifications in gene expression regulation. *Cell*, 169(7), 1187–1200.

Royzman, I., & Orr-Weaver, T. L. (1998). S phase and differential DNA replication during Drosophila oogenesis. *Genes to Cells*, 3(12), 767–776. <http://doi.org/10.1046/j.1365-2443.1998.00232.x>

Rubin, T., Macaisne, N., & Huynh, J.-R. (2020). Mixing and Matching Chromosomes during Female Meiosis. *Cells*, 9(3), 696. <http://doi.org/10.3390/cells9030696>

Rust, K., Byrnes, L. E., Yu, K. S., Park, J. S., Sneddon, J. B., Tward, A. D., & Nystul, T. G. (2020). A single-cell atlas and lineage analysis of the adult Drosophila ovary. *Nature Communications*, 11(1), 5628. <http://doi.org/10.1038/s41467-020-19361-0>

Rymond, B. C., & Rosbash, M. (1985). Cleavage of 5' splice site and lariat formation are independent of 3' splice site in yeast mRNA splicing. *Nature*, 317(6039), 735.

Rørth, P. (1998). Gal4 in the Drosophila female germline. *Mechanisms of Development*, 78(1), 113–118. [http://doi.org/10.1016/S0925-4773\(98\)00157-9](http://doi.org/10.1016/S0925-4773(98)00157-9)

Sahai-Hernandez, P., Castanieto, A., & Nystul, T. G. (2012). Drosophila models of epithelial stem cells and their niches. *WIREs Developmental Biology*, 1(3), 447–457. <http://doi.org/10.1002/wdev.36>

Salles, C., Mével-Ninio, M., Vincent, A., & Payre, F. (2002). A germline-specific splicing generates an extended ovo protein isoform required for Drosophila oogenesis. *Developmental Biology*, 246(2), 366–376.

Sanchez, C. G., Teixeira, F. K., Czech, B., Preall, J. B., Zamparini, A. L., Seifert, J. R. K., ... Lehmann, R. (2016). Regulation of Ribosome Biogenesis and Protein Synthesis Controls Germline Stem Cell Differentiation. *Cell Stem Cell*, 18(2), 276–

290. <http://doi.org/10.1016/J.STEM.2015.11.004>

Sarkar, K., Kotb, N. M., Lemus, A., Martin, E. T., McCarthy, A., Camacho, J., ...

Rangan, P. (2021, November). A feedback loop between heterochromatin and the nucleopore complex controls germ-cell to oocyte transition during *Drosophila* oogenesis.

Cold Spring Harbor Laboratory. <http://doi.org/10.1101/2021.10.31.466575>

Sarov, M., Barz, C., Jambor, H., Hein, M. Y., Schmied, C., Suchold, D., ... Schnorrer, F.

(2016). A genome-wide resource for the analysis of protein localisation in *Drosophila*.

eLife, 5, e12068. <http://doi.org/10.7554/eLife.12068>

Sass, G. L., Comer, A. R., & Searles, L. L. (1995). The ovarian tumor protein isoforms of

Drosophila melanogaster exhibit differences in function, expression, and localization.

Developmental Biology, 167(1), 201–212.

Schäfer, T., Strauß, D., Petfalski, E., Tollervey, D., & Hurt, E. (2003). The path from

nucleolar 90S to cytoplasmic 40S pre-ribosomes. *The EMBO Journal*, 22(6), 1370–

1380.

Schupbach, T., & Wieschaus, E. (1989). Female sterile mutations on the second chro-

mosome of *Drosophila melanogaster*. I. Maternal effect mutations. *Genetics*, 121(1),

101–117.

Schupbach, T., & Wieschaus, E. (1991). Female sterile mutations on the second chro-

mosome of *Drosophila melanogaster*. II. Mutations blocking oogenesis or altering egg

morphology. *Genetics*, 129(4), 1119–1136.

Schüpbach, T. (1987). Germ line and soma cooperate during oogenesis to establish the dorsoventral pattern of egg shell and embryo in *Drosophila melanogaster*. *Cell*, *49*(5), 699–707. [http://doi.org/10.1016/0092-8674\(87\)90546-0](http://doi.org/10.1016/0092-8674(87)90546-0)

Schwarzacher, H. G., & Wachtler, F. (1993). The nucleolus. *Anatomy and Embryology*, *188*(6), 515–536.

Sekiguchi, T., Hayano, T., Yanagida, M., Takahashi, N., & Nishimoto, T. (2006). NOP132 is required for proper nucleolus localization of DEAD-box RNA helicase DDX47. *Nucleic Acids Research*, *34*(16), 4593–4608. <http://doi.org/10.1093/nar/gkl603>

Senturk, E., & Manfredi, J. J. (2013). P53 and Cell Cycle Effects After DNA Damage. *Methods in Molecular Biology (Clifton, N.J.)*, *962*, 49–61. http://doi.org/10.1007/978-1-62703-236-0_4

Serano, T. L., Cheung, H.-K., Frank, L. H., & Cohen, R. S. (1994). P element transformation vectors for studying *Drosophila melanogaster* oogenesis and early embryogenesis. *Gene*, *138*(1), 181–186. [http://doi.org/10.1016/0378-1119\(94\)90804-4](http://doi.org/10.1016/0378-1119(94)90804-4)

Seydoux, G., & Braun, R. E. (2006). Pathway to Totipotency: Lessons from Germ Cells. *Cell*, *127*(5), 891–904. <http://doi.org/10.1016/j.cell.2006.11.016>

Sezgin, M., & Sankur, B. (2004). Survey over image thresholding techniques and quantitative performance evaluation. *Journal of Electronic Imaging*, *13*(1), 146–166.

Shachak, A., Shuval, K., & Fine, S. (2007). Barriers and enablers to the acceptance of bioinformatics tools: A qualitative study. *Journal of the Medical Library Association : JMLA*, *95*(4), 454. <http://doi.org/10.3163/1536-5050.95.4.454>

Shi, J., Jin, Z., Yu, Y., Zhang, Y., Yang, F., Huang, H., . . . Xi, R. (2021). A Progressive Somatic Cell Niche Regulates Germline Cyst Differentiation in the Drosophila Ovary. *Current Biology*, 31(4), 840–852.e5. <http://doi.org/10.1016/j.cub.2020.11.053>

Shu, X. E., Swanda, R. V., & Qian, S.-B. (2020). Nutrient Control of mRNA Translation. *Annual Review of Nutrition*, 40(1), 51–75. <http://doi.org/10.1146/annurev-nutr-120919-041411>

Slaidina, M., Gupta, S., Banisch, T. U., & Lehmann, R. (2021). A single-cell atlas reveals unanticipated cell type complexity in Drosophila ovaries. *Genome Research*, gr.274340.120. <http://doi.org/10.1101/gr.274340.120>

Slaidina, M., & Lehmann, R. (2014). Translational control in germline stem cell development. *The Journal of Cell Biology*, 207(1), 13 LP–21. <http://doi.org/10.1083/jcb.201407102>

Sloan, K. E., Warda, A. S., Sharma, S., Entian, K. D., Lafontaine, D. L. J., & Bohnsack, M. T. (2017). Tuning the ribosome: The influence of rRNA modification on eukaryotic ribosome biogenesis and function. *RNA Biology*, 14(9), 1138–1152. <http://doi.org/10.1080/15476286.2016.1259781>

Smolko, A. E., Shapiro-Kulnane, L., & Salz, H. K. (2018). The H3K9 methyltransferase SETDB1 maintains female identity in Drosophila germ cells. *Nature Communications*, 9(1), 4155.

Soldner, F., & Jaenisch, R. (2018). Stem Cells, Genome Editing, and the Path to Translational Medicine. *Cell*, 175(3), 615–632. <http://doi.org/10.1016/j.cell.2018.09.010>

- Sonoda, J., & Wharton, R. P. (1999). Recruitment of Nanos to hunchback mRNA by Pumilio. *Genes & Development*, 13(20), 2704–2712. <http://doi.org/10.1101/gad.13.20.2704>
- Sonoda, J., & Wharton, R. P. (2001). Drosophila Brain Tumor is a translational repressor. *Genes & Development*, 15(6), 762–773. <http://doi.org/10.1101/gad.870801>
- Spradling, A. (1993). Developmental genetics of oogenesis. *The Development of Drosophila Melanogaster*.
- Spradling, Allan C. (1993). Germline cysts: Communes that work. *Cell*, 72(5), 649–651. [http://doi.org/10.1016/0092-8674\(93\)90393-5](http://doi.org/10.1016/0092-8674(93)90393-5)
- Spradling, A. C., De Cuevas, M., Drummond-Barbosa, D., Keyes, L., Lilly, M., Pepling, M., & Xie, T. (1997). The Drosophila Germarium: Stem Cells, Germ Line Cysts, and Oocytes. *Cold Spring Harbor Symposia on Quantitative Biology*, 62, 25–34. <http://doi.org/10.1101/SQB.1997.062.01.006>
- Spradling, Allan C., & Rubin, G. M. (1981). DROSOPHILA GENOME ORGANIZATION: CONSERVED AND DYNAMIC ASPECTS. *Annual Review of Genetics*, 15(1), 219–264. <http://doi.org/10.1146/annurev.ge.15.120181.001251>
- Spradling, Allan, Drummond-Barbosa, D., & Kai, T. (2001). Stem cells find their niche. *Nature*, 414(6859), 98–104. <http://doi.org/10.1038/35102160>
- Spradling, Allan, Fuller, M. T., Braun, R. E., & Yoshida, S. (2011). Germline stem cells. *Cold Spring Harbor Perspectives in Biology*, 3(11), a002642. <http://doi.org/10.1101/cshperspect.a002642>

- Studier, F. W. (2005). Protein production by auto-induction in high-density shaking cultures. *Protein Expression and Purification*, 41(1), 207–234. <http://doi.org/10.1016/j.pep.2005.01.010>
- Subtelny, A. O., Eichhorn, S. W., Chen, G. R., Sive, H., & Bartel, D. P. (2014). Poly(A)-tail profiling reveals an embryonic switch in translational control. *Nature*, 508, 66.
- Szostak, E., & Gebauer, F. (2013). Translational control by 3'-UTR-binding proteins. *Briefings in Functional Genomics*, 12(1), 58–65. <http://doi.org/10.1093/bfgp/els056>
- Tadauchi, T., Matsumoto, K., Herskowitz, I., & Irie, K. (2001). Post-transcriptional regulation through the HO 3'-UTR by Mpt5, a yeast homolog of Pumilio and FBF. *The EMBO Journal*, 20(3), 552–561. <http://doi.org/10.1093/emboj/20.3.552>
- Tadros, W., & Lipshitz, H. D. (2009). The maternal-to-zygotic transition: A play in two acts. *Development*, 136(18), 3033 LP–3042. <http://doi.org/10.1242/dev.033183>
- Tafforeau, L., Zorbas, C., Langhendries, J.-L., Mullineux, S.-T., Stamatopoulou, V., Mullier, R., ... Lafontaine, D. L. J. (2013). The Complexity of Human Ribosome Biogenesis Revealed by Systematic Nucleolar Screening of Pre-rRNA Processing Factors. *Molecular Cell*, 51(4), 539–551. <http://doi.org/10.1016/J.MOLCEL.2013.08.011>
- Tanentzapf, G., Devenport, D., Godt, D., & Brown, N. H. (2007). Integrin-dependent anchoring of a stem-cell niche. *Nature Cell Biology*, 9(12), 1413–1418. <http://doi.org/10.1038/ncb1660>
- Tang, F., Barbacioru, C., Wang, Y., Nordman, E., Lee, C., Xu, N., ... Surani, M. A. (2009). mRNA-Seq whole-transcriptome analysis of a single cell. *Nature Methods*, 6(5), 377–382. <http://doi.org/10.1038/nmeth.1315>

- Tang, H., Hornstein, E., Stolovich, M., Levy, G., Livingstone, M., Templeton, D., ... Meyuhas, O. (2001). Amino Acid-Induced Translation of TOP mRNAs Is Fully Dependent on Phosphatidylinositol 3-Kinase-Mediated Signaling, Is Partially Inhibited by Rapamycin, and Is Independent of S6K1 and rpS6 Phosphorylation. *Molecular and Cellular Biology*, 21(24), 8671–8683. <http://doi.org/10.1128/MCB.21.24.8671-8683.2001>
- Tanneti, N. S., Landy, K., Joyce, E. F., & McKim, K. S. (2011). A Pathway for Synapsis Initiation during Zygote in Drosophila Oocytes. *Current Biology*, 21(21), 1852–1857. <http://doi.org/10.1016/j.cub.2011.10.005>
- Tarun Jr, S. Z., Wells, S. E., Deardorff, J. A., & Sachs, A. B. (1997). Translation initiation factor eIF4G mediates in vitro poly(A) tail-dependent translation. *Proceedings of the National Academy of Sciences of the United States of America*, 94(17), 9046–9051. <http://doi.org/10.1073/pnas.94.17.9046>
- Tasnim, S., & Kelleher, E. S. (2018). P53 is required for female germline stem cell maintenance in P-element hybrid dysgenesis. *Developmental Biology*, 434(2), 215–220.
- Tastan, Ö. Y., Maines, J. Z., Li, Y., McKearin, D. M., & Buszczak, M. (2010). Drosophila Ataxin 2-binding protein 1 marks an intermediate step in the molecular differentiation of female germline cysts. *Development*, 137(19), 3167–3176. <http://doi.org/10.1242/dev.050575>

Tcherkezian, J., Cargnello, M., Romeo, Y., Huttlin, E. L., Lavoie, G., Gygi, S. P., & Roux, P. P. (2014). Proteomic analysis of cap-dependent translation identifies LARP1 as a key regulator of 5'TOP mRNA translation. *Genes and Development*, 28(4), 357–371.
<http://doi.org/10.1101/gad.231407.113>

Temme, C., Simonelig, M., & Wahle, E. (2014). Deadenylation of mRNA by the CCR4-NOT complex in Drosophila: Molecular and developmental aspects. *Frontiers in Genetics*, 5, 143. <http://doi.org/10.3389/fgene.2014.00143>

Teng, T., Thomas, G., & Mercer, C. A. (2013). Growth control and ribosomopathies. *Current Opinion in Genetics & Development*, 23(1), 63–71.
<http://doi.org/10.1016/J.GDE.2013.02.001>

Texada, M. J., Jørgensen, A. F., Christensen, C. F., Koyama, T., Malita, A., Smith, D. K., ... Rewitz, K. F. (2019). A fat-tissue sensor couples growth to oxygen availability by remotely controlling insulin secretion. *Nature Communications*, 10(1).
<http://doi.org/10.1038/s41467-019-09943-y>

Theunissen, T. W., & Jaenisch, R. (2017). Mechanisms of gene regulation in human embryos and pluripotent stem cells. *Development*, 144(24), 4496 LP–4509.
<http://doi.org/10.1242/dev.157404>

Theurkauf, W. E., Alberts, B. M., Jan, Y. N., & Jongens, T. A. (1993). A central role for microtubules in the differentiation of Drosophila oocytes. *Development (Cambridge, England)*, 118(4), 1169–80.

Thomas, P. D., Campbell, M. J., Kejariwal, A., Mi, H., Karlak, B., Daverman, R., ... Narechania, A. (2003). PANTHER: A Library of Protein Families and Subfamilies Indexed by Function. *Genome Research*, 13(9), 2129–2141. <http://doi.org/10.1101/gr.772403>

Thoreen, C. C., Chantranupong, L., Keys, H. R., Wang, T., Gray, N. S., & Sabatini, D. M. (2012). A unifying model for mTORC1-mediated regulation of mRNA translation. *Nature*, 485(7396), 109–113. <http://doi.org/10.1038/nature11083>

Tiaden, A. N., Breiden, M., Mirsaidi, A., Weber, F. A., Bahrenberg, G., Glanz, S., ... Richards, P. J. (2012). Human serine protease HTRA1 positively regulates osteogenesis of human bone marrow-derived mesenchymal stem cells and mineralization of differentiating bone-forming cells through the modulation of extracellular matrix protein. *Stem Cells (Dayton, Ohio)*, 30(10), 2271–2282. <http://doi.org/10.1002/stem.1190>

Tirronen, M., Lahti, V.-P., Heino, T. I., & Roos, C. (1995). Two otu transcripts are selectively localised in Drosophila oogenesis by a mechanism that requires a function of the otu protein. *Mechanisms of Development*, 52(1), 65–75.

Tschochner, H., & Hurt, E. (2003). Pre-ribosomes on the road from the nucleolus to the cytoplasm. *Trends in Cell Biology*, 13(5), 255–263.

Twombly, V., Blackman, R. K., Jin, H., Graff, J. M., Padgett, R. W., & Gelbart, W. M. (1996). The TGF-beta signaling pathway is essential for Drosophila oogenesis. *Development*, 122(5), 1555 LP–1565.

- Tye, B. W., Commins, N., Ryazanova, L. V., Wühr, M., Springer, M., Pincus, D., & Churchman, L. S. (2019). Proteotoxicity from aberrant ribosome biogenesis compromises cell fitness. *eLife*, 8, e43002. <http://doi.org/10.7554/eLife.43002>
- Umen, J. G., & Guthrie, C. (1995). The second catalytic step of pre-mRNA splicing. *Rna*, 1(9), 869.
- Upadhyay, M., Cortez, Y. M., Wong-Deyrup, S., Tavares, L., Schowalter, S., Flora, P., ... Rangan, P. (2016). Transposon Dysregulation Modulates dWnt4 Signaling to Control Germline Stem Cell Differentiation in Drosophila. *PLOS Genetics*, 12(3), e1005918. <http://doi.org/10.1371/journal.pgen.1005918>
- Valdez, B. C., Henning, D., So, R. B., Dixon, J., & Dixon, M. J. (2004). The Treacher Collins syndrome (TCOF1) gene product is involved in ribosomal DNA gene transcription by interacting with upstream binding factor. *Proceedings of the National Academy of Sciences*, 101(29), 10709–10714. <http://doi.org/10.1073/pnas.0402492101>
- Van Buskirk, C., & Schüpbach, T. (2002). Half pint regulates alternative splice site selection in Drosophila. *Developmental Cell*, 2(3), 343–353.
- VanInsberghe, M., van den Berg, J., Andersson-Rolf, A., Clevers, H., & van Oudenaarden, A. (2021). Single-cell Ribo-seq reveals cell cycle-dependent translational pausing. *Nature*, 597(7877), 561–565. <http://doi.org/10.1038/s41586-021-03887-4>
- Venema, J., Cile Bousquet-Antonelli, C., Gelugne, J.-P., Le Caizergues-Ferrer, M., & Tollervey, D. (1997). Rok1p Is a Putative RNA Helicase Required for rRNA Processing, 17(6), 3398–3407.

- Venema, J., & Tollervey, D. (1995). Processing of pre-ribosomal RNA in *Saccharomyces cerevisiae*. *Yeast*, 11(16), 1629–1650. <http://doi.org/10.1002/yea.320111607>
- Vessey, J. P., Schoderboeck, L., Gingl, E., Luzi, E., Rieffler, J., Di Leva, F., ... Macchi, P. (2010). Mammalian Pumilio 2 regulates dendrite morphogenesis and synaptic function. *Proceedings of the National Academy of Sciences*, 107(7), 3222 LP–3227. <http://doi.org/10.1073/pnas.0907128107>
- Vincent, N. G., Charette, J. M., & Baserga, S. J. (2017). The SSU processome interactome in *Saccharomyces cerevisiae* reveals potential new protein subcomplexes. *RNA*, rna.062927.117. <http://doi.org/10.1261/rna.062927.117>
- Vlachos, A., & Muir, E. (2010). How I treat Diamond-Blackfan anemia, 116, 3715–3723. <http://doi.org/10.1182/blood-2010-02-251090>
- Wahl, M. C., Will, C. L., & Lührmann, R. (2009). The spliceosome: Design principles of a dynamic RNP machine. *Cell*, 136(4), 701–718.
- Wang, X., & Page-McCaw, A. (2018). Wnt6 maintains anterior escort cells as an integral component of the germline stem cell niche. *Development (Cambridge, England)*, 145(3). <http://doi.org/10.1242/dev.158527>
- Wang, Y., Liu, J., Huang, B. O., Xu, Y.-M., Li, J., Huang, L.-F., ... Yang, W.-M. (2015). Mechanism of alternative splicing and its regulation. *Biomedical Reports*, 3(2), 152–158.
- Warren, A. J. (2018). Molecular basis of the human ribosomopathy Shwachman-Diamond syndrome. *Advances in Biological Regulation*, 67, 109–127. <http://doi.org/10.1016/j.jbior.2017.09.00>

- Watanabe-Susaki, K., Takada, H., Enomoto, K., Miwata, K., Ishimine, H., Intoh, A., ... Asashima, M. (2014). Biosynthesis of ribosomal RNA in nucleoli regulates pluripotency and differentiation ability of pluripotent stem cells. *Stem Cells*, 32(12), 3099–3111.
- Watkins, N. J., & Bohnsack, M. T. (2012). The box C/D and H/ACA snoRNPs: Key players in the modification, processing and the dynamic folding of ribosomal RNA. *Wiley Interdisciplinary Reviews: RNA*, 3(3), 397–414. <http://doi.org/10.1002/wrna.117>
- Webster, P. J., Liang, L., Berg, C. A., Lasko, P., & Macdonald, P. M. (1997). Translational repressor bruno plays multiple roles in development and is widely conserved. *Genes & Development*, 11(19), 2510–2521. <http://doi.org/10.1101/gad.11.19.2510>
- Wei, Youheng, Bettedi, L., Kim, K., Ting, C.-Y., & Lilly, M. (2019). The GATOR complex regulates an essential response to meiotic double-stranded breaks in Drosophila. *eLife*, 8, e42149. <http://doi.org/10.7554/eLife.42149>
- Wei, Youheng, Reveal, B., Reich, J., Laursen, W. J., Senger, S., Akbar, T., ... Lilly, M. A. (2014). TORC1 regulators Iml1/GATOR1 and GATOR2 control meiotic entry and oocyte development in Drosophila. *Proceedings of the National Academy of Sciences*, 111(52), E5670–E5677.
- Wei, Yuehua, & Zheng, X. F. S. (2009). Sch9 partially mediates TORC1 signaling to control ribosomal RNA synthesis. *Cell Cycle*, 8(24), 4085–4090.
- Wickham, H. (2016). *Ggplot2: Elegant graphics for data analysis*. Springer-Verlag New York.

- Wilcockson, S. G., & Ashe, H. L. (2019). Drosophila Ovarian Germline Stem Cell Cytosensor Projections Dynamically Receive and Attenuate BMP Signaling. *Developmental Cell*, 50(3), 296–312.e5. <http://doi.org/10.1016/j.devcel.2019.05.020>
- Will, C. L., & Lührmann, R. (2001). Spliceosomal UsnRNP biogenesis, structure and function. *Current Opinion in Cell Biology*, 13(3), 290–301.
- Will, C. L., & Lührmann, R. (2011). Spliceosome structure and function. *Cold Spring Harbor Perspectives in Biology*, 3(7), a003707.
- Woolnough, J. L., Atwood, B. L., Liu, Z., Zhao, R., & Giles, K. E. (2016). The Regulation of rRNA Gene Transcription during Directed Differentiation of Human Embryonic Stem Cells. *PLOS ONE*, 11(6), e0157276. <http://doi.org/10.1371/journal.pone.0157276>
- Wullschleger, S., Loewith, R., & Hall, M. N. (2006). TOR signaling in growth and metabolism. *Cell*, 124(3), 471–484.
- Xie, T., & Li, L. (2007). Stem cells and their niche: An inseparable relationship. *Development*, 134(11), 2001 LP–2006. <http://doi.org/10.1242/dev.002022>
- Xie, T., & Spradling, A. C. (1998). Decapentaplegic Is Essential for the Maintenance and Division of Germline Stem Cells in the Drosophila Ovary. *Cell*, 94(2), 251–260. [http://doi.org/10.1016/S0092-8674\(00\)81424-5](http://doi.org/10.1016/S0092-8674(00)81424-5)
- Xie, T., & Spradling, A. C. (2000). A Niche Maintaining Germ Line Stem Cells in the Drosophila Ovary. *Science*, 290(5490), 328–330. <http://doi.org/10.1126/science.290.5490.328>

Xue, S., & Barna, M. (2012). Specialized ribosomes: A new frontier in gene regulation and organismal biology. *Nature Reviews Molecular Cell Biology*, 13(6), 355–369. <http://doi.org/10.1038/nrm3359>

Yamashita, Y. M., & Fuller, M. T. (2005). Asymmetric stem cell division and function of the niche in the Drosophila male germ line. *International Journal of Hematology*, 82(5), 377–380. <http://doi.org/10.1532/IJH97.05097>

Yan, D., & Perrimon, N. (2015). Spenito is required for sex determination in Drosophila melanogaster. *Proceedings of the National Academy of Sciences*, 112(37), 11606–11611.

Yang, S. Y., Baxter, E. M., & Van Doren, M. (2012). Phf7 controls male sex determination in the Drosophila germline. *Developmental Cell*, 22(5), 1041–1051.

Yang, Y.-G. Y., Hsu, P. J., Chen, Y.-S., & Yang, Y.-G. Y. (2018). Dynamic transcriptomic m 6 A decoration: Writers, erasers, readers and functions in RNA metabolism. *Cell Research*, 28(6), 616.

Yelick, P. C., & Trainor, P. A. (2015). Ribosomopathies: Global process, tissue specific defects. *Rare Diseases*, 3(1), e1025185. <http://doi.org/10.1080/21675511.2015.1025185>

Yerlikaya, S., Meusburger, M., Kumari, R., Huber, A., Anrather, D., Costanzo, M., ... Loewith, R. (2016). TORC1 and TORC2 work together to regulate ribosomal protein S6 phosphorylation in *Saccharomyces cerevisiae*. *Molecular Biology of the Cell*, 27(2), 397–409.

Yi, C., & Pan, T. (2011). Cellular dynamics of RNA modification. *Accounts of Chemical Research*, 44(12), 1380–1388.

You, K. T., Park, J., & Kim, V. N. (2015). Role of the small subunit processome in the maintenance of pluripotent stem cells. *Genes & Development*, 29(19), 2004–9.
<http://doi.org/10.1101/gad.267112.115>

Yu, H., Jin, S., Zhang, N., & Xu, Q. (2016). Up-regulation of GTPBP4 in colorectal carcinoma is responsible for tumor metastasis. *Biochemical and Biophysical Research Communications*, 480(1), 48–54. <http://doi.org/10.1016/j.bbrc.2016.10.010>

Zaccaï, M., & Lipshitz, H. D. (1996). Differential distributions of two adducin-like protein isoforms in the Drosophila ovary and early embryo. *Zygote*, 4(2), 159–166.

Zahradkal, P., Larson, DawnE., & Sells, BruceH. (1991). Regulation of ribosome biogenesis in differentiated rat myotubes. *Molecular and Cellular Biochemistry*, 104(1-2).
<http://doi.org/10.1007/BF00229819>

Zamore, P. D., Bartel, D. P., Lehmann, R., & Williamson, J. R. (1999). The PUMILIO-RNA interaction: A single RNA-binding domain monomer recognizes a bipartite target sequence. *Biochemistry*, 38(2), 596–604. <http://doi.org/10.1021/bi982264s>

Zemp, I., & Kutay, U. (2007). Nuclear export and cytoplasmic maturation of ribosomal subunits. *FEBS Letters*, 581(15), 2783–2793.

Zhang, K., & Smith, G. W. (2015). Maternal control of early embryogenesis in mammals. *Reproduction, Fertility, and Development*, 27(6), 880–896.
<http://doi.org/10.1071/RD14441>

Zhang, Q., Shalaby, N. A., & Busczak, M. (2014). Changes in rRNA transcription influence proliferation and cell fate within a stem cell lineage. *Science*, 343(6168), 298–301.

Zhang, Yandong, Forys, J. T., Miceli, A. P., Gwinn, A. S., & Weber, J. D. (2011). Identification of DHX33 as a Mediator of rRNA Synthesis and Cell Growth. *Molecular and Cellular Biology*, 31(23), 4676–4691. <http://doi.org/10.1128/MCB.05832-11>

Zhang, Yanping, & Lu, H. (2009). Signaling to P53: Ribosomal Proteins Find Their Way. *Cancer Cell*, 16(5), 369–377. <http://doi.org/10.1016/j.ccr.2009.09.024>

Zhang, Yi, Wang, Z.-H., Liu, Y., Chen, Y., Sun, N., Gucek, M., ... Xu, H. (2019). PINK1 Inhibits Local Protein Synthesis to Limit Transmission of Deleterious Mitochondrial DNA Mutations. *Molecular Cell*, 73(6), 1127–1137.e5. <http://doi.org/10.1016/j.molcel.2019.01.013>

Zhao, B. S., & He, C. (2015). Pseudouridine in a new era of RNA modifications. *Cell Research*, 25(2), 153.

Zhao, G.-Q., & Garbers, D. L. (2002). Male germ cell specification and differentiation. *Developmental Cell*, 2(5), 537–547.

Zhou, R., Mohr, S., Hannon, G. J., & Perrimon, N. (2013). Inducing RNAi in Drosophila Cells by Transfection with dsRNA. *Cold Spring Harbor Protocols*, 2013(5), pdb.prot074351–pdb.prot074351. <http://doi.org/10.1101/pdb.prot074351>

Zielke, N., Korzelius, J., van Straaten, M., Bender, K., Schuhknecht, G. F. P., Dutta, D., ... Edgar, B. A. (2014). Fly-FUCCI: A versatile tool for studying cell proliferation

in complex tissues. *Cell Reports*, 7(2), 588–598.